STUDIES OF GAS-LIQUID-PARTICLE MIXING IN STIRRED VESSELS

Submitted for the degree of Doctor of Philosophy

in the University of London by:

Colin Michael Chapman, B.Sc. (Eng.)

Ramsay Memorial Laboratory,

Department of Chemical and
Biochemical Engineering,

University College London,

Torrington Place,

London WC1E 7JE

September 1981

ABSTRACT

Measurements of impeller speed, power consumption and gas holdup were combined with visual observations of the extent of gas dispersion and particle suspension in three phase systems for a wide size range of fully baffled, agitated vessels (tank diameters from 0.29 to 1.83 m).

Several common impeller geometries were examined and a minimum mixing condition with regard to gas dispersion was specified for each type. Where the impeller had previously been characterized (e.g. the six-bladed disc turbine) in gas-liquid systems, this minimum condition coincided with those generally accepted in the literature.
The minimum mixing condition with regard to particle suspension was taken to be when no particle remained at rest on the base for more than one to two seconds. A system was defined as efficiently mixed when both gas dispersion and particle suspension criteria were simultaneously satisfied for the minimum power input.

The effect of well-suspended particles on the gas-liquid hydrodynamics in the vessel was negligible, but if large quantities of particles were settled out on the vessel base, gas dispersion was affected. On the other hand, aeration had an adverse influence on particle suspension, and increased impeller speeds and powers were necessary to maintain the particles in the just-suspended state if the system was sparged with gas. Consequently the result of aerating a system which was operating at the ungassed just-suspended condition was sedimentation of the solids. The severity of this sedimentation was dependent on impeller geometry, and at one extreme could result in complete sedimentation of all the solids for a very small change in operating conditions. A qualitative method is presented which gives an indication of the likely extent of sedimentation.

Of the impellers investigated, the disc turbine and mixed flow impeller pumping upwards are shown to provide the most stable and efficient operation at high gas rates. A tentative procedure for designing a disc turbine agitated system is proposed and is supported by data collected over the whole vessel size range. A novel theoretical approach to estimating gas-liquid mass transfer coefficients is utilised to produce data which support the use of disc turbines and mixed flow impellers pumping upwards as the most efficient impellers in a three phase system.

ACKNOWLEDGEMENTS

I would like to thank everyone who has shown interest in this work, especially my fellow postgraduate students, past and present, who have been a source of encouragement.

In particular I am very grateful to:-

Professor P.N. Rowe, for providing the facilities for this research.

Messrs. D. Montgomery, L. Coates, D. Cheeseman, K. Wheatley, H. MacGillivray and all the other technical staff.

The academic staff for their constant advice and help, particularly Dr. L. Gibilaro for the work on mass transfer.

The S.R.C. for the provision of a research studentship and I.C.I. for their contribution of financial assistance and experimental facilities, particularly Dr. J.C. Middleton and Mr. M. Cooke for their advice and assistance.

Finally and with particular gratitude, to Professor A.W. Nienow for his enthusiasm, guidance and friendship.

Addenda

Page	Line	Change
38	13	"demonstrated in Fig. 3.6" to "demonstrated by another set of data in Fig 3.6"
59	17	"regime, a very ..." to "regime, then assuming plug flow through the impeller region, a very ..."
189	2	"$\frac{dC_L}{dt} = 0$" to "$\frac{dC_L}{dt} = 0$ (since in Eqn. 8.18, the denominator is zero at t=0 and hence $\frac{dC_L^*}{dt}$ must also be zero otherwise $k_L A$ would have an instantaneously infinite value at zero time. Also, the step change is imposed on the gas phase and hence – as with two C.S.T.R.s in series – the response in the liquid phase will lead to $\frac{dC_L^*}{dt} = 0$)"
208	1	"4 and 7 suggests" to "4 and 7 – regarding the significant deviations in $(\varepsilon_T)_{JS}$ between the two sets of vessels (UCL and ICI) – suggests ..."

To Mum and Dad, and my wife Dominique

who tried to correct all my spelling

misteaks. (sic)

"Two's company, three's a crowd."

CONTENTS

CHAPTER 1.

INTRODUCTION

1.1. Three Phase Contacting in Stirred Vessels

Both gas-liquid and particle-liquid dispersions in mechanically agitated vessels have been the subject of much research. However, the suspension of solid particles whilst simultaneously dispersing a gas in a liquid continuum has received very little attention, despite numerous applications in the process industries.

The requirements of many three phase reaction and absorption systems can be satisfied by using fixed bed or trickle bed reactors, though these do not ensure uniform ageing or complete contacting of the solid phase. Additional power input to the system, in the form of mechanical agitation, enhances transport properties and allows greater flexibility than can be obtained with either fixed beds or three phase fluidised beds. Thus mechanical agitation of gas-liquid-particle dispersions has a significant role to play. Typical applications include various hydrogenations and oxidations, fermentations, waste water treatment, evaporative crystallizers and froth flotation cells.

1.2. Motivation and Objectives

The motivation for this work is the lack of knowledge with regard to any interaction there may be between the mechanisms responsible for gas dispersion and particle suspension respectively. The importance of gaining this knowledge was demonstrated when Arbiter et al.[1] reported a sudden and catastrophic sedimentation of particles in a froth flotation cell, if a critical gas flow was exceeded.

Therefore, the overall objective of this thesis is to provide a solid basis of information and to eventually lead to the description of a design method for the stable operation of a three phase agitated system, based on:-

1. Examining the individual two phase systems (gas-liquid and

solid-liquid) and combining visual observation with experimental data to gain any new information required, particularly with regard to:-

(a) Scale up in solid-liquid systems.

(b) Gas dispersion capability of axial and mixed flow impellers.

2. Using the bases established in (1) above to study the major interactions of gas dispersion on solid suspension,and vice versa, in three phase systems.

The approach taken to achieve the objectives set out above was initially to use a six-bladed disc turbine, which has been widely used and characterized in terms of both its gas-liquid and solid-liquid dispersion roles, to examine the effect of a wide range of variables on a three phase system and thereby gain an insight to the most important phenomena at work. The next step was to consider other types of impeller and define where each type might be most suitable. However, this stage required some preliminary work to be done, particularly on the behaviour of axial flow impellers in gas-liquid systems, since this field was not well documented in the literature. Having reached the position whereby some recommendations could be made on the most suitable system for a given duty, then a further check was instituted by evaluating the gas-liquid mass transfer rates of the various impeller systems.

1.3. Terminology and Main Parameters

In order to simplify presentation of data, various dimensionless groups will be used throughout this thesis. They can each be ascribed a physical interpretation.

The power number (Po) is the ratio of pressure forces producing flow to inertial forces and is analogous to a drag coefficient.

$$Po = \frac{P}{\rho_L N^3 D^5} \quad \text{or} \quad Po_g = \frac{P_g}{\rho_L N^3 D^5} \qquad 1.1$$

The flow number (Fl) represents the ratio of gas inlet rate to impeller pumping rate.

$$Fl = \frac{Q}{ND^3} \qquad 1.2$$

The Reynolds number (Re) is the ratio of inertial to viscous forces.

$$Re = \frac{\rho_L N D^2}{\mu} \qquad 1.3$$

Both Reynolds number and power number, whether in two or three phase systems, are calculated on the basis of liquid properties.

Gas rates are often referenced to vessel size, either as a superficial velocity (V_S) based on the cross sectional area of the vessel, or as tank volumes per minute (vvm). In this work vvm are most commonly used, for reasons explained in Chapter 3.

The major parameters examined were the two minimum mixing requirements. For a constant gas rate, the minimum mixing requirement for the gas phase is the impeller speed (N_{CD}) at which the gas is just dispersed throughout the vessel. For the solid phase, the minimum requirement is the impeller speed (N_{JS}) at which no particle remains on the base for more than one to two seconds. The justification for choosing these criteria is explained fully in Chapters 3 and 4 respectively. A further criterion examined was the gas-liquid mass transfer capability of various impellers.

1.4. Layout of Thesis

The nature of the thesis lends itself to presentation in self contained sections. Firstly, Chapter 2 describes the equipment and techniques common to all the work. Chapters 3 and 4 deal with the two phase systems, gas-liquid and solid-liquid respectively. The

third and main section, formed by Chapters 5, 6 and 7, contains the work on three phase systems, describing general interactions in Chapter 5, and the more detailed effects of liquid or particle and equipment properties in Chapters 6 and 7. With regard to particle suspension, impeller type is a crucial parameter in obtaining an optimum design. Chapter 8 examines the gas-liquid mass transfer capability of several impellers to determine their overall suitability. The final chapter draws together the major conclusions and suggests further work.

CHAPTER 2.

EQUIPMENT AND TECHNIQUES

2.1. Introduction

Equipment and procedures relating to specific chapters will be dealt with in those chapters. The techniques and apparatus described here cover the various tanks, impellers, particles and liquids used, along with the methods employed to make visual observations and to measure impeller speed, power consumption and gas holdup.

2.2. The Tanks

The bulk of the work was carried out in a baffled 0.56 m diameter vessel (T_{56}) which is shown in Plate 1. However, one of the objectives of this work was to examine the effects of scale up and therefore another four baffled tanks were used with diameters of 0.29 m (T_{29}), 0.30 m (T_{30}), 0.91 m (T_{91}) and 1.83 m (T_{183}). Details of all these vessels are given in Table 2.1. The two largest (T_{183}, T_{91}) and one of the smallest (T_{30}) vessels were located at ICI Corporate Laboratory (Plate 2).

Fig. 2.1 shows a schematic representation of the standard geometry employed in all the tanks used, though gas sparger, impeller mounting and shaft length and thickness varied between the tanks. Although the effect of varying impeller clearance is briefly examined later (Chapters 4 and 7), a clearance from the base of one quarter of the tank diameter was chosen as standard since low clearances have been shown to enhance particle suspension capability[2] whilst this clearance has also been recommended as the optimum for gas dispersion in disc turbine agitated systems.[3] In order to maintain geometric similarity whilst varying impeller type, this clearance was also used for impellers other than disc turbines.

T_{56} was an open topped 0.56 m diameter cylindrical vessel, with four 10% baffles, constructed of Perspex and encased in a square

PAGE
NUMBERS
CUT OFF
IN
ORIGINAL

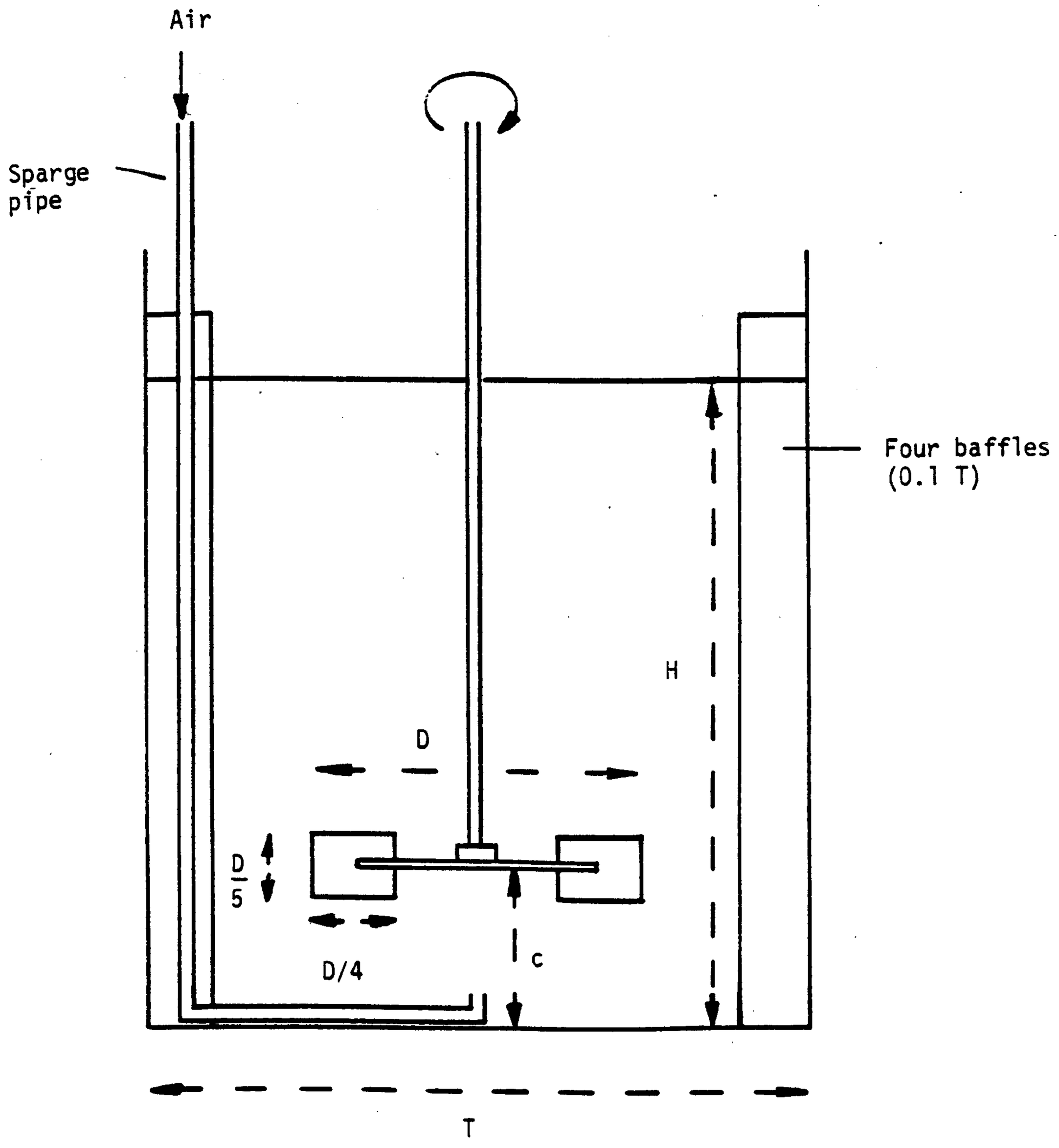

Fig. 2.1 Schematic Representation of the Standard Geometry Employed

H = T

c = 0.25 T

(a)

(b)

Plate 1. (a) General view of Experimental Rig (T_{56}) and Ancillary Equipment showing (b) a close up of the motor-air bearing-load cell assembly.

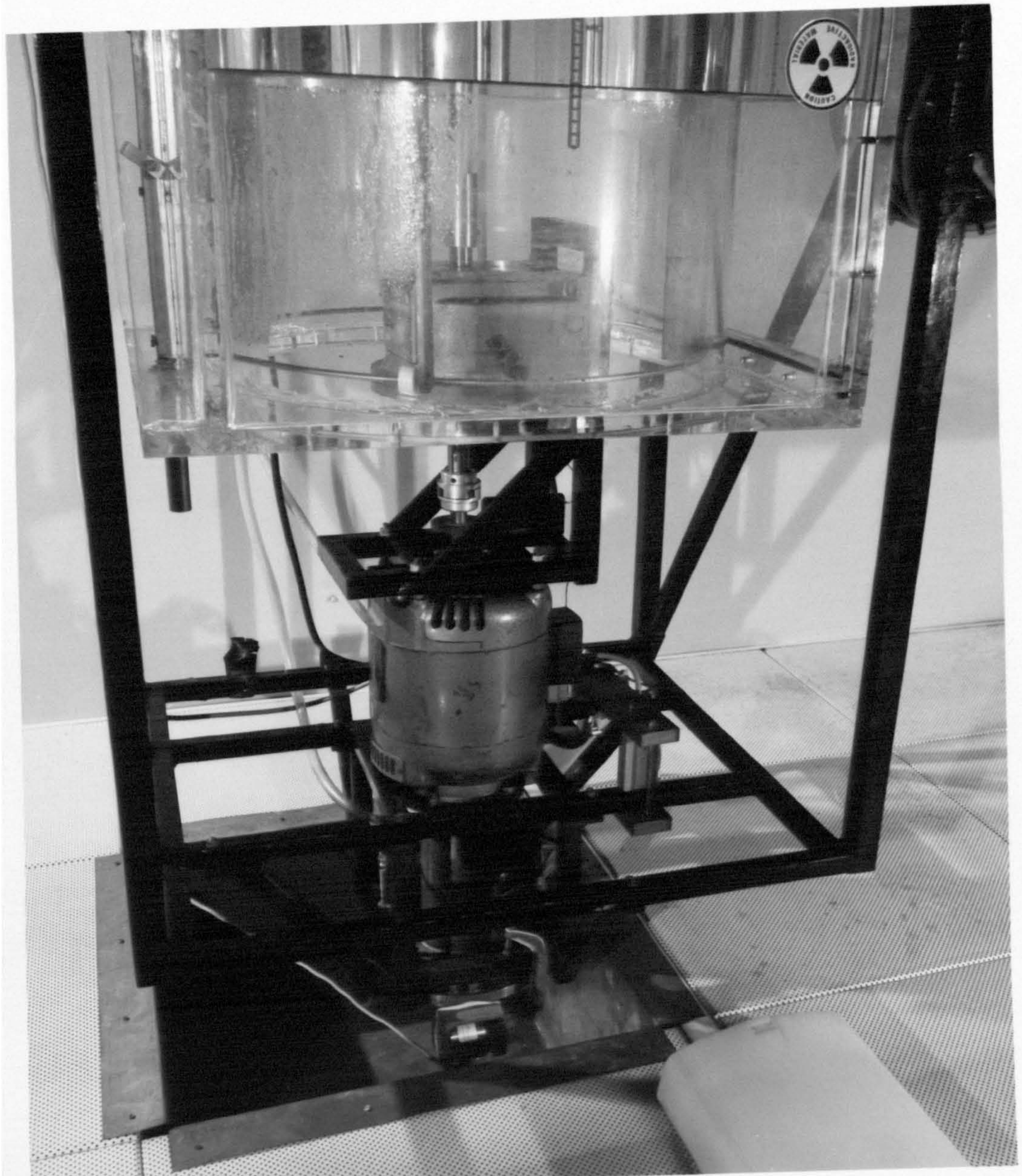

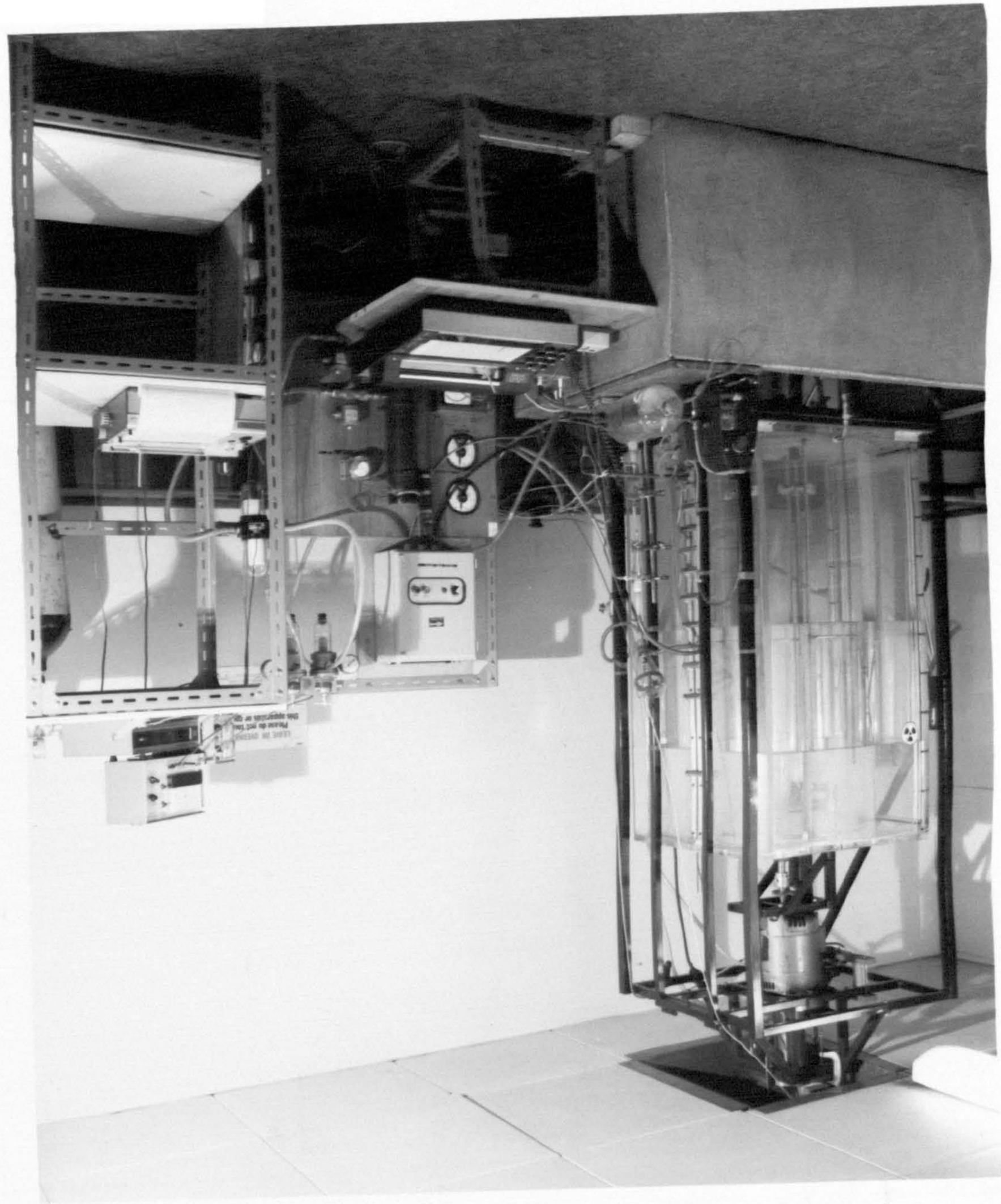

(a)

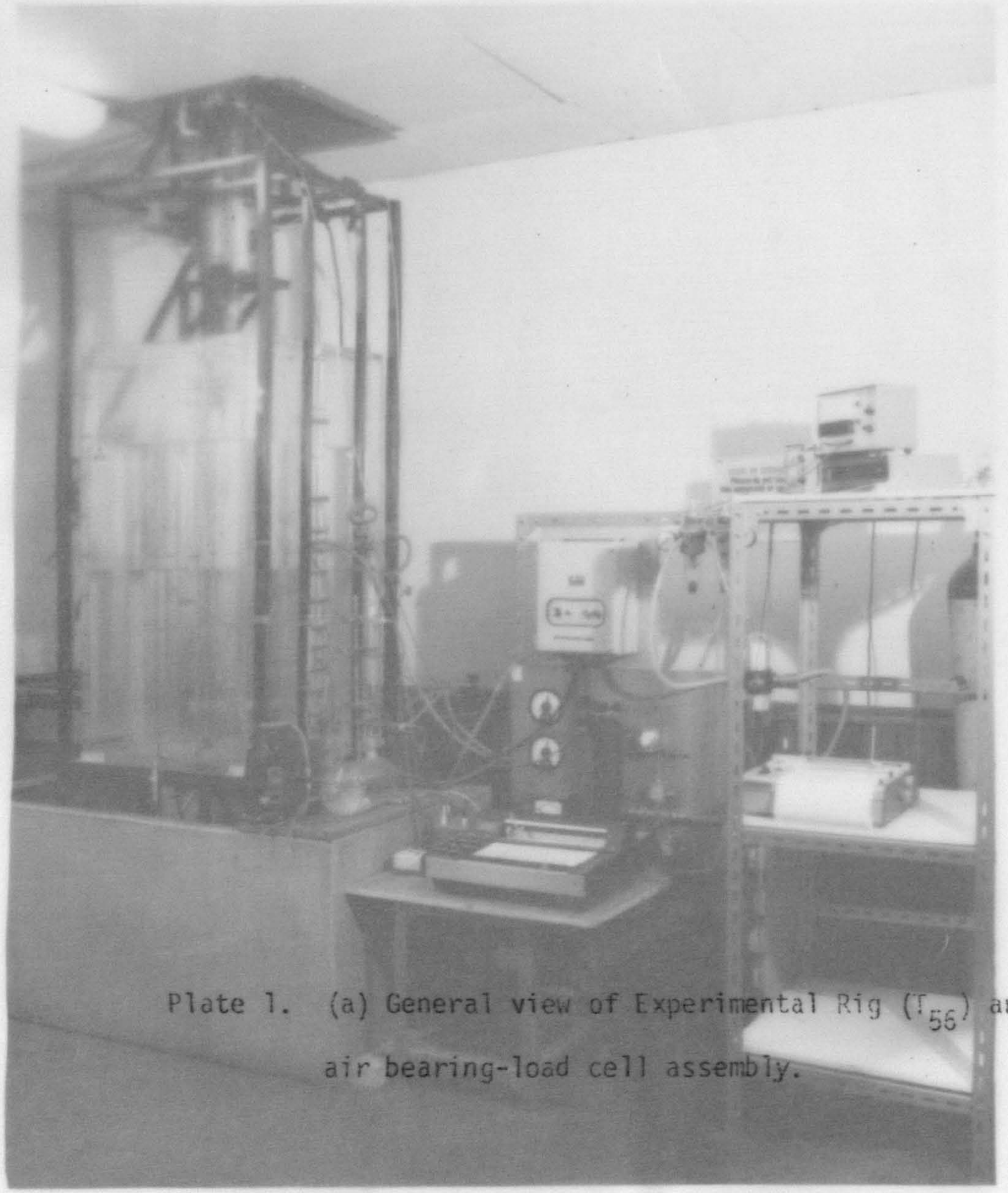

(b)

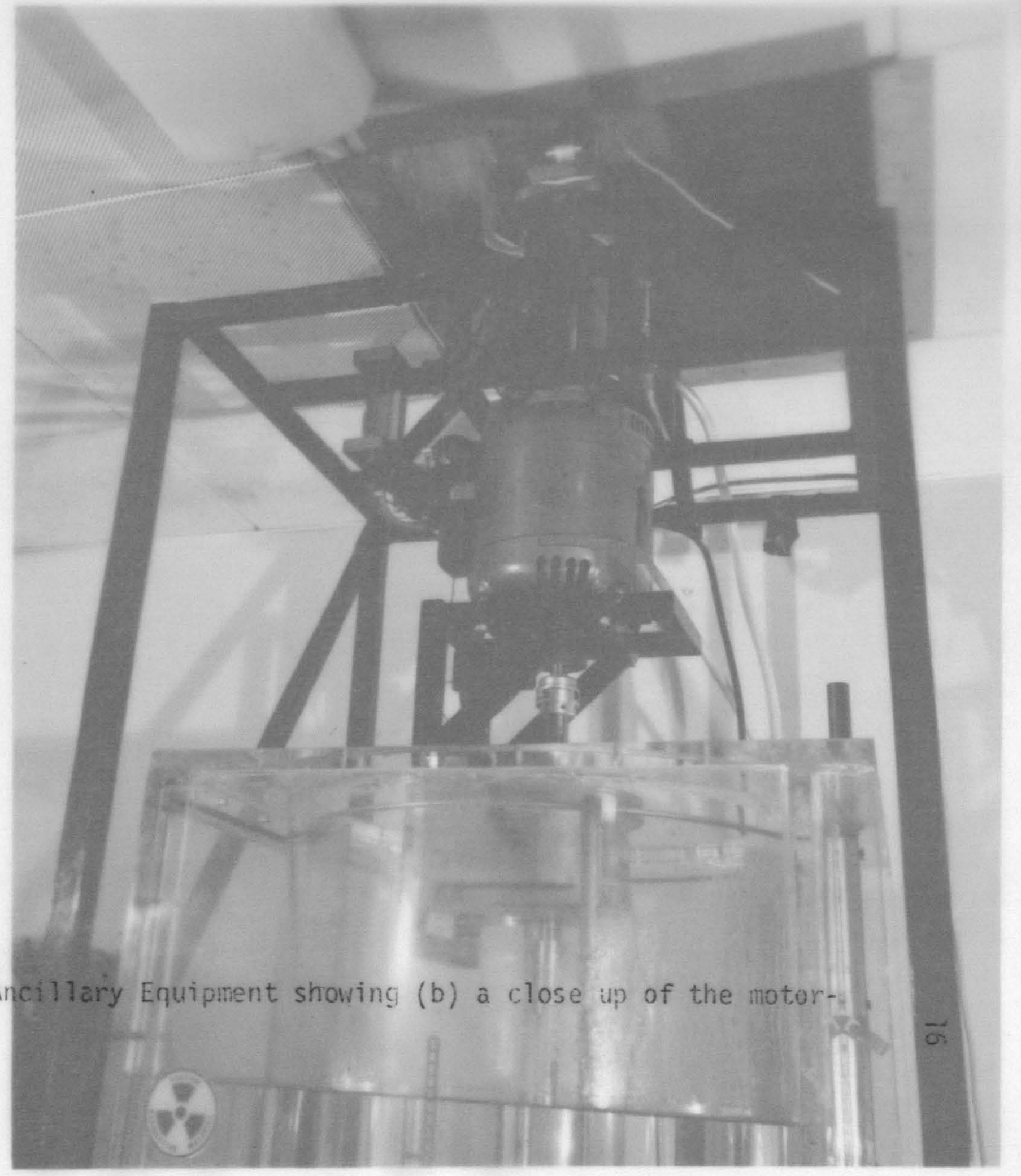

Plate 1. (a) General view of Experimental Rig (T_{56}) and Ancillary Equipment showing (b) a close up of the motor-air bearing-load cell assembly.

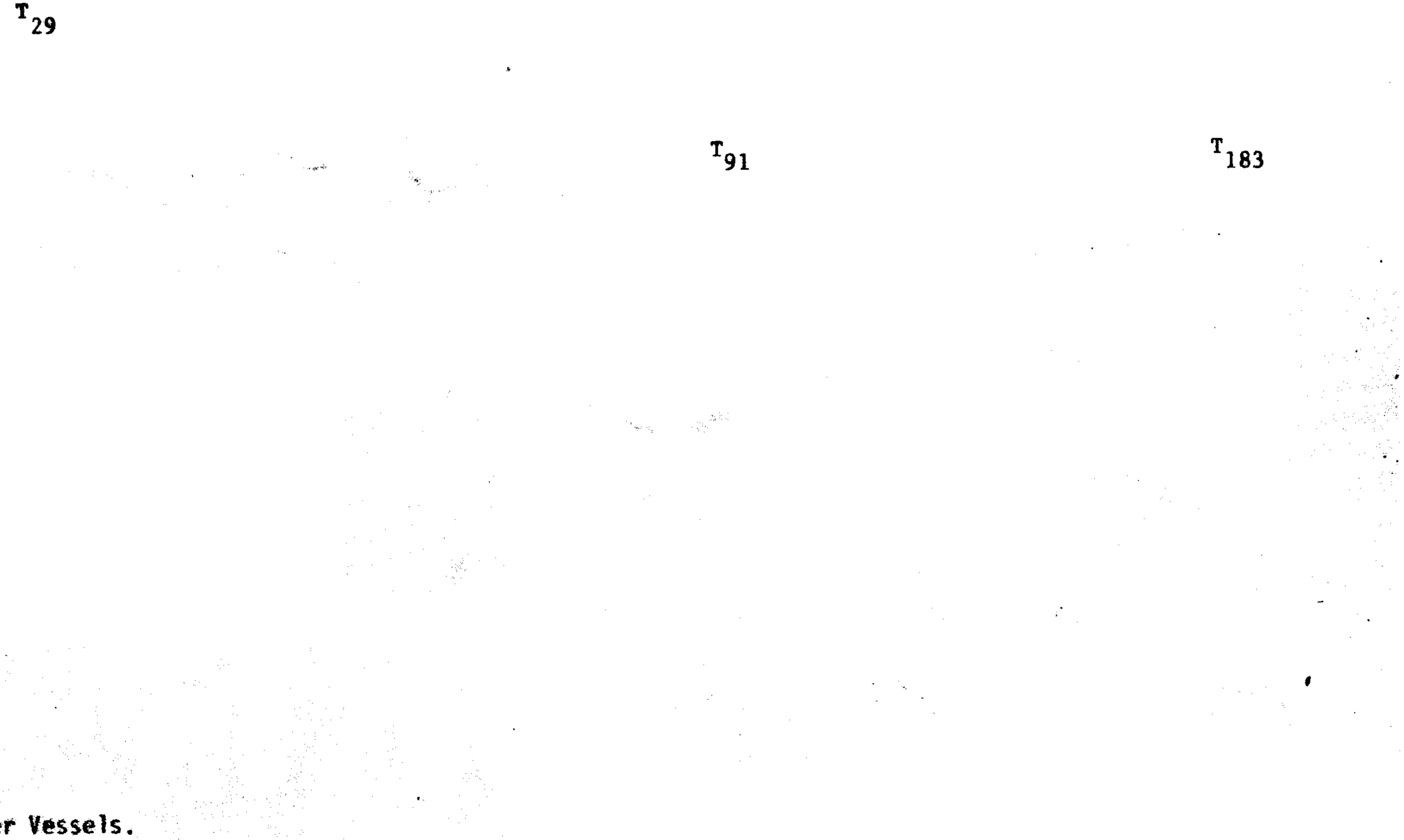

Plate 2. Other Vessels.

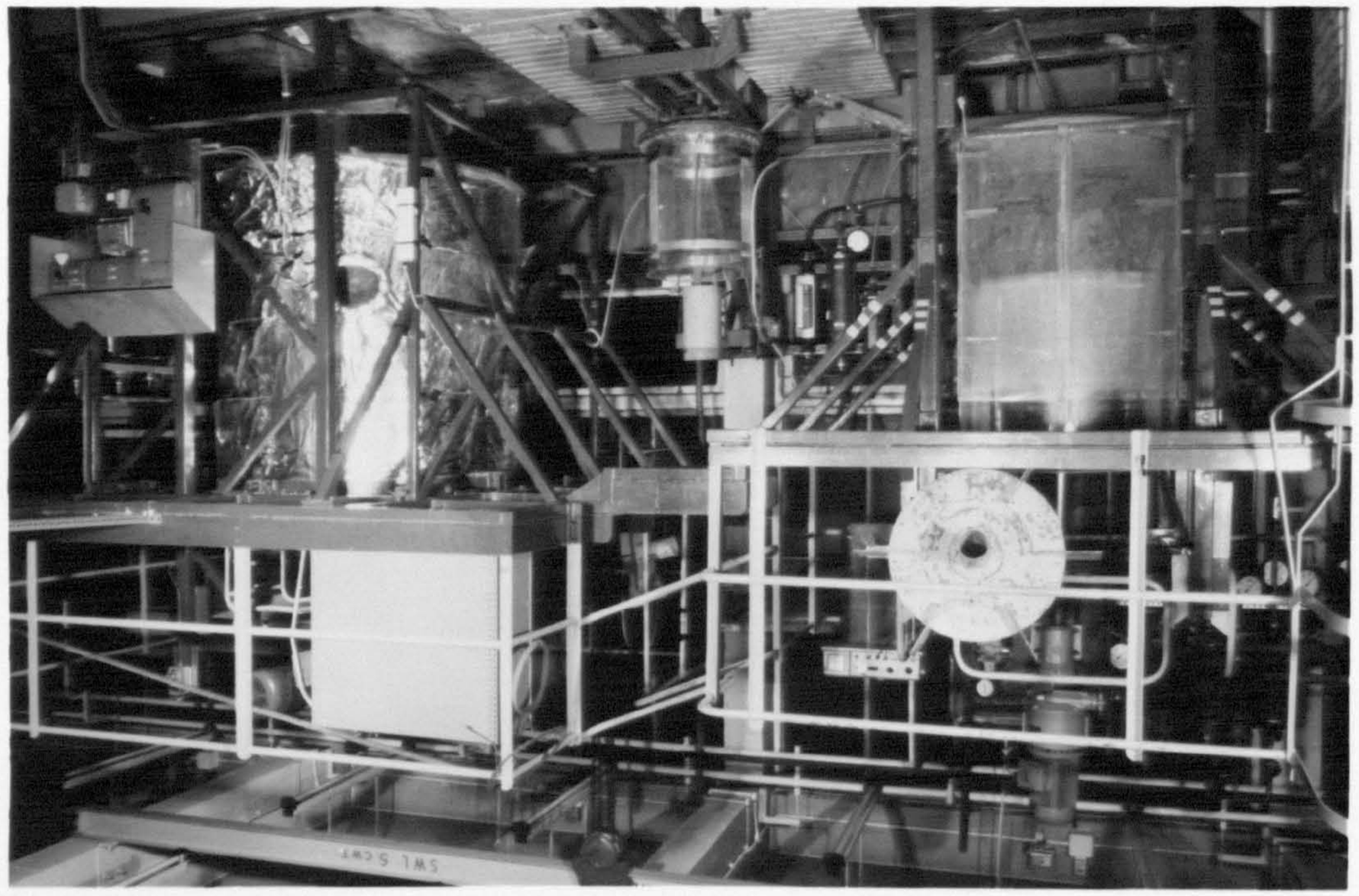

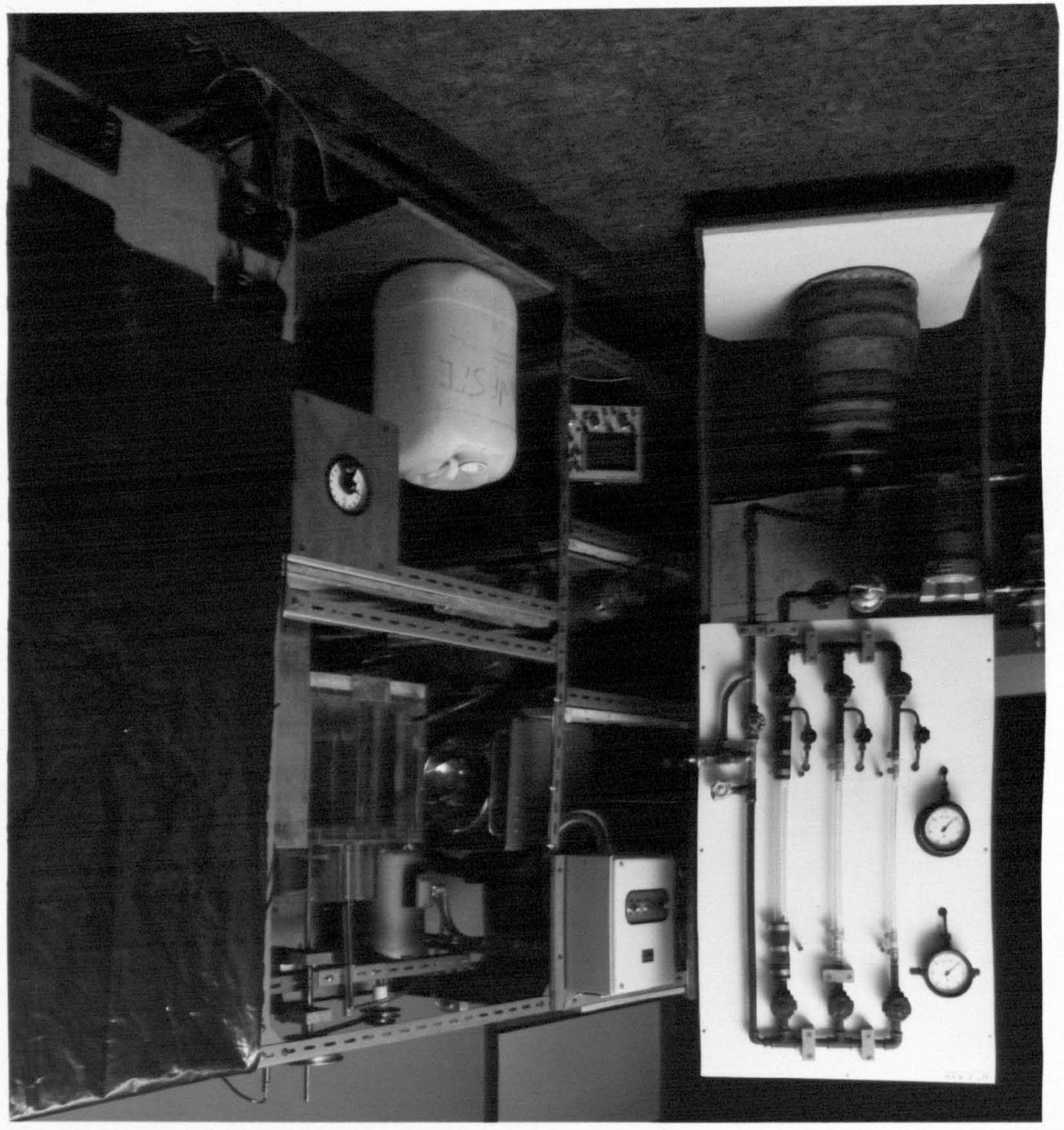

T29

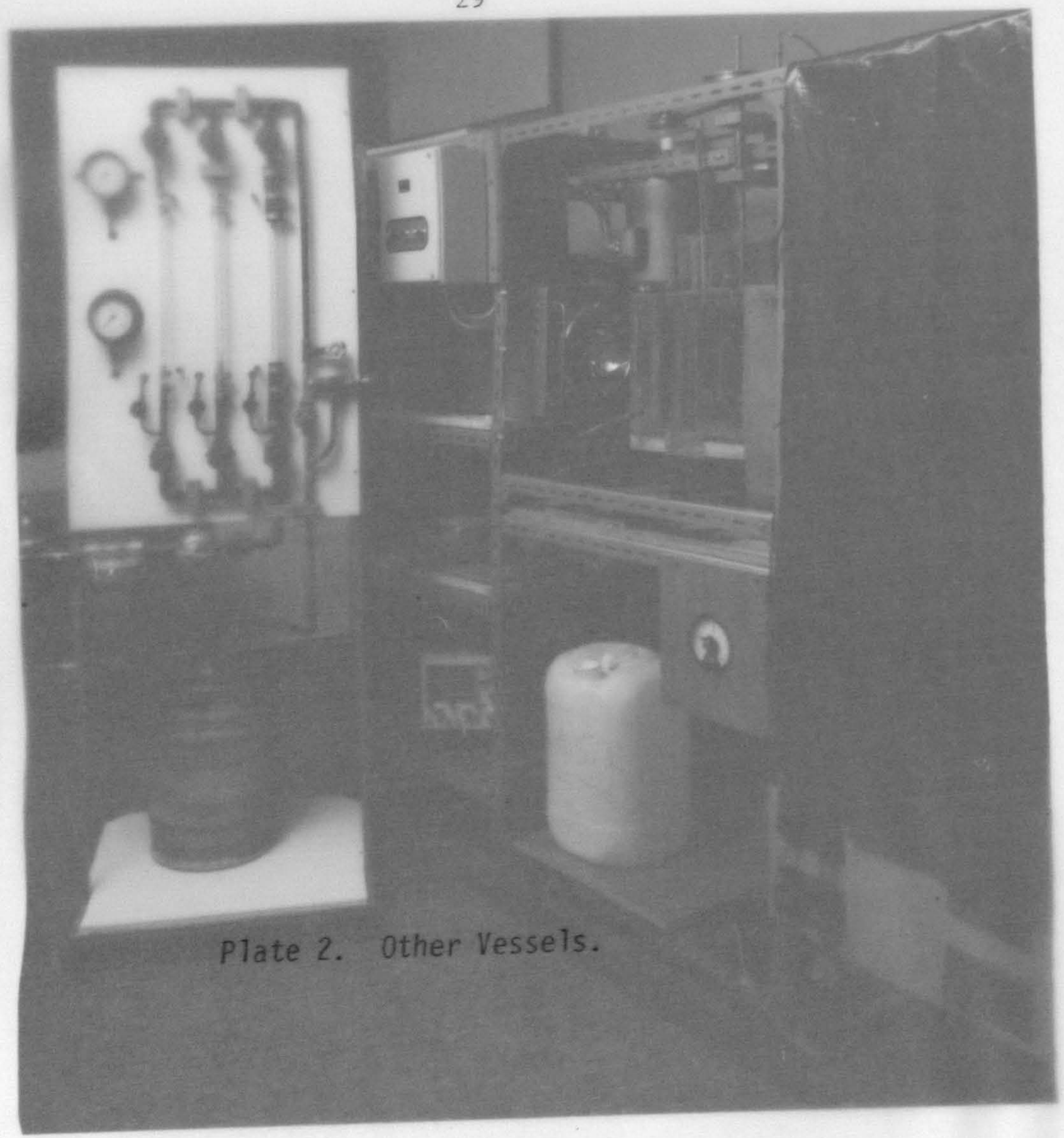

Plate 2. Other Vessels.

T91

T183

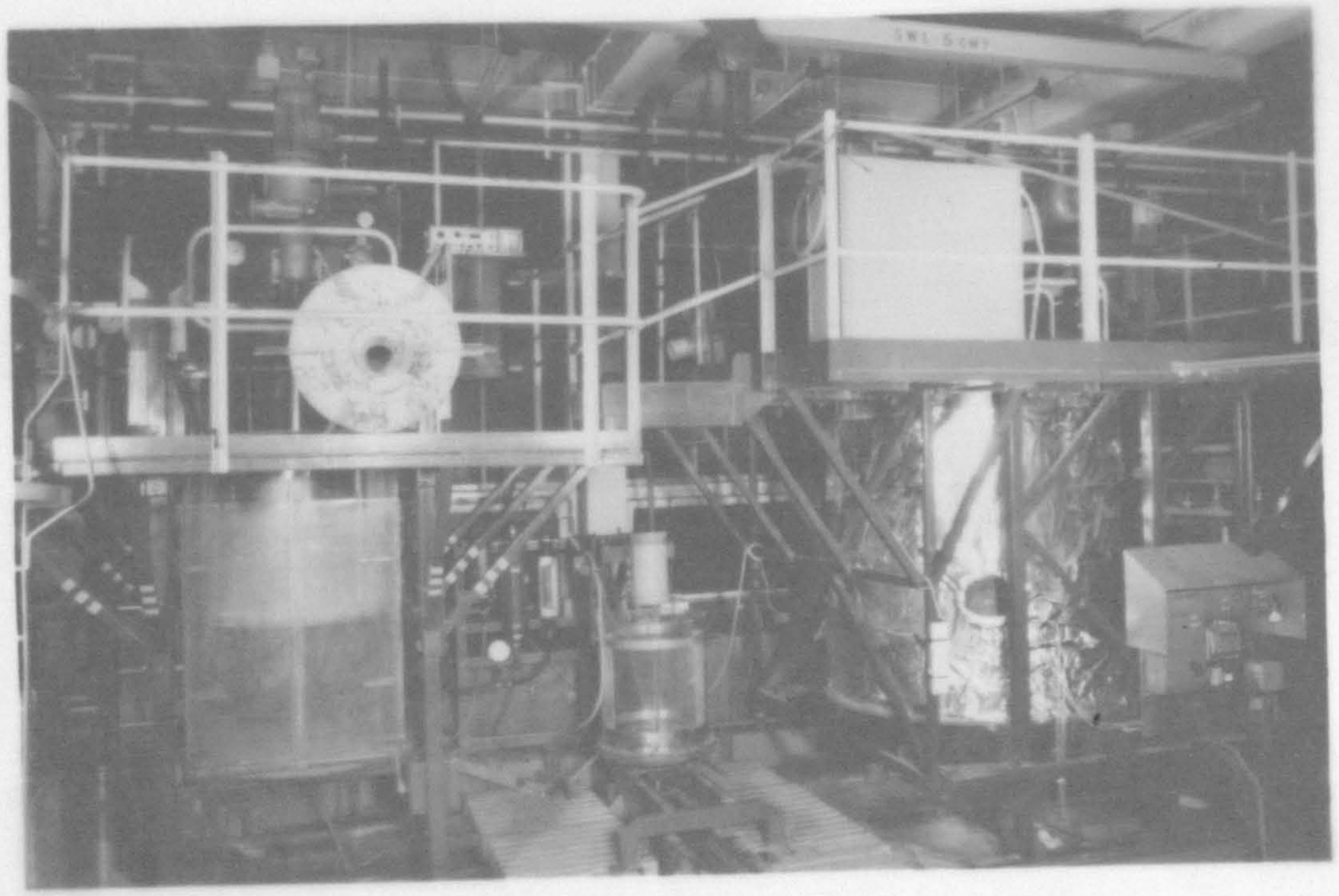

section tank to allow distortion free viewing, which was also possible through the flat Perspex base. Water was circulated between the jacket and vessel which enabled the vessel contents to be controlled at 25^{o} C $\pm$ 1^{o} C. This was achieved by means of two temperature sensors in the vessel linked to an external heating-cooling circuit controlled by solenoid valves and a Fielden temperature controller. The motor which drove the impellers was a NECO 0.75 horsepower (560 Watts) direct current electric motor. The output shaft from the motor either drove the impeller directly or passed via a flexible coupling to a fixed ratio gearbox mounted below the motor by a bracket. Two gearboxes were used, of 6.49 and 2.85 to 1 reductions, allowing a wide range of torques and speeds to be applied to the system. The complete motor and gearbox assembly was suspended via a flange from a journal and thrust plate air bearing (Plate 1) which allowed the torque reacting on the assembly to be measured by a Datasense 100 (Transducers (C.E.L.) Ltd.) load cell. The length of the shaft necessitated a Teflon support bearing on the base of the vessel, which also acted as the gas sparger via three slots in the bearing around the base of the shaft. Careful checks on the power consumption showed that frictional losses caused by the bearing were negligible, even when particles were present in the system. However, care was taken to ensure that either air or water was always being flushed through the bearing in the presence of solids. The gas supply to the vessel was compressed air which passed through a humidifier before its flowrate was measured by calibrated gas rotameters.

The maximum gas flow through the bearing was approximately 2.9×10^{-3} $m^3 s^{-1}$ (1.25 vvm). The maximum impeller speed attainable was about 16 rps but depended on impeller size, gearbox reduction and gas rate. The speed was measured via an electrical tachometer which

	T_{29}	T_{30}	T_{56}	T_{91}	T_{183}
Diameter (T), m	0.29	0.30	0.56	0.91	1.83
Liquid height (H), m	0.29	0.30	0.56	0.91	1.68
Volume (V_L), m^3	0.0192	0.0212	0.138	0.592	4.41
Baffle width, %	10	10	10	10	10
Sparger	Pipe Point Source	Pipe Point Source	Three point Bottom bearing source	Pipe Point Source	Pipe Point Source
Temperature Control	Water Jacket	None	Water Jacket	None	None
Material of Construction	Perspex and Glass	Perspex	Perspex	Perspex	Polypropylene with Perspex windows
Geometry	Cylindrical with flat base				
Viewing	Through sides and base				Via windows in side and base

Table 2.1 Vessels Employed in this Study

used an electromagnetic sensor to detect the rotation of a 60 tooth cog wheel attached to the shaft just below the motor. Accuracy of within $\pm$ 1% was possible with this system. Impeller power was estimated from the impeller speed and torque by Eqn. 2.1:-

$$P = 2\pi \times \text{Impeller Torque} \times N \qquad 2.1$$

Although torque fluctuations increased with increasing speed, power measurements were reproducible to within $\pm$ 6%.

The smallest tank (T_{29}) was of similar construction to T_{56}. Speed measurements were made with a Smith's handheld tachometer. However, in this case, torque measurements were obtained by measuring the angular deflection of the tank against a calibrated spring with the whole vessel located on an air bearing[4]. The gas was introduced via a single point pipe sparger, as it was for T_{30}, T_{91} and T_{183} also. Similarly, the impeller shaft terminated at the impeller for all the tanks except T_{56}. T_{30} was essentially similar to T_{29} except that it had no external jacket and operated at ambient temperature. The methods used to obtain speed and power measurements were identical to those used for T_{29}. The object of using two tanks of such similar dimensions was simply to check reproducibility and ensure any scale effects were genuine.

The 0.91 m diameter tank had no temperature controlling water jacket but one quadrant was encased by Perspex and the resulting volume filled with water to allow accurate viewing. Torque measurements were obtained by strain gauges on the shaft but otherwise the tank was similar to the others.

The largest vessel, T_{183}, was fabricated from Polypropylene and was the only vessel with limited viewing of the sides and base. Perspex portholes in the centre of the base and at various locations in the walls enabled restricted visual observations to be made. Torque measurements were made by estimating the deflection of the

motor and gearbox assembly mounted on ball bearings against a calibrated spring, giving a reproducibility of approximately $\pm$ 10%. The liquid level in T_{183} was 1.68 m ($H = 11 \frac{T}{12}$) due to the limited height of the vessel.

2.3. The Impellers

A range of impeller sizes was used in this work, though generally they were either one half, one third or one quarter of the appropriate tank diameter. When the effect of varying impeller diameter was not being investigated directly, a large part of the work was carried out with D = T/2 impellers since larger impellers have been shown to be the most energy efficient for both solid suspension and gas dispersion duties in their respective two phase systems.[2,5]

Besides the standard six-bladed disc turbine (DT) shown in Fig. 2.1, impellers with other blade geometries were used. Those employed in T_{56} are shown in Plate 3 and detailed in Table 2.2. Table 2.3 gives details of the impellers used in all the other tanks.

2.4. Liquids and Particles

De-ionised water was used during virtually all experiments carried out in T_{29} and T_{56}. It was regularly replaced to ensure consistent bubble coalescence behaviour. The other vessels used tap water due to the excessive quantities required to fill them.

The effect of increasing liquid viscosity was briefly examined (Chapters 4 and 6) using various concentrations of sugar solution in T_{29}. Viscosity measurements were made with a Deer Rheometer.

Table 2.4 presents details of the particles used in this study in order of increasing particle density. A range of density differences ($\rho_S - \rho_L$) between 50 Kgm^{-3} and 1900 Kgm^{-3} was examined. The Surface to Volume (Sauter) mean diameter of the particles was calculated where possible from the results of a sieve analysis. The exceptions to this procedure were: firstly the Dowex ion exchange resin beads

D-T/4 DT

D-T/3 DT

D-T/2 DT

D-T/4 4MFD

D-T/4 6MFD

D-T/2 4MFD

D-T/2 ADT

D-T/2 AFD

D-T/2 4MFU

Plate 3. Impellers used in T_{56}

Anthracite

Sand

Glass Powder

Plate 4. Non-Spherical Particles.

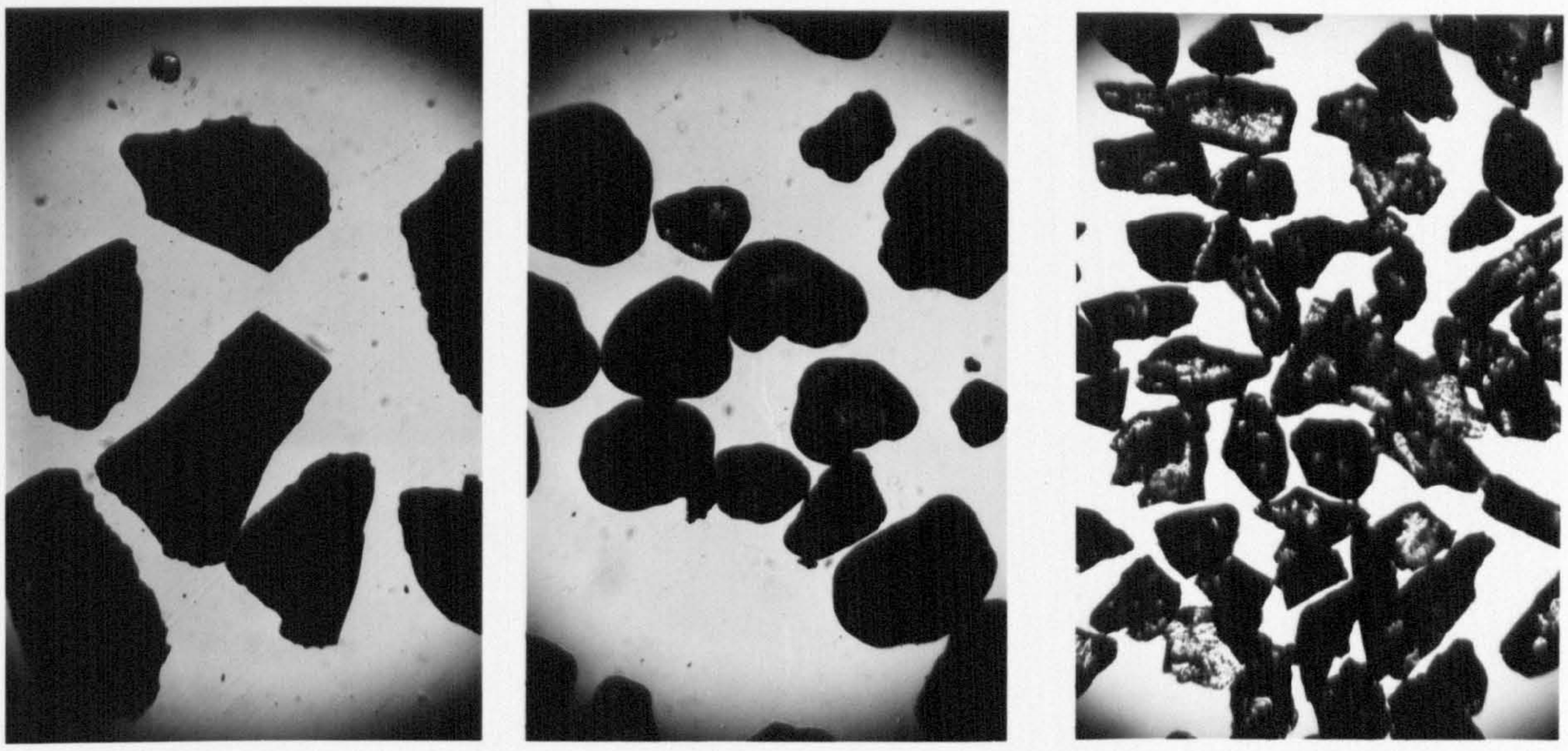

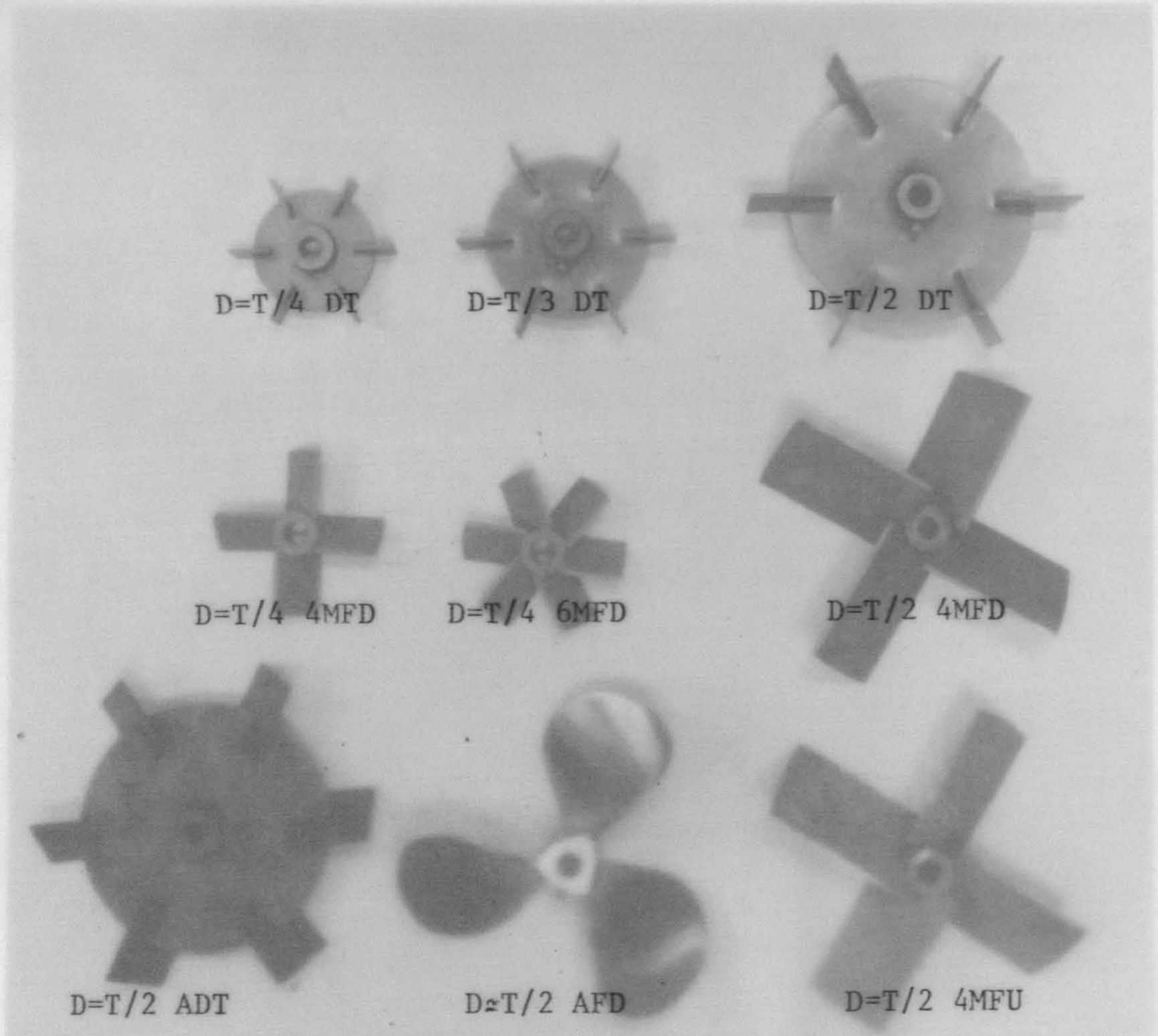

Plate 3. Impellers used in T_{56}

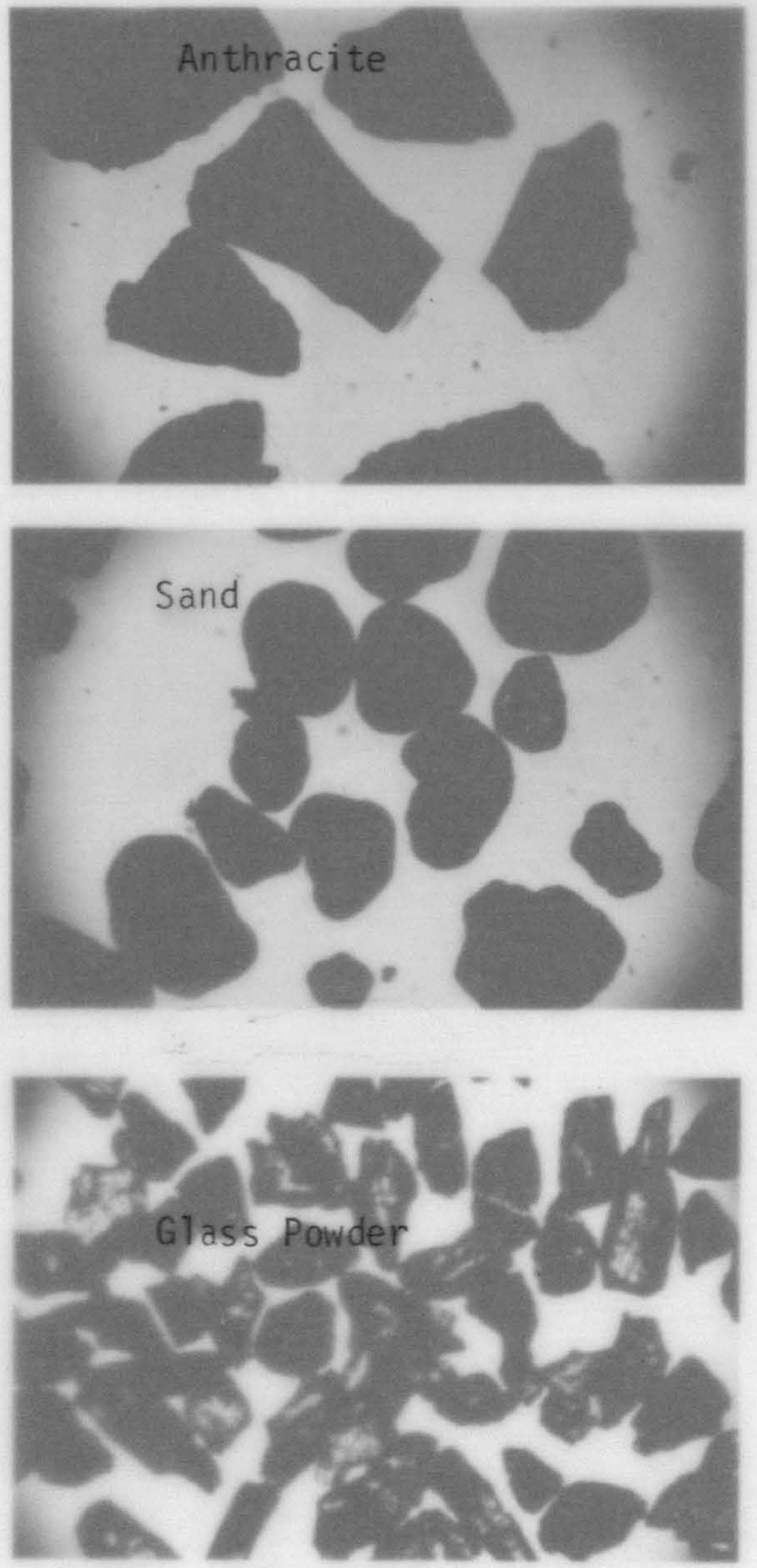

Plate 4. Non-Spherical Particles.

Type - see Plate 3	Notation	No. of blades	Diameters (D) m	Vertical height of blade, m	Horizontal height of blade, m	Blade and Disc thickness, mm	Angle or Pitch of blade
Disc Turbine	DT	6	0.14	D/5	D/4	3.2	-
			0.187	D/5	D/4	3.2	-
			0.28	D/5	D/4	3.2	-
Angled Blade Disc Turbine	ADT	6	0.28	0.039	D/4	2.5	45^{o}
Mixed Flow Impeller Pumping Up	4 MFU	4	0.28	D/5	0.120	3.2	45^{o}
Mixed Flow Impeller Pumping Up	4 MFD	4	0.14	D/5	0.050	3.2	45^{o}
			0.28	D/5	0.120	3.2	45^{o}
Mixed Flow Impeller Pumping Down	6 MFD	6	0.14	D/5	0.050	3.2	45^{o}
Marine Propeller	AFD	3	0.29	Not constant - see Plate 3			1.5 D

Table 2.2 Impellers Used in T_{56}

Tank	Notation	No. of blades	Diameter m	Vertical height of blade m	Horizontal height of blade m	Blade and Disc thickness, mm	Angle or Pitch of blade
T_{29}	DT	6	0.145	D/5	D/4	3.2	-
	4 MFD	4	0.145	0.029	0.055	3.2	45^o
	4 MFD	4	0.072	0.015	0.025	1.6	45^o
T_{30}	DT	6	0.15	D/5	D/4	2.0	-
T_{91}	DT	6	0.457	D/5	D/4	4.8 disc 6.35 blade	-
	4 MFD	4	0.457	0.0984	0.159	6.35*	45^o
T_{183}	DT	6	0.902	0.175	D/4	6.35 disc 9.5 blade	-
	4 MFD	4	0.794	0.165	0.349	9.5	45^o

* The central horizontal portion of each blade was double this thickness

Table 2.3 Impellers Used in Other Tanks

Particles	Shape	Size Range μm	Surface to Volume Mean Size (d_p) μm	Density (ρ_s) Kgm^{-3}
Polystyrene	spherical	250 - 355	302	1050
Diakon	spherical	420 - 710	583	1200
Dowex Ion Exchange Resin	spherical	500 ± 100	-	1250
Anthracite	flat and irregular (sphericity ≃ 0.4 - 0.5)	500 - 600	-	1400
Glass Powder	Granular (sphericity ≃ 0.7)	250 - 355	309	2200
Soda Glass Ballotini	spherical	180 - 250	206	2480
Sand	Granular (sphericity ≃ 0.9)	300 - 710	470	2650
Lead Glass Ballotini	spherical	80 - 105	-	2900
		440 - 530	-	2900
		850 - 1000	-	2900
		2500 - 2800	-	2900

Table 2.4 Particles Employed in this Study

which were examined under a microscope fitted with a graticule as they were unsuitable for sieving, and secondly the lead glass Ballotini whichwere obtained very closely sieved and thus no further analysis was undertaken. The shape of the anthracite was such that only an approximate size range was obtained. The particle size distributions were made up from the closely sieved lead glass Ballotini fractions.

The size ranges quoted in Table 2.4 are such that a minimum of 90% of the particles fall within that range. The large quantities of sand used, especially in T_{183}, made sieving to obtain a closer size fraction impracticable. Plate 4 shows the non-spherical anthracite, sand and glass powder particles. The sand had a sphericity (surface area of sphere with the same volume as the particle,divided by the surface area of the particle) of approximately 0.9 whereas the sphericity of the glass powder was around 0.7 and the anthracite 0.4 to 0.5.

2.5. Holdup Measurements

Gas holdup, ε, was evaluated by observing the rise in level of the dispersion surface under aerated conditions and dividing this rise in level by the total aerated height of the dispersion. A point midway between two baffles was chosen as the measuring position since surface level varied across the tank, particularly near the baffles. The low values of holdup obtained in air-water systems combined with the fluctuations in level of the dispersion surface led to measurements only being reproducible to within $\pm$ 15 to 20% for the mixed flow impellers which tended to cause the more violent surface fluctuations (particularly the 4 MFU). The disc turbine results were reproducible to within $\pm$ 10%.

2.6. Other Techniques Employed in This Thesis

Two basic techniques are presented for characterizing particle suspension. The first involved visual observation of the vessel base

and assessment of the impeller speed, N_{JS}, at which the last particle remained at rest on the base for less than one to two seconds. The second was a less subjective method and involved measuring a maximum in particle concentration sampled from a point near the vessel base by either separating and weighing the particles or monitoring the amount of light scattered by the particles in the sample stream. These techniques are described in detail in Chapters 4 and 5.

Fast response oxygen electrodes were used to measure the oxygen concentration in both the liquid phase and the gas phase in order to determine mass transfer coefficients. Details of this method are presented in Chapter 8.

CHAPTER 3.

GAS-LIQUID SYSTEMS

3.1. Introduction

The dispersion of gas in a liquid by mechanical agitation has been the subject of numerous investigations. One of the most popular agitators used in these studies has been the six-bladed disc turbine, since the disc forces all the inflowing gas to pass through the high shear impeller region, ensuring efficient break up of the gas stream into bubbles and effective dispersion of the bubbles throughout the vessel. The disc turbine and other radial flow impellers have also been used in particle suspension studies[6] and shown to be less energy-effective than axial and mixed flow impellers such as the marine propeller and angled blade impellers.

In order to define a satisfactorily mixed three phase system, clear definitions of adequately mixed gas-liquid and particle-liquid systems must first be established. The purpose of this chapter is to characterize the gas-liquid mixing requirements and how they affect the potential of the system to suspend solids, particularly for axial and mixed flow impellers which have received little attention in the literature. This will be achieved by combining visual observations with impeller power and gas holdup measurements.

3.2. Literature Survey

3.2.1. Power Consumption

Over the past ten to fifteen years, much work has been done to explain the variation of impeller power consumption with impeller speed and gas rate in gas-liquid dispersions. The bulk of this work has been carried out using six-bladed disc turbine impellers and has led to an understanding of the existence of, and the role played by, gas filled cavities which cling to the back of the turbine blades. Rennie and Valentin[7] showed evidence of gas collection in the low

pressure regions behind the blades in 1968. Subsequently Nienow and Wisdom[8] and Van't Riet and Smith[9] have demonstrated how the nature and size of the cavities change with gas rate and impeller speed. Fig. 3.1 shows the three types of cavity observed at various speeds by Nienow and Wisdom for a given gas rate. At low speeds a large cavity covered the whole rear face of the blade (Fig. 3.1a). As speed increased so the cavity shape modified itself to fit the shape of the trailing vortex (Fig. 3.1b) and at still higher speeds the breakaway points moved inwards along the blade (Fig. 3.1c) forming vortex cavities. From this work has emerged an understanding of the manner in which gassed power changes with the hydrodynamic conditions in the impeller region.

Gassed power data are commonly presented in two ways, both of which are basically gassed power number (Po_g) plotted against flow number (Fl). Fig. 3.2a shows the effect of increasing gas rate at constant impeller speed, and Fig. 3.2b the effect of increasing impeller speed at constant gas rate. Considering firstly Fig. 3.2a: since impeller speed is constant, then plotting the gassed power number will also represent the variation of the gassed power and the ratio of gassed power to ungassed power, for a particular system.

i.e. $$Po_g = \frac{P_g}{\rho N^3 D^5} = Po.\frac{P_g}{P} \propto P_g \qquad 3.1$$

and since Po is constant in turbulent systems then Fig. 3.2a represents the response of Po_g, P_g and P_g/P to gas rate variations (N constant $\Rightarrow Q/ND^3 \propto Q$). As a small amount of gas is admitted to the system it migrates to the low pressure regions forming vortex cavities behind the impeller blades and therefore increasing the pressure in this area. The consequence of this is a reduced pressure difference over the blade and a slight drop in drag and power consumption. Bruijn et al.[10] suggest that as gas rate is further raised,

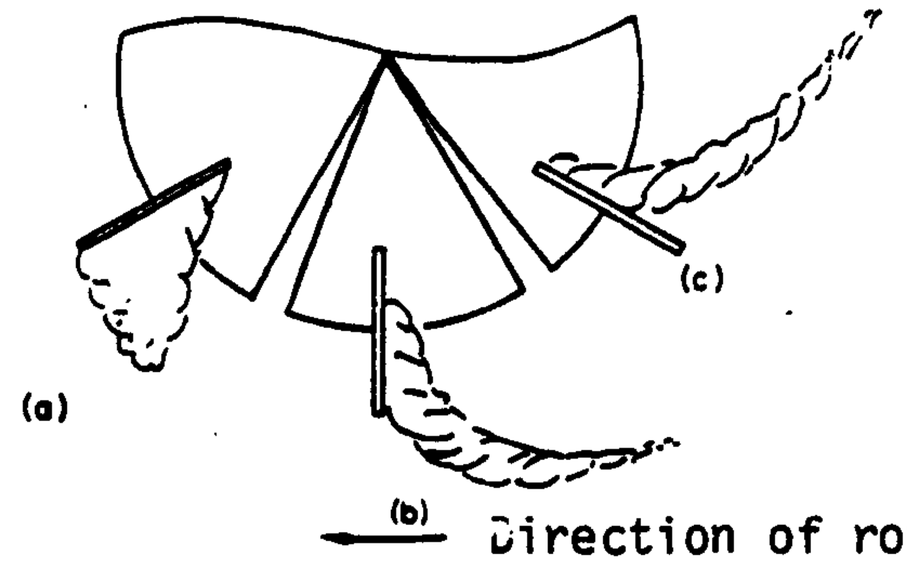

Fig. 3.1[8] Changing Cavity Shape (DT)

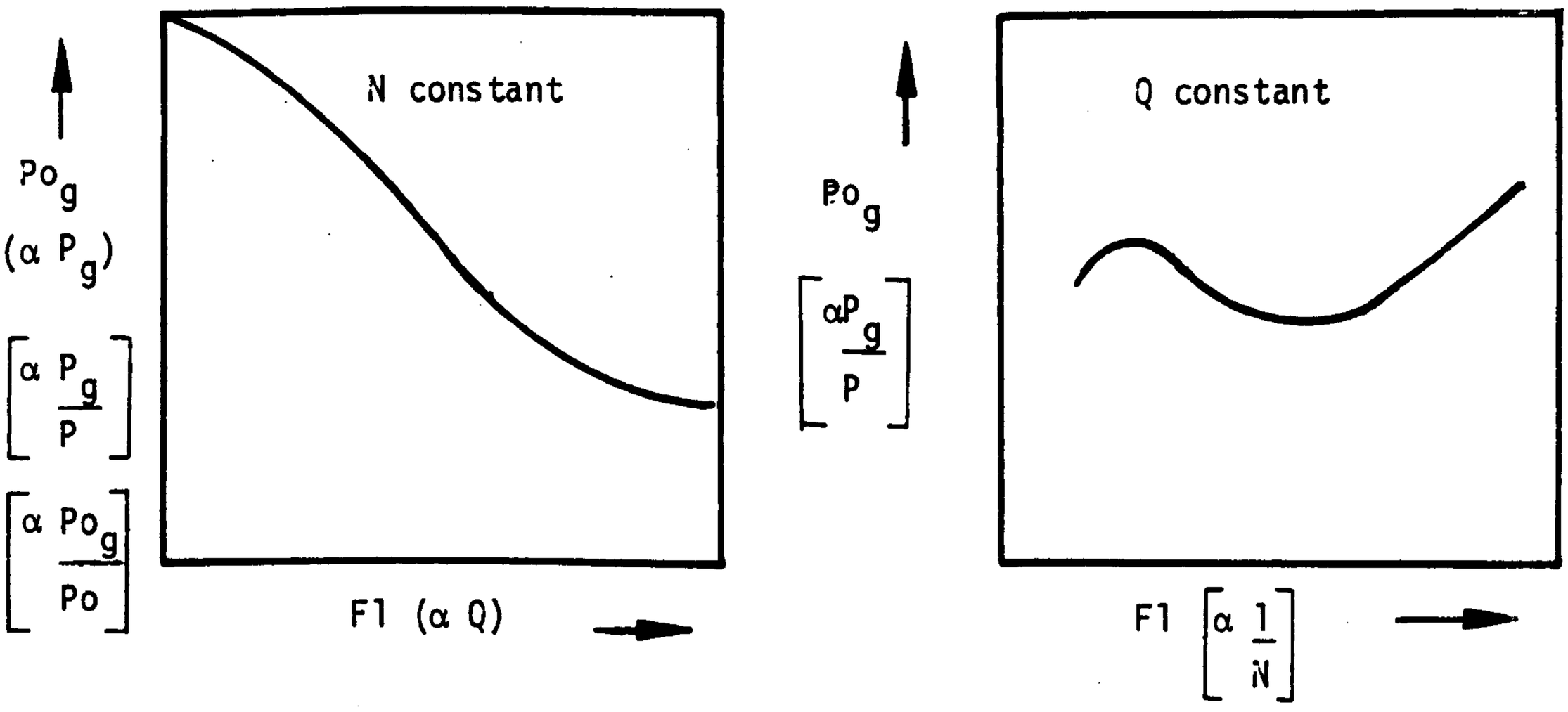

Fig. 3.2 Power Number (Po_g) versus Flow Number (F1) for (a) Constant Impeller Speed and (b) Constant Gas Rate (DT)

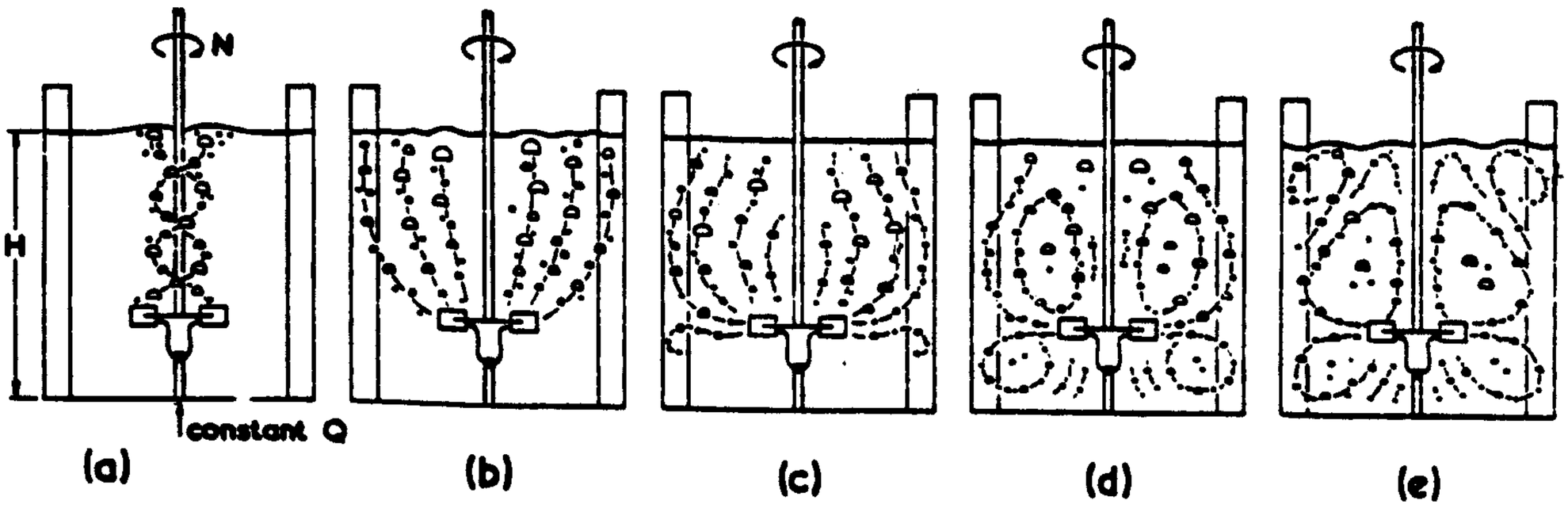

Fig. 3.3[5] Bulk Flow patterns with increasing speed, N for a disc turbine

an increasing number of large cavities form, streamlining the impeller and further reducing drag. Eventually all six cavities reach a maximum size and the impeller pumping capacity is reduced to a minimum. Warmoeskerken et al.[11] have proposed that three large cavities form simultaneously, causing a definite drop in the power consumption at a given gas rate, after which any further decrease can be explained by the reduction in the mean density of the pumped fluid. Oyama et al.[12] suggested that the rate of decrease of power number at a given gas rate (or flow number) described the gas dispersion ability of the impeller. Thus as the power number drops rapidly due to an increase in the quantity of gas in the impeller region, the pumping rate and dispersion capability of the impeller also drop suddenly.

Fig. 3.2b has been interpreted by Nienow et al.[5] Again the gassed power number is equivalent to a constant multiplied by the ratio P_g/P if Po is considered to be constant in the turbulent region, independent of Reynolds number. However Po_g is not proportional to P_g alone since impeller speed is changing at constant gas rate. In this case the flow number is inversely proportional to impeller speed. At low speeds the tips of the bladesare surrounded by liquid and the power number remains high because of the presence of two low pressure vortices at the back of each blade.[8] As impeller speed is increased, a large cavity forms over the upper half of the blade causing a reduction in Po_g. At a slightly higher speed the cavity covers the whole of the back face of the blade and a minimum occurs in the gassed power number. Further increases in speed cause a rise in the power number as the size and number of large cavities fall[10] and their shape tends towards those of vortex cavities (Fig. 3.1) so that less of the rear of the blade is blanketed by gas. At high enough impeller speeds, recirculation of gas to the impeller becomes significant and the power number drops slightly again.[5,13] The

impellerspeed required to achieve the resulting maximum is commonly designated N_R.[5]

To summarize, the power consumption of a disc turbine impeller can be quite satisfactorily explained by existing data on the gas-liquid hydrodynamics in the impeller region. However, this level of understanding does not exist for other types of impeller.

Brauer and Schmidt-Traub[14] proposed two mechanisms by which a downward pumping propeller dispersed gas. At low sparge rates the bubbles formed simply by the action of the downward liquid flow over the gas entry pipe, and were thence distributed about the vessel. At higher gas loadings the buoyancy of the gas overcame the liquid downflow and a "bell-shaped gas cushion" formed below the hub of the propeller. Bubbles were sheared off from this cushion by the liquid downflow and dispersed, some travelling into the impeller itself and forming a cavity which clung to the rear of the blade. Unfortunately, although the authors measured power consumption, the only reference made to the results was that the ratio of gassed to ungassed power did not fall below 0.6, compared to about 0.3 to 0.5 for a disc turbine. No attempt was made to present and interpret the power measurements in the light of the above observations.

3.2.2. Flow Patterns and Minimum Mixing Requirements

Fig. 3.3 shows the bulk mixing stages that were observed by Wisdom[3] when the impeller speed was increased for a particular gas rate. These stages are detailed below:-

(a) Negligible dispersion.

(b) Upper part of vessel acting as bubble column.

(c) Gas circulation in the upper part of the vessel with occasional movement in the lower region.

(d) Gas circulating throughout the whole vessel.

(e) Secondary loops form.

Nienow and Wisdom[15] defined the transition between (d) and (c)

as the onset of flooding, and used this transition as the minimum requirement for bulk gas mixing. Thus the gas phase was considered adequately mixed provided the impeller speed was greater than that required to just disperse the gas throughout the whole vessel. Rushton and Bimbenet[16] defined the flooding point as the transition between Figs. 3.3c and 3.3b. However, this implies that the lower portion of the vessel contains no gas and is therefore being unproductive. Westerterp et al.[17] have also defined a minimum rate of agitation based on interfacial area measurements but this has the disadvantage of being more complicated to detect. The definition of the flooding point as defined by Nienow has the advantage that it corresponds closely with the minimum in the Po_g versus Fl plot (Fig.3.2b).[5]

From the above it can be seen that the definition of the flooding point is still not well established. Nienow's interpretation of the flooding point has recently been defined[18] as N_{CD}, which is the condition investigated throughout this work.

3.3. Equipment and Experiments

The bulk of the work presented in this chapter was carried out in T_{56} using impellers of diameter 0.28 m at a clearance of 0.14 m from the base. The exceptions to this were firstly the disc turbine, which has been well characterized at this clearance (i.e. T/4, Section 3.2) but not at lower clearances where there is evidence of enhanced particle suspension capability.[2] Thus a clearance of 0.093 m (T/6) was examined for various diameter impellers. The second exception was the MFD impellers, which are commonly used in industry, where the influence of impeller diameter and number of blades was also investigated. Some additional data from other size tanks have been included as necessary.

The experiments were generally performed by observing the flow patterns, using the bubbles and sometimes tracer particles as aids,

for various fixed gas rates over a wide range of impeller speeds. The speed at which the gas was completely dispersed, N_{CD}, was assessed and linked to power and holdup measurements,obtained as described in Chapter 2.

3.4. Results: Comparison of V_S and vvm

Gas rates are commonly scaled as either superficial velocities based on the tank cross sectional area, or specific velocities based on the tank volume. The latter is usually referenced to a minute rather than a second as the resulting rate of 1 vvm is a common industrial operating value.

When comparing the impeller speed and power required to perform a given duty over a wide scale range, it would be preferable for the power number of the impeller to be independent of scale. With this objective, the power number data for a disc turbine impeller of diameter T/2 in T_{30}, T_{56} and T_{91} were examined. The data for T_{29} and T_{183} were ignored since variations in the minor dimensions of the impeller caused the ungassed power numbers in the systems to differ (Table 4.7). Table 3.1 shows the gassed power number evaluated by taking the mean of the value at the minimum and peak in a Fig. 3.2b type plot of each tank size.

Gas Rate	Po or Po_g		
	T_{30}	T_{56}	T_{91}
0	5.9	6.0	6.1
0.5 vvm	4.8	4.4	4.6
1.0 vvm	3.2	3.1	3.2
$5x10^{-3}$ ms^{-1}	3.2	4.4	5.2
10^{-2} ms^{-1}	-	3.1	4.2

(a) Disc Turbine c = T/4, D = T/2

Gas Rate	Po or Po_g	
	T_{56}	T_{91}
0	5.3	5.2
0.5 vvm	4.0	4.2
1.0 vvm	3.15	3.2
$5x10^{-3}$ ms^{-1}	3.85	4.5
10^{-2} ms^{-1}	3.1	3.8

(b) c = T/6 Disc Turbine D = T/2

Table 3.1 Effect of Scale Up Criterion on Po_g

These data show Po_g to be relatively independent of tank size if gas rate is scaled in terms of tank volumes, compared to a strong dependence on scale if superficial velocities are kept constant. Thus vvm were chosen for scaling gas rates as they seemed to give a more sensible basis for comparison of speeds and powers on scale up.

3.5. Results: Comparison of Impellers

Bearing in mind the significance of Figs. 3.2a and 3.2b, each will be used to demonstrate different concepts. The initial parts (3.5.1 - 3.5.4) of this section describe the mode of gas dispersion by the various impellers. These observations were obtained by fixing a value of the gas rate and varying the impeller speed to cover the full range of hydrodynamic conditions, thus the power measurements are presented in the same manner (as in Fig. 3.2b). An attempt is made to interpret the resulting plots in terms of the observed dispersion characteristics.

The effect of gas rate on the capability of an impeller to circulate and impart energy to the dispersion at a constant impeller speed is reflected in the decrease in the ratio P_g/P (and therefore Po_g). This is shown by data presented as in Fig. 3.2a and a comparison is drawn between the impellers in Section 3.5.8.

The minimum conditions for gas dispersion are compared in Section 3.5.6 and holdup compared in Section 3.5.7.

3.5.1. Four-bladed Mixed Flow Impeller Pumping Up (4 MFU)

The impeller discharge stream and gas sparge were co-current in this system and consequently at low impeller speeds the impeller pumping action aided the buoyancy of the gas and caused it to bubble straight up through the impeller region with little or no dispersion (Fig. 3.4a). The forces due to the radial component of velocity in the impeller discharge stream became significant at higher speeds in comparison with the bubble buoyancy and therefore a portion of the gas would be dispersed to the walls before rising to the surface (Fig. 3.4b). Higher speeds caused the locus of bubble movement to resemble the vortex in the free liquid surface of an unbaffled tank operating at high impeller speeds, yet the region below the impeller remained virtually devoid of bubbles. Further increases in speed resulted in the gas being just dispersed below the impeller as the bubbles followed the flow loops depicted in Fig. 3.4c. Still higher speeds caused bubble velocities within the loop to increase and eventually the loops themselves to oscillate vigorously up and down the lower regions of the tank (Fig. 3.4d). However, the upper portion of the vessel often remained relatively quiescent. It was not possible to detect any cavity formation by simple visual observation. Nevertheless, the gassed power data plotted as gassed power number against flow number for three gas rates (Fig. 3.5) can be interpreted from the bulk mixing patterns observed.

The effect ofsparging gas into the base of the vessel is to cause liquid circulation. Thus at very low impeller speeds the gas induced liquid flow aids impeller rotation, since the impeller pumps in the same direction, thereby producing a lower power number than expected. However, as speed is increased, the contribution of this

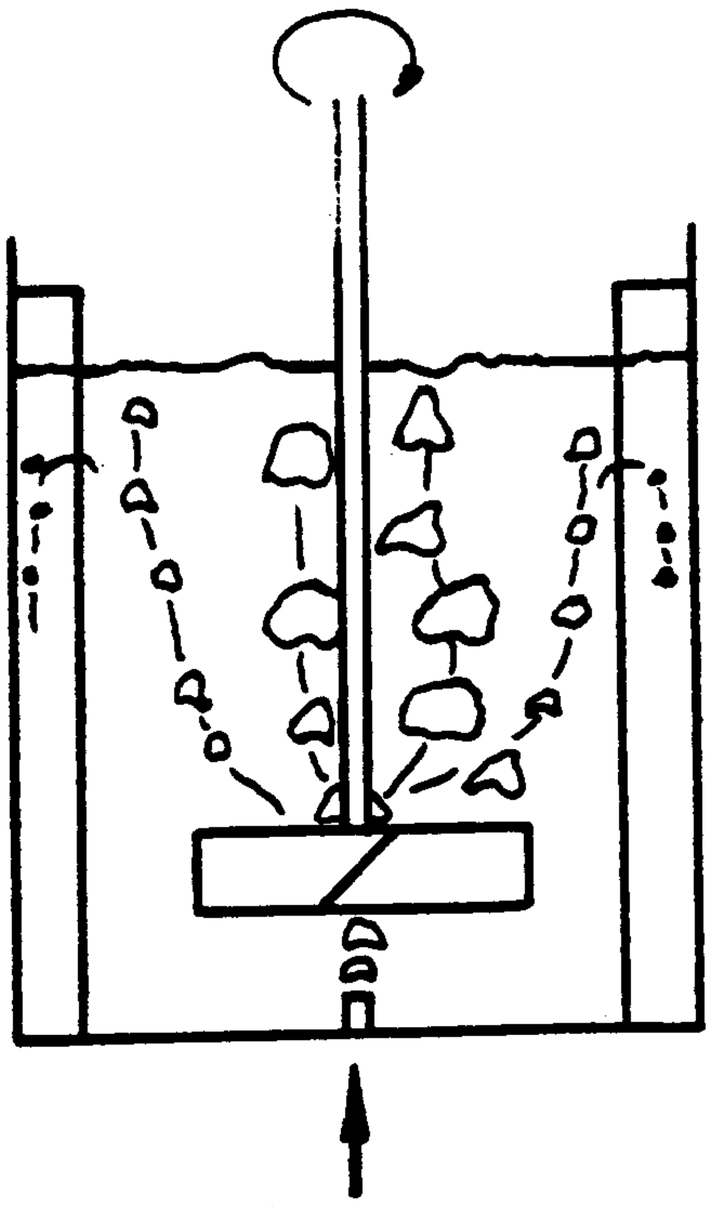

(a)

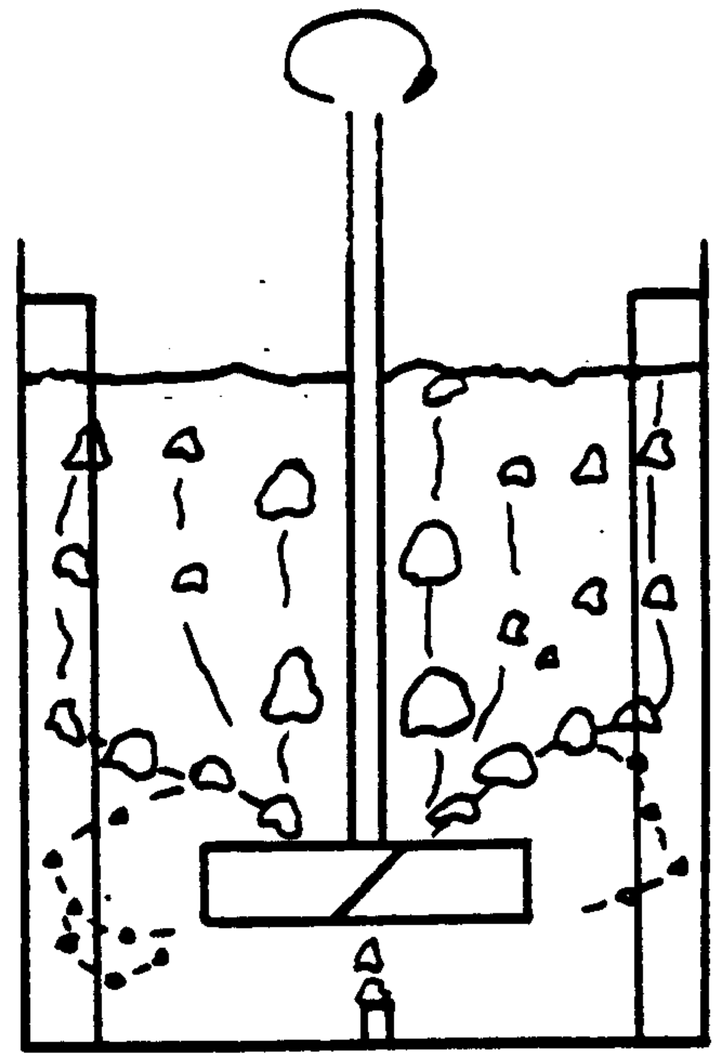

(b)

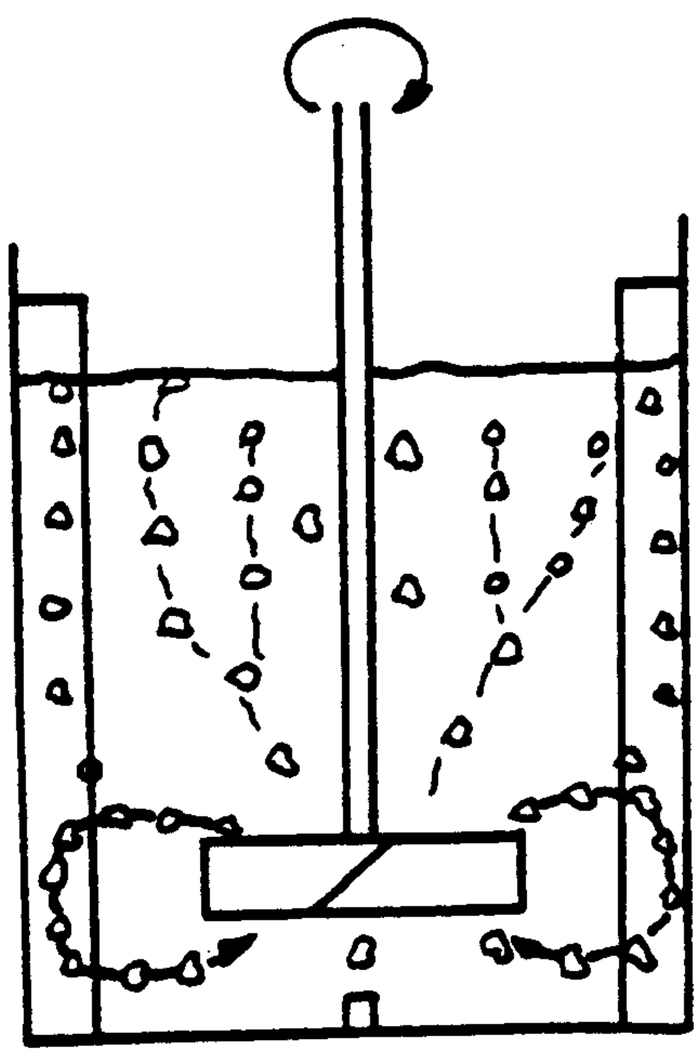

(c)

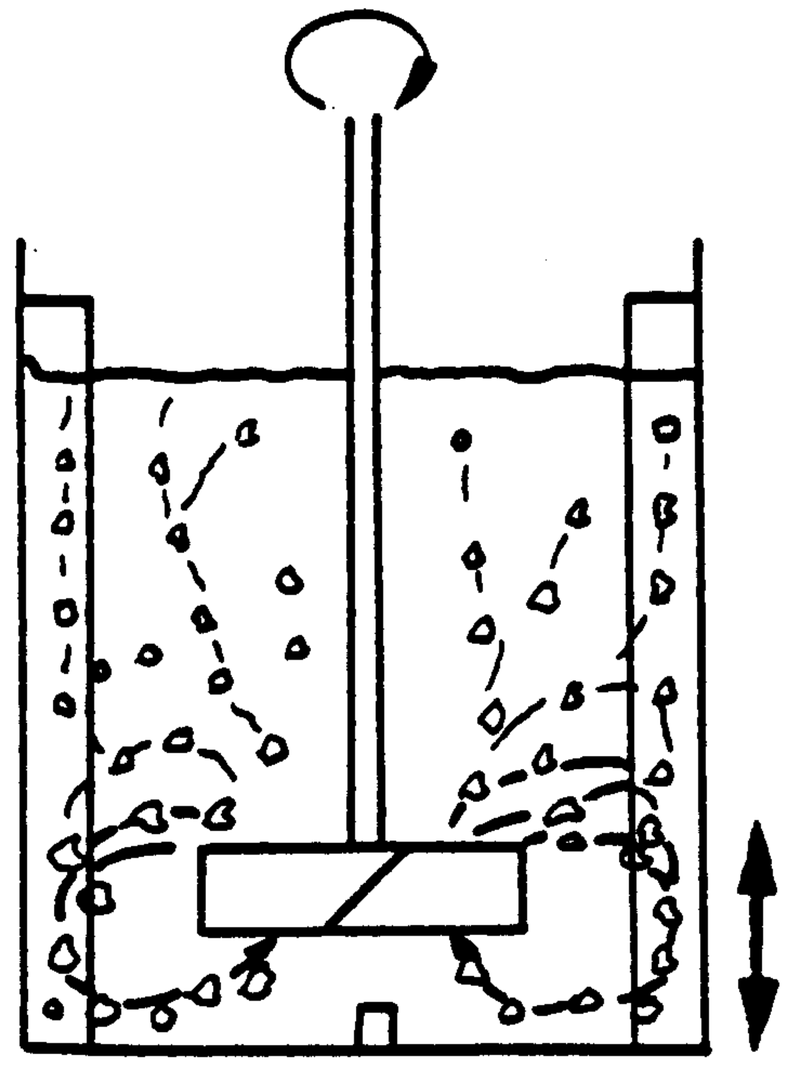

(d)

Fig. 3.4 Bulk flow Patterns with Increasing Speed for 4 MFU Impellers

effect becomes negligible compared to the liquid flow generated by the impeller, and the power number therefore increases. As the gas flow just forms the recirculation loops (Fig. 3.4c) so the power number reaches its maximum, and further increases in speed produce additional gas flow to the impeller via recirculation, and a reduction in power number.

The definition of good gas dispersion was taken as the speed, N_{CD}, corresponding with the maximum in the power curve, that is the point where gas was just circulated to the lower portions of the vessel (i.e. the transition from Fig. 3.4b to 3.4c). Inspection of Fig. 3.5 shows the gassed power number (and therefore gassed power consumption) to be relatively independent of gas rate when compared to the disc turbine. This point is further demonstrated in Fig. 3.6 where the power number variation with Reynolds number is shown for gassed and ungassed systems.

The position of the ungassed data suggests that $P_g/P > 1$ under some conditions, which is difficult to explain and could largely be due to the higher fractional errors in the data at low speeds. However, the power number-Reynolds number plot does show how little effect gas rate has on power number up to very high impeller speeds, not withstanding the trends previously described. This point is further demonstrated by the very small increase in speed necessary to just disperse the gas with large increases in gas rate (i.e. N_{CD} is virtually independent of Q), especially when compared with other impellers (see Section 3.5.6). The relative independence of power consumption and of mixing characteristics appears to be due to the co-current overall flow of gas and liquid through the impeller. However, a study of the gas and liquid flows in the impeller region is needed before the phenomena can be more precisely explained.

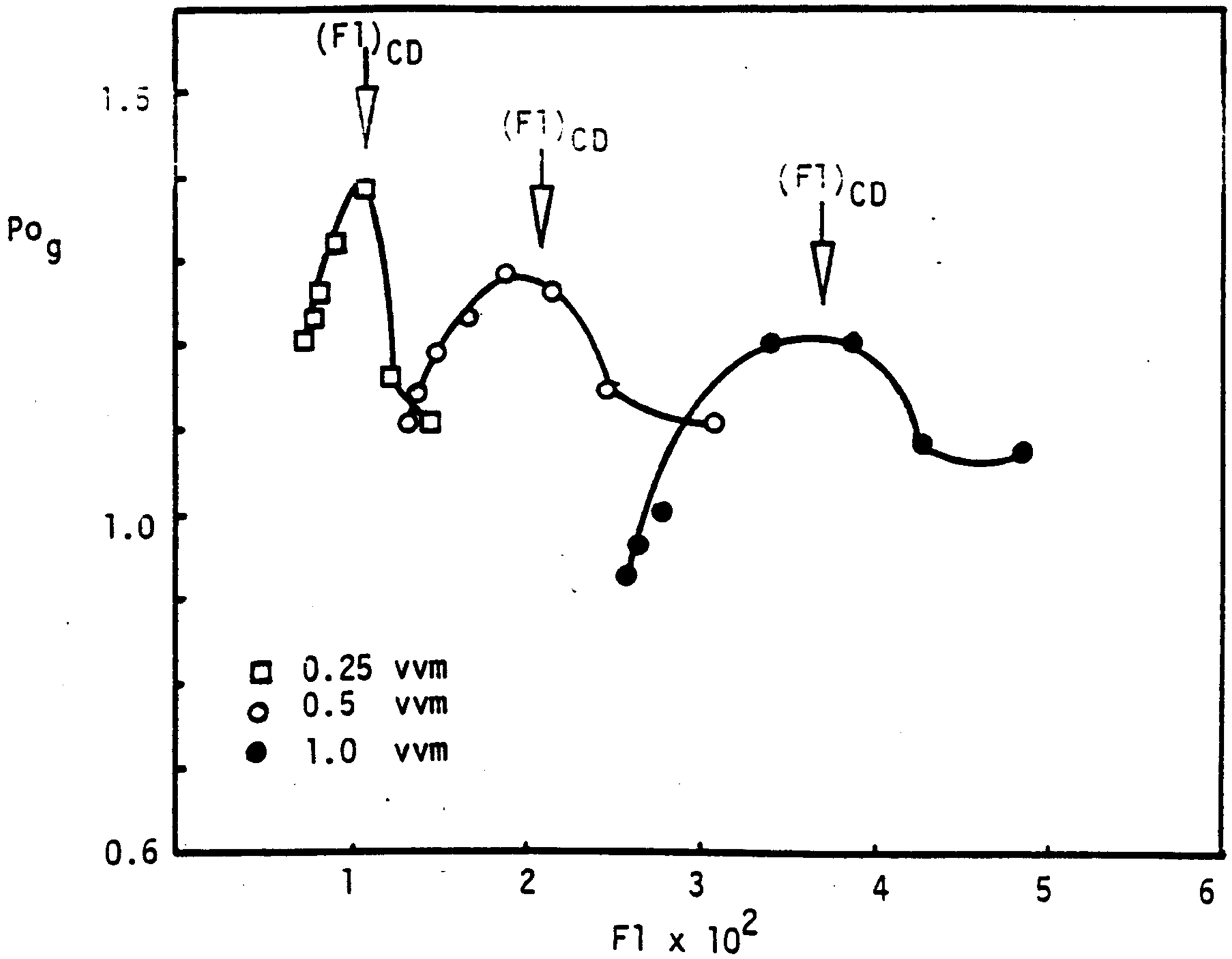

Fig. 3.5 Power Number versus Flow Number for a 4 MFU Impeller
(D = T/2, C = T/4, T_{56})

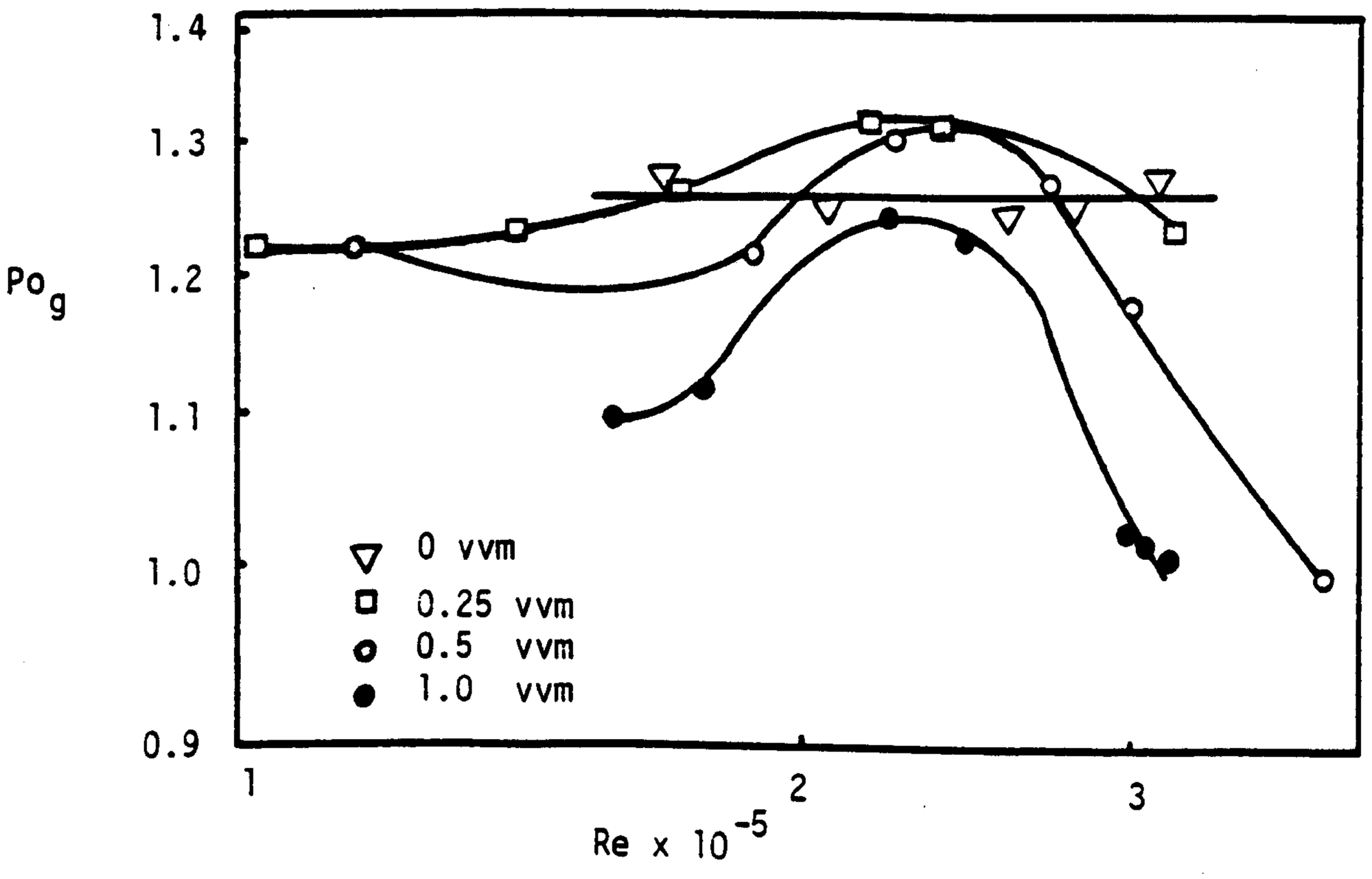

Fig. 3.6 Power Number versus Reynolds Number for a 4 MFU Impeller
(D = T/2, C = T/4, T_{56})

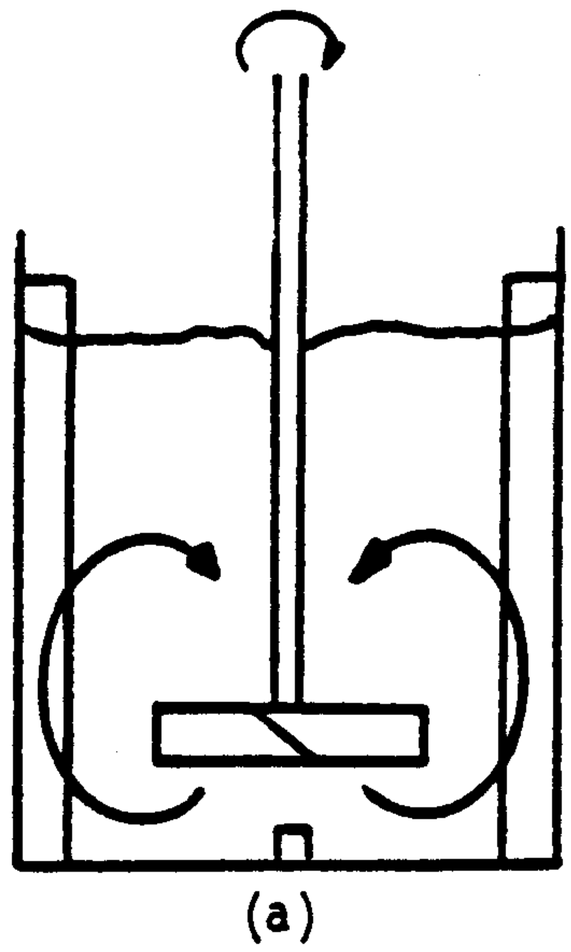

(a)

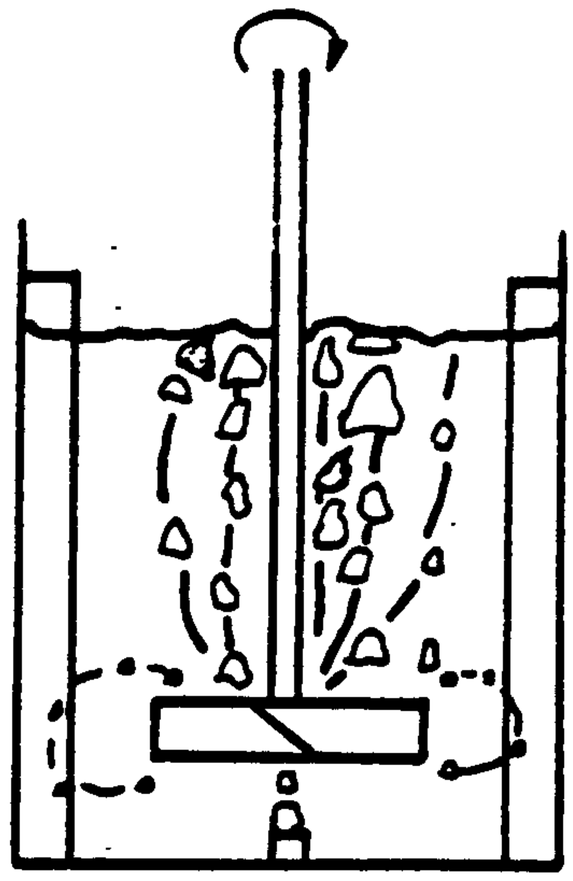

(b)

constant Q

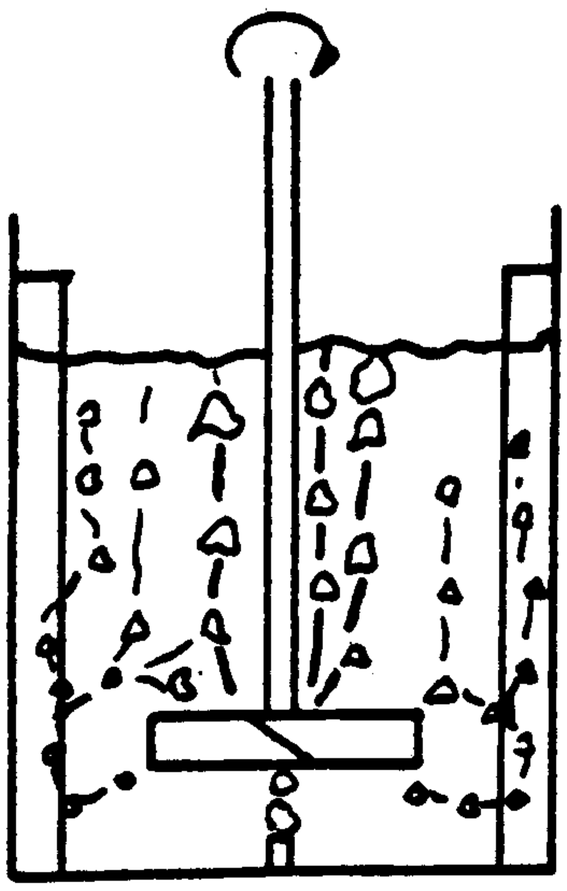

(c)

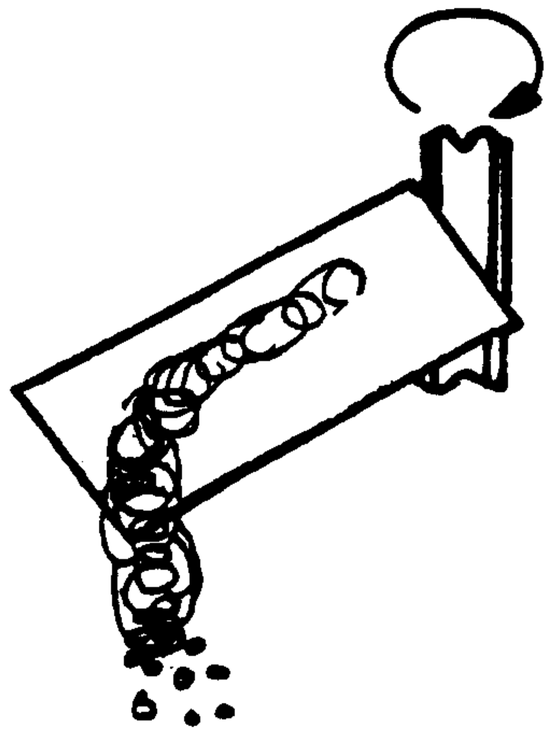

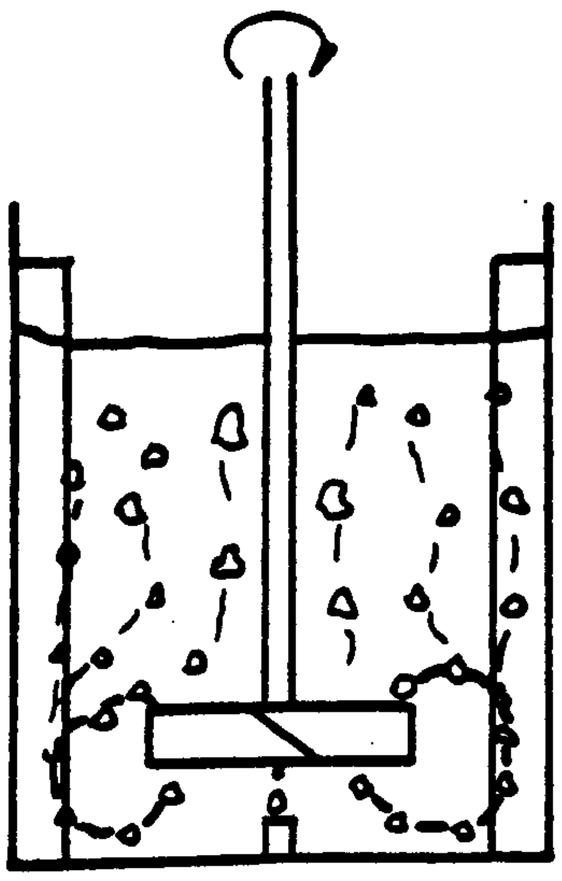

(d)

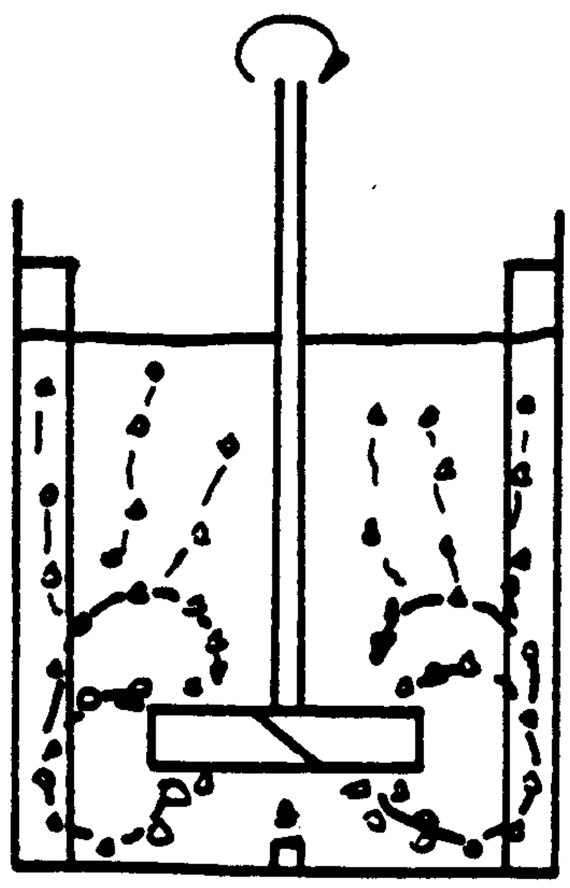

(e)

Fig. 3.7 Bulk Flow Patterns with Increasing Speed for a 4 MFD Impeller

3.7 (a)-(c) would occur except that in (c) no gas filled cavities were visible at any stage and the dominance of the upward gas flow would occasionally falter and gas surge gently towards the base. A further small increase in speed resulted in the impeller's pumping action becoming dominant and the gas suddenly being thoroughly and vigorously dispersed throughout the lower regions of the vessel. This condition was unstable and after a period of time the gas phase would revert to a non-dispersed condition. Thus the system would oscillate between that depicted in Fig. 3.7c and that in Fig. 3.7e without any external stimulus. The periodicity of these fluctuations appeared to be random and was marked by sharp variations in the power drawn by the impeller. Fig. 3.8a shows the torque output varying with time at constant impeller speed and gas rate. The higher torque value corresponds to the gas phase being well dispersed and the lower to negligible dispersion. This chronic instability in the flow occurred over a narrow range of impeller speeds, with some hysteresis, until a speed was reached above which the gas phase remained well dispersed and the power at the higher level. The plot of power number against flow number (Fig. 3.9a) shows the dispersion behaviour of the 0.14 m diameter 4 MFD impeller can be considered to have three hydrodynamic regimes. The first shows a decreasing power number as speed increases. The second shows an oscillation in power number between two extremes, the upper of which is approximately equivalent to that obtained in an ungassed system for the same Reynolds number (Fig. 3.9b). The third shows power number once again decreasing with increasing impeller speed.

Tatterson et al.[20] used stereoscopic visualization techniques to identify two major types of flow associated with this type of impeller in single phase liquid systems. They found that on their smaller scale equipment (D = T/3 = 0.102 m, 6 blades), the formation

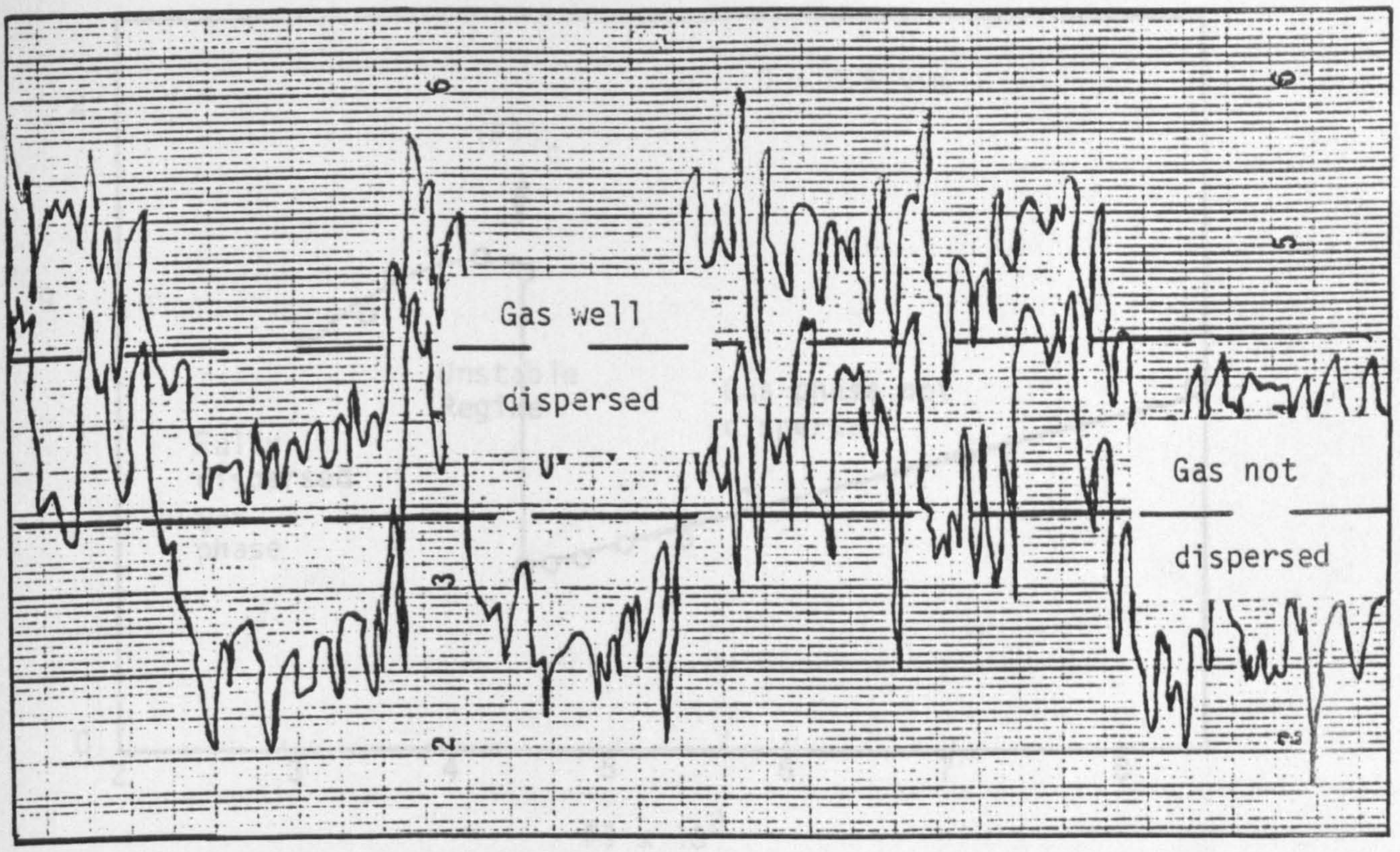

(a) D = T/4 Q = 0.5 vvm

(b) D = T/2 Q = 0.5 vvm

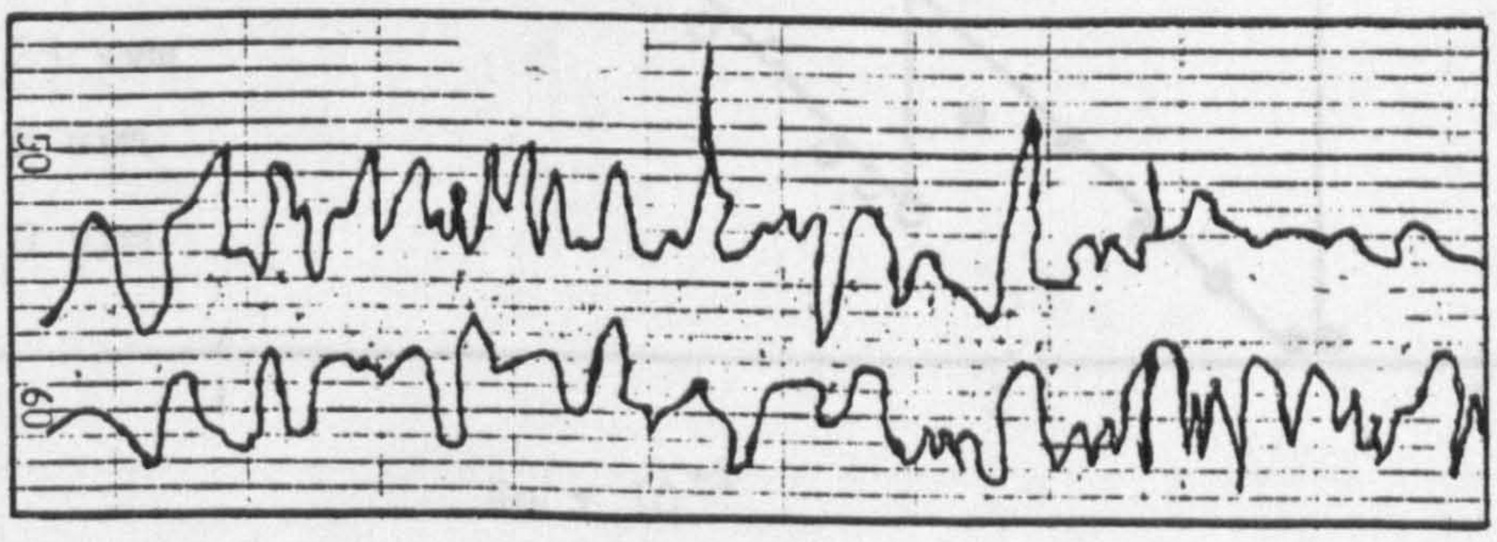

(c) D = T/2 Unaerated

Fig. 3.8 Torque Fluctuations on Aerating a 4 MFD Impeller (T_{56}, C = T/4)

(a)

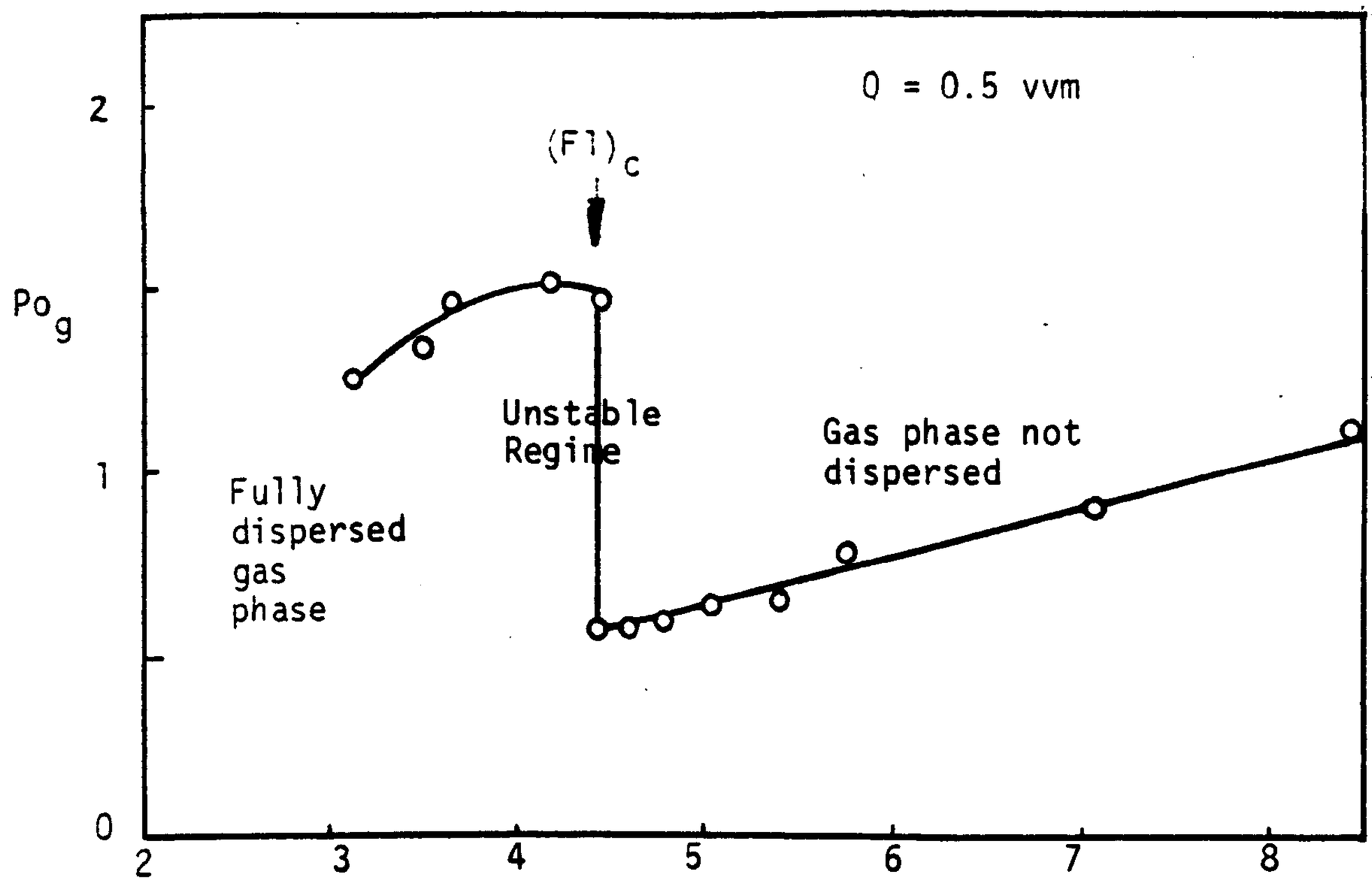

(b)

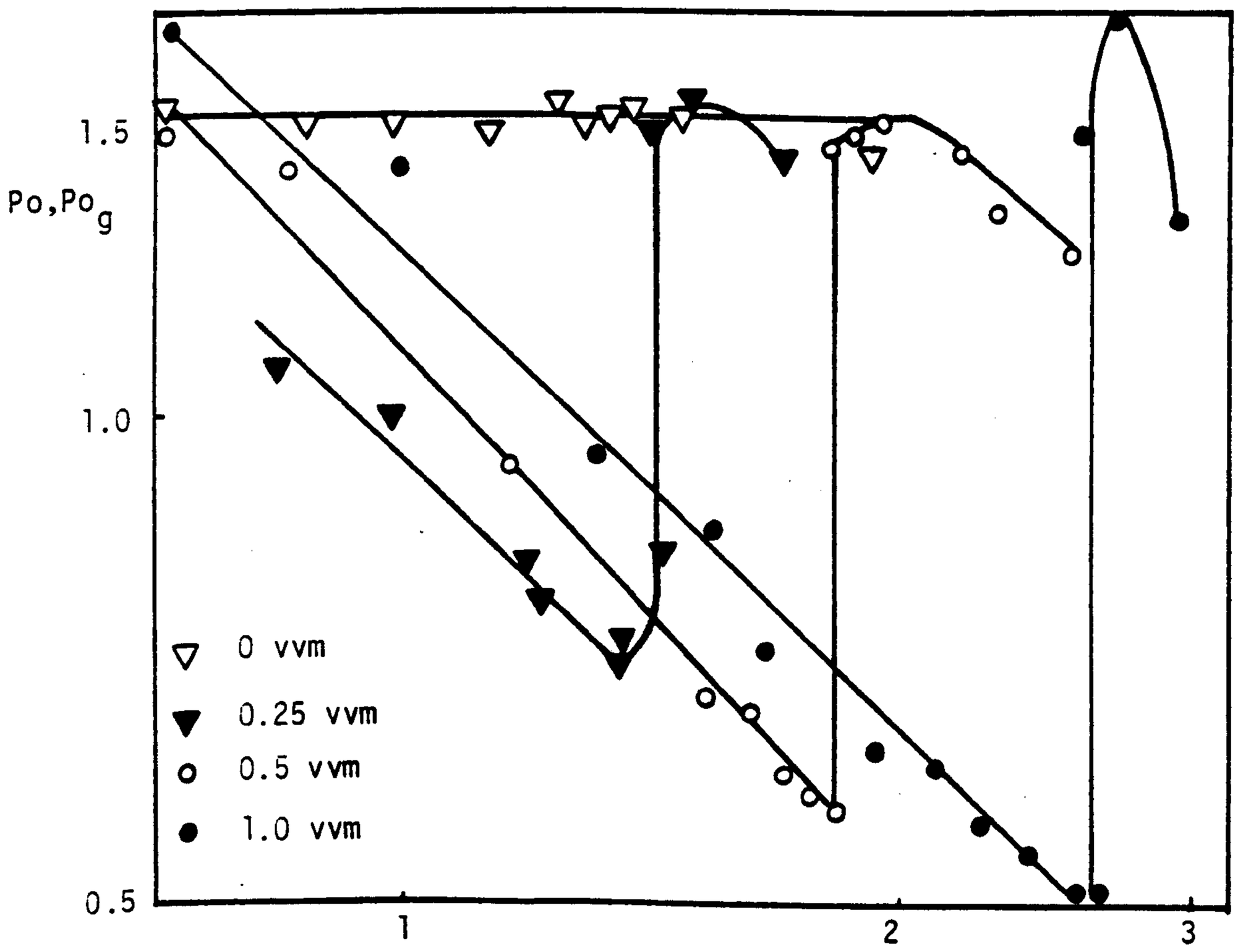

Fig. 3.9 Plots of (a) Power Number versus Flow Number and (b) Power Number versus Reynolds Number for a D = T/4 4 MFD Impeller (C = T/4, T_{56})

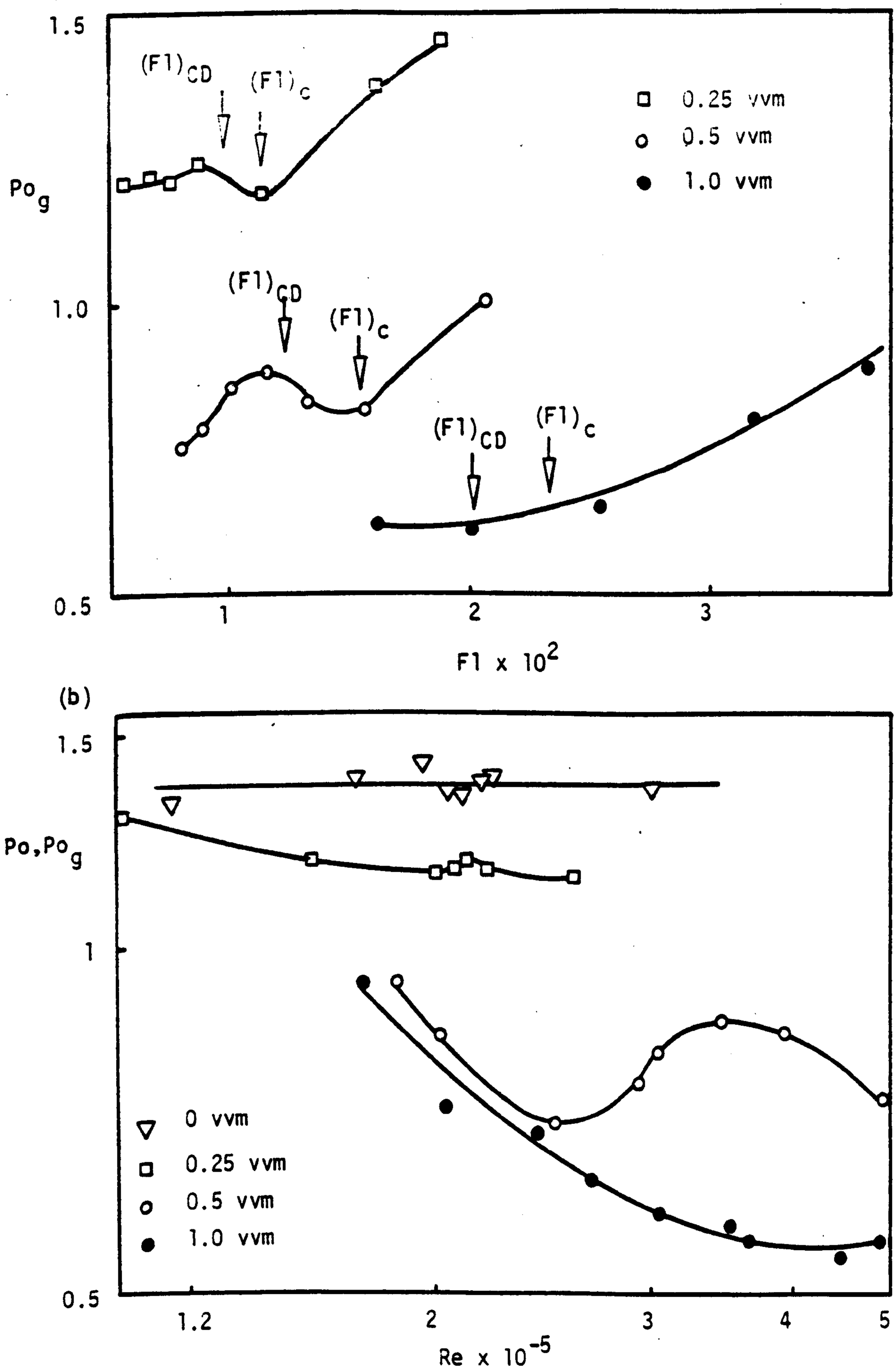

Fig. 3.10 Plots of (a) Power Number versus Flow Number and (b) Power Number versus Reynolds Number for a D = T/2 4 MFD Impeller (C = T/4, T_{56})

of high speed jets leaving the impeller region and directed towards the tank base dominated the flow. On the larger scale (D = T/3 = 0.305 m, 4 blades) they found that a trailing vortex formed inside the rear end edge of the blade and was either pulled along behind the blade or shed and moved away radially with a slight downward vertical velocity. The high speed jets had a negligible effect on the large scale where flow around the impeller was fairly ordered, but the jets were found to occasionally cause severe pulsing on the smaller scale, resulting in strong vertical draughts through the impeller.

In the light of these observations, combined with those of Brauer and Schmidt-Traub[14] as described in Section 3.2.1 for a marine propeller, a plausible explanation of the behaviour demonstrated in Fig. 3.9a for the 0.14 m diameter impeller emerges. At low speeds the gas flow dominates the impeller yet power number decreases as speed increases. This trend is similar to that displayed in a disc turbine system and also in the large mixed flow impeller system (Fig. 3.10) and suggests the increasing presence of gas in the impeller region, possibly within the trailing vortices although these were not observed for the 0.14 m impeller. The pulsing of the high speed jets and consequent strong downdraught could have an exaggerated effect in a gassed system, resulting in the observed power and flow oscillations with the gas being dispersed before it reaches the impeller by the periodically dominant liquid flow. This would explain the slight hysteresis and why the power number returned to the value in an ungassed system (Fig. 3.9b). Recirculation of gas to the impeller would explain a further decrease in power number when the gas phase was well dispersed.

The larger impeller (0.28 m diameter) showed less dramatic surges in flow. Nevertheless, these surges were easily detected both visually and by inspection of the variation in impeller torque (Fig.

3.8b) especially at 0.5 vvm. Fig. 3.10a demonstrates the more gentle nature of this characteristic behaviour. Once again the oscillations in torque developed most rapidly at an impeller speed corresponding to the rise in the power number, at which speed the gas was periodically well dispersed (Fig. 3.7d). The presence of gas filled cavities was observed in the "non-dispersed" region of Fig. 3.10a (Fig. 3.7c) and their increasing size would explain the fall in power number. The power number for the 0.28 m impeller never attains the ungassed value (Fig. 3.10b), suggesting that the vortices observed by Tatterson et al. filled with gas and these had a constant presence, with vortex shedding accounting for the power and flow oscillations. Again, recirculation could explain a subsequent fall in power number.

Neither incomplete gas dispersion nor fluctuations in power consumption are desirable operating conditions. Thus it is vital that these regimes be identified and avoided by using a sufficiently high impeller speed for a given gas rate.

The fluctuations in torque and gas dispersion started at some speed N_c and faded out at some higher speed, at which point the gas was well dispersed and power consumption steady. This higher speed constituted the minimum mixing requirement, N_{CD}, for this impeller type. Table 3.2 shows the magnitude of this unstable regime for the two 4 MFD impeller sizes in T_{56}.

Impeller Diameter. D m	Gas Rate vvm	Q m^3s^{-1}	N_c (s^{-1})	N_{CD} (s^{-1})
0.14	0.25	$0.575\times10_3^{-3}$	6.9	6.9
	0.5	1.15×10^{-3}	9.4	9.6
	1.0	2.30×10^{-3}	13.3	15.25
0.28	0.25	$0.575\times10_3^{-3}$	2.3	2.6
	0.5	1.15×10^{-3}	3.3	4.2
	1.0	2.30×10^{-3}	4.4	5.2

Table 3.2 Critical Speeds for the 4 MFD Impeller in T_{56}

The regime in which flow was unstable appears to become larger as both gas rate and impeller size increase.

Based on the dispersion mechanism discussed above, the critical impeller speed (N_C) at which gas is first just dispersed throughout the vessel is given by the point where the liquid downflow from the impeller just overcomes the upflow of gas from the sparger and prevents direct gas flow into the impeller region. Considering a momentum balance in the vertical direction on the downward liquid pumped from the impeller (mass flowrate G_L) at velocity U_L and the upward gas and entrained liquid flow from the sparger (mass flowrate G_{GL}) at velocity U_{GL}. At the critical condition, the outward flow $G_L + G_{GL}$ leaves the control volume horizontally so that it makes no contribution to this balance. At this point then, the upward and downward momentum must be equal.

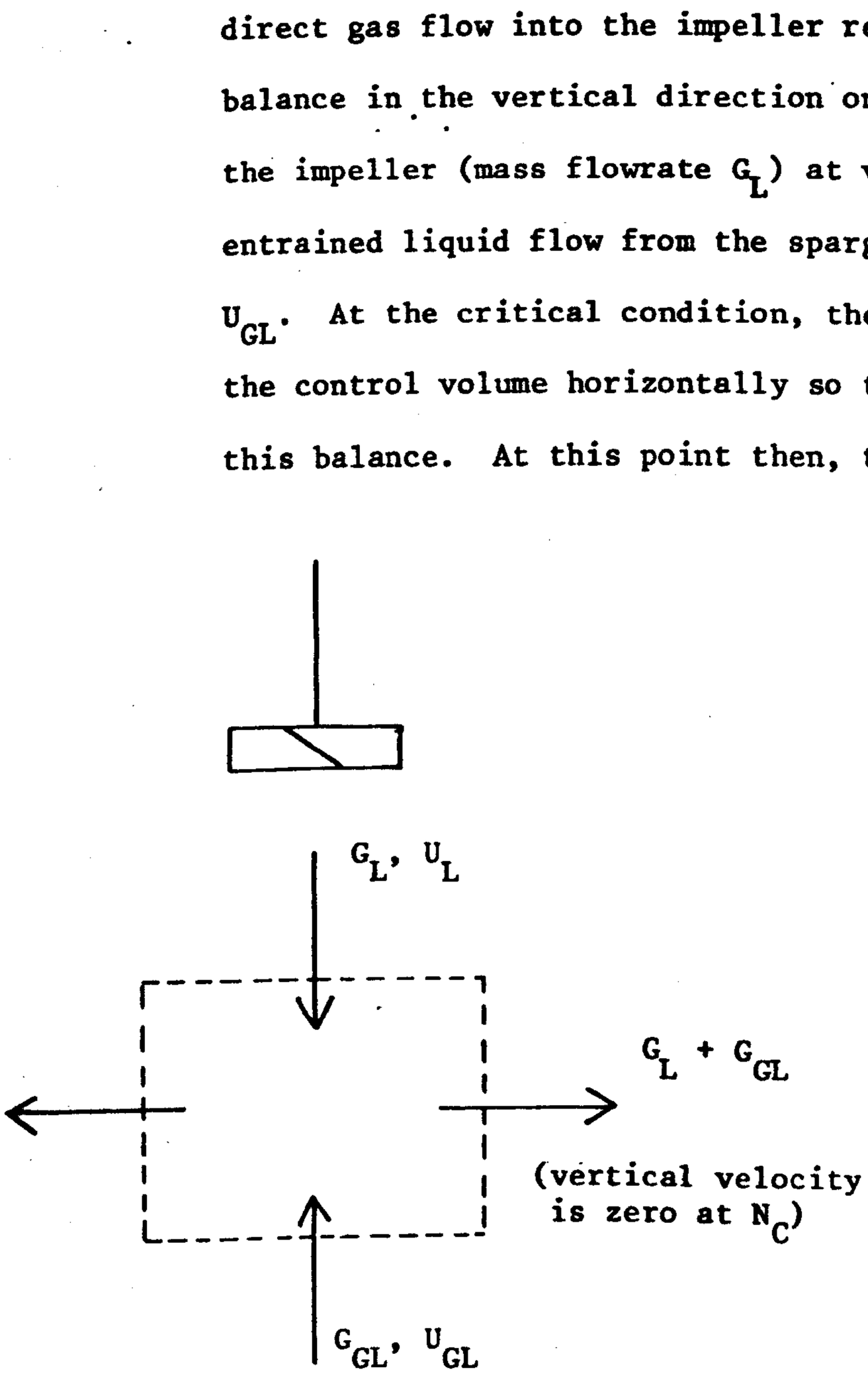

Fig. 3.11 Ideal Picture of Flows Through a Control Volume Below a 4MFD Impeller.

$$\text{ie} \quad G_L U_L = G_{GL} U_{GL} \qquad 3.2$$

The volumetric downflow of liquid will be proportional to $N_C D^3$ and the average velocity of flow proportional to $N_C D$. Hence:

$$\left.\begin{aligned} G_L &\propto N_C D^3 \\ \text{and} \quad U_L &\propto N_C D \end{aligned}\right) \qquad 3.3$$

Assuming that for the upwards flow:

$$G_{GL} \propto Q \quad \text{and} \quad U_{GL} \propto U_b \qquad 3.4$$

then by combining 3.3 and 3.4 with 3.2:

$$\frac{G_{GL}U_{GL}}{G_L U_L} = K^{\dagger}\left[\frac{Q\ U_b}{N_C{}^2 D^4}\right] = 1$$

or

$$\frac{QU_b}{N_C{}^2 D^4} = Y, \text{ a constant.} \qquad 3.5$$

Consider the gas stream leaving the sparger as distinct bubbles. The volume of the bubbles[21] is given by:

$$V_b = 1.138\ \frac{Q^{1.2}}{g^{0.6}} \qquad 3.6$$

for a single sparger orifice. If the bubbles are assumed to be perfect spheres then, from Eqn. 3.6, the bubble diameter is given by:

$$d_b \propto Q^{0.4} \qquad 3.7$$

and since bubble rise velocity is proportional to the square root of bubble diameter,[21] assuming no interaction between the bubbles, then bubble velocity is only a very weak function of gas rate and will be considered as independent of it.

i.e.

$$\frac{Q}{N_C{}^2 D^4} = Y' \Rightarrow Y'' = \frac{Q^{0.5}}{N_C D^2} \qquad 3.8$$

i.e.

$$N_C = \frac{Q^{0.5}}{Y'' D^2} \qquad 3.9$$

where Y' and Y'' are also constants.

The data presented in Table 3.2 along with data for a single gas rate and impeller size from T_{29}, T_{91} and T_{183} were used to evaluate Y''. Fig. 3.12a shows that Y'' was not in fact constant over a large size range, as Eqn. 3.9 implies, but that there was a dependence on impeller size of:

$$Y'' \propto D^{-0.37} \qquad 3.10$$

(a)

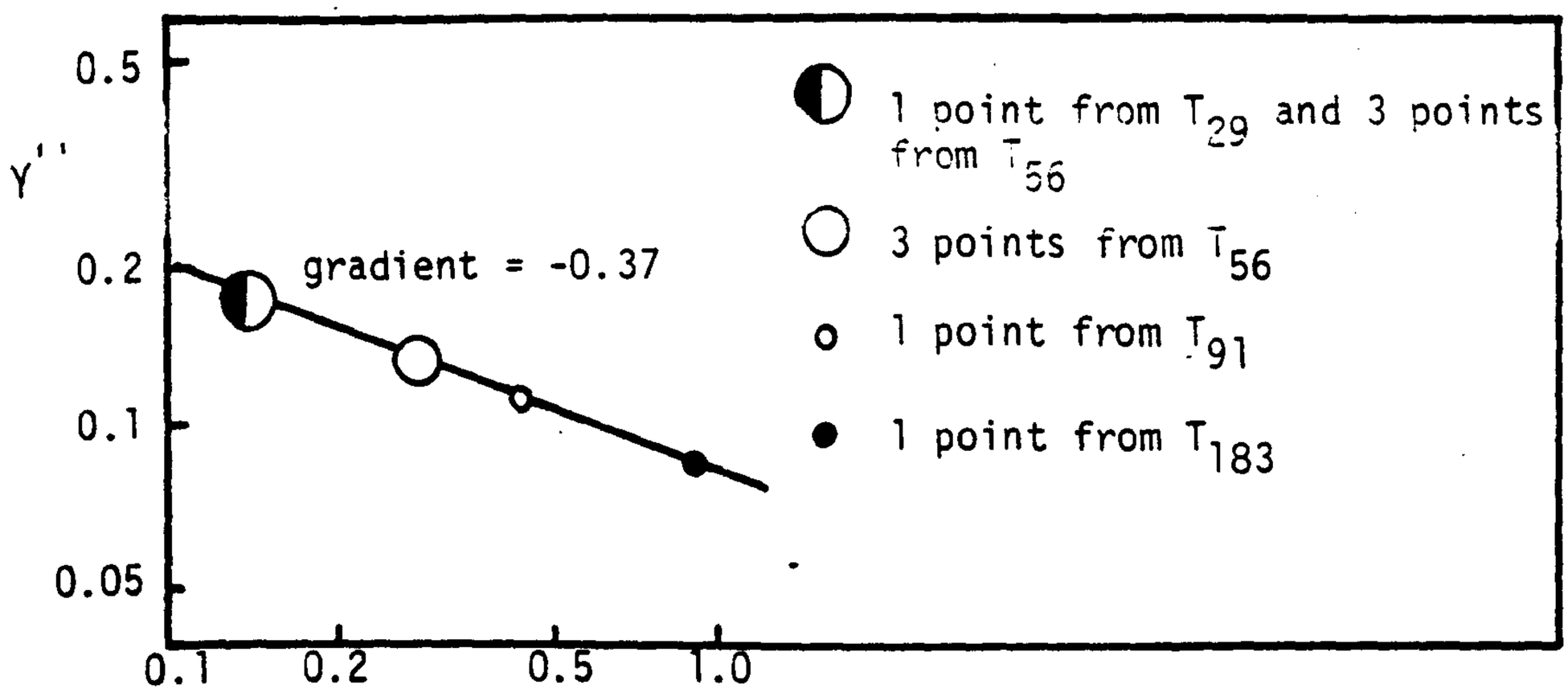

(b)

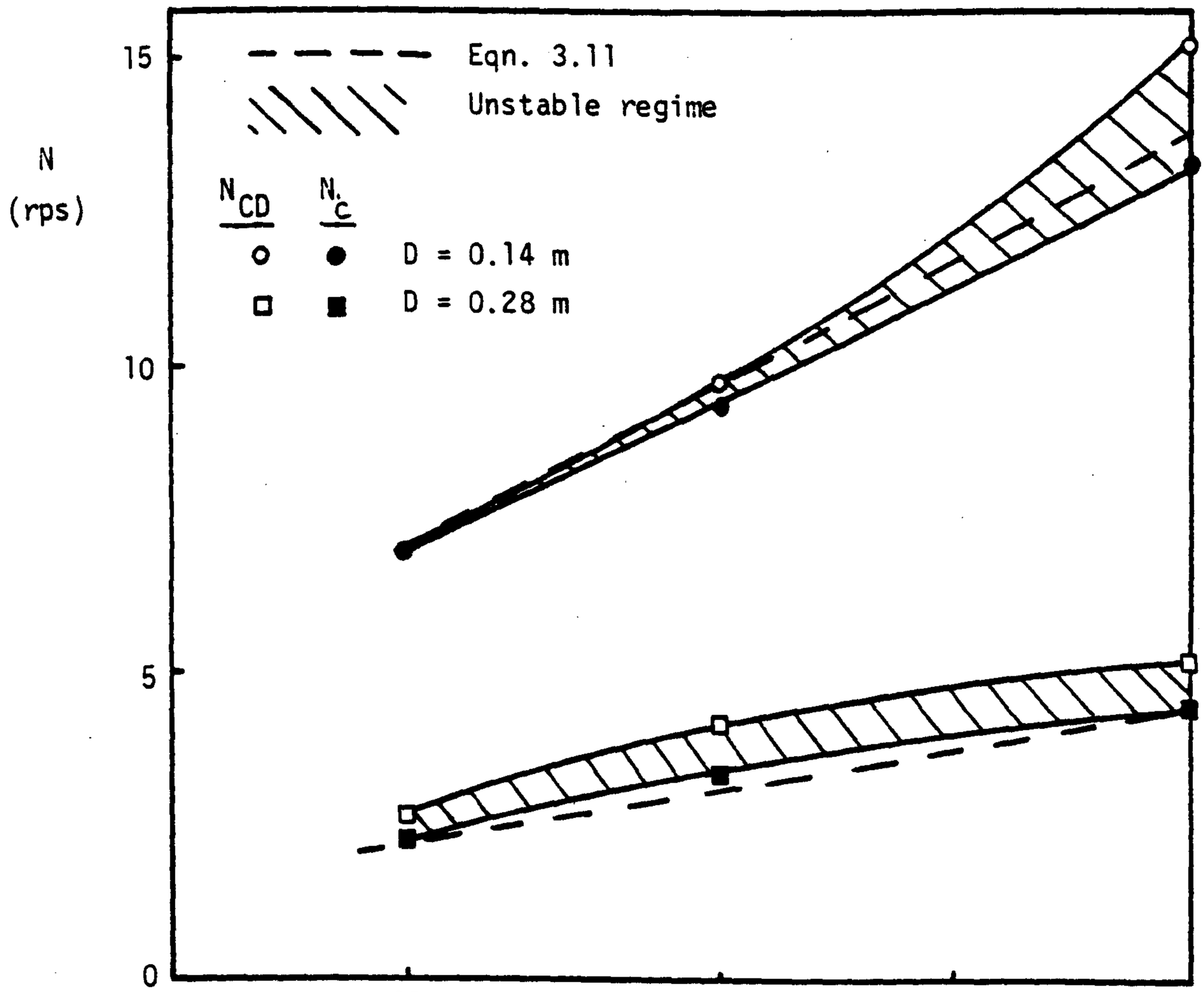

Fig. 3.12 (a) Y'' versus D
(b) Comparison of Eqn. 3.11 with Experimental Observations (T_{56}, c = T/4)

This additional factor, not predicted by the reasoning set out above, was probably the result of changing hydrodynamics with scale as outlined by Tatterson et al.[20] If Eqn. 3.10 is combined with Eqn.3.9 and the constants evaluated, then the resulting expression is:

$$N_C = \frac{11.7\ Q^{0.5}}{D^{1.63}} \qquad 3.11$$

The similarity between Eqn. 3.11 and that derived by Nienow et al.[5] to predict the flooding point of a disc turbine (see Fig.3.19) is perhaps surprising when the differing mechanisms of dispersion are considered. Fig. 3.12b shows the predicted value of N_C (from Eqn. 3.11) along with the region of instability, from which an idea of the safety margins required to ensure $N > N_{CD}$ can be obtained.

3.5.3. Six-bladed Mixed Flow Impellers Pumping Down (6 MFD)

Additional experiments using a six-bladed 0.14 m diameter impeller yielded no change in the overall characteristics described for the four-bladed impeller. However, N_{CD} was lower and the unstable region narrower for the six-bladed version, supporting Van't Riet's[22] observations that increasing the number of blades increases gas dispersion efficiency. Fig. 3.13 demonstrates the effect of increasing the number of blades.

3.5.4. Axial Flow Impellers Pumping Down (AFD)

The 0.29 m diameter marine propeller (AFD) has a less significant radial component of flow than the mixed flow 45^{o} impellers. Thus the upper regions of the vessel behaved as a bubble column even under conditions of extreme agitation. Otherwise, the mode of dispersion in the impeller region was very similar to that observed for the 0.28 m 4 MFD impeller (Fig. 3.7) in all respects.

The power number-flow number plot, however, did not follow a similar pattern to the mixed flow impeller. In this case a steady drop in power number occurred over the complete range investigated

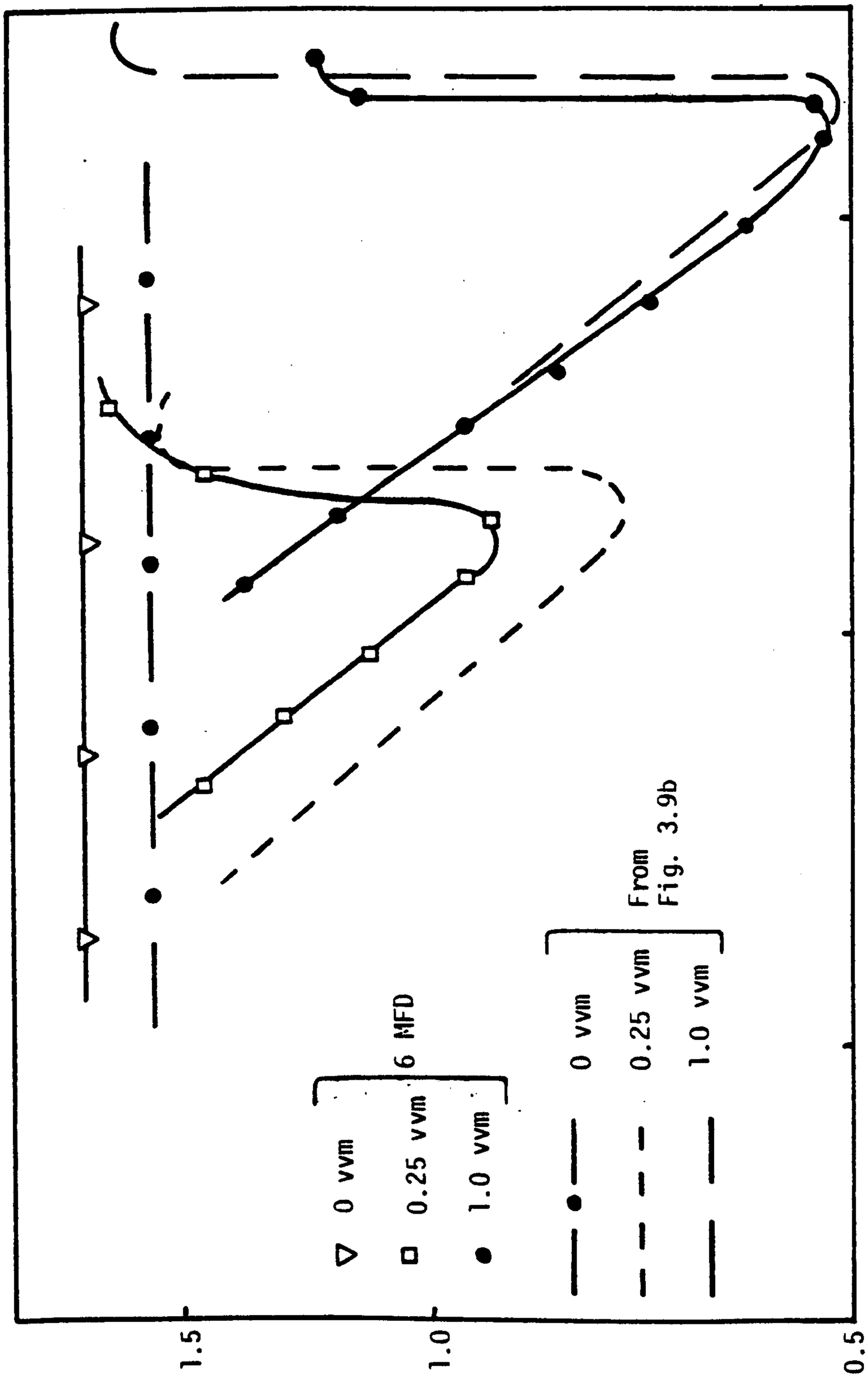

Fig. 3.13 Comparison of 6 MFD Impeller with Data for the 4 MFD Impeller (from Fig. 3.9b)
(D = T/4, c = T/4, T_{56})

(Fig.3.14), up to speeds well above that necessary to disperse the gas throughout the tank. The torque oscillations, which developed in the same manner as for the 4 MFD impeller (most noticeably at around the speed necessary to just disperse the gas), caused large instantaneous variations in power number. The mean value is shown in Fig. 3.14a with the limiting values marked for two speeds to demonstrate the extent of the fluctuations.

Fig. 3.14b clearly shows that, at low gas rates, the power consumption in a two-phase system was higher than that in single phase systems, until very high speeds had been reached. Again, as with the smaller mixed flow impeller, Po_g tends to the ungassed value at high speeds, but this time from a higher value. This could confirm Brauer et al's[14] dispersion mechanism at low gas rates, with the gas being dispersed from below the impeller region at sufficiently high speeds. Although the gas bubble they observed below the impeller was not noticed at higher gas rates, the gas filled cavities were clearly visible at lower speeds for all gas rates in a similar position and of similar shape to that depicted in Fig. 3.7c for the 4 MFD. One major difference between Brauer's work and this was the pitch of the propeller which was 1.5 D here, but never more than 0.75 D in Brauer's work.

A surprising aspect was the increase in power consumption caused at all but very high speeds for the lower gas rates. In this case it did not appear to be due to experimental errors, but was a genuine effect. Van't Riet[22] observed similar behaviour by a concave-bladed turbine but was unable to explain it. A possible explanation for the AFD impeller is that the presence of a relatively small number of bubbles attached to the rear face of the blade, in the low pressure, high velocity region, may upset the laminar flow around the blade, encouraging turbulence and separation and therefore

(a)

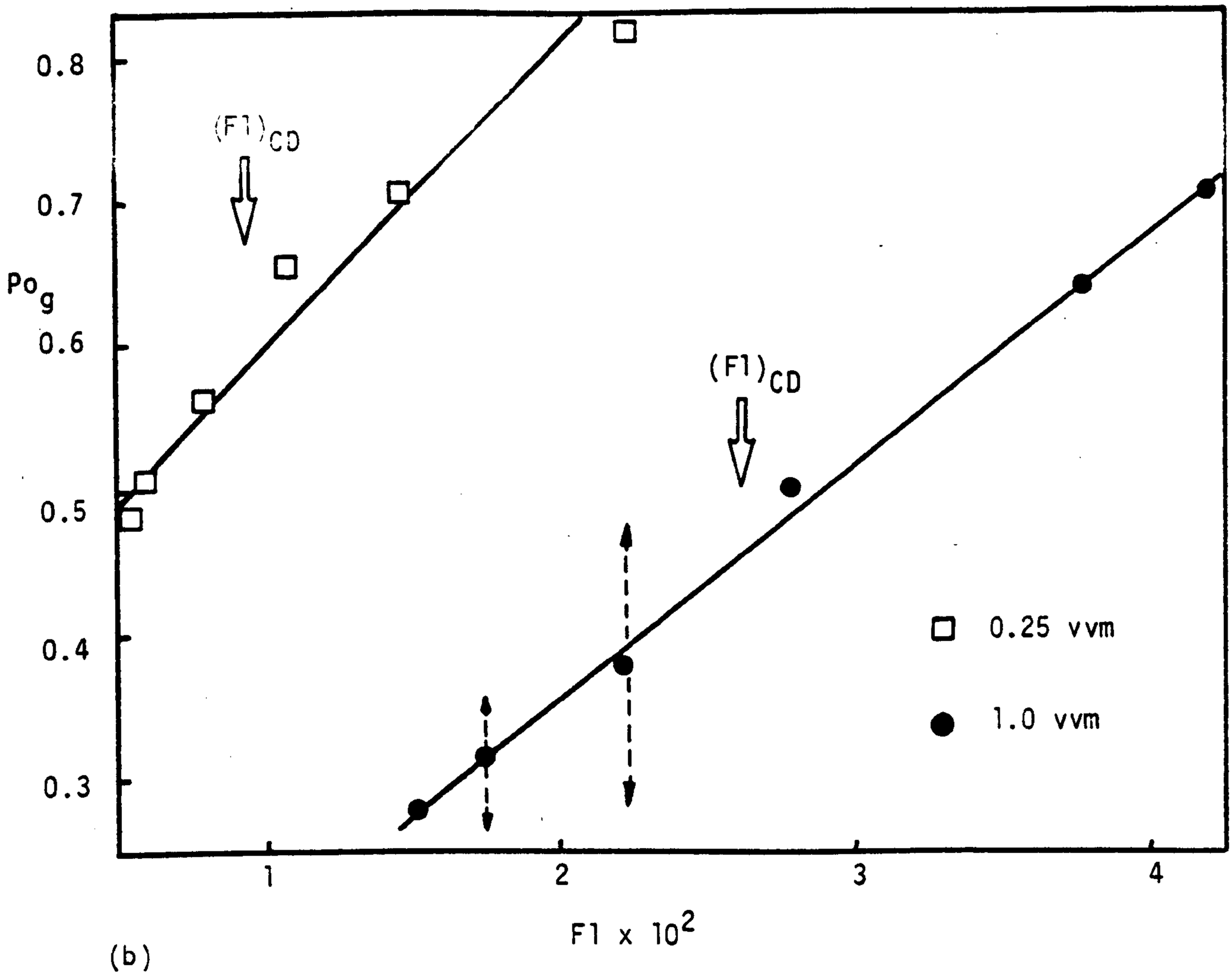

(b)

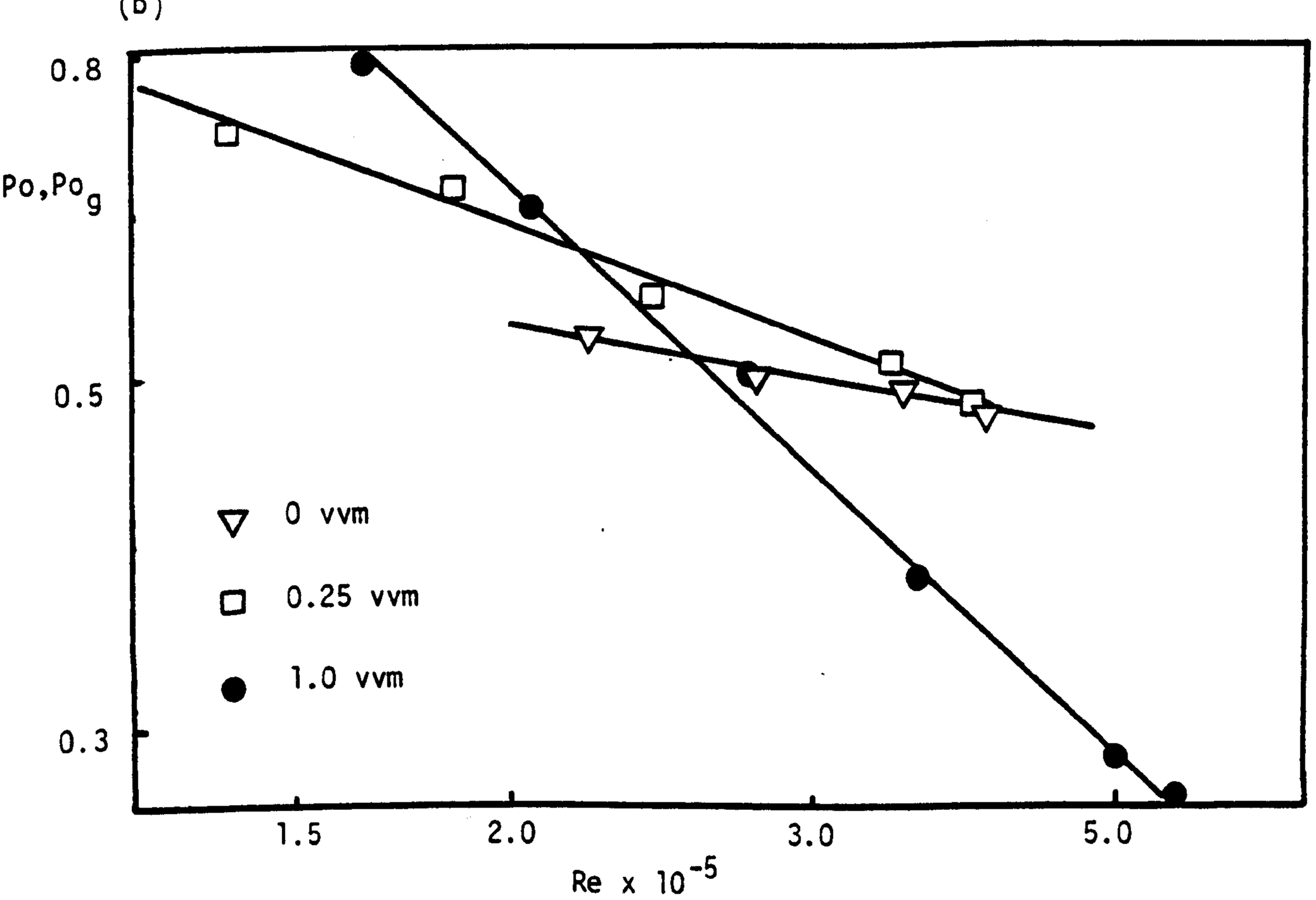

Fig. 3.14 (a) Power Number versus Flow Number and
(b) Power Number versus Reynolds Number for the AFD Impeller
($D \approx T/2$, $C = T/4$, T_{56})

increasing drag and power consumption. Higher gas rates probably have a significant effect on the local pressure behind the blade and thus reduce drag. At constant gas rates, increases in speed caused a steady decline in the power number. Also, the rate of decline increased with increasing gas rate (Fig. 3.14b), presumably due to the increasing rate at which gas migrated to the suction side of the blades as either Q or N increased.

With gas dispersion being a very gradual process and without convenient discontinuities to aid identification, the purely visual assessment of the point where gas was just well dispersed, N_{CD}, was very difficult to define accurately. However, the fluctuations in power consumption did increase at about N_{CD}, but over the range of gas rates examined (0.25 to 1 vvm) N_{CD} appeared to be a weaker function of gas rate then it had been for the MFD impellers.

3.5.5. Disc Turbines

This section deals with both the standard disc turbine (DT) at a clearance of 0.093 m (T/6) and the angled-blade disc turbine (ADT, c = 0.14 m = T/4), since both displayed very similar behaviour in gassed systems. The DT has previously been well charactized at higher clearances.

Standard Disc Turbine

The 0.28 m disc turbine displayed exactly similar dispersion characteristics at both T/4 and T/6 clearances. However, in ungassed systems, the smaller 0.187 m (T/3) diameter impeller forced a single loop axial type flow, though with a much higher tangential velocity component than either the mixed flow or axial flow impellers, causing a swirling motion of tracer particles on the base (Fig. 3.15a). When gas was introduced, flow reverted to the normal radial type described earlier (Section 3.2) at low speeds (Fig. 3.15b). As the impeller speed was increased so the same pattern as shown in Fig. 3.3 occurred

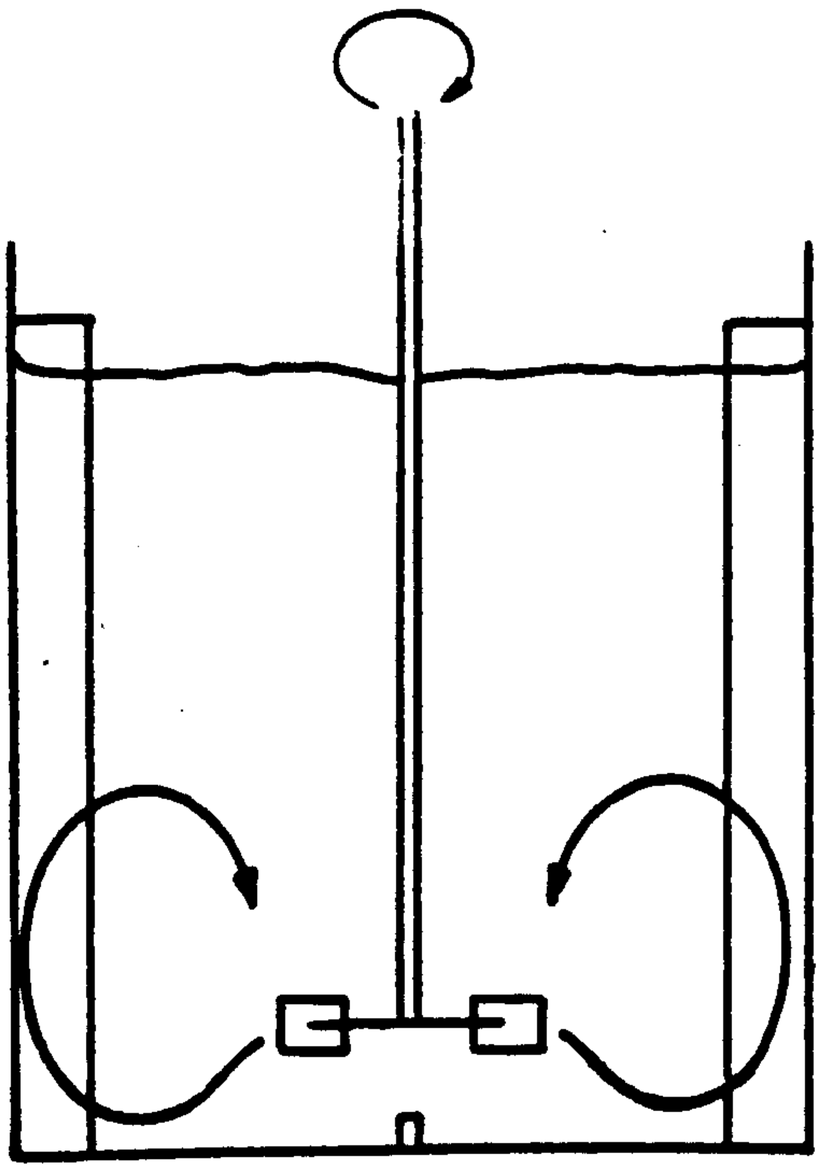

$Q = 0$

(a)

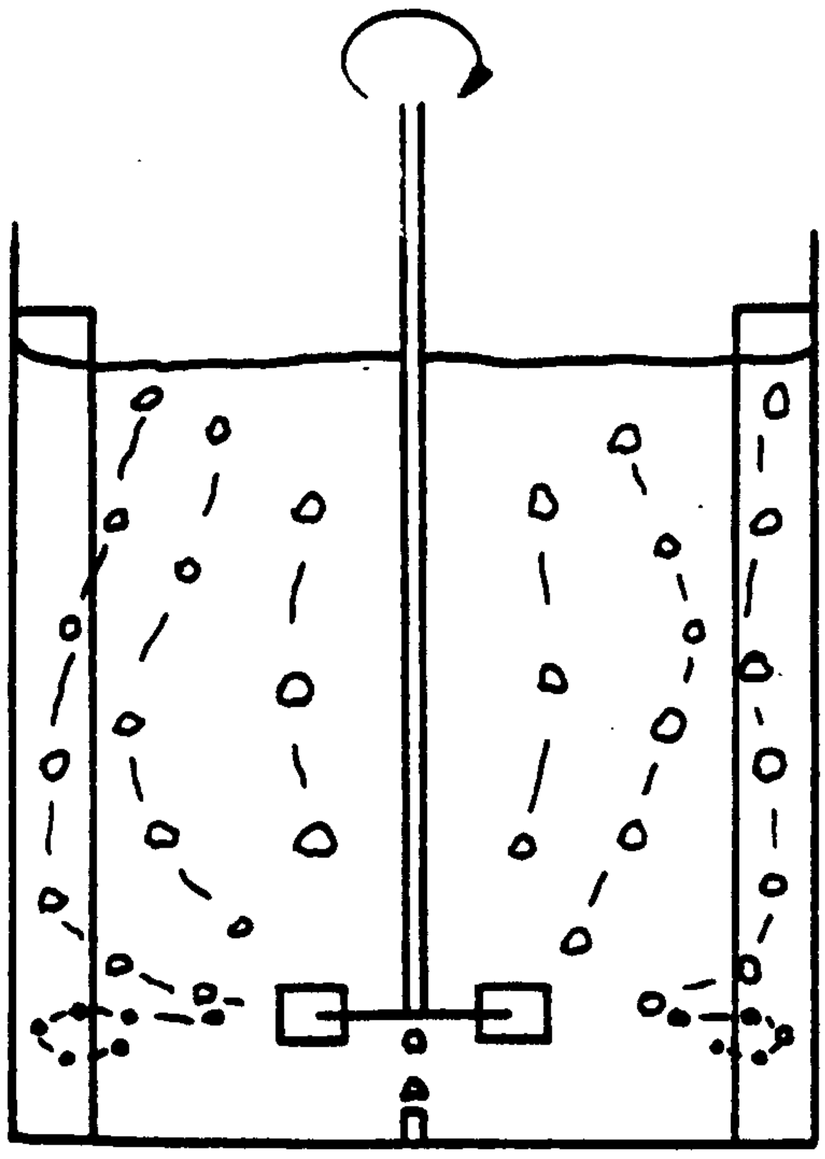

(b)

constant Q

$N < N_{CD}$

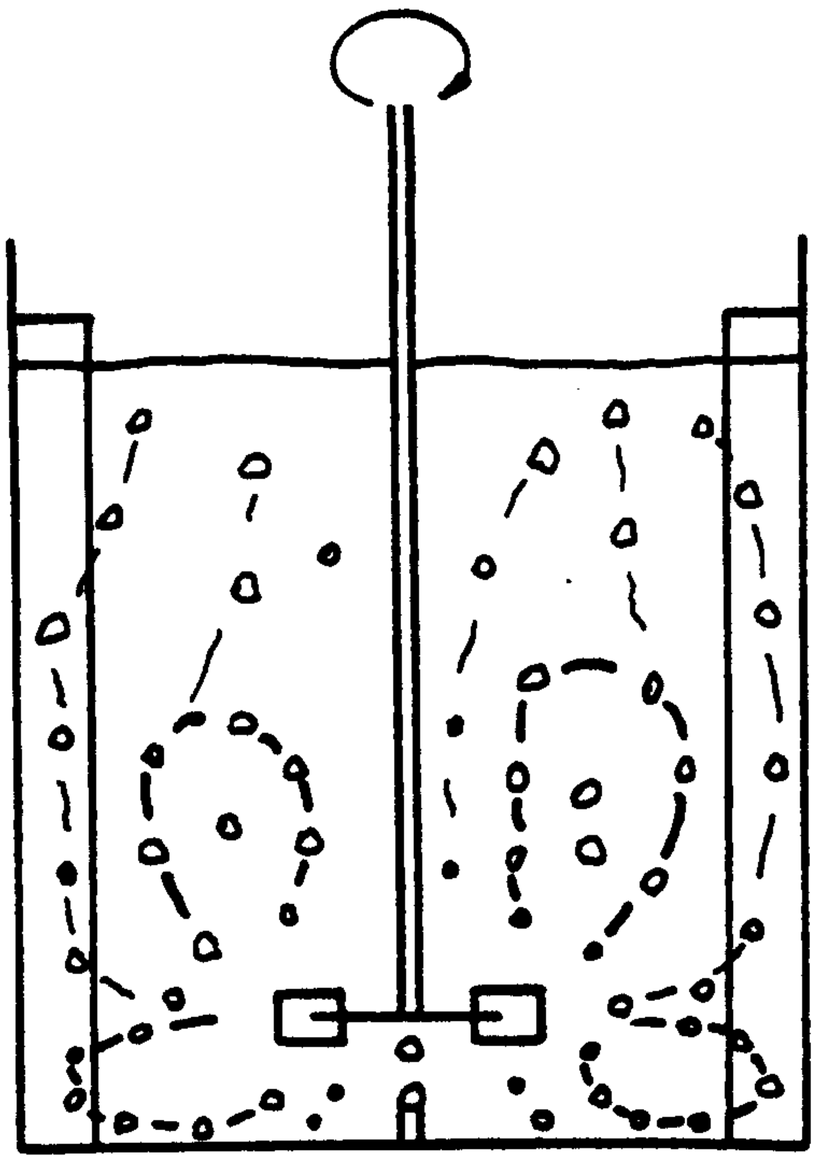

$N \geq N_{CD}$

(c)

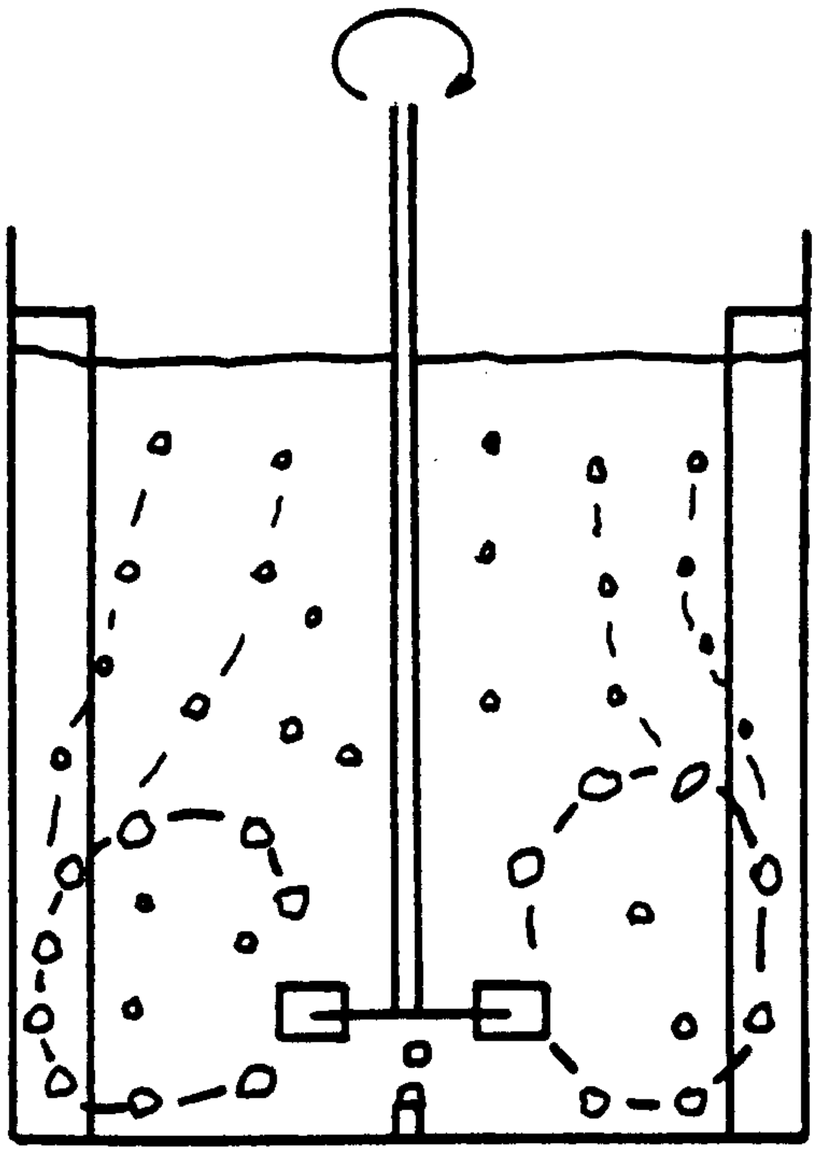

$N > N_c$

(d)

Fig. 3.15 Bulk Flow Patterns for a D = T/3 DT at a clearance of T/6

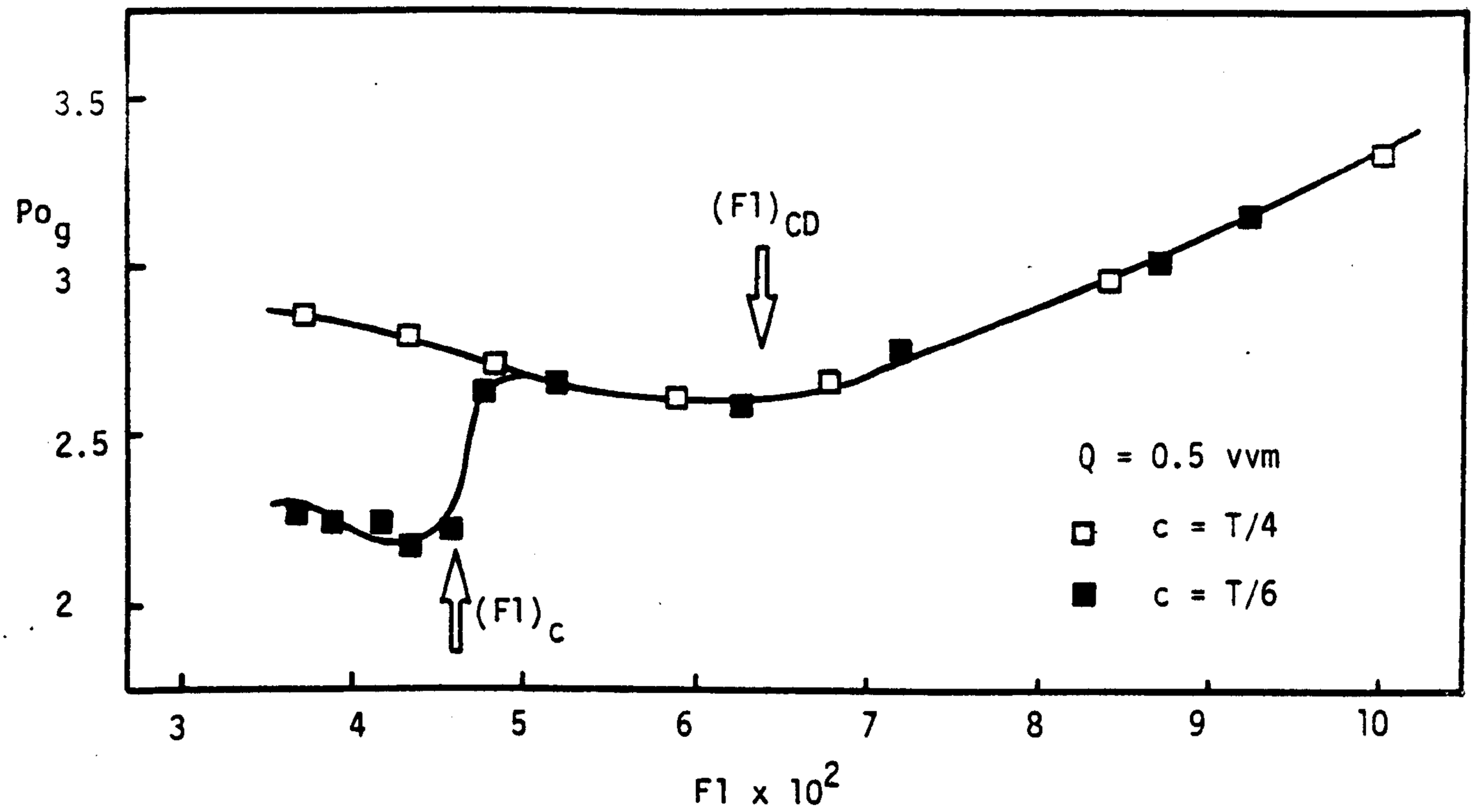

Fig. 3.16 Effect of clearance (c) on the Po_g - Fl plot for a D = T/3 DT. (T_{56})

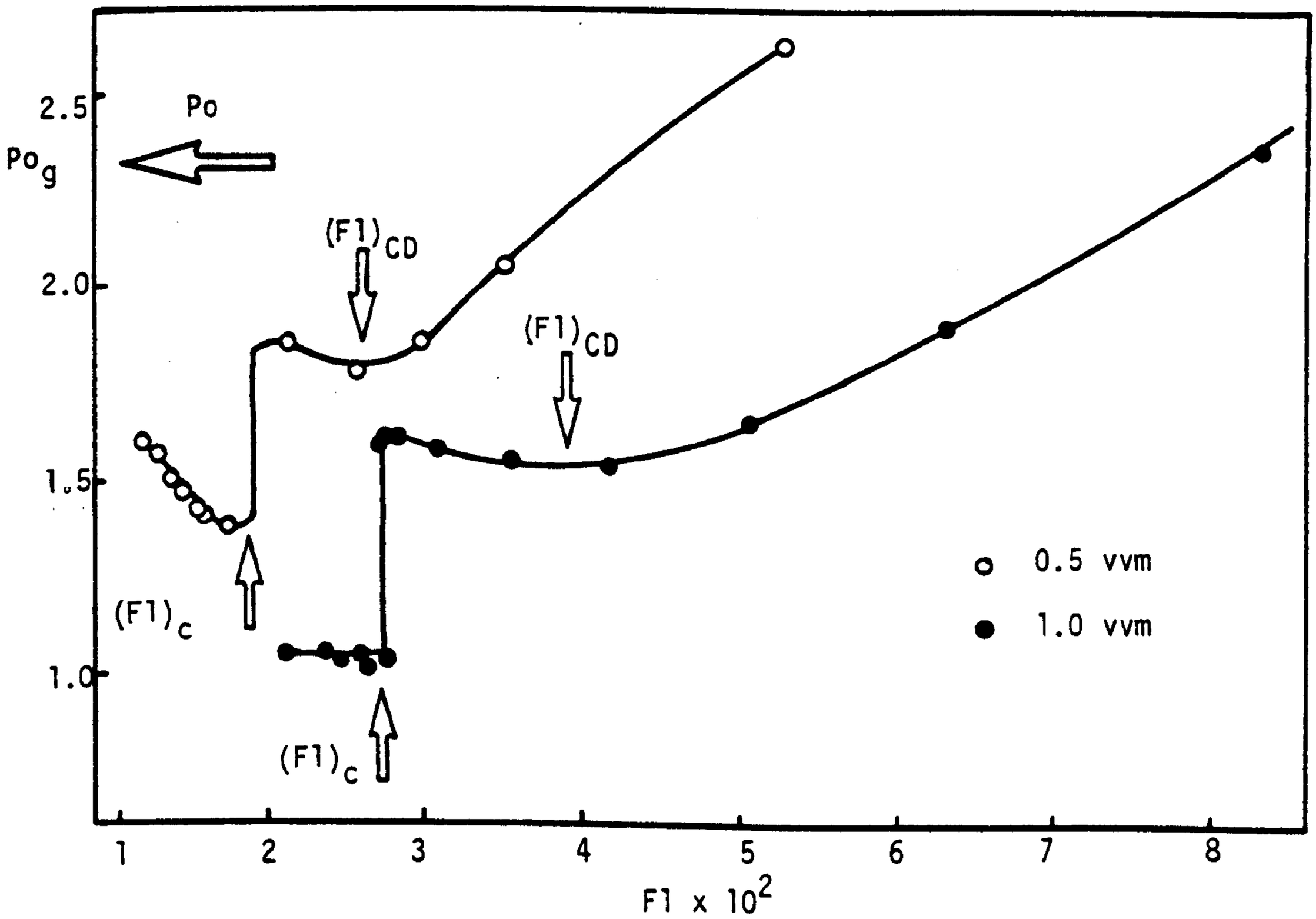

Fig. 3.17 Power Number versus Flow Number for the ADT Impeller (D = T/2, C = T/4, T_{56})

until N_{CD} was reached (Fig. 3.15c) and exceeded. At some speed in excess of N_{CD}, similar torque oscillations to those previously described (Fig. 3.8) suddenly set in, corresponding to a change from the radial flow pattern (Fig. 3.15c) to the axial flow pattern (Fig. 3.15d). This axial flow pattern was equivalent to the unaerated pattern shown in Fig. 3.15a. The gas phase remained well dispersed at all times for $N > N_{CD}$ and the power demand eventually became steady again. Fig. 3.16 demonstrates the effect this transition has on the power number-flow number plot.

The flow demonstrated in Fig. 3.15a has previously been noted in smaller vessels at lower clearances[2] and appears to be caused by the discharge stream dipping immediately it leaves the impeller region and flowing along the base until it turns up at the wall. Thus the introduction of gas must reduce the pumping capacity of the impeller such that the lower part of the discharge stream cannot dip until a sufficiently high impeller speed is reached(which was above N_{CD} and the associated minimum in Fig. 3.16 in all the cases examined) to restore the necessary discharge rate and transform the flow pattern. The drop in power number is logical considering the lower power number of impellers producing this type of flow.

All the work carried out with disc turbine impellers confirmed that the visually observed minimum speed for dispersion, N_{CD}, was attained at the same speed, or at slightly lower speeds than those which corresponded to the minimums in the gassed power number-flow number curves. Thus for the purpose of this thesis, it will be considered that the minimum in the gassed power number-flow number curves corresponded with N_{CD}.

Angle-bladed Disc Turbine (ADT)

This impeller (D = 0.28 m, C = 0.14 m = T/4) followed exactly the dispersion mechanism depicted in Fig. 3.15 for the disc turbine.

In this case the blade angle promotes the downward axial component of the discharge stream, which is overcome by the gas at low speeds. Fig. 3.17 shows the power number-flow number plot which is also identical to that for the disc turbine (Fig. 3.16) but with power numbers reduced to approximately one half of the value for a geometrically similar disc turbine system at $N < N_C$. At the transition speed a 30 - 40% fall in power number occurs and thereafter for $N > N_C$, the ADT power number is only a third of that of the disc turbine.

Additional checks at higher impeller clearances indicated a stable, predominantly radial double-looped type flow (as with the standard disc turbine) independent of gas rate, due to the discharge stream impinging on the wall before reaching the base and therefore turning downward.

Wisdom[3] has shown that within the well mixed regions, that is $N_R > N > N_{CD}$, the volume of gas in the impeller region is approximately proportional to the flow number. Since the transition speed (N_C) always occurred within this regime, a very simple model can be developed to predict N_C.

The total volume of the impeller region will be equal to δD^3 where δ is related to the blade dimensions. For a given gas rate, Q, the volume of gas in the impeller region is given by the product of the total volume (δD^3) and the ratio of gas flow to total output,

i.e. Volume of gas in impeller region = $\delta D^3 \frac{Q}{\delta N D^3}$ 3.12

Thus the volume of liquid in the impeller region is given by the difference between the total volume and the gas volume:

$$\text{Liquid volume in impeller region} = \delta D^3 - \left[\delta D^3 \frac{Q}{\delta N D^3}\right] \qquad 3.13$$

It then follows that:

$$\text{Liquid pumping rate} = N\left[\delta D^3 - \frac{Q}{N}\right] \qquad 3.14$$

Logically, Eqn. 3.14 reduces to the total output rate, (δND^3) minus the gas flow rate (Q). If the flow transition occurs at a speed, N_C, where the liquid pumping rate of the impeller just equals some critical value (e.g.β m^3s^{-1}) and is therefore sufficient to restore an axial type flow pattern, then:

$$N_C(\delta D^3 - \frac{Q}{N_C}) = \beta \qquad 3.15$$

i.e. $$Q = \delta D^3 N_C - \beta \qquad 3.16$$

Unfortunately only a very limited amount of data were obtained for both the ADT and the 0.187 m DT. This data is presented in Fig. 3.18 and an interesting result is that the gradient of the line through the disc turbine data gives a δ value of 0.115. An idea of the actual value of δ is given by the volume swept out by the impeller blades, that is:

$$\delta D^3 = \left[\frac{\pi D^2}{4} \times \frac{D}{5}\right] - \left[\frac{\pi}{4}\left(\frac{D}{2}\right)^2 \times \frac{D}{5}\right] = 0.118\ D^3 \qquad 3.17$$

i.e. $$\delta = 0.118 \qquad 3.18$$

Significantly more data are needed to confirm this approach, which obviously breaks down for D = 0.28 m where no flow transition was observed.

3.5.6. Dispersion Speeds

The definition of N_{CD} in relation to each impeller system has been dealt with in previous sections. Fig. 3.19 draws all the data together for two impeller sizes in T_{56}.

It is not surprising that the disc turbine disperses the gas at the lowest speeds. Nienow's correlation is in good agreement with experimental results, especially for the 0.28 m impeller. The angle-bladed disc turbine requires slightly higher speeds but both appear to have a similar dependence on gas flow rate. The 4 MFU impeller results show that N_{CD} is virtually independent of gas rate which concurs with the remarks made in Section 3.5.1. The data for the

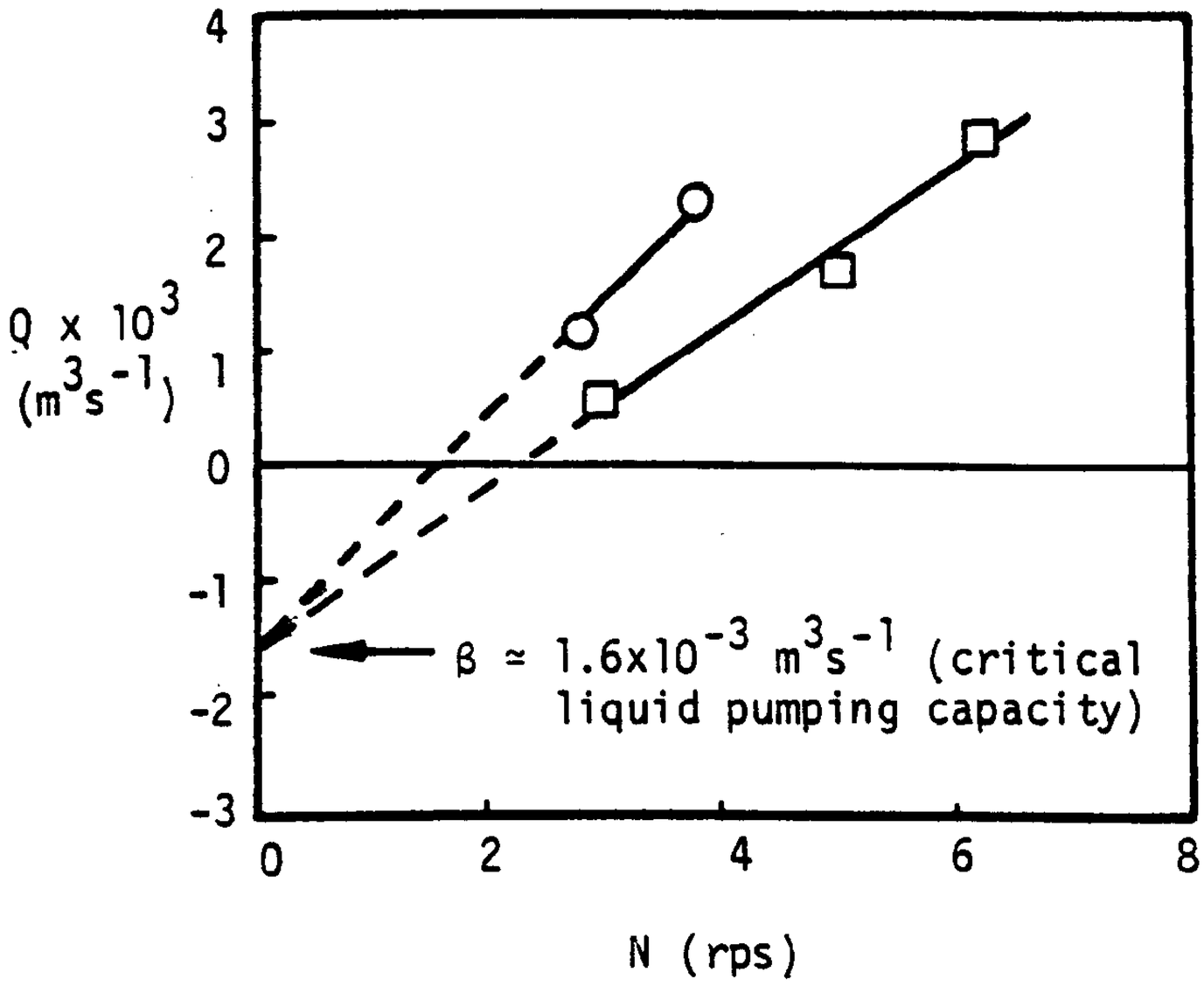

Fig. 3.18 Gas Rate versus Critical Speed for Flow Transition (T_{56})

□ DT D = T/3 c = T/6

○ ADT D = T/2 c = T/4

propeller are probably the most prone to error for reasons described earlier but follow a similar trend to the 4 MFD which requires the highest speeds to achieve dispersion. Fig. 3.20 demonstrates the magnified effect of these higher speeds in terms of the power demand necessary to disperse the gas for the larger impellers.

3.5.7. Holdup

The data reported here were obtained either in a two phase gas-liquid system or with a very low solids concentration (1 - 3% by weight). No effect of solids concentration on holdup was found at these low concentrations (see Chapter 5).

Fig. 3.21 shows that, for the 0.28 m impellers, holdup correlates very well with specific power (power per unit mass of liquid), irrespective of impeller type at a gas rate of 1 vvm. There is some divergence from the line at low specific powers, but, as shown in the figure, this generally occurs for $N < N_{CD}$ (or $\varepsilon_T < (\varepsilon_T)_{CD}$) where the gas flow dominates and makes accurate measurements more difficult. A similar treatment for gas rates of both 0.25 vvm and 0.5 vvm led to a clear power relationship of:

$$\varepsilon \alpha \varepsilon_T^{0.31} \qquad 3.19$$

The results for the 0.14 m impellers yielded the same power dependence but with wider scatter from the mean and slightly lower absolute values for a given gas rate and specific power input.

The holdup was then plotted against gas rate for all impeller types for specific power inputs of 0.5, 1.0 and 1.5 $W.Kg^{-1}$. This yielded a 0.67 power dependence on gas rate. Thus:

$$\varepsilon \alpha \varepsilon_T^{0.31} Q^{0.67} \qquad 3.20$$

This relationship is commonly expressed in terms of superficial gas velocity, V_S, and if so produces the following relationship (Eqn. 3.21) which is shown in Fig. 3.22 along with the data for both impeller sizes and all three gas rates.

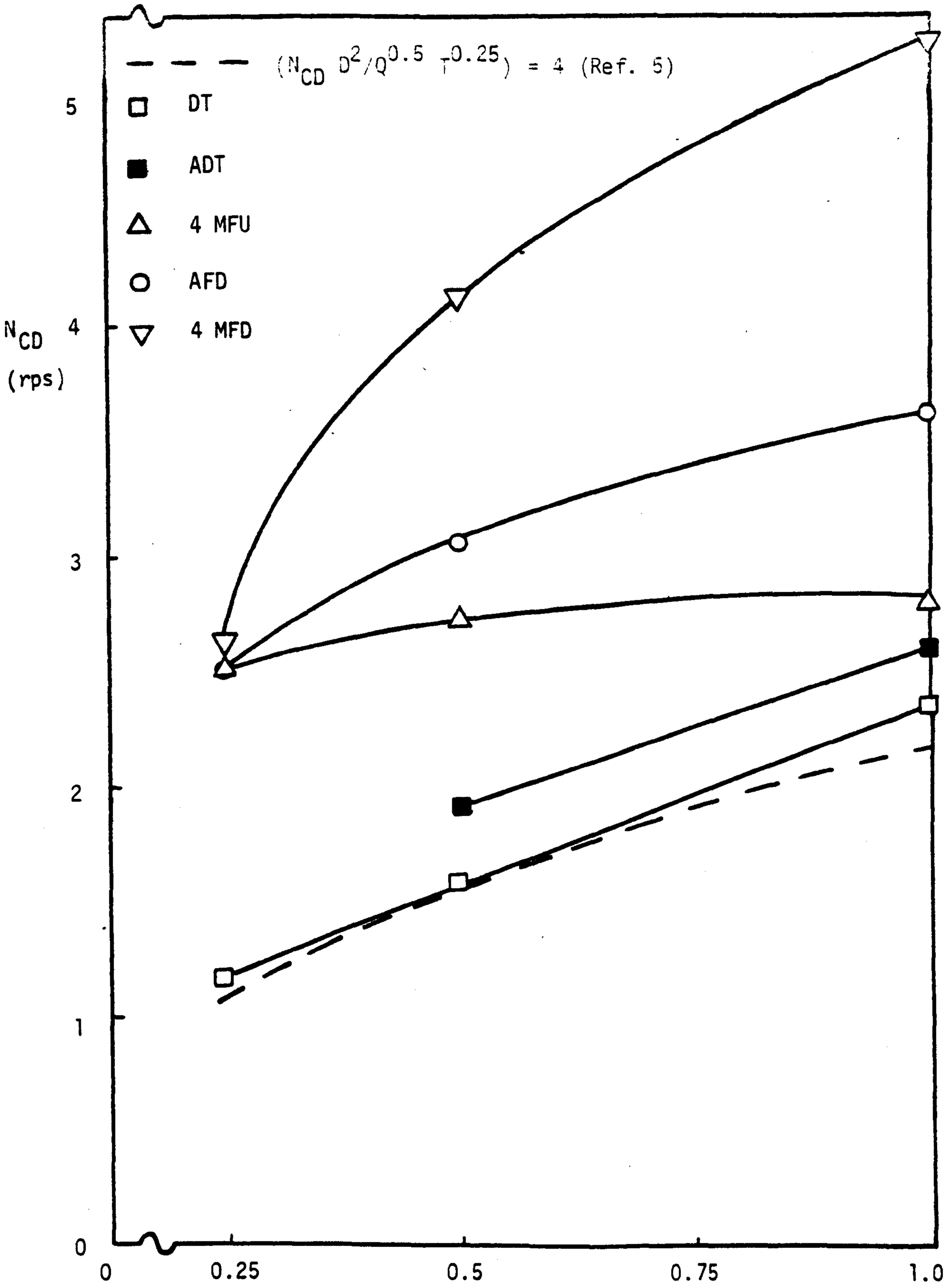

Fig. 3.19a N_{CD} versus Q for Various Impeller Types
($D = T/2$, $c = T/4$, T_{56})

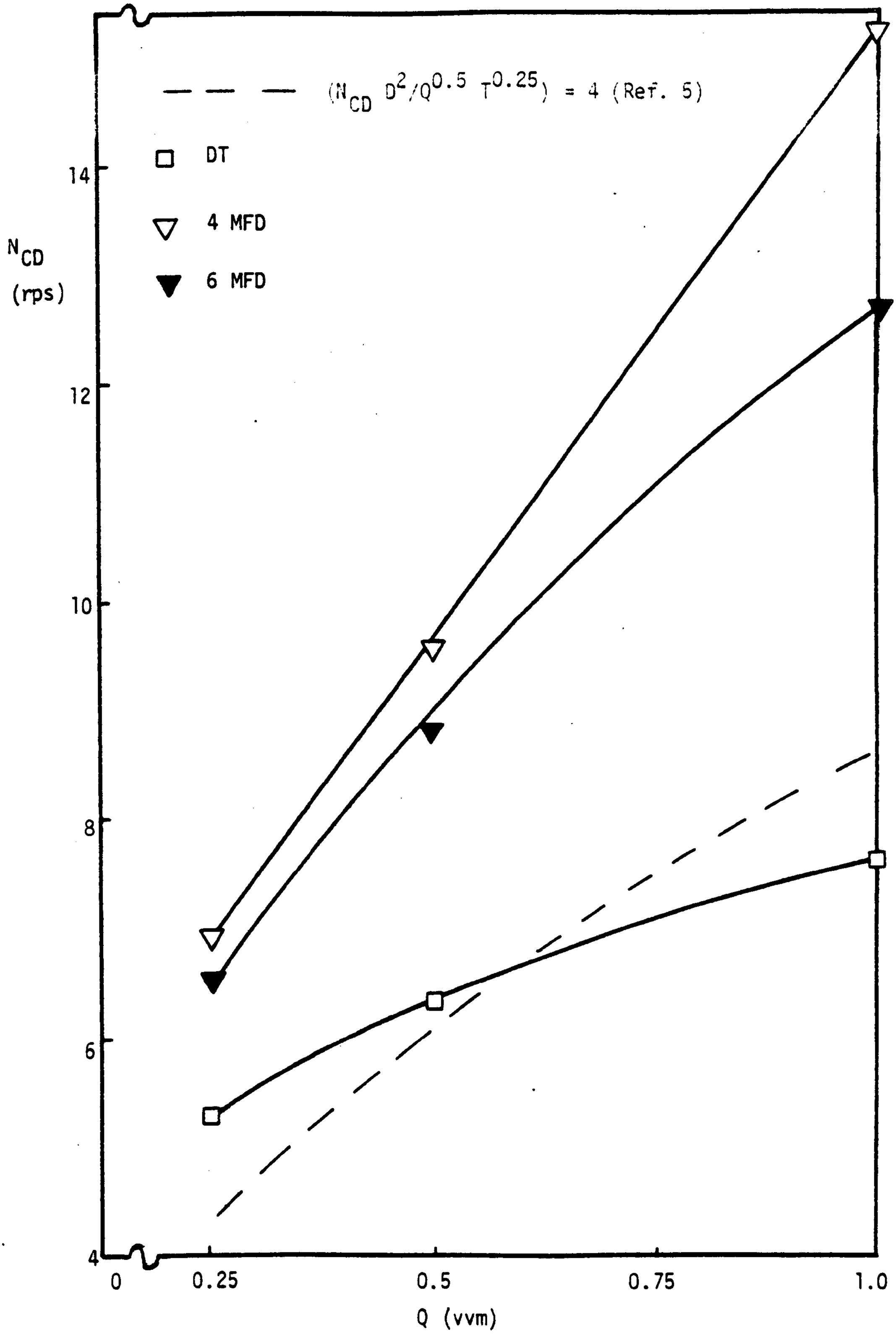

Fig. 3.19b N_{CD} versus Q for Various Impeller Types
($D = T/4$, $c = T/4$, T_{56})

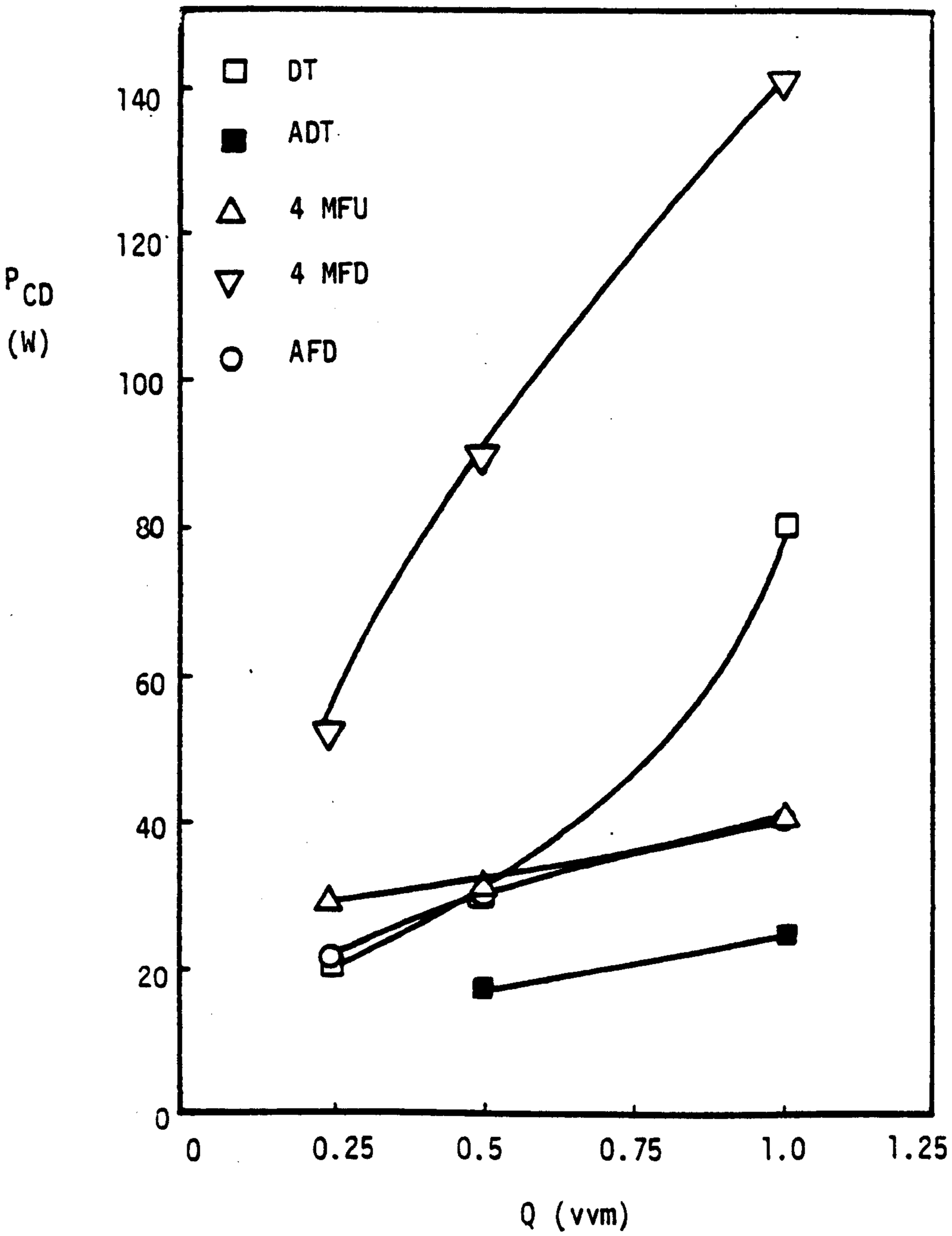

Fig. 3.20 Power Necessary to Achieve N_{CD} for Various Impeller Types

(D = T/2, c = T/4, T_{56})

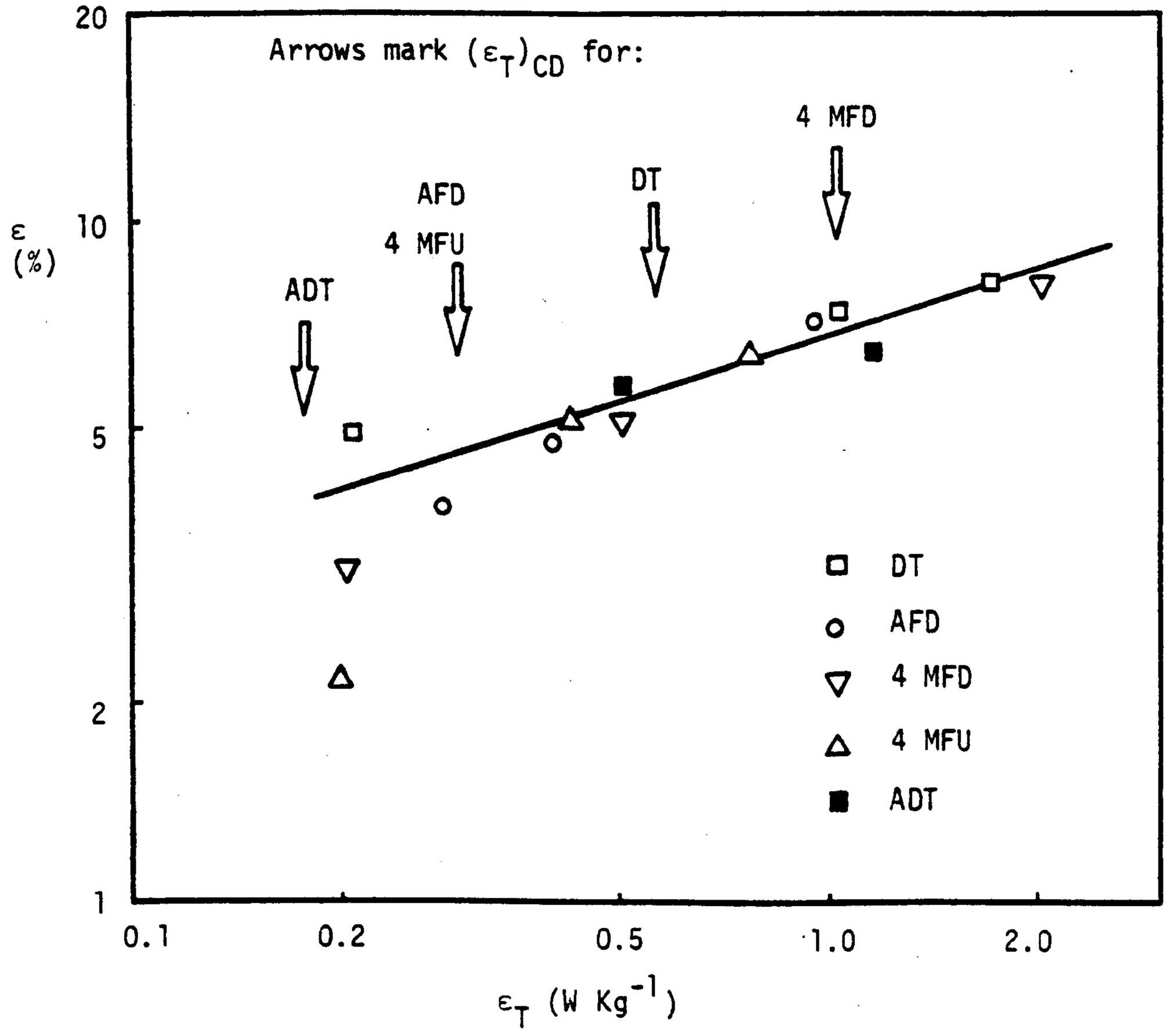

Fig. 3.21 Gas holdup (ε) versus Specific Power Input (ε_T) for all Impeller Types

(D = T/2, c = T/4, T_{56}, Q = 1.0 vvm)

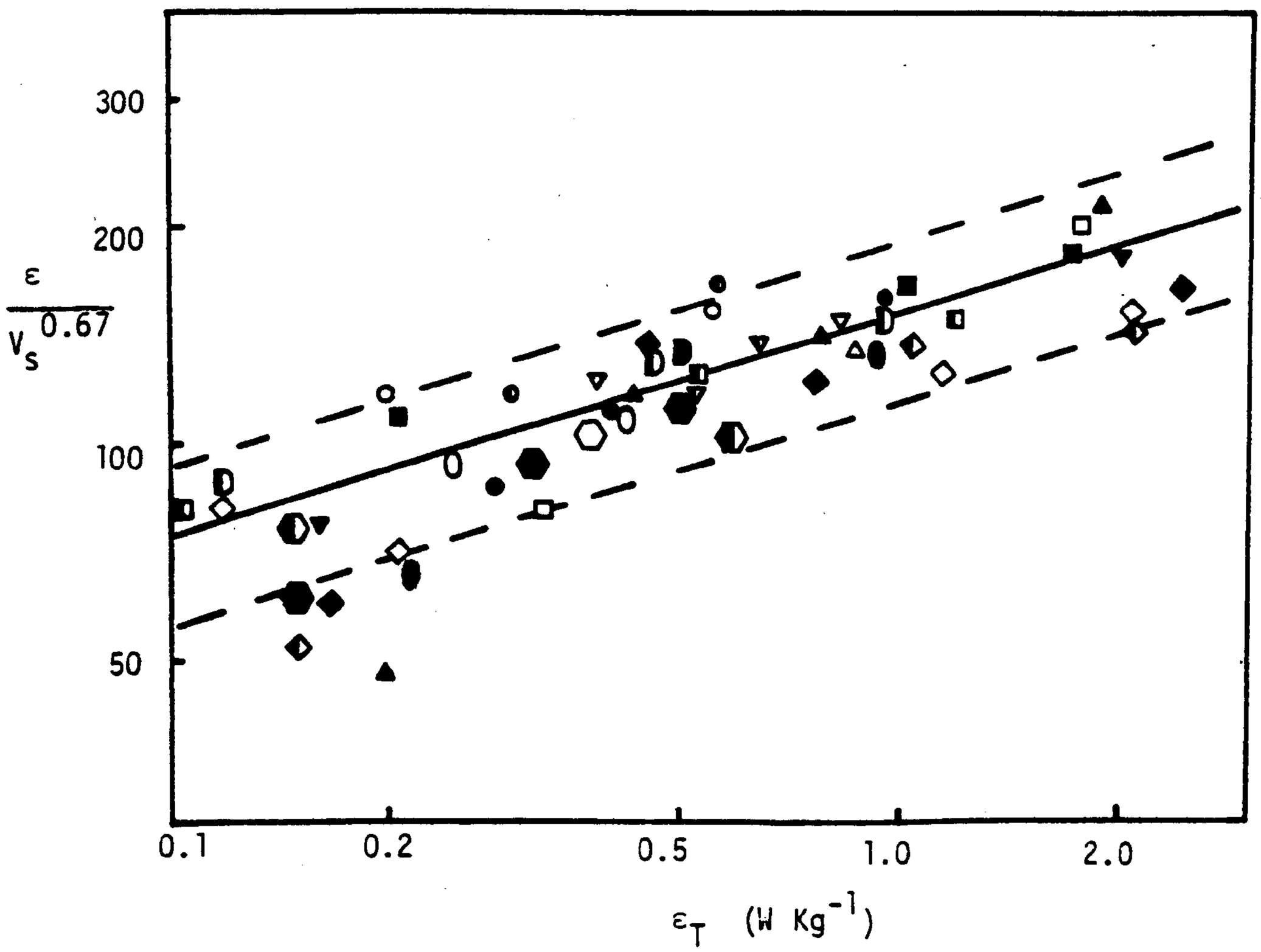

Fig. 3.22 Gas Holdup Correlation for all Impeller Types and Sizes in T_{56} (c = T/4)

□ DT, D = T/2

◇ DT, D = T/4

D ADT, D = T/2

o AFD, D = T/2

▲ 4 MFU, D = T/2

▽ 4 MFD, D = T/2

⬡ 4 MFD, D = T/4

O 6 MFD, D = T/4

Open Symbol = 0.25 vvm

Half Closed Symbol = 0.5 vvm

Closed Symbol = 1.0 vvm

$$\varepsilon = 17.9\ \varepsilon_T^{0.31}\ V_S^{0.67} \pm 25\% \qquad 3.21$$

The above expression is almost identical to Van't Riet's[22] relationship for several types of disc turbine:

$$\varepsilon = 13\ \varepsilon_T^{1/3}\ V_S^{2/3} \qquad 3.22$$

Inspection of Fig. 3.22 shows that, except for a few results, again at very low power inputs, all the data falls within a 25% band either side of the line representing Eqn. 3.21. This is a reasonable spread considering that the experimental errors involved in measuring ε were sometimes of the order of $\pm$ 20%.

3.5.8. The Effect of Gas Rate on Power Consumption

Fig. 3.23 shows how gassed power falls with increasing gas rate for a constant impeller speed. The ratio Po_g/Po is proportional to P_g for reasons explained in Section 3.2.1. The significance of these curves in relation to particle suspension will be discussed in detail later (Chapter 7). However, their characteristic shapes confirm some of the observations made earlier in this chapter.

The curves for all the impellers (Fig. 3.23) were calculated for impeller speeds well above N_{CD}. The 4 MFD initially showed a gradual fall in gassed power, which became steeper as the dispersing effect of the impeller was overcome by the gas flow. A further increase in gas rate produced little change in the gassed power since the gas flow completely dominated the impeller pumping action.

The propeller showed an increase in power on the admission of gas to the system as mentioned previously, with a gradual fall-off as gas rate increased further. The power consumption of the 4 MFU was fairly independent of gas rate until sparge rate exceeded 0.5 vvm. The standard disc turbine produced a continuous gradual decline in gassed power. Too few data were collected for the ADT to warrant presentation in this figure.

The 0.14 m impeller curves (Fig. 3.23b) were also calculated at

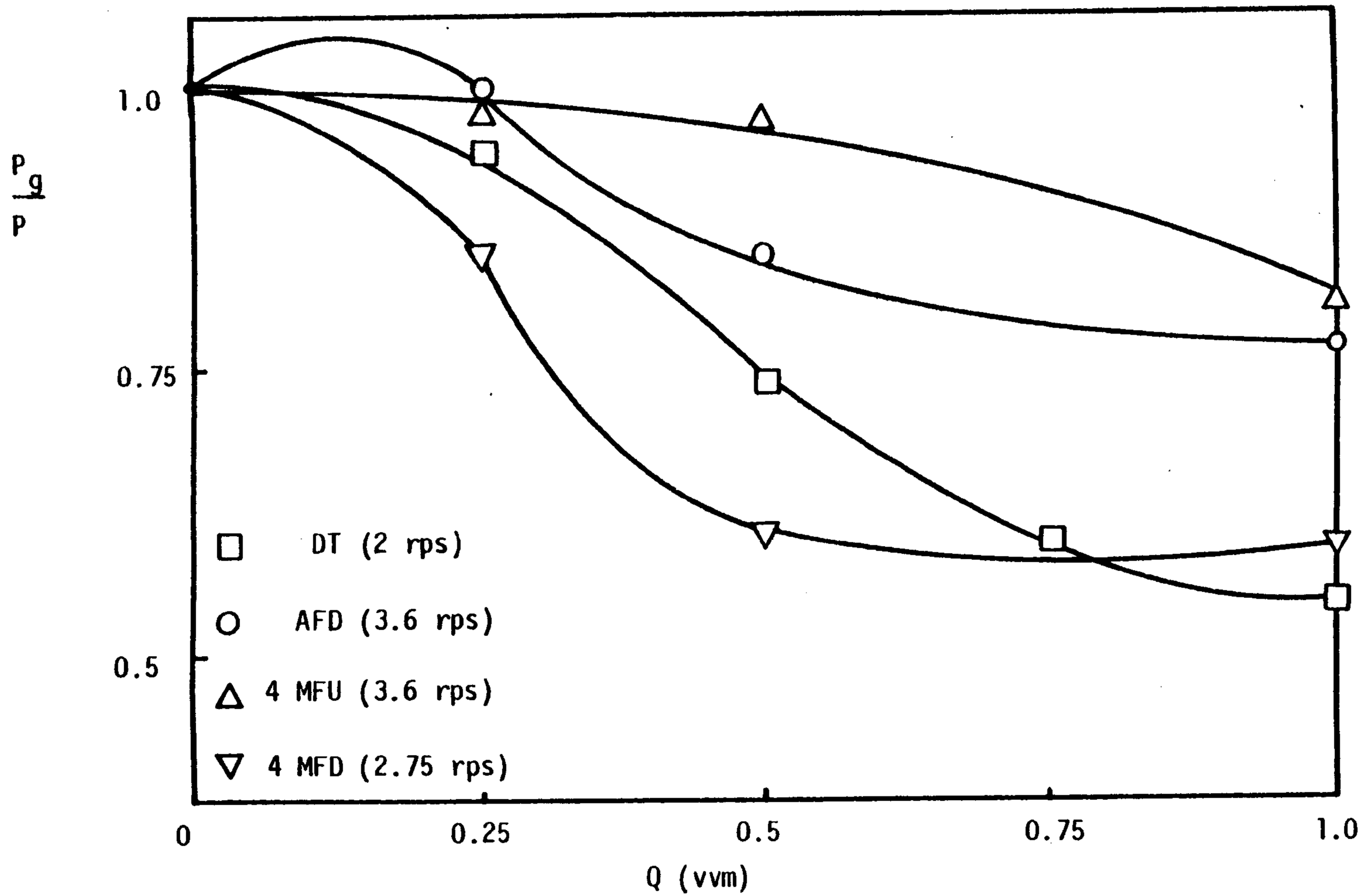

Fig. 3.23a Decrease in the Gassed to Ungassed Power Ratio (P_g/P) with Aeration Rate ($D = T/2$, $c = T/4$, T_{56})

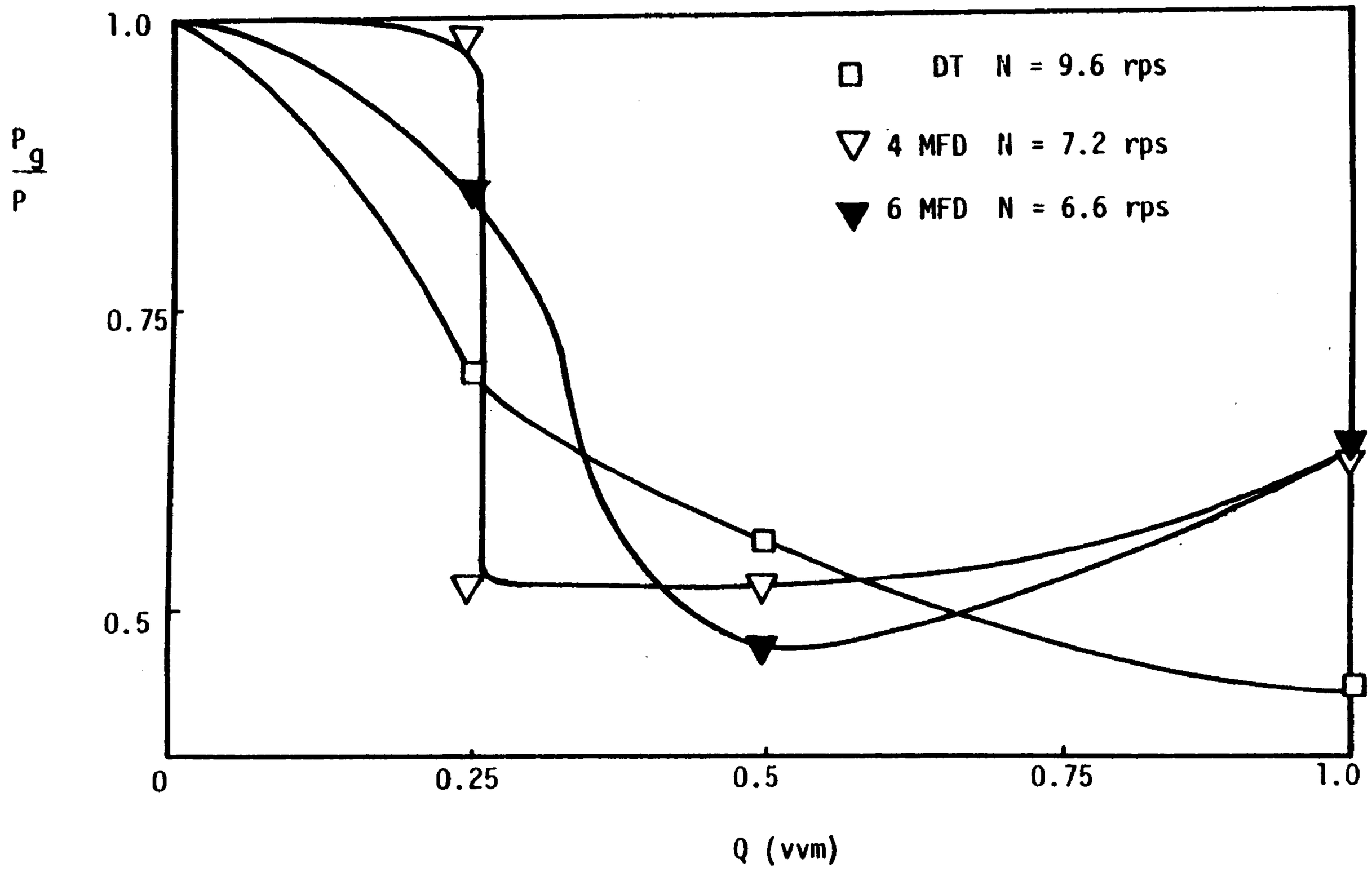

Fig. 3.23b Decrease in the Gassed to Ungassed Power Ratio (P_g/P) with Aeration Rate ($D = T/4$, $c = T/4$, T_{56})

$N > N_{CD}$. Again the disc turbine showed a gradual decrease in gassed power with increasing gas rate, only starting to level out as the impeller became flooded with gas at $Q \simeq 1$ vvm. Both the mixed flow impellers produced a sudden drop in gassed power as the gas phase changed from being dispersed to "chimneying" up the shaft. Thereafter the power demand levelled off and then rose slightly for further increases in gas rate, caused by increasing opposition to the motion of the impeller.

Thus sharp drops in gassed power seem to be associated with a sudden decrease in the capability of the impeller to circulate fluid throughout the vessel. This results in the impeller flooding with gas in the case of the mixed flow impellers pumping downwards, producing a transition from a well dispersed gas phase to a non-dispersed gas phase.

3.6. Conclusions

Surprisingly, only the 4 MFD impeller was less energy efficient than the disc turbine with regard to gas dispersion. However, the criterion used to define N_{CD} for the AFD impeller was somewhat uncertain and the consequences of aeration with regard to particle suspension have yet to be established. Gas holdup was dependent only on gas sparge rate and specific power input, provided the gas phase was well dispersed, though axial and mixed flow impellers achieved lower specific power inputs due to their low power numbers.

The effect of bubble size and flow patterns on mass transfer coefficients must be assessed before impellers producing an axial component of flow can be recommended. This is done in Chapter 8. A major drawback of this type of impeller lies in the flow instabilities caused when the direction of gas flow is opposed to the direction of the impeller discharge.

CHAPTER 4.

SOLID-LIQUID SYSTEMS

4.1. Introduction

Both the experimental investigation and the theoretical-empirical modelling of particle suspension in an agitated liquid continuum have received much attention in the literature. However, all the theoretical models proposed have serious limitations and although various empirical correlations have been widely confirmed on small scale equipment, there is a paucity of data to support them on larger scale vessels.

A very large majority of the work referred to above has concentrated on the impeller speed, N_{JS}, necessary to just fully suspend the particles. Below this speed the total surface area of solid is not efficiently utilized and above this speed the rate of many transfer processes increases only slowly.[23,24]

The purpose of this chapter can be defined as follows:

1. To combine a review of the relevant literature with experimental observations to establish the major factors affecting particle suspension, with particular regard to those factors which may be influenced by aeration.
2. To report the data from the many runs carried out at zero gas rate in the course of the three phase work. Where these data confirm already well established results they will be dealt with briefly. On the other hand, the implications of the data that are not well established in the literature especially those relating to scale up and to a lesser degree, the use of mixed flow impellers, will be emphasized.

4.2. Literature Survey

4.2.1. Suspension Criteria

The definition of N_{JS} is commonly taken as the speed at which no

particle is visually observed to remain at rest on the tank base for more than one or two seconds.[2,6,25,26,27] A more recent and less subjective definition is the impeller speed for which the particle concentration just above the base of the vessel is a maximum,[28] or shows a discontinuity[29] with impeller speed. The estimation of this speed involves measuring local solids concentration in situ or by withdrawing a sample from the vessel. Bourne and Sharma[28] showed experimentally that for a wide range of geometries and particulate solids, a peak occurred when a graph of solids concentration in the withdrawn sample was plotted against impeller speed (Fig.4.1), provided the sample was withdrawn from near the base of the vessel.

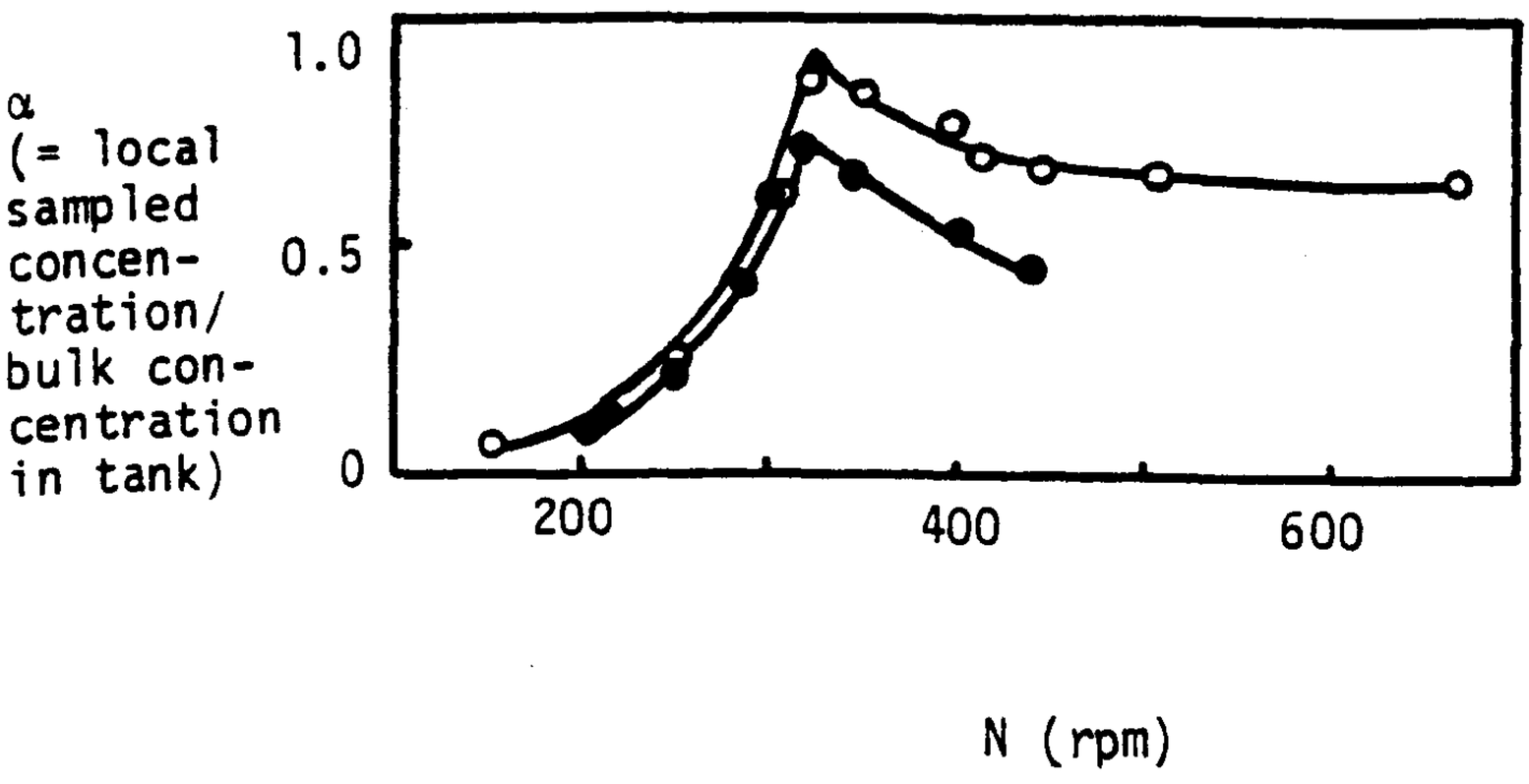

Fig. 4.1 Local Particle Concentration versus Impeller Speed for Two Sampling Locations[28]

The peak was found to coincide with the visually observed value of N_{JS}. Using a light transmission technique to measure concentration, Musil[29] obtained similar results in situ.

The maximum shown in Fig. 4.1 can be explained as follows. At low speeds the majority of the particles rest on the bottom, producing a very low concentration reading just above the base. As speed is increased so the particles are gradually suspended and hence the local concentration just above the base increases. Eventually a speed is reached when the source of particles on the base is practically exhausted but the upper regions of the dispersion have very low particle holdups. Thus further speed increases tend to homogenise the suspension and therefore reduce the local concentration near the base, producing a maximum as shown in Fig. 4.1. However, this rather idealized description does not always apply. Musil also noted that occasionally a 'kink' or discontinuity, in the form of a sharp decrease in gradient rather than a peak, would occur. In this case it was explained as being due to the conical tank base providing an additional source of particles at speeds above the critical suspension speed.

4.2.2. Correlations and Theories

The work of Zwietering in 1958[6] still represents the most complete investigation on N_{JS} (1 - 2 seconds on base criterion) in terms of both the variety and range of variables studied (Table 4.1). He completed over a thousand experiments in systems of similar geometry to those examined in this work, and analysed the results using dimensional analysis to yield a purely empirical expression for N_{JS} (Eqn. 4.1)

$$N_{JS} = \frac{S\, \nu^{0.1}\, d_p^{0.2} \left[\frac{\Delta\rho\, g}{\rho_L}\right]^{0.45} X^{0.13}}{D^{0.85}} \qquad 4.1$$

Author	Impeller Type	Variable Range Investigated					
		D (m)	T (m)	$\Delta\rho$ (Kg m^{-3})	d_p μm	X % by wt.	$\mu x10^3$ (Kg $m^{-1}s^{-1}$)
Zwietering[6]	AFD, DT, Vaned Disc, 2 bladed Paddle	0.06-0.2	0.15-0.6	560-1810	125-850	0.5-20	0.32-9.3
Conti and Baldi[30]	8 bladed DT 8 bladed ADT	0.024-0.076	0.12-0.23	1414-1800	42-1200	2-20	0.645-7.8
Nienow[2,32]	DT, 4 MFD, 2 blade Paddle	0.035-0.145	0.14-0.29	530-1660	153-9000	0.1-10	1.0
Narayanan et al.[25]	8 bladed flat Paddle	0.035-0.07	0.11-0.14	140-1600	106-600	2.5-20	1.0
Subbarao and Taneja[33]	AFD	0.051	0.16	1666-2010	63-3070	30 (by vol.)	1.0
Musil and Vlk[34]	3 MFD (24^o) 6 MFD	0.15-0.315	0.6	-	700-1100	4-8	-
Weisman and Efferding[27]	6 blade paddles	0.051-0.10	0.14-0.29	-	45-140	-	-

Table 4.1 Experimental Conditions Investigated by Various Authors

The exponents of ν, d_p, $(\Delta\rho\ g/\rho_L)$ and X were found to be independent of impeller type, vessel size, impeller clearance and impeller to tank diameter ratio. The dimensionless constant, S, accounted for these system geometry variables. Graphs were presented giving S values for five impeller types at various impeller to tank diameter ratios (D/T) and various impeller clearances (c). It was found that in all cases except one, S (and hence N_{JS}) was reduced as the impeller was positioned closer to the base. The surprising exception was the disc turbine impeller which was reported to have S values independent of c for $T/7 \leq c \leq T/2$. Nienow[2] has since shown that disc turbines do indeed show a reduction in S with decreasing clearances, due to increased flow near the vessel base.[38]

The extensive range of geometries examined by Zwietering, together with the advantage of having an expression (Eqn. 4.1) which allows N_{JS} to be estimated for a wide range of conditions has resulted in this work being the most widely recommended basis for design.[31] At first sight, the purely empirical approach adopted appears to preclude any insight being gained into the mechanisms responsible for causing suspension. However, the very fact that all the parameters specifying the liquid and particle properties have the same exponents independent of the agitation geometry at least suggests that the same mechanism applies to all the geometries investigated. Several attempts have been made to theoretically model a mechanism describing suspension. It is through these that an understanding of some of the phenomena at work can be gained.

Narayanan et al.[25] derived an expression for N_{JS} based on a balance of the vertical forces acting on a particle, assuming no slip between the particle and the fluid. However, the necessary knowledge of fluid velocities was obtained from the mean circulation time data of Holmes et al.[39] and does not consider the local conditions on the

vessel base. Subbarao and Taneja[33] recently proposed a fairly simplistic model based on a balance of the fluid velocity and particle settling velocity for a propeller agitated system. The particle settling velocity was estimated from a correlation for the porosity of a liquid fluidised bed as a function of liquid velocity. The experimental data, however, does not fit the postulate well, even after some empirical adjustments.

Two other theoretical approaches have been based on energy balances. Kolar[37] proposed that the mixing energy at the critical condition was related to the energy dissipated by a particle moving at its terminal settling velocity in a still fluid. The obvious drawback of this approach is the relevance of this settling velocity to the actual settling velocity in a highly turbulent dispersion.

Perhaps the most successful attempt is due to Baldi et al.[26] They postulated that suspension was due to turbulent eddies which had a scale of the order of, or proportional to, the particle size. Energy transferred to the particles from these eddies lifted them off the base to a height proportional to the particle diameter, from which they were suspended. Thus an energy balance could be performed on the basis that the kinetic energy imparted by the eddies was proportional to the potential energy gained by the particle. This energy balance led to the specification of a dimensionless group Z,(Eqn. 4.2) which was related to the ratio of the energy dissipated on the tank base, $(\varepsilon_T)_B$ (responsible for suspension) to the average energy dissipation in the tank (ε_T).

$$Z = \left[\frac{\Delta\rho\ g}{\rho_L}\right]^{1/2} \frac{T\ d_p^{1/6}}{P_o^{1/3}\ D^{5/3}\ N_{JS}} \qquad 4.2$$

If $(\varepsilon_T)_B$ is proportional to ε_T, then it implies that Z is a constant, which coincides with the empirical relationship put forward by Kneule[23] for predicting the optimum impeller speed for the dis-

solution of salt crystals. However, Baldi et al. related $(\varepsilon_T)_B$ / ε_T to a modified Reynolds number by analogy with the decay of turbulence downstream from a grid.

$$Re^* = \frac{D^3 N_{JS}}{\nu T} \qquad 4.3$$

Experimental data obtained with eight bladed disc turbines (and later angled blade disc turbines[30]) showed Z to be a function of Re^*, with the nature of the function itself generally dependent on system geometry (Eqns. 4.4, 4.6). Nevertheless, providing the above relationship is known, an expression for N_{JS} can be deduced from their work (Eqns. 4.5, 4.7). The dependence of N_{JS} on particle concentration, X, was not accounted for in the model, but allowed for empirically and agreed very closely with Zweitering's relationship.[6]

Two examples of their results are given below:

1. Eight-bladed disc turbine, C/D = 0.5:

$$Z = \text{constant} \simeq 2 \qquad 4.4$$

$$\text{i.e. } N_{JS} = 1.03 \left[\frac{g\,\Delta\rho}{\rho_L}\right]^{1/2} \frac{d_p^{1/6}\, T\, X^{0.134}}{Po^{1/3}\, D^{5/3}} \qquad 4.5$$

2. Eight-bladed disc turbine, C/D = 1:

$$Z \propto (Re^*)^{0.2} \qquad 4.6$$

$$\text{i.e. } N_{JS} \propto \nu^{0.17} \left[\frac{g\,\Delta\rho}{\rho_L}\right]^{0.42} \frac{d_p^{0.14}\, T\, X^{0.11}}{Po^{0.28}\, D^{1.89}} \qquad 4.7$$

Thus these authors suggest that the exponents on the various parameters vary slightly with geometry but are nonetheless still very close to those proposed in Eqn. 4.1.

All attempts to model particle suspension described above can be thought of as utilizing one of two approaches. The first is the concept of drag forces exerted by the fluid on the particle. The second is the analysis of the turbulent properties of the system. Both approaches lack a rigorous method of relating the flow parameters

(velocity profiles, fluctuating velocities, dissipation rates, etc.) on the base of the vessel - from where particles are suspended - to their values at the impeller which are more easily measured. It may simply be the case that the method employed by Baldi et al.[26] to achieve this by employing the Re^* concept is superior to, for instance, Narayanan's approach, utilizing mean circulation times, since comparison of the exponents on various parameters (Table 4.2) shows that Baldi's model (Eqns. 4.5 and 4.7) comes closest to the experimental values found by Zwietering.[6] Also, visual observation of the base supports the concept that suspension is due to random turbulent motion, particularly for radial flow impellers.

Author	Exponent on X	ν	Δρ	d_p	D (T constant)
Zwietering[6]	0.13	0.1	0.45	0.2	-2.35(R) -1.67 (A)
Nienow[2]	0.12	-	0.43	0.21	-2.25 (R)
Pavlushenko[35]	-	0.2	-	0.4	-2.5 (A)
Oyama[36]	≈ 0	-	1.0	1.3	-1.67 (?)
Weisman[27]	0.17	terminal velocity			< -1.67 (R)
Kneule[23]	0.17	-	0.5	0.17	-1.67 (M)
Kolar[37]	0.10	terminal velocity			-2.24 (A, M)
Narayanan[25]	0.22	-	0.5	< 0.5	-2.00 (R)

R - Radial flow impeller. A - Axial flow impeller. M - mixed flow impeller

Table 4.2[31] Exponents Found by Other Authors

The well established efficiency,in terms of power consumption, with which axial flow impellers cause suspension, when compared with radial flow impellers[6,32], is somewhat confusing in the light of observations suggesting that these impellers produce higher flow but lower turbulence intensity than radial flow impellers.[40] This

would suggest that the enhanced drag forces resulting from the higher volumetric pumping rate of the axial flow impellers are primarily responsible for suspension. An alternative explanation might be that the path length between the impeller and the point from which particles are last suspended is less for an axial flow impeller, reducing the probability of the turbulent eddies decaying. Also, axial flow impellers invariably require a higher impeller speed to perform a given suspension duty[6] and it is only the very low power numbers which make them energy-efficient.

Many other postulates have been put forward for prediction of N_{JS}[27,41] but their criteria have been based on the position of the upper interface rather than suspension from the base, though the two are not necessarily connected. Perhaps a promising approach is consideration of the particle in relation to the boundary layers on the vessel base, but a recent attempt at analysing this situation[42] was not helpful.

On balance, Zwietering's[6] work remains the most useful in terms of estimating N_{JS}. However, consideration of Baldi et al's[26] theoretical approach does suggest that, assuming all other parameters are unaffected, the introduction of gas to the system, if resulting in a decrease in power number, would result in an increase in N_{JS} being necessitated, since, for constant Z, $N_{JS} \alpha Po^{-1/3}$.

4.3. Experimental

This chapter contains results obtained in all the tanks (see Chapter 2). However, once again the bulk of the work was carried out in T_{56} and where results were obtained from other vessels it will be clearly stated. All the experimental data are contained in Appendix 1.

The critical impeller speed at which the particles were just-suspended, N_{JS}, was determined visually by observing the base of the

tank via a mirror placed directly underneath it. The base was illuminated by a Photoflood light to aid observation. N_{JS} was adjudged to have been reached when none of the particles remained at rest on the tank base for more than one to two seconds. This measurement was repeatable to approximately $\pm$ 5% on average, though occasionally only to $\pm$ 10%. The position on the base from which the last particles were suspended depended on the impeller geometry. The radial flow impellers suspended particles last from an annulus around the centre of the base, particularly at the 4 points in line with the baffles. The axial and mixed flow impellers tended to suspend the last particles from around the periphery.

The speed at which the concentration near the base reached a maximum, designated N_{PJS}, was also measured. However, the results presented in this chapter were all obtained by visual observation of the base as described above. The experimental details and results relating to N_{PJS} are presented in Chapter 5 along with the three phase data, allowing a more detailed comparison between N_{JS} and N_{PJS}.

4.4. Results

The results will be presented in three sections. The first will briefly deal with the effect on N_{JS} of varying particle and liquid properties. The next section will deal with system properties such as impeller type, geometry and scale. The final section will draw together all the data for comparison with the work discussed in Section 4.2.2.

4.4.1. Particle and Liquid Properties

Particle Density

Examination of Eqns. 4.1 and 4.5 shows $\Delta\rho$ ($=\rho_S-\rho_L$), the density difference between the solid and the liquid phases, to be the most influential of the particle parameters on N_{JS}, in that it has the highest exponent. Since the liquid medium was water in every case,

the $\Delta\rho$ term was varied by using particles of very different densities, allowing a range of $50 \leq \Delta\rho \leq 1900$ Kg m^{-3} to be examined. A linear regression analysis of the data for seven different particle densities gave:

$$N_{JS} \propto \Delta\rho^{0.40} \qquad 4.8$$

with a correlation coefficient of 0.96 (Fig. 4.2). This is slightly lower than previous exponents but was obtained over a much larger range for $\Delta\rho$. The data used in the analysis were standardized to a particle diameter of three hundred microns and concentration of 1% using a D = T/3 disc turbine by means of the relationships presented in this section.

Particle Concentration

Particle concentration, X, was varied over a ten fold range for the D = T/2 disc turbine (3 - 30%) and also from 1 to 3% for the D = T/3 disc turbine. Though a higher exponent ($N_{JS} \propto X^{0.14}$) was found for the D = T/3 impeller, considerably less data over a narrower range was available than for the D = T/2 DT, which gave $N_{JS} \propto X^{0.11}$ (Fig. 4.3). Combination of these data with those available for the 4 MFU and the 4 MFD at 3% and 20% gave an average exponent of 0.12.

i.e. $$N_{JS} \propto X^{0.12} \qquad 4.9$$

Zwietering defined X slightly differently, as the mass ratio of solid to liquid, multiplied by 100, compared to the definition here and elsewhere[2,26] of mass ratio of solid to suspension, multiplied by 100. The effect of interchanging definitions with a constant exponent is, however, very small, even at high X, due to the very weak dependence of N_{JS} on concentration.

Particle Diameter and Size Distributions

Once again, good agreement was obtained with previous workers. Size was varied over nearly a thirty fold range (Fig. 4.4) and the relationship found to be:

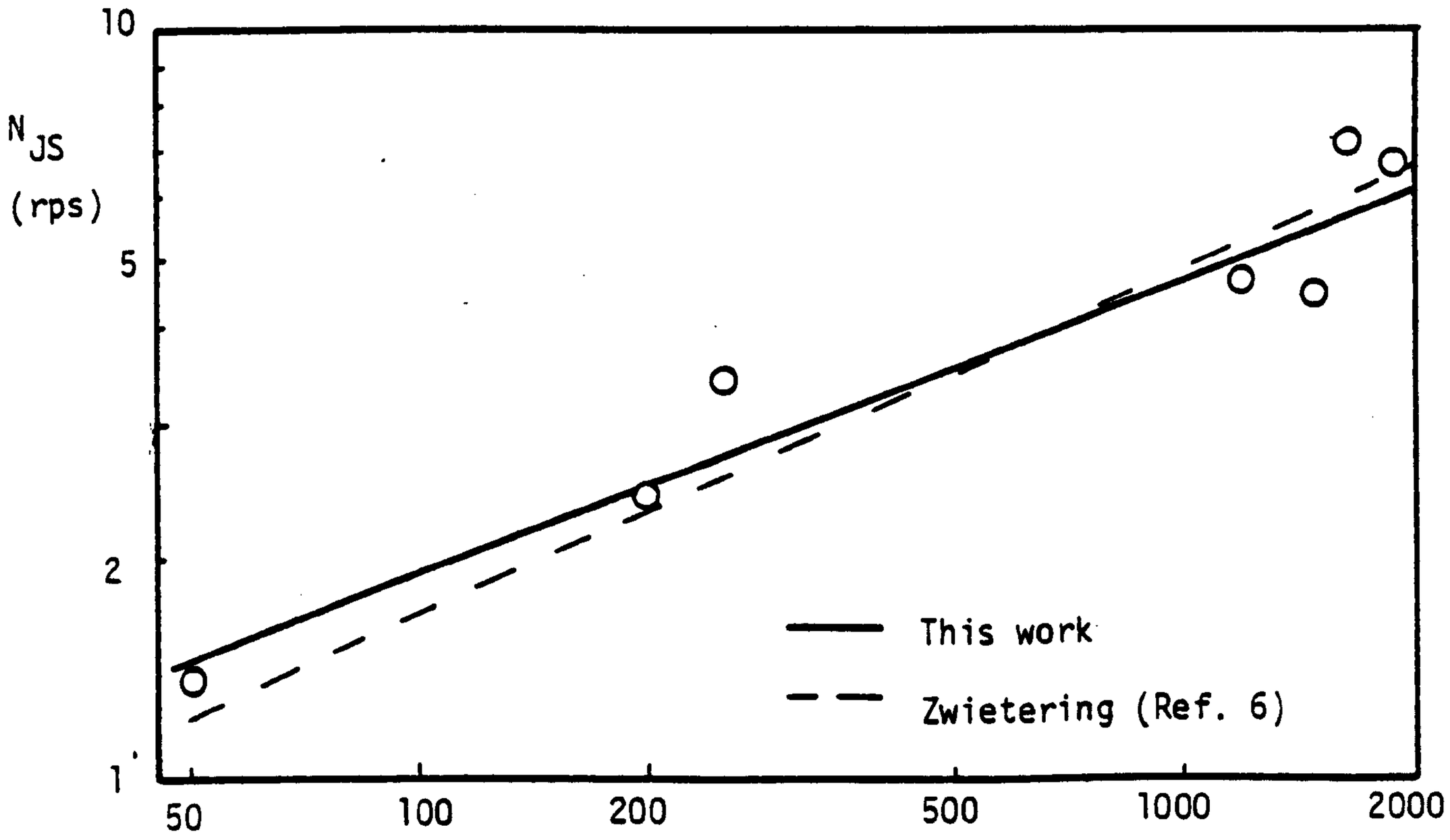

Fig. 4.2 The Relationship between N_{JS} and $\Delta\rho$
(T_{56}, D = T/3, c = T/4, DT, X = 1%, d_p = 300 μm)

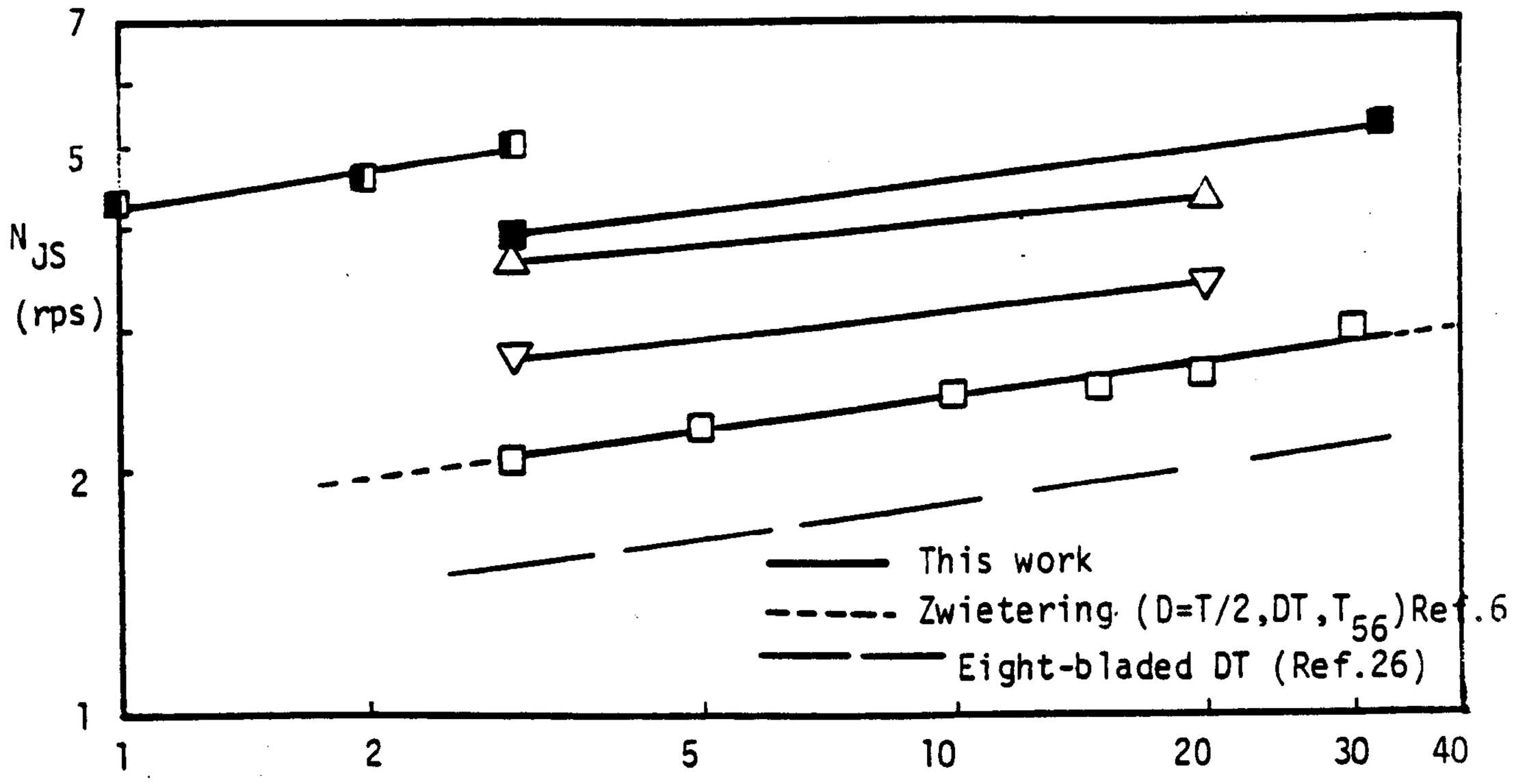

Fig. 4.3 Relationship between N_{JS} and X
(T_{56}, c = T/4, d_p = 206 μm, Δρ = 1480 Kg m^{-3})

■ D = T/2 DT, T_{29} ▽ D = T/2 4 MFD, T_{56}

◧ D = T/3 DT, T_{56} △ D = T/2 4 MFU, T_{56}

□ D = T/2 DT, T_{56}

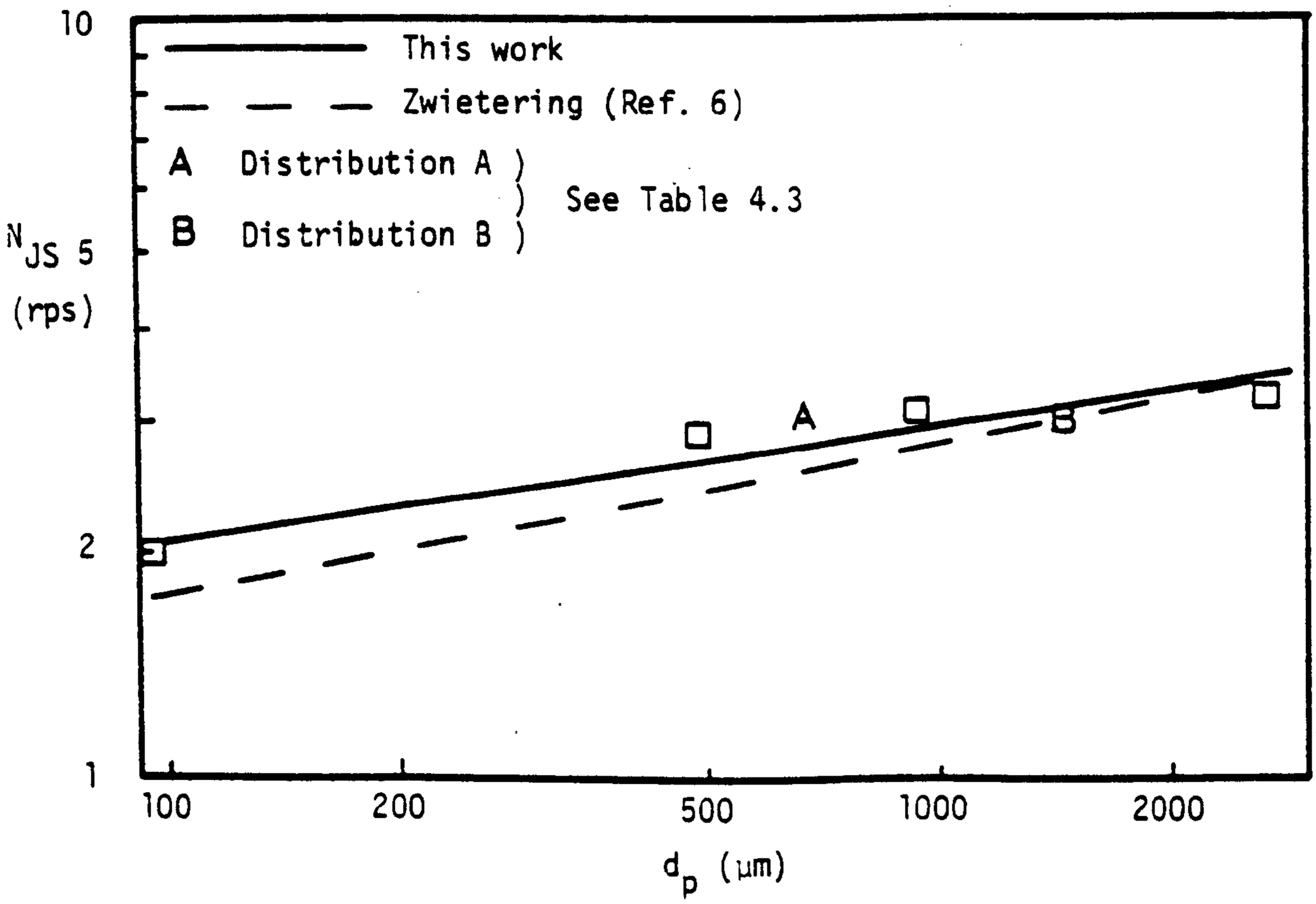

Fig. 4.4 The Relationship between N_{JS} and d_p
(D = T/2 DT, T_{56}, c = T/4, X = 1%, Δρ = 1900 Kg m^{-3})

$$N_{JS} \propto d_p^{0.15} \qquad 4.10$$

with a correlation coefficient of 0.95.

Very little work has been reported on the behaviour of wide size distributions, though Baldi et al.[26] observed a bimodal distribution to behave similarly to a unimodal distribution with a mean diameter calculated on the basis of mass percentage. Table 4.3 gives details of the distributions used in this work, both of which had a Sauter mean diameter of 485 microns.

d_p (μm)	Mass fraction A	B
92.5	0.050	0.111
485	0.505	0.189
925	0.445	0.300
2650	0	0.400
Sauter Mean d_p (μm)	485	485
Mass Mean d_p (μm)	660	1440
N_{JS} (rps)	3.07	3.0

Table 4.3 Size Distributions

The N_{JS} results for distributions A and B are plotted as A and B respectively in Fig. 4.4 according to their mass mean diameters, and tend to confirm Baldi's conclusion.

Particle Shape

With the exception of the anthracite, all the other particles were basically spherical or iso-dimensional in shape. The anthracite was very angular and predominantly flat in shape (see Chapter 2). Insufficient variety in shape was available to make an attempt at analysing the data in terms of a shape factor. A significant increase

in the speed and power required to suspend the anthracite was necessary over and above that predicted by the use of Eqns. 4.8, 4.9 and 4.10 with all other data. For example, a speed of 5.3 rps was required to just-suspend a 1% concentration of the particles with a D = T/3 disc turbine, compared to just 4.95 rps being required to suspend a 3% particulate dispersion of soda glass Ballotini with identical system geometry. Based on the anthracite result, N_{JS} for the Ballotini should have been 8.2 rps. The very sudden and spurting particle motion on the base was in contrast to the smoother fluctuations in movement associated with spherical particles.

Despite this significant effect, apparently due to shape, on N_{JS}, the effect of changing impeller diameter from D = T/3 to D = T/4 resulted in the relationship $N_{JS} \alpha D^{-2.5}$ which is very close to the dependence predicted by Zwietering when the S factor is accounted for ($N_{JS} \alpha D^{-2.35}$).

Liquid Viscosity

The kinematic viscosity was increased from 10^{-6} to 5×10^{-6} $m^2 s^{-1}$ in T_{29} but no significant effect on N_{JS} was observed. N_{JS} may have decreased slightly, but only by an amount equivalent to less than the experimental error involved in measuring N_{JS}. The configuration used was that for which Baldi et al.[26] predict N_{JS} to be independent of viscosity, though Zwietering finds a very weak dependence.

4.4.2. System Properties

Impeller Type

Table 4.4 lists the impeller speed and specific power input necessary to achieve N_{JS} with a 3% soda glass Ballotini suspension.

Impeller	N_{JS} rps	$(\epsilon_T)_{JS}$ W Kg^{-1}	Po (-)
AFD	3.55	0.33	0.5
4 MFD	2.75	0.35	1.4
ADT	2.67	0.54	2.2
DT	2.02	0.61	5.9
4 MFU	3.6	0.72	1.2

Table 4.4 Comparison of Impellers in T_{56}

$D \simeq T/2$ 3% soda glass Ballotini

Inspection of this table shows the axial and mixed flow impellers with the discharge stream downwards to be the most energy efficient, in accordance with all previous work. The 4 MFU, of which the discharge stream is directed away from the vessel base, is not surprisingly the least energy efficient, though not markedly less so than the disc turbine. However, an advantage of the 4 MFU, particularly over the AFD and the 4 MFD, was the increased homogeneity with high concentration dispersions. At low concentrations there was no visible difference between the homogeneity produced by each impeller type.

Impeller Diameter

Analysis of Zwietering's data for propellers and disc turbines shows that in the former case, $S \alpha (T/D)^{0.82}$, and in the latter, $S \alpha (T/D)^{1.5}$. If this information is combined with $N_{JS} \alpha D^{-0.85}$ (Eqn. 4.1), then for changing impeller diameter in a given system (constant T) we have:

$$N_{JS} \alpha D^{-1.67} \quad \text{- AFD impellers} \qquad 4.11$$

$$N_{JS} \alpha D^{-2.35} \quad \text{- DT impellers} \qquad 4.12$$

Results from the 0.14 and 0.28 4 MFD impellers in T_{56} produced good agreement with Zwietering's results (Eqn. 4.11) for a propeller,

giving (Fig. 4.5):

$$N_{JS} \alpha D^{-1.5} \qquad 4.13$$

Similarly the data from the three DT diameters (T/4, T/3 and T/2) in T_{56} and the T/2 and T/4 impellers in T_{29} (Fig. 4.5) yielded:

$$N_{JS} \alpha D^{-2.45} \qquad 4.14$$

These exponents are significantly higher than those proposed by Baldi et al. in Eqns. 4.5 and 4.6. However, this could be due to the differences in the impellers (eight blades against six here) or the nature itself of Baldi's postulate which proposes that the exponent is a function of C/D, and since C is kept constant in this work, then this suggests a changing exponent with impeller diameter.

The variation of the power required to just-suspend particles is often deduced from the above relationships on the basis that the power number (Po) is constant for all D, and thus for disc turbines from Eqns. 4.14 and 1.1:

$$P \alpha N^3 D^5 \Rightarrow P_{JS} \alpha D^{-2.35} \qquad 4.15$$

However, the data presented in Fig. 4.6 does not entirely support this prediction due partly to the power number changing with impeller diameter, as shown in Table 4.5.

T (m)	D (m)	Po (-)
0.56	0.28	5.95
0.56	0.187	5.5
0.56	0.14	5.1
0.29	0.145	4.8
0.29	0.097	3.15

Table 4.5 Variation of Po with D for Disc Turbine Impellers

Bates et al.[43] measured power numbers for radial impellers without discs and showed up to 20% variation in Po with impeller dia-

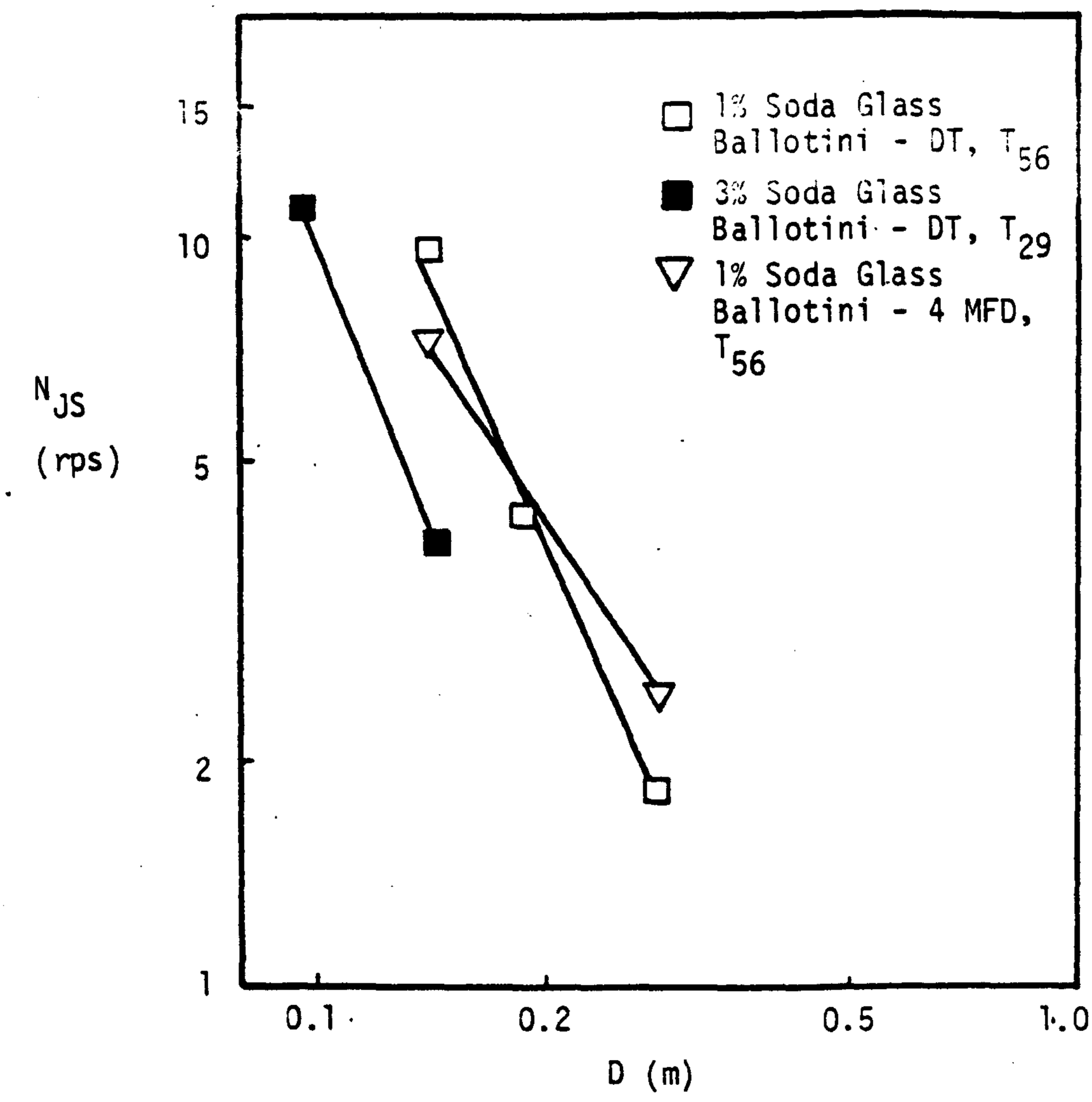

Fig. 4.5 Effect of Impeller Size on N_{JS} (c = T/4)

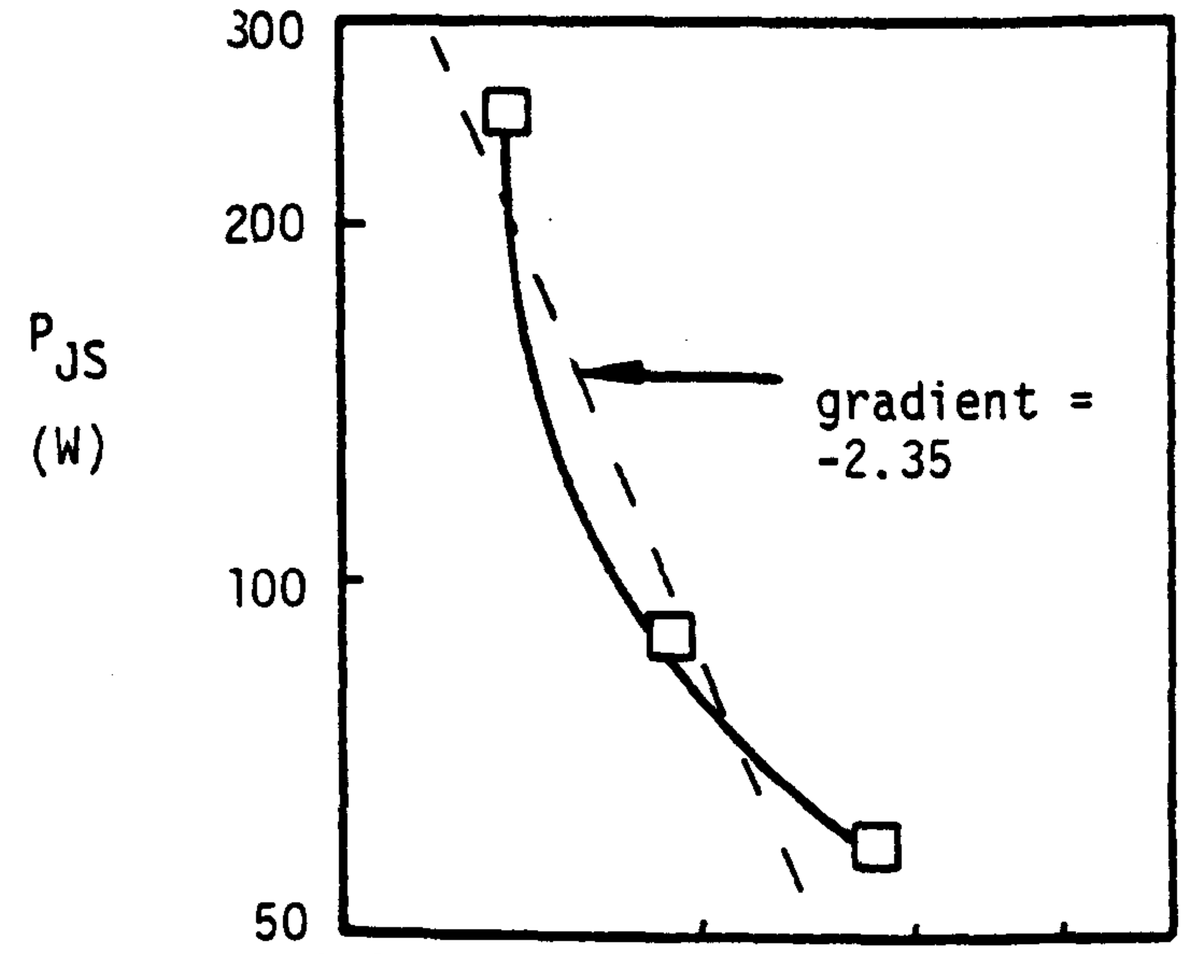

Fig. 4.6 Power Consumption to Achieve N_{JS} versus Impeller Diameter
(T_{56}, DT, c = T/4, 1% Soda Glass Ballotini)

meter. Nienow and Miles[38] also showed an increase in Po with D/T, and further pointed out the considerable effect that minor dimensions have on the power number, particularly the disc thickness to blade height ratio. The considerably lower values obtained in T_{29} (Table 4.5) could therefore be explained by the doubling of this ratio from 0.055 to 0.11 on scaling down from T_{56} to T_{29} for a T/2 impeller. This is further supported by the Po value of 5.9 obtained from T_{30} with this ratio equal to 0.067, fairly close to that in T_{56}.

Number of Blades

As with gas dispersion, increasing the number of blades from four to six on the MFD (0.14 m diameter) impeller produced an increase in efficiency. Slightly lower powers (13%) and speeds (≃ 9%) were required to just suspend a 1% concentration of soda glass Ballotini.

Impeller Clearance

Though Zwietering found N_{JS} to be independent of impeller clearance (c) for disc turbines, provided $T/7 \leq c \leq T/2$, it has since been shown to have a significant effect on N_{JS}[2]. Table 4.6 shows the savings in speed and power achieved with a D = T/3 DT.

T_{56} Disc Turbine			D = T/3	3% Soda Glass Ballotini		
c (-)	N_{JS} rps	P_{JS} W	$(Po)_{JS}$ (-)	S this data	S -Zwietering[6]	S -Nienow[2]
T/6	4.28	82	4.6	5.8	7.5	6.5
T/4	4.95	151	5.5	6.7	7.5	7.8
T/2	5.90	240	5.4	8.0	7.5	-

Table 4.6 Effect of Impeller Clearance (c) on N_{JS}

The power savings produced by the lower speeds necessary to achieve N_{JS} at small c were enhanced by the decrease in power number

that also occurred as clearance was decreased. Thus even reducing the clearance by 0.047 m, from T/4 to T/6, virtually halved the power input necessary to just-suspend the particles. This trend was observed on all scales, but to a much lesser degree with larger vessels, the power reduction being critically dependent on the power number reduction, which varied due to minor dimension inconsistencies, etc.

The reduction in Po with c has been previously reported and was explained by Bates et al.[43] as being due to the disc affecting suction into the impeller, but they did not observe the changing flow pattern mentioned in Section 3.5.5. The data presented in Table 4.6 are in good agreement with that presented by Bates et al. Nienow and Miles[38] also noted this effect. The apparently anomalous reduction in Po at c = T/2 (Table 4.6) was due to the onset of surface aeration.

The dimensionless group, S, was evaluated from Eqn. 4.1. The same trend as noted by Nienow[2] occurred but the values were 11 - 14% lower. Both sets of data encompassed Zwietering's value. Musil and Vlk[34] reported N_{JS} to be independent of c for $c \leq T/3$, but their work was carried out in a conical based vessel.

Scale Up

The data presented in Fig. 4.7 represent N_{JS} values for a 1% concentration of sand over a very wide range of vessel sizes and indicates that there was no noticeable change in behaviour outside the scale ranges previously examined by other workers. The difference in gradients between the three impeller types represented (DT, 4 MFD, 4 MFU) is negligible and gives:

$$N_{JS} \propto T^{-0.76} \quad \text{for } D = T/2 \text{ and } c = T/4 \qquad 4.16$$

This result is slightly lower than Zwietering's value (exponent of 0.85) and slightly higher than Baldi et al's for c/D = 0.5 (exponent of 0.67). On the basis of the exponent in Eqn. 4.16, then the specific power input at N_{JS}, assuming Po remains constant, would

be given by:

$$P \alpha N^3 D^5 \Rightarrow (\varepsilon_T)_{JS} \alpha N_{JS}^3 D^2 \qquad 4.17$$

i.e. $$(\varepsilon_T)_{JS} \alpha D^{-0.28} \qquad 4.18$$

since $D \alpha T$ for constant D/T on scaling. This implies a slight reduction in $(\varepsilon_T)_{JS}$ on scale up. Zwietering suggests a stronger relationship ($(\varepsilon_T)_{JS} \alpha D^{-0.55}$) and Baldi implies firstly that $(\varepsilon_T)_{JS}$ remains constant on scale up for a disc turbine in this geometry (c/D = 0.5) and secondly that this relationship is a function of geometry, which might explain the widely diverging opinions in the literature. Although the data presented in Fig. 4.7 for disc turbines produce a good straight line relationship, it can be seen that the data from the tanks at U.C.L. (T_{29} and T_{56}) fall slightly below the line and those from the tanks at ICI (T_{30}, T_{91} and T_{183}) slightly above the line. In terms of power dissipation, this effect is drastically emphasized as indicated by the results in Table 4.7, plotted in Fig. 4.8. This figure reveals a serious anomaly between the results obtained at U.C.L. and those obtained at ICI, though each set is self consistent, for both impeller types tested (i.e. DT and 4 MFD).

The data for the disc turbines clearly falls into two sets and the results obtained with a 4 MFD impeller in T_{91} also implies that a much higher power input was necessary to cause suspension than would have been estimated on the basis of the T_{29} and T_{56} (U.C.L. tanks) results. If the data from each set of tanks is considered separately, then the rate of reduction of $(\varepsilon_T)_{JS}$ on scale up is in each case of the same order as the value predicted by Eqn. 4.18. This suggests that some phenomena not previously considered is at work since the same particles were used in each experiment. One possible explanation might be the lack of consideration given to solid-solid interactions such as the surface roughness or surface fungal growth of the vessels interacting with particle shape and roughness. If this were so then

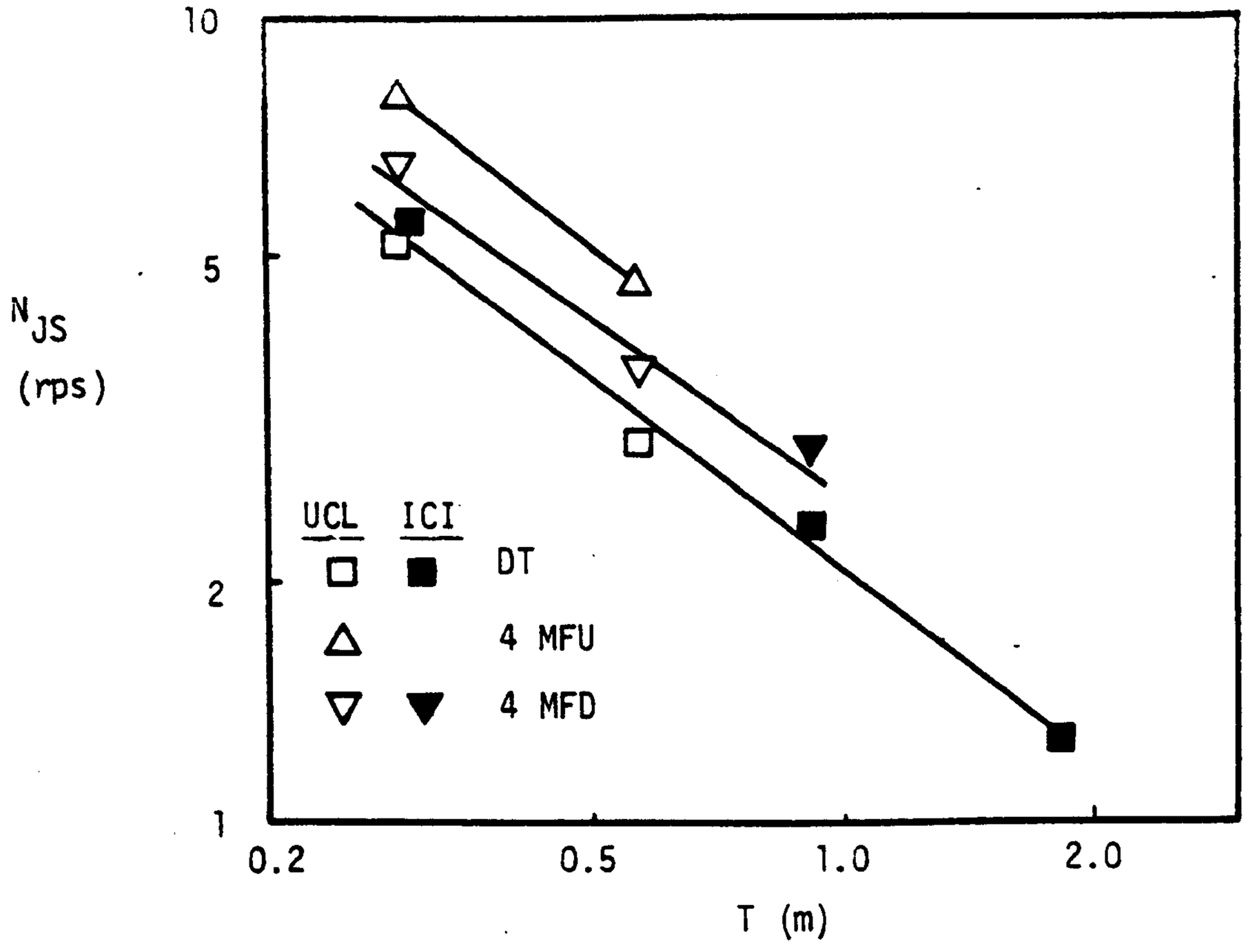

Fig. 4.7 Effect of Scale (Tank Size) on N_{JS} (D = T/2, c = T/4, 1% Sand)

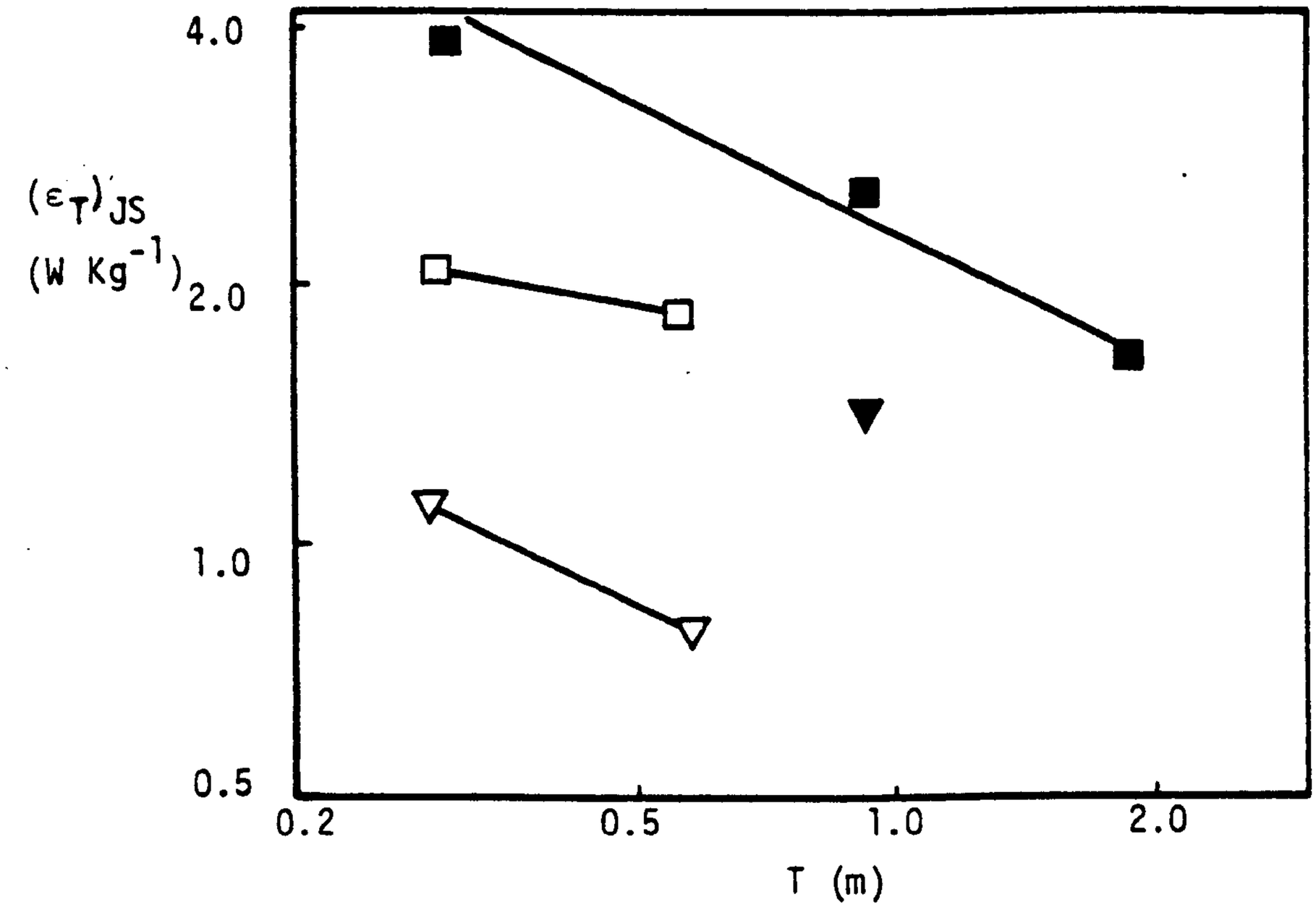

Fig. 4.8 Effect of Scale on $(\epsilon_T)_{JS}$
(details and symbols as Fig. 4.7)

(a) D = T/2 Disc Turbines c = T/4 1% Sand

T (m)	N_{JS} (rps)	$(\varepsilon_T)_{JS}$ ($W\ Kg^{-1}$)	$(Po)_{JS}$ (-)
0.29	5.03	2.1	4.8
0.30	5.58	3.8	5.95
0.56	2.92	1.8	5.9
0.91	2.32	2.55	6.15
1.83	1.28	1.6	5.8

(b) D = T/2 4 MFD c = T/4 1% Sand

T (m)	N_{JS} (rps)	$(\varepsilon_T)_{JS}$ ($W\ Kg^{-1}$)	$(Po)_{JS}$ (-)
0.29	6.45	1.1	1.2
0.56	3.63	0.78	1.3
0.91	2.87	1.4	1.8*

(c) D = T/2 4 MFU c = T/4 1% Sand

T (m)	N_{JS} (rps)	$(\varepsilon_T)_{JS}$ ($W\ Kg^{-1}$)	$(Po)_{JS}$ (-)
0.29	7.83	2.2	1.4
0.56	4.67	1.6	1.2

Table 4.7 Effect of Scale Up on the Just-Suspended Condition

* Probably due to the double thickness of blade incorporated in this impeller and general non standard construction.

it would make it exceedingly difficult to propose any sensible scale up relationships since it would be virtually impossible to keep the internal surfaces of very large industrial scale vessels as clean and smooth as small scale bench vessels. Further work is necessary to clarify the validity of this suggestion but brief tests with an exceedingly rough false base in T_{56} had a negligible effect on N_{JS}. Other factors which may have had some small effect but seem unlikely to fully explain the above results include the variation of power numbers (Table 4.7) and the possibility of slightly superior lighting quality on T_{29} and T_{56} varying the condition identified as just-suspended.

4.4.3. Comparison of Data with the Literature

Considering the geometry employed in the bulk of this work, i.e. DT, D = T/2, c = T/4 => c/D = 0.5, then from Eqn. 4.1 and the constant(S) quoted by Zwietering[6]:

$$N_{JS} = \frac{4\ \nu^{0.1}\ d_p^{0.2}}{D^{0.85}} \left[\frac{\Delta\rho\ g}{\rho_L}\right]^{0.45} \chi^{0.13} \qquad 4.19$$

by substituting for a 1% concentration water system and rearranging, Eqn. 4.19 becomes:

$$2 = \frac{d_p^{0.167}}{N_{JS}} \left[\frac{\Delta\rho\ g}{\rho_L}\right]^{0.5} \frac{T}{D^{1.67}} \left[\frac{d_p^{.033}}{D^{0.18}} \left[\frac{\Delta\rho\ g}{\rho_L}\right]^{-0.05}\right] \qquad 4.20$$

$$\text{i.e.} \qquad 2 = Po^{1/3}.\ Z\ \frac{d_p^{.033}}{D^{0.18}} \left[\frac{\Delta\rho\ g}{\rho_L}\right]^{-0.05} \qquad 4.21$$

where Z is defined by Eqn. 4.2.

Using the measured power number of 5.95 for the geometry under consideration (Table 4.7a) then:

$$Z = 1.1\ \frac{D^{0.18}}{d_p^{0.033}} \left[\frac{\Delta\rho\ g}{\rho_L}\right]^{0.05} \qquad 4.22$$

If the same procedure is repeated using the S value proposed by Nienow[2] to allow for impeller clearance variations with otherwise

similar geometries, then the resulting expression is given by Eqn.4.23.

$$Z = 0.98 \frac{D^{0.18}}{d_p^{0.033}} \left[\frac{\Delta\rho\, g}{\rho_L}\right]^{0.05} \qquad 4.23$$

Since the exponents on the density and particle size terms in Eqns. 4.22 and 4.23 are very small, then it is possible to evaluate with very little error the parameter Z for each vessel size (D/T constant) according to the empirical correlation found by Zwietering[6] and modified by Nienow[2] for a very wide range of particle properties. Thus in Fig. 4.9, the Z values predicted by Zwietering and Nienow for each vessel size are marked on the right and left hand vertical axis respectively, along with the value found by Baldi *et al.* for an eight-bladed disc turbine. The data points in Fig. 4.9 are the experimental results (Appendix 1) from this work for the geometry under consideration (DT, D = T/2, c = T/4) plotted as Z against Re^* evaluated according to Eqns. 4.2 and 4.3. The data appear to support Baldi *et al*'s conclusion that Z = constant $\neq f(Re^*)$ for this configuration, giving a mean value of Z ($\bar{Z}$) of 1.17, with a standard deviation from the mean (σ_Z) of $\pm$ 0.15 ($\pm$ 13%), over the complete scale range. This result seems very reasonable when compared with the value reported for an eight-bladed disc turbine of Z = 2, implying lower N_{JS} values which supports the proposition that increasing the number of blades leads to increased suspension efficiency (Section 4.4.2).

The data from T_{56} and T_{29} agree quite well with the Z values predicted by Zwietering's correlation (Eqns. 4.1, 4.22) but the agreement with Nienow's results (Eqn. 4.23) is still better. However, the results for T_{30}, T_{91} and T_{183} fall well below the Z values predicted by either Eqns. 4.22 or 4.23, implying much higher N_{JS} values than predicted. This supports observations made in Section 4.4.2. Cliff *et al.*[44] recently presented N_{PJS} data obtained in T_{91} during a

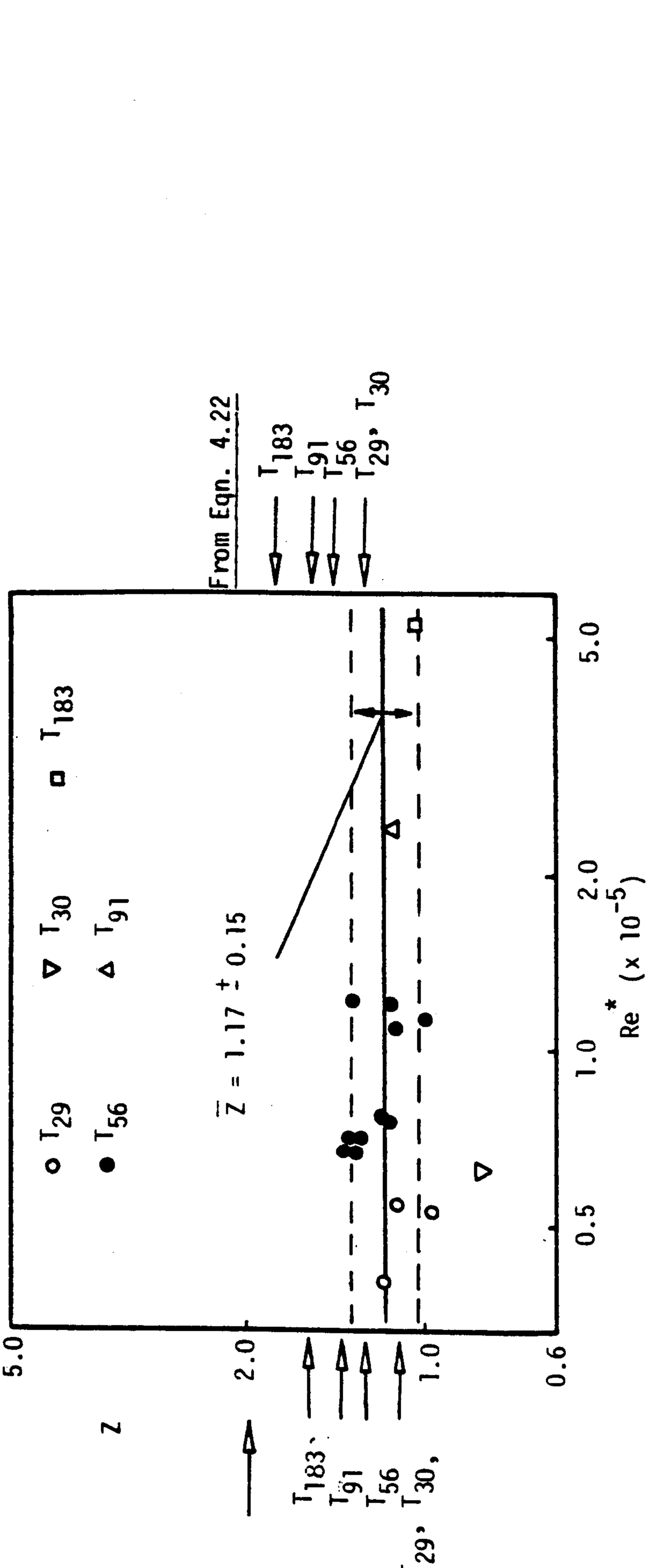

Fig. 4.9 Comparison of Experimental Data with Z values predicted by Zwietering[6] and Mlenow[2]

(D = T/2, DT, c = T/4)

separate study using a propeller and also found their experimental values well above the N_{JS} values predicted according to Eqn. 4.1.

The data for the configuration considered above (DT, c/D = 0.5) fit Baldi et al's model quite well. Fig. 4.10 presents experimental data for other impeller configurations (Appendix 1). The relationships between Z and Re^* deduced from Fig. 4.10 are given in Table 4.8 along with the resulting exponents on the various parameters evaluated from these relationships and Eqns. 4.2 and 4.3. The relationship between Z and Re^* for each DT geometry is in general agreement with that found by Baldi et al.

	Source	Geometry	Exponent on					
			$(Re^*)^+$	ν^{++}	d_p^{++}	X^{++}	$\left[\frac{\Delta\rho\, g}{\rho_L}\right]^{++}$	T^{++}
A	This work - Sections 4.4.1.and 4.4.2.	All	-	0.0	0.15	0.12	0.40	-0.76
B	Zwietering - Eqn.4.1.	All	-	0.1	0.20	0.13	0.45	-0.85
C	Baldi's model using the relationships estimated from the experimental data in Fig.4.9 and 4.10	DT c/D = 0.5	0	-	0.17	0.13	0.5	-0.67
D		DT c/D = 1	0.3	0.23	0.13	0.10	0.38	-0.98
E		DT c/D = 0.75	0.3	0.23	0.13	0.10	0.38	-0.98
F		4 MFD c/D = 1	-0.14	-0.54	0.26	0.21	0.77	0.05
G		4 MFD c/D = 0.5	-0.35	-0.16	0.19	0.16	0.58	-0.45
H		4 MFU c/D = 0.5	0.09	0.08	0.15	0.12	0.46	-0.78

$^+$ signifies $Z \alpha (Re^*)^+$. $^{++}$ signifies $N_{JS} \alpha \nu^{++}$, d_p^{++}, etc.

Table 4.8 Application of Baldi et al's[26] model to various impeller Configurations

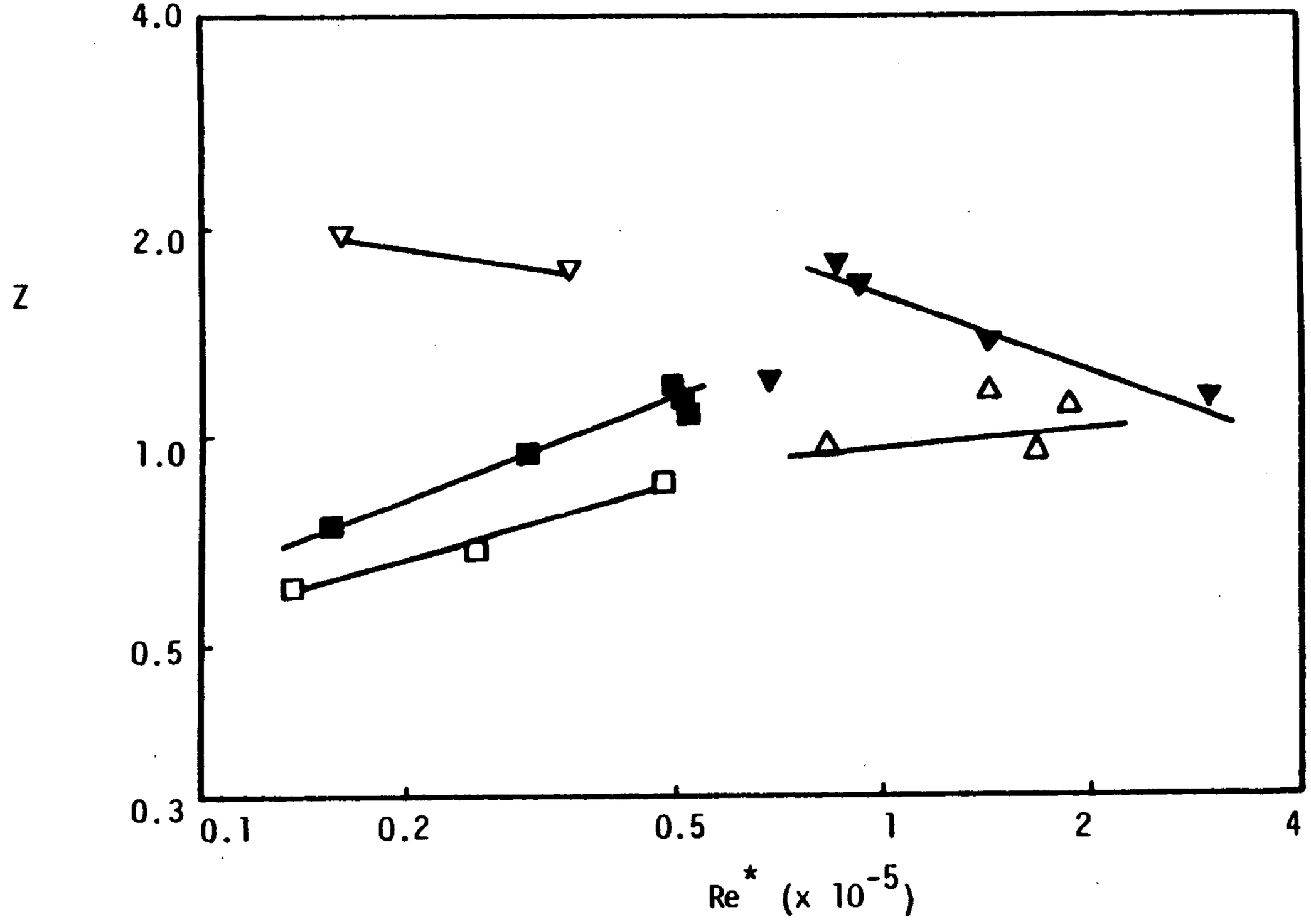

Fig. 4.10 Z versus Re^* for Various Impeller Configurations

▼ 4 MFD c/D = 0.5 ■ DT c/D = 0.75

▽ 4 MFD c/D = 1.0 □ DT c/D = 1.0

△ 4 MFU c/D = 0.5

It is evident from the exponents presented in Table 4.8 that Baldi's model does not match the experimentally observed exponents on the major parameters (line A) for the configurations given in lines F and G, and thus reveals the limitations of this approach when applied to impellers producing an axial component of flow, especially considering the insensitivity of those exponents to all geometrical variations as revealed by this work and supported by Zwietering and Nienow.

Therefore, on balance, it appears to be more consistent to use the empirical method of estimating N_{JS}. The dimensionless approach recommended by Zwietering produces exponents which are broadly supported by this work. Also Figs. 4.2 to 4.4 show how closely Zwietering's predictions agree with the experimental data presented here. The modified S values presented by Nienow appear to give a more accurate estimation of N_{JS} than Zwietering's original data for disc turbines.

S values calculated from the data of Nienow and Miles[32] for 4 MFD impellers show large variations for constant T/D ratio, but reflect an increase in N_{JS} over that predicted for a propeller from Zwietering's correlation. This work shows lower speeds were necessary when using 4 MFD impellers (compared to AFD), though higher powers (Section 4.4.2). However,some variation in S was also found for constant T/D ratio (as shown in Appendix 1) for both 4 MFD and 4 MFU impellers. The mean S values are presented in Table 4.9 for the configurations studied with an impeller clearance of T/4. The error limits shown are for one standard deviation from the mean value.

Configuration c = T/4	S values		
	Zwietering[6]	Nienow[2,32]	This work+
DT D = T/2	4.0	4.5	4.25 ± 11%
DT D = T/3	7.5	8.0	7.1 ± 12%
DT D = T/4	12	12	12.2 ± 6%
4 MFD D = T/2	-	4.6 and 7.8	5.8 ± 14%
4 MFD D = T/4	-	10.1 and 12.3	7.1 ± 0%
4 MFU D = T/2	-	-	7.4 ± 12%
AFD D ≃ T/2	6	-	6.8 (1 result)
ADT D = T/2	-	-	5.1 (1 result)

+ These values do not account for data obtained in T_{30}, T_{91} or T_{183}.

Table 4.9 Comparison of S values

4.5. Conclusions

The general trends found in this work confirm those put forward by Zwietering[6] and his correlation (Eqn. 4.1) remains the soundest basis for design. One reservation is concerned with the recommendation of scale up with decreasing specific power input ($(\varepsilon_T)_{JS} \propto T^{-0.55}$) deduced from Eqn. 4.1. The relationship derived in this work over a wider scale range ($(\varepsilon_T)_{JS} \propto D^{-0.28}$) suggests a more conservative approach to scale up and agrees well with the rules used in industrial practice ($(\varepsilon_T)_{JS} \propto D^{-0.25}$).[45] Also, the exponent proposed by Zwietering was actually deduced by dimensional analysis and his experimental data give $(\varepsilon_T)_{JS} \propto D^{-0.34}$ to $(\varepsilon_T)_{JS} \propto D^{-0.82}$ depending on impeller type.

The model proposed by Baldi et al.[26] appears to work well for some geometries but not at all well for others. However, it represents the best attempt at a theoretical analysis of suspension.

The only reasonable explanation for the anomalous results

obtained in the large scale vessels (and T_{30}) appears to be that another factor not previously considered affects suspension. A suggested cause is an interaction between the particles and the internal surface of the vessel, but further work is required to clarify this.

Despite prolific work on the subject over the last half century, little significant advance has been made on the empirical relationship found by Zwietering in terms of the understanding and prediction of particle suspension. This demonstrates the complexity of the topic and suggests that clarification is unlikely to be forthcoming until more accurate models of flow behaviour and of liquid-solid, solid-solid interactions are available.

CHAPTER 5.

INTRODUCTION TO THREE PHASE SYSTEMS

5.1. Introduction

The importance of ensuring that the discontinuous phase is well dispersed in the continuous phase has been firmly established for a wide variety of multiphase reaction and transfer systems. Hence in the literature there has been much attention paid to establishing criteria which define this state. In the context of this work, there are two criteria, N_{CD} and N_{JS}, which relate to gas-liquid and solid-liquid dispersions respectively. These criteria have been characterized in the previous two chapters.

The simultaneous satisfaction of both these criteria is equally vital in three phase systems. However, very little work exists in the literature on this topic. The little there is suggests that important additional interactions occur in three phase situations and reveals that the straightforward application of principles deduced in two phase systems is an unreliable form of design.

The objective of this chapter is to ascertain the major interactions between the gas dispersion and particle suspension mechanisms as a basis for examining in detail the effect of the major variables on N_{JS} and N_{CD} simultaneously in Chapters 6 and 7.

5.2. Literature Survey

Three phase slurry reactions have long formed a source of much published work. Though they are often carried out in stirred vessels, the emphasis is usually on the reaction kinetics and there is generally very little consideration given to the hydrodynamics involved. A recent review paper[46] quoted Zwietering's correlation with respect to ensuring complete suspension, but made no observations with respect to any effect of the gassing on suspension speeds.

The first work to deal with the interactions of aeration and

suspension was published in 1969 by Arbiter, Harris and Yap[1] in the field of froth flotation. They noticed that drastic sedimentation of suspended particles occurred on aeration if a critical air flow number (Fl) was exceeded. The critical flow number was a function of particle size and coincided with a sudden drop in the ratio P_g/P with flow number. The results of this work are difficult to relate directly to that presented in this thesis, since the impeller and shroud geometry used in flotation cells is very different from the more standard arrangements considered here. The sudden drop in P_g/P was explained as being due to particles blocking the suction parts of the impeller, which could not happen in an unshrouded system. They also noted that sedimentation was achieved gradually by increases in gas rate or decreases in impeller speed in systems which did not display this critical fall in P_g/P. However, the major conclusions drawn from their work appear to be relevant to this investigation. They are:

1. Aeration caused a decrease in power consumption and particle sedimentation was associated with this decrease.
2. A sudden fall in P_g/P caused a corresponding catastrophic loss of suspension.

Zlokarnik and Judat[47] proposed a self inducing tube stirrer combined with a propeller as an efficient means of simultaneously dispersing gas and suspending solids. A complex empirical relationship was given for the critical Reynolds number at which particles were suspended by this configuration, but no term accounting for aeration was included in it. The justification for this was presumably their claim that the gas had a negligible effect on the propeller pumping rate when introduced to the system in this manner. The correlation reduces to a form very similar to that proposed by Baldi *et al.*[26] in two phase systems. Oldshue [48] also briefly considered three phase systems but was mainly concerned with transfer process and

made no mention of the hydrodynamics.

The work of Queneau et al.[49] further demonstrates the wide range of operations where a knowledge of the hydrodynamic state of a three phase system is essential. The overall objective of their work was to specify scale up requirements for the upgrading of an atmospheric leaching plant to produce nickel from nickel-copper mattes. They observed that a loss of suspension occurred at high gas rates, low speed or small impeller diameter and low power input. Though they observed the superior energy efficiency of a propeller over a radial turbine and also the savings available on lowering the radial impeller, these tests were carried out without aeration. It was also noted that multiple impellers were less efficient for suspension than a single impeller for equal power input. A graph was presented of P_g/P against Fl, showing particle sedimentation to occur for $P_g/P < 0.5$. However, in some cases they reported no settling out even when the impeller was flooded with gas. All the work was completed in an 11 inch diameter vessel with gas rates up to approximately 0.8 vvm. Particle diameters were mostly less than 50 microns. It is difficult to draw any positive conclusions from this work, since suspension and sedimentation of the particles were not defined in terms of a standard criterion, e.g. N_{JS}. However, no comments were made that implied extreme sedimentation as reported by Arbiter et al.[1]

Since this project began, work has been published relating specifically to the interaction of aeration on N_{JS} and suspension on gas-liquid hydrodynamics. Wiedmann et al.[50] presented data obtained in two tanks (T = 0.2 m and 0.45 m) over a very wide range of gas rates (up to Q > 10 vvm) for various particle-liquid conditions and utilizing both disc turbines and propellers. Several important qualitative conclusions can be drawn from their work, though their absolute data values imply suspension was achieved at speeds some 50%

lower than this work, or that of Zwietering[6] or Nienow[2] would predict, and must therefore be regarded as slightly suspect. Both N_{JS} and $(\varepsilon_T)_{JS}$ were found to increase as gas rate increased, more so for the propeller than the disc turbine. The minimum mixing requirement for the gas phase, N_{CD}, was found to be independent of particle conditions ($\Delta\rho$, X, d_p etc.) and to be achieved at lower speeds than N_{JS}. These characteristics were explained solely in terms of the fluid flows induced by the ascending bubbles upsetting and reducing the output flow from the impeller.

Subbarao and Taneja[33] investigated propeller agitated three phase dispersions in a 16.4 cm diameter vessel with the gas sparger situated above the impeller. A model was derived for predicting N_{JS} in two phase systems (see Chapter 4) but implied amongst other things that N_{JS} increased with impeller diameter and, not surprisingly, the data did not fit the theory very well. They also assumed that, on aeration, an entrained liquid flow - proportional to sparge rate - would be set up in a counter current direction to the propeller induced flow and hence hinder suspension. The resulting relationship implied that, on aeration, an increase in N above that necessary to just suspend the particles in a two phase system was required, and this increase was proportional to the gas rate. The data obtained seemed to support this postulate but with a lot of scatter and only for very low gas rates. As a result of this they defined a critical flow number (equivalent to $Q/(N-N_{JS})D^3 = 5\times10^{-3}$) for which suspension was just achieved. It was also noted that, with a sufficiently high gas rate, all the particles could be sedimented and that a flow number evaluated at these conditions agreed closely with the critical flow number proposed by Arbiter et al.[1] However, this was probably a coincidence since the mechanism which caused particles to sediment suddenly in Arbiter's work (mentioned earlier) was not possible in the

open geometry used in this work, where sedimentation was not sudden and an order of magnitude increase in gas rate was necessary to completely collapse the suspension.

There are, then, clear indications of aeration affecting the suspension of solid particles. However, the explanations put forward to account for this effect are not satisfactory. Consequently, no clear method of designing a three phase stirred tank system has emerged and this, therefore, forms the major objective of this thesis.

5.3. Experimental

5.3.1. Equipment and Techniques

The presence of particles sometimes hindered visual observation of the extent of gas dispersion. However, the criteria established in Chapter 3, in terms of the power responses of each impeller, always enabled N_{CD} to be detected.

N_{JS} was detected by visual observation of the base, as described in the previous chapter. It was found that it sometimes took two to three minutes to attain steady state as regards particle motion, especially at high gas rates. Nevertheless, even when the gas was dispersed throughout the tank, the gradual decrease in particles on the base with increasing speed, and the critical N_{JS} condition, could be clearly observed.

The peak or kink in the sampled concentration versus speed plot, N_{PJS}, was determined for polystyrene, glass powder and sand particles. The results relating to sand were obtained on three scales, i.e. T_{56}, T_{91} and T_{183}, allowing comparison with N_{JS} in T_{56} and T_{91} where viewing of the base was unrestricted. Only limited vision of the base was possible in T_{183}.

Two techniques were used to obtain N_{PJS}, the second superseding the first. Both involved withdrawing a sample from the tank at a height of 0.10 m from the base. Musil[29] found no effect of sampling

height on N_{PJS} provided that the probe height was between 0.08 H and 0.25 H from the base. Tests were carried out in both T_{56} and T_{183} and this result was confirmed. The orientation of the probe to the flow was also found to have a negligible effect on N_{PJS}, though a substantial one on the actual quantity of solids sampled. No attempt was made to achieve isokinetic sampling and hence gain actual concentration data since this is exceedingly difficult in a stirred vessel. However, an advantage of this technique was that no calibration was required since the sampled concentration was proportional to the actual local concentration at the sample point, and so the position of the peak was not affected.[28] Some unsuccessful attempts were made to make concentration measurements in situ (Appendix 2), which were complicated by the presence of gas. Thus it was necessary to withdraw a sample before analysis.

Initially the concentration data were obtained by extracting a sample, drying and weighing it. The impeller speed was set at the required value and the system allowed to reach steady state. The dispersion was then sucked from the vessel at a linear velocity of approximately 0.4 ms^{-1} which was of a similar order of magnitude to the velocities in the vessel and also sufficient to prevent any particles setting out of suspension in the pipes (greater than five times the terminal velocity of the particle[51]). The particles settled out in the aspirator (Fig. 5.1a) and any gas extracted from the vessel also separated. The liquid was sucked through the peristaltic pump and via a damping bottle through a calibrated rotameter before returning to the vessel via the bottom bearing (if the vessel was being sparged, the liquid was sent to waste). The sample was collected over a minimum of three minutes, more normally five or ten, to ensure that the result was time averaged. The aspirator contents were then filtered to extract the particles, which were later dried and weighed,

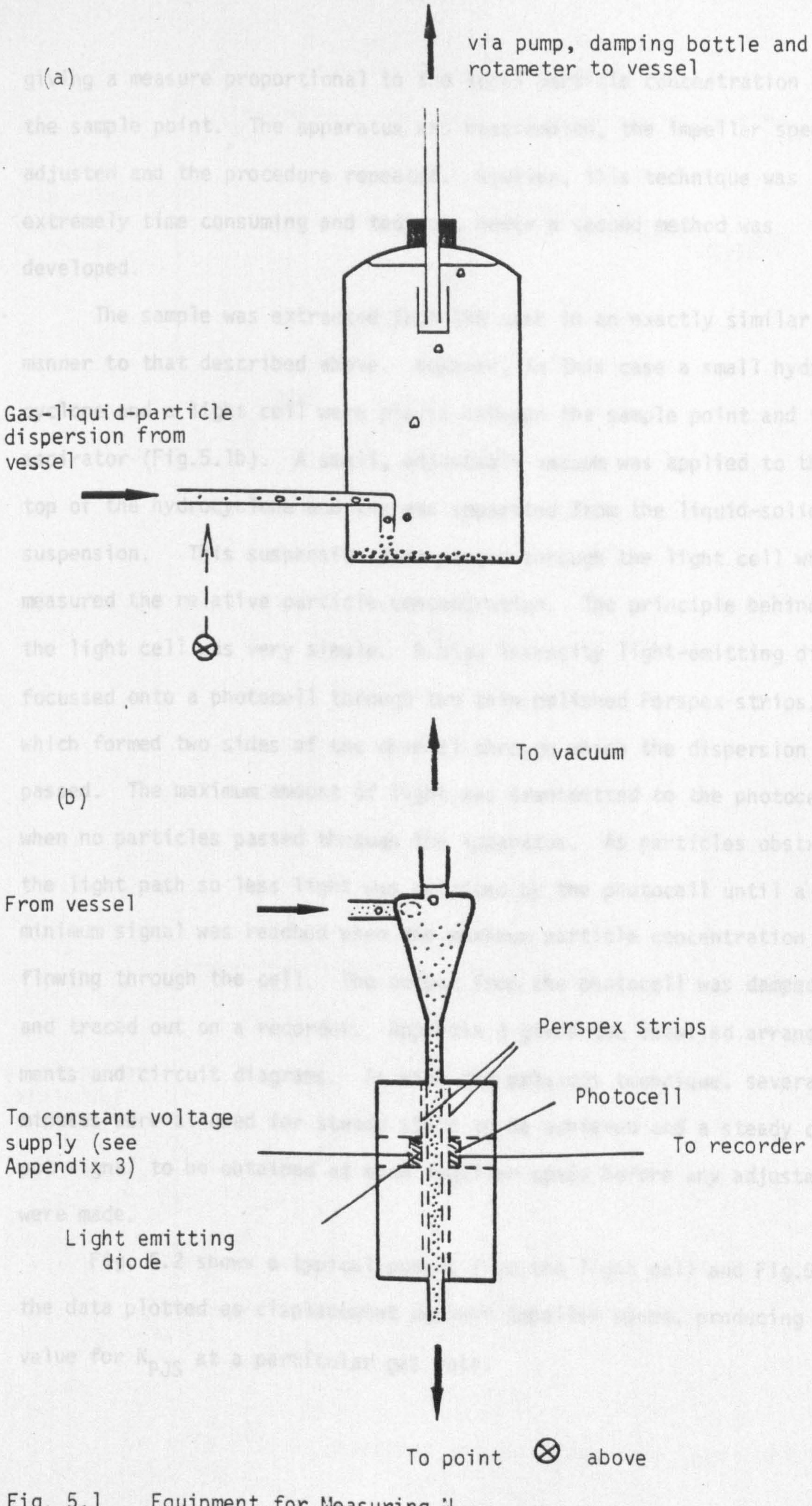

Fig. 5.1 Equipment for Measuring N_{PJS}

giving a measure proportional to the local particle concentration at the sample point. The apparatus was reassembled, the impeller speed adjusted and the procedure repeated. However, this technique was extremely time consuming and tedious, hence a second method was developed.

The sample was extracted from the tank in an exactly similar manner to that described above. However, in this case a small hydrocyclone and a light cell were placed between the sample point and the aspirator (Fig.5.1b). A small, adjustable vacuum was applied to the top of the hydrocyclone and the gas separated from the liquid-solid suspension. This suspension then passed through the light cell which measured the relative particle concentration. The principle behind the light cell was very simple. A high intensity light-emitting diode focussed onto a photocell through two thin polished Perspex strips, which formed two sides of the channel through which the dispersion passed. The maximum amount of light was transmitted to the photocell when no particles passed through the apparatus. As particles obstructed the light path so less light was detected by the photocell until a minimum signal was reached when the maximum particle concentration was flowing through the cell. The output from the photocell was damped and traced out on a recorder. Appendix 3 gives the detailed arrangements and circuit diagrams. As with the previous technique, several minutes were allowed for steady state to be achieved and a steady output signal to be obtained at each impeller speed before any adjustments were made.

Fig. 5.2 shows a typical output from the light cell and Fig.5.3 the data plotted as displacement against impeller speed, producing a value for N_{PJS} at a particular gas rate.

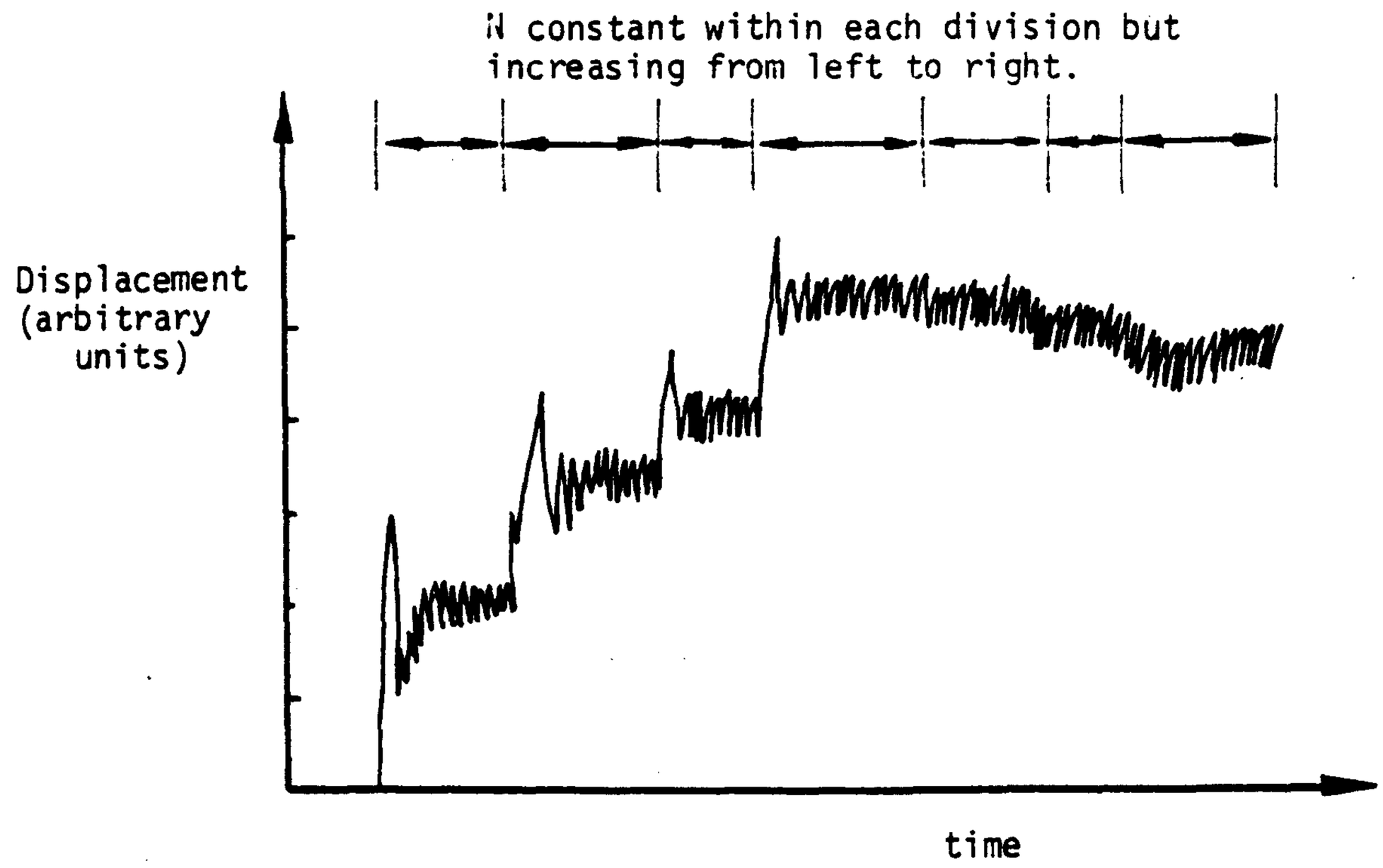

Fig. 5.2 Typical output from Light Cell

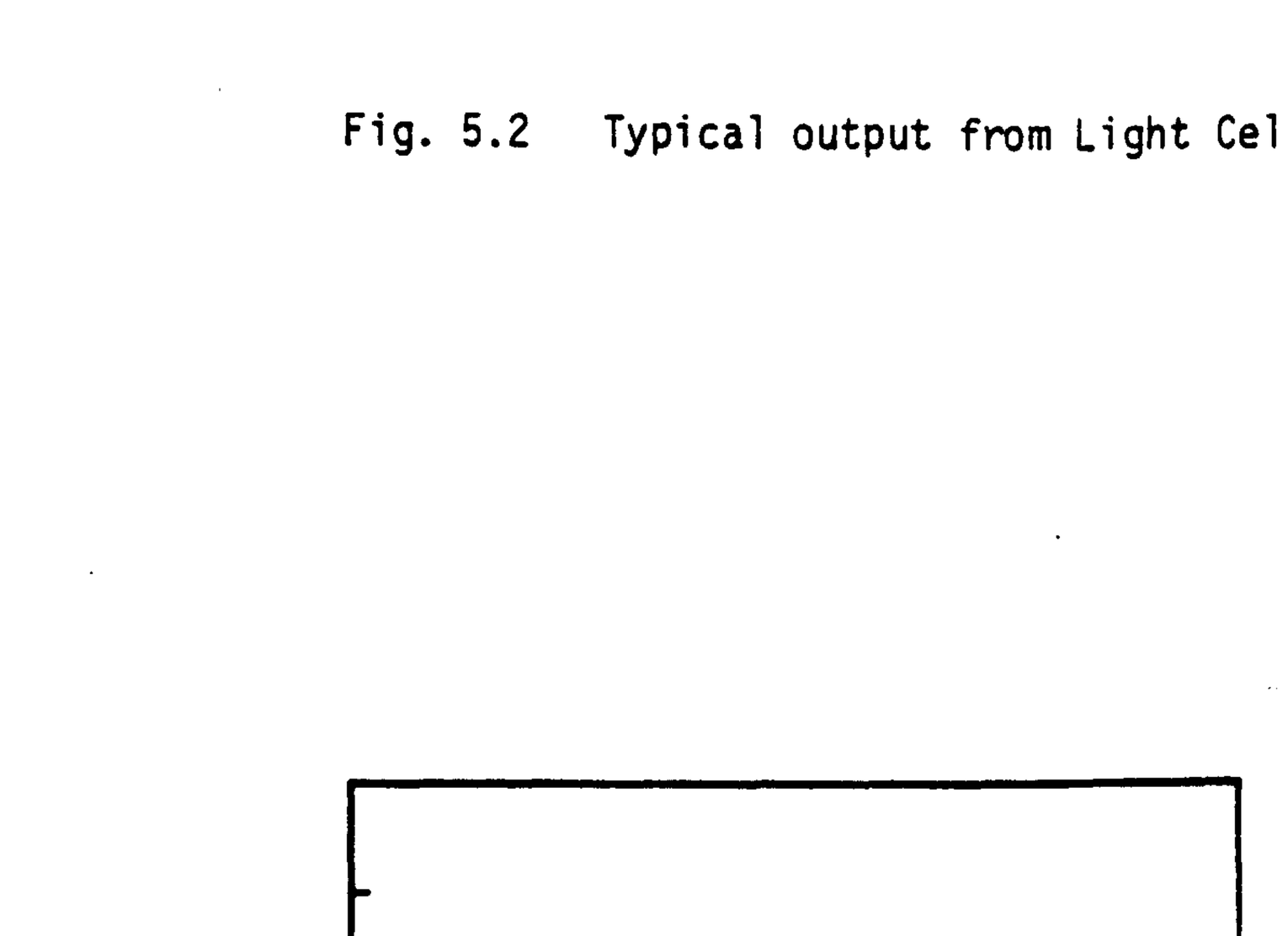

Fig.5.3 Displacement against N for data from Fig.5.2.

5.3.2. Comparison of N_{JS} and N_{PJS}

A major advantage of establishing a suspension criterion based on N_{PJS} would be its usefulness in large scale vessels where visual observation is not possible. Also it should be less prone to operator error than a visual assessment.

Tests were carried out over a wide range of tank-impeller-particle combinations for two phase and three phase systems. Table 5.1 presents both the N_{PJS} and N_{JS} data. A distinct peak or kink was obtained in every case. Generally a peak (Fig. 5.4) was obtained when the impeller clearance was T/4 and a kink (Fig. 5.5) when the impeller clearance was T/6. As shown in Table 5.1, the initial tests with a glass powder suspension showed excellent agreement between N_{JS} and N_{PJS}, with a clear peak obtained for speeds at worst 6% lower than the visually observed N_{JS} speeds, supporting the work in the literature.[28] However, later results showed increased differences between the two criteria, with N_{PJS} always achieved at lower speeds than N_{JS}. These differences were sometimes over 30% of N_{JS} for the "heavier" particles ($\Delta\rho > 1000$ Kg m^{-3}), which implies a very significant difference between P_{JS} and P_{PJS}. The differences between N_{JS} and N_{PJS} were emphasized in the case of the polystyrene particles ($\Delta\rho = 50$ Kg m^{-3}), where N_{PJS} decreased with increasing gas rate in contrast to N_{JS}, which increased with Q. In fact, N_{PJS} was achieved with no impeller action whatever at a gas rate of approximately 0.7 vvm. This was presumably due to the almost neutral density particles being sufficiently suspended by the liquid movement, provoked by the gas upflow, to cause a peak (Fig. 5.6). Thus, although it has been firmly established over a wide range of particles, tank sizes and gas rates, that a definite criterion exists and can be defined by concentration measurements near the base, it is clear that this criterion generally gives a different speed to that assessed visually, though sometimes they

Impeller Type	Impeller size D and clearance c	Tank	Particles	Gas rate, Q (vvm)	N_{JS} (rps)	N_{PJS} (rps)	$\left[\frac{N_{JS}-N_{PJS}}{N_{JS}}\right] \times 100$ (%)	Comments
DT	D = T/4 c = T/4	T_{56}	Polystyrene X = 1%	0 0.25 0.5	2.6 4.6 5.7	1.77 1.62 1.13	32 65 80	P P P
DT	D = T/3 c = T/4	T_{56}	Glass Powder X = 0.3%	0 0.25 0.5 0.75 1.0 1.25	3.8 4.3 4.85 5.5 6.08 6.37	3.8 4.17 4.58 5.42 6.07 6.37	0 0.3 6 1.5 0.16 0	P P P P P P
6MFD	D = T/4 c = T/4	T_{56}	Soda glass Ballotini X = 1%	0.25	7.51	6.73	10.4	P
DT	D = T/2 c = T/4	T_{56}	Soda glass Ballotini X = 3%	0.5	2.49	2.31	7.2	P *
DT	D = T/2 c = T/4	T_{56}	Sand X = 1%	0 0.25 1	2.92 3.05 3.62	2.2 2.5 2.9	26 18 20	P * P * P *
DT	D = T/2 c = T/6	T_{56}	Sand X = 1%	0 0.25 1	2.55 2.9 3.47	2.18 2.47 2.88	14.5 15 17	K * K * K *

continued overleaf

Impeller Type	Impeller size D and clearance c	Tank	Particles	Gas rate, Q (vvm)	N_{JS} (rps)	N_{PJS} (rps)	$\left[\frac{N_{JS}-N_{PJS}}{N_{JS}}\right]_{(\%)} \times 100$	Comments
4 MFD	D = T/2 c = T/4	T_{56}	Sand X = 1%	0 0.25 1	3.63 3.8 5.68	2.62 2.62 4.62	28 31 19	P * P * P *
DT	D = T/2 c = T/4	T_{91}	Sand X = 1%	0 0.25 1	2.31 2.62 3.1	1.75 1.72 2.17	24 34 30	P * P * P *
DT	D = T/2 c = T/6	T_{91}	Sand X = 1%	0 0.25 1	2.3 2.6 2.9	1.72 1.77 2.12	25 32 27	K * K * K *
DT	D = T/2 c = T/4	T_{183}	Sand X = 1%	0 0.25 0.5 1	1.28 1.58 1.75 1.75	1.11 1.18 1.27 1.45	13 25 27 17	P P P K
DT	D = T/2 c = T/6	T_{183}	Sand X = 1%	0 0.25 1	1.42 1.5 1.75	1 1.17 1.28	30 22 27	K K K

P indicates a peak was obtained e.g. Fig. 5.4.
K indicates a decrease in gradient e.g. Fig. 5.5.
* indicates light cell used to obtain measurements

Table 5.1 Comparison of N_{JS} and N_{PJS} Data

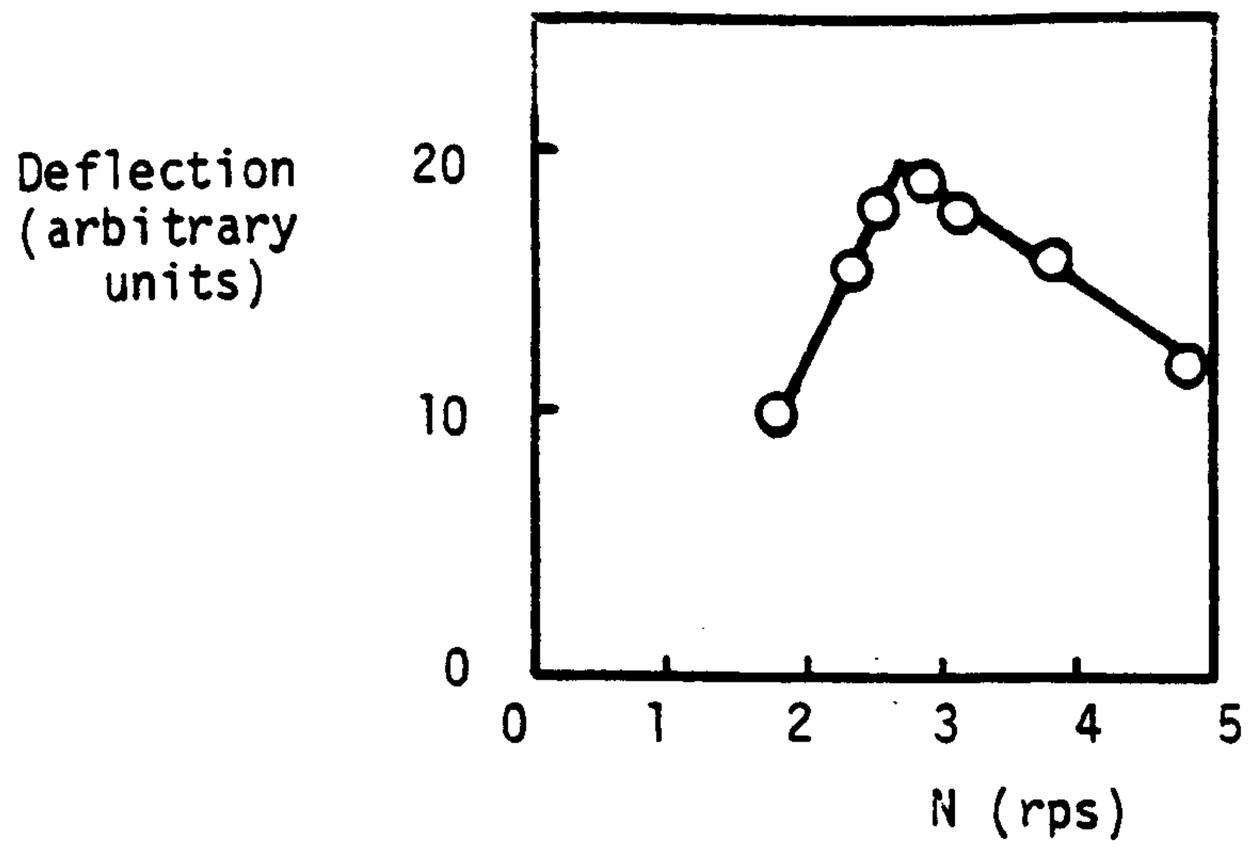

Fig.5.4 Deflection versus N
(T_{56}, 4 MFD, D = T/2, c = T/4, 1% Sand, Q = 0 vvm)

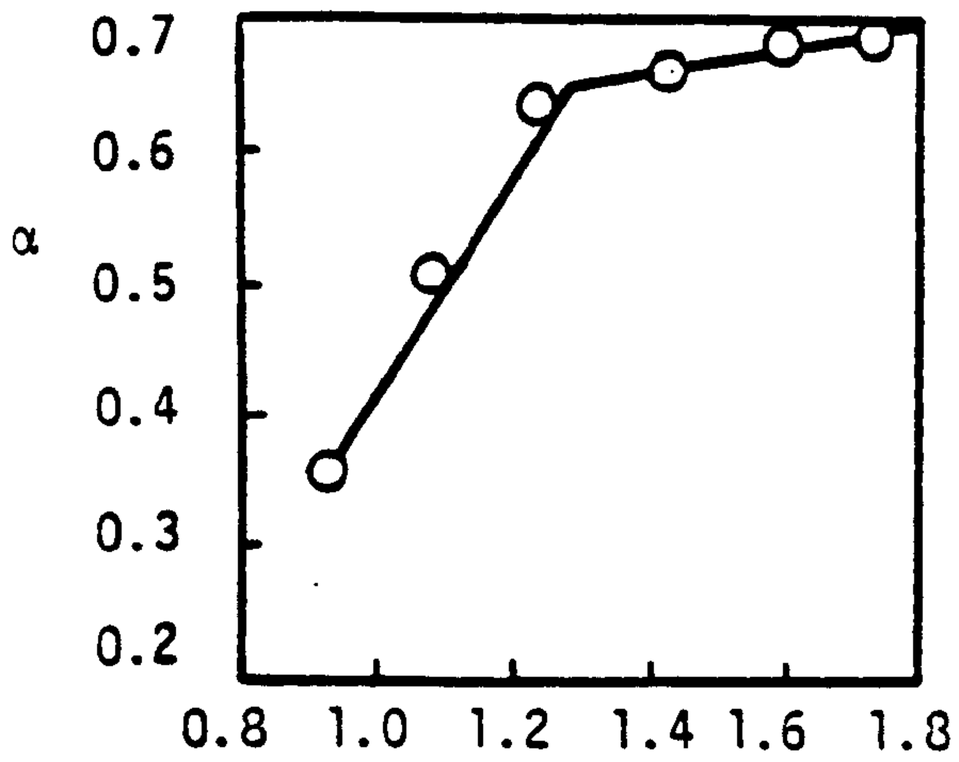

Fig.5.5 α versus N
(T_{183}, DT, D = T/2, c = T/6, 1% Sand, Q = 1.0 vvm)

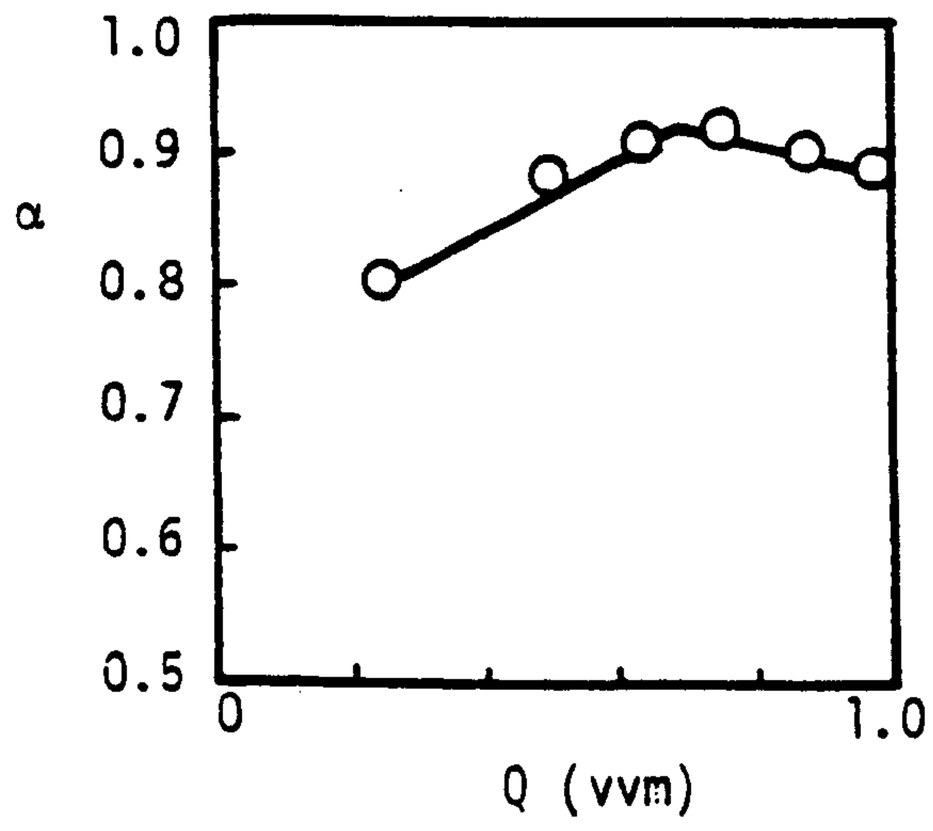

Fig.5.6 α versus Q
(T_{56}, 1% polystyrene, N = 0)

coincide.

In order to maintain consistency throughout this work the use of N_{JS} will be adhered to, as in Chapter 4. In a few instances, where the presentation of N_{PJS} data aids the qualitative explanation of a point, the concentration-impeller speed results will be shown.

5.4. Major Interactions

The major interactions between gas dispersion and solid suspension are described in this section for disc turbine impellers. This impeller type has been well documented in the literature in terms of both its particle suspension and gas dispersion capabilities. Having established in this chapter the major consequences of combining these two duties for a well documented system, in the following two chapters the basis formed in Chapters 3 and 4 will be used to present and discuss the characteristics of other systems and examine in detail the effects of all the major variables.

5.4.1. Effect of Particles on Gas-Liquid Hydrodynamics

The importance of particle effects on the gas-liquid hydrodynamics will be assessed by examining the manner in which particle size, density and concentration affect the speed at which the gas phase is completely dispersed, N_{CD}, the gassed power number, Po_g, and the overall gas holdup, ε.

The variation of both particle size (d_p) and density (ρ or $\Delta\rho$) had negligible effect on N_{CD}, Po_g or ε at the low concentrations investigated. However, this was not true of particle concentration. Fig. 5.7 shows how a ten fold increase in X affected the Po_g versus Fl plot for a D = T/2 disc turbine situated at c = T/4. Consider first the absolute values of the power numbers. The figure shows that, at this gas rate (0.5 vvm), concentration has a small effect on Po_g provided that the particles are suspended, i.e. for $N \geq N_{JS}$. However, at $N \leq N_{CD}$, the concentration of particles in the system had a very

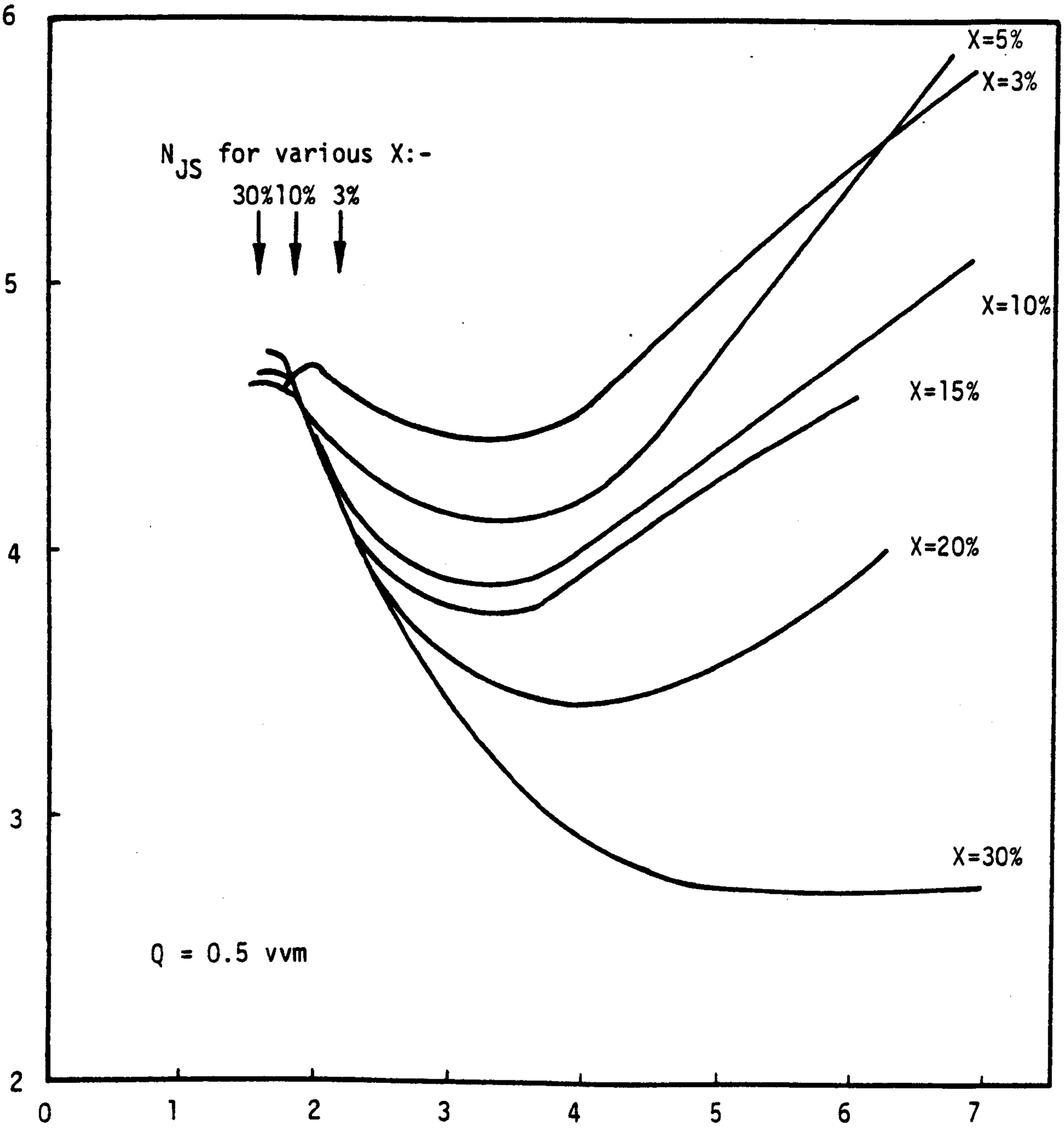

Fig. 5.7 Effect of Particle Concentration on Po_g - F1 plot.
(T_{56}, DT, D = T/2, c = T/4).

significant effect on the gassed power number. An explanation for this phenomenon is the false base formed by the particles effectively reducing impeller clearance at low speeds, which causes a decrease in power number similar to that observed in Section 4.4.2. As N tended to N_{JS} (as indicated in Fig. 5.7) so particles were suspended, the false base removed and the power numbers tended to a common value. Table 5.2 demonstrates the variation of power number with concentration for various gas rates, at the just-suspended condition.

Q vvm ↓	X→	Po or Po_g for a particular concentration, X					
		3	5	10	15	20	30
0		6.0	6.15	6.0	6.2	6.3	6.7
0.25		5.7	5.5	5.4	5.6	5.6	-
0.5		4.6	4.55	4.6	4.7	4.7	5.0
1.0		3.1	3.1	3.2	3.2	3.3	3.5

Table 5.2 Po_g as a function of X for various gas rates

(DT T_{56} D = T/2 c = T/4 Soda glass Ballotini)

This table shows that the power number generally increased as particle concentration increased, at the just-suspended condition. This is not surprising since Po and Po_g were calculated on the basis of the liquid properties and the effective density in the impeller region will increase in the presence of particles of greater density than the liquid. A 30% concentration implies an increase of approximately 20% in the overall density (assuming homogeneity and Q = 0) and thus 20% increase in Po since ρ was actually taken as the value for the liquid only. Since Po does not show a 20% increase, then this suggests that either the dispersion is not homogenious or Po is insensitive to X for other reasons. The data in Table 5.2 demonstrate that similar fractional increases in Po_g were observed with X, as for Po, of the order of 10% for the concentration range examined.

The second observation drawn from Fig. 5.7 involves the position of the minimum in the Po_g - Fl plot which marks N_{CD}, the speed at which the gas phase is taken as being just-dispersed. For low concentrations ($X \leq 15\%$), N_{CD} is independent of concentration. However, at the higher concentrations ($X > 15\%$), N_{CD} was achieved at lower speeds (higher Fl). In these cases, at low speeds, the particle bed was so close to the impeller that gas was easily dispersed and also the overall liquid flow pattern tended to the characteristic axial flow loops (as with low clearances - Section 3.5.5) and their associated lower power numbers and torque fluctuations. As particle bed heights diminished with increasing speed, so all the power number - flow number curves converged.

Fig. 5.8 shows gas holdup, ε, against solids concentration for the constant gas rate and speeds given in the figure. Considering that the experimental error involved in measuring ε was up to $\pm$ 10% for disc turbines, it is difficult to conclude anything other than the fact that a negligible change occurs in holdup, though it would appear that there may be a small decrease of ε with particle concentration. Van Den Berg[52] concluded that no change in interfacial area occurred on the addition of particles of $75\mu m \leq d_p \leq 600\mu m$ and $X \leq 4\%$ following measurements made using a sulphite oxidation technique in a 29 cm diameter vessel. Alternatively, Joosten et al.[53] observed a decrease in gas holdup at very high solids concentrations, though no quantitative details are given, and supported this with evidence that, in three phase fluidisedbeds, high particle volume fraction encourages bubble coalescence and a decrease in gas holdup.[54,55]

In conclusion, for the range of variables investigated, the effect of particles on the gas-liquid hydrodynamics of a three phase system is virtually negligible provided that the system is well mixed, i.e. $N > N_{JS}$ and $N > N_{CD}$. If either or both of the discontinuous

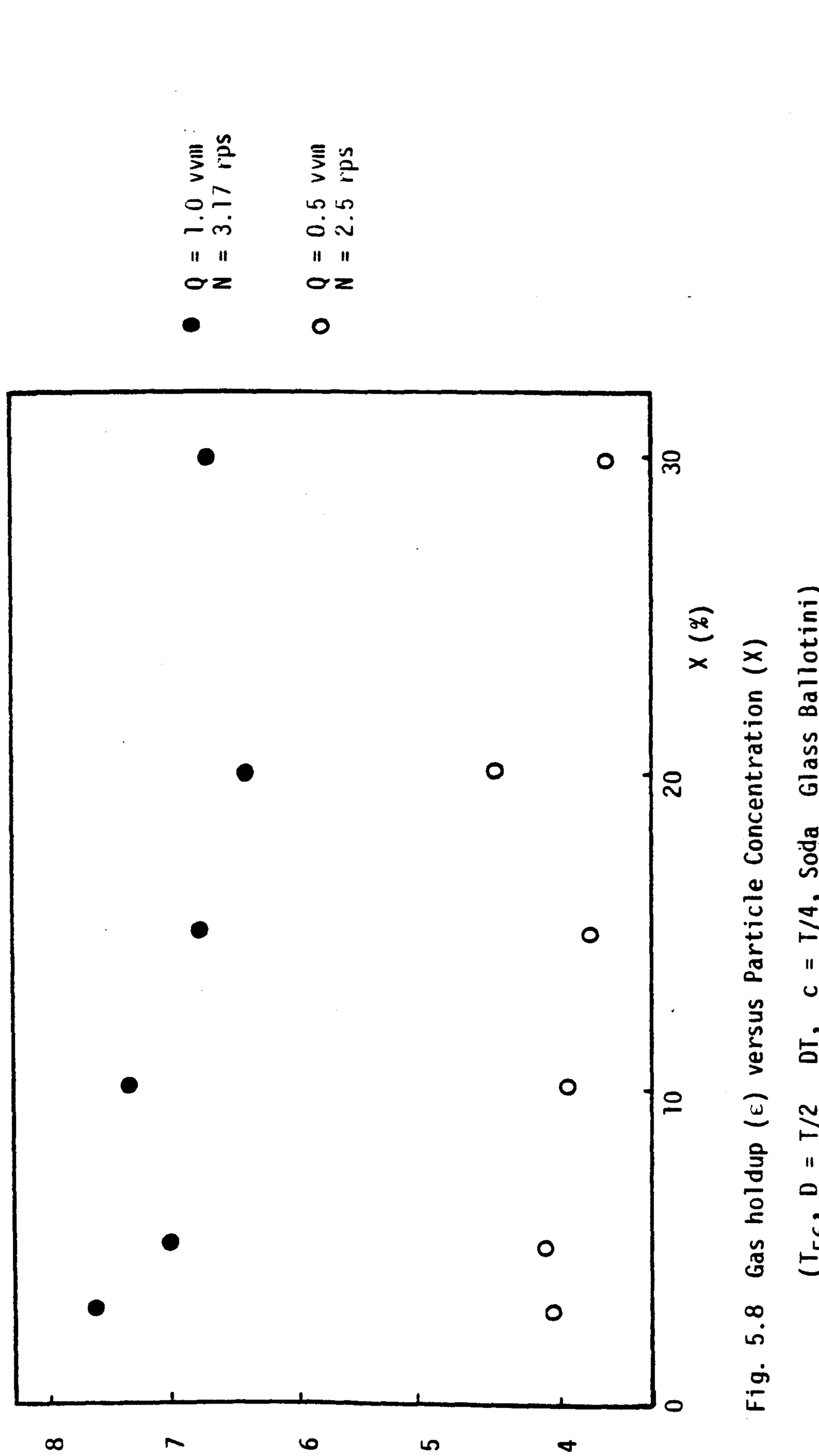

Fig. 5.8 Gas holdup (ε) versus Particle Concentration (X)
(T_{56}, D = T/2 DT, c = T/4, Soda Glass Ballotini)

phases are not well dispersed, then very high particle concentrations may have a significant effect.

5.4.2. Effect of Gas on Solid-Liquid Hydrodynamics

Consider an agitated suspension of particles at its critical condition with no aeration, i.e. $N = (N_{JS})_{Q = 0}$. The effect on sparging a small amount of gas into this system was to cause slight sedimentation such that, for the same impeller speed, the particles were no longer just-suspended, i.e. $N < (N_{JS})_{low\ Q}$. Further increases in Q led to more sedimentation such that, again for the same speed, $N << (N_{JS})_{high\ Q}$. It was demonstrated in Chapter 3 that, as gas rate increased, so the pumping capacity and ability of the impeller to circulate fluid decreased. The manner in which it did so was linked to graphs of power number against flow number for constant speed. In Chapter 4 it was established that either drag forces, local energy dissipation and associated turbulent eddies, or both, were probably responsible for suspension. Any decrease in pumping capacity will clearly decrease local velocities on the vessel base and hence affect these parameters, thereby reducing the ability of the system to suspend particles. However, the dramatic collapse of suspension observed by Arbiter[1] did not occur. A decrease in Q caused re-suspension, as did an increase in N.

Further, it was found that a unique combination of gas rate and impeller speed resulted in the just-suspended condition being achieved. This also applied to the N_{PJS} condition and was well illustrated by the results obtained for glass powder (Fig. 5.9). A clear peak was obtained when plotting normalized concentration, α (= sample concentration/bulk concentration), over a range of impeller speeds for Q = 0.25 vvm, in the same way as a peak was obtained in an unaerated system. If N was held constant at 4.1 rps $(=(N_{PJS})_{Q = 0.25vvm})$ and gas rate varied, then a peak again resulted at a gas rate of 0.25 vvm.

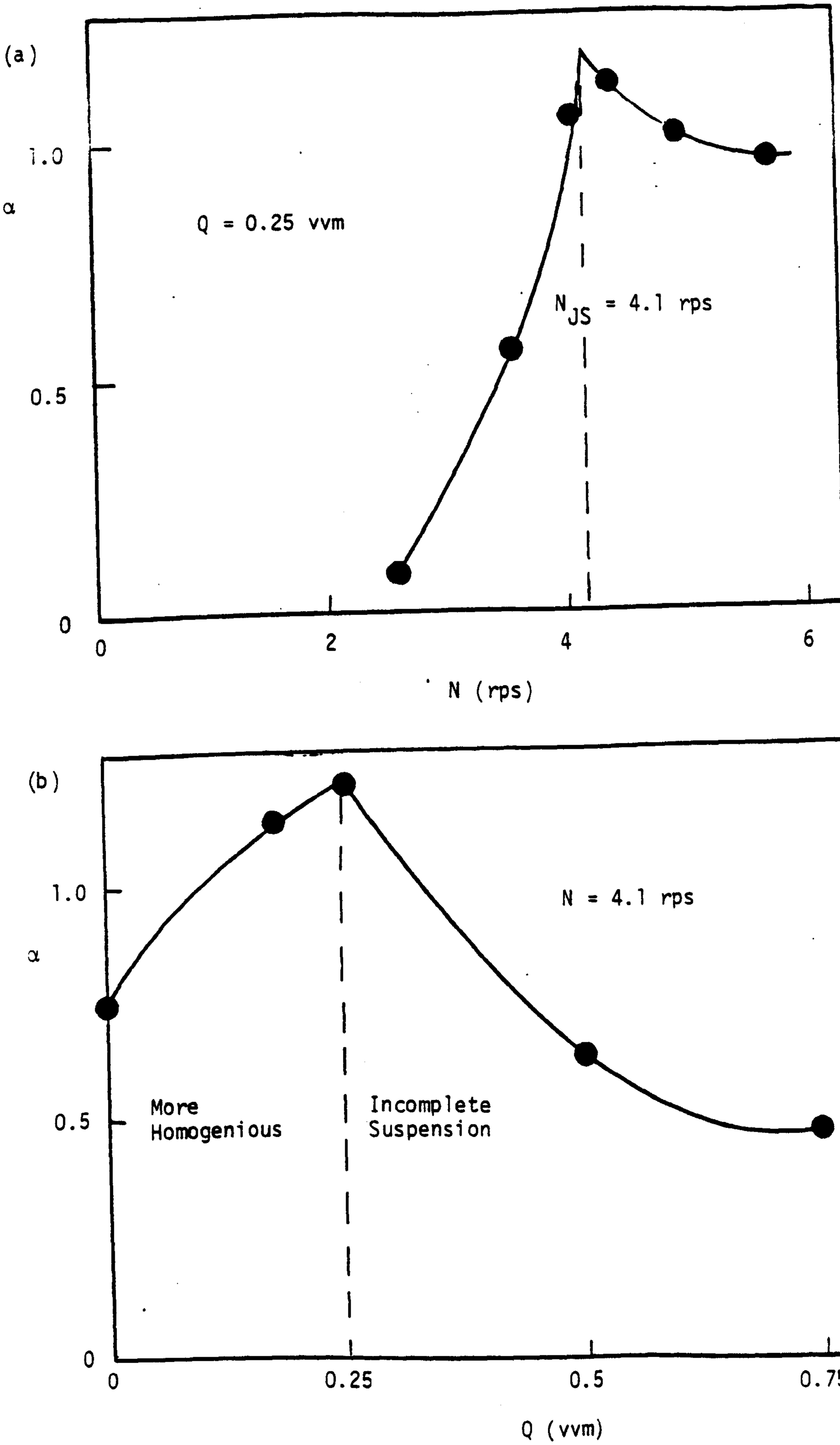

Fig. 5.9 Sampling Results for a Glass Powder Suspension.

(T_{56}, D = T/3 DT, c = T/4, X = 0.3%).

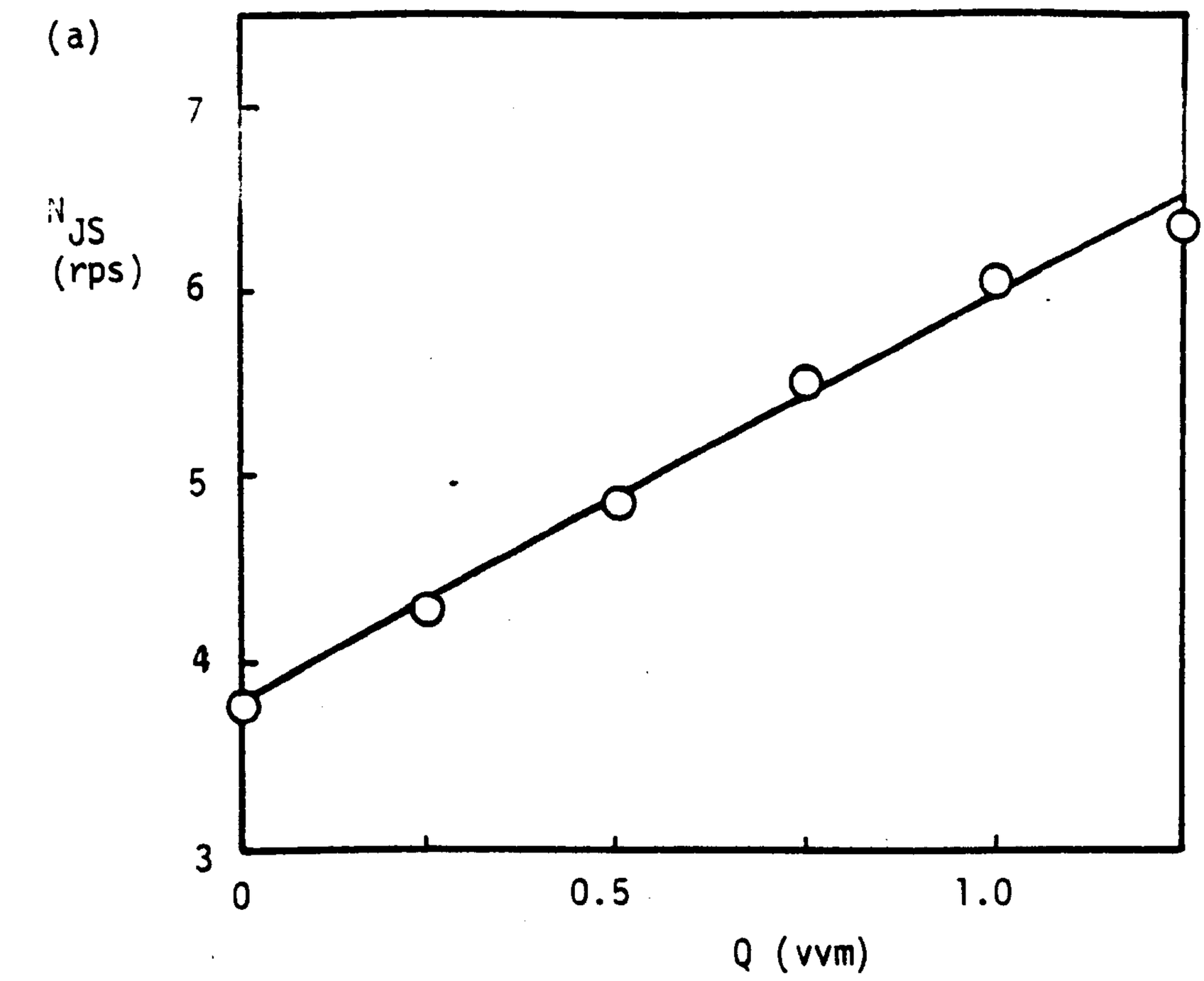

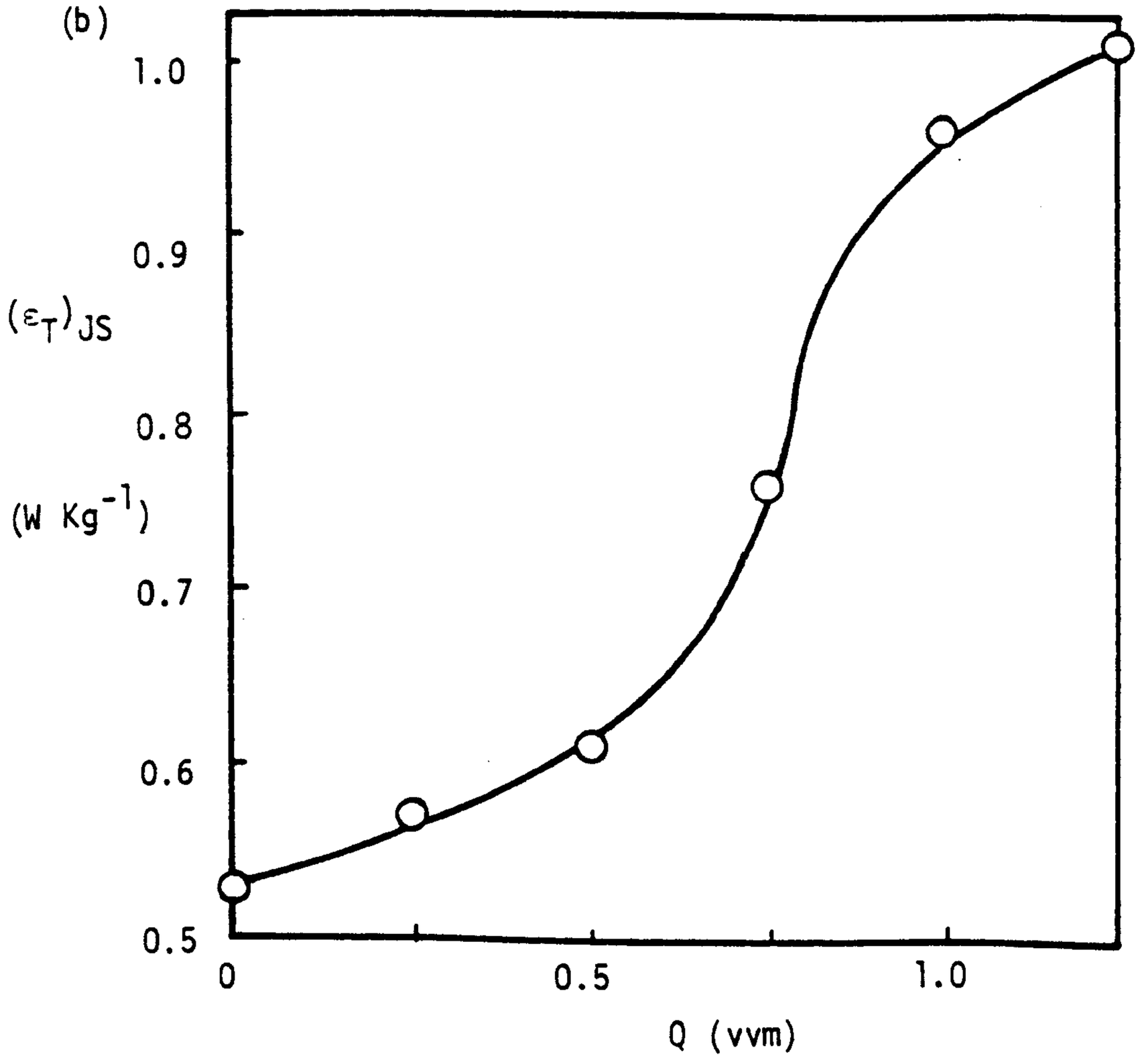

Fig. 5.10 Effect of Gas Rate on (a) N_{JS} and (b) $(\varepsilon_T)_{JS}$ (T_{56}, D = T/3 DT, c = T/4, 0.3% Glass Powder).

Higher gas rates (Q > 0.25 vvm) resulted in sedimentation and at lower gas rates (Q < 0.25 vvm) the dispersion was homogenised such that for Q = 0, 4.1 rps > $(N_{JS})_{Q=0}$. Fig. 5.10a shows how N_{JS} increased linearly with gas rate for the same glass powder system. Also, the rate of increase was such that it overcame the reduction in power that occurs on aeration and resulted in a net increase in the power input required to cause suspension (Fig. 5.10b). Thus a greater power input is necessary to cause suspension under aerated conditions than unaerated, suggesting that the gas presence has an additional effect other than a reduction of flow from the impeller region, in the form of damping local turbulence and velocities near the vessel base.

The gas phase was generally well dispersed before the particles were just-suspended, i.e. $N_{CD} < N_{JS}$. Exceptions to this are discussed in detail in Chapters 6 and 7. However, from the effects described above it is clear that an allowance must be made for the influence of aeration on particle suspension.

5.5. Conclusions

The small amount of work in the literature suggests that aeration of a particle-liquid dispersion has important consequences on the degree of solid suspension. After initial examination of the effects of both aeration on solid suspension and particles on gas dispersion, this suggestion is clearly supported. By examining in detail the consequences of varying both the particle-liquid and equipment variables, especially with regard to the interaction of Q on N_{JS} which appears to be the more significant, a far more complete picture of the characteristics of a three phase system will emerge.

CHAPTER 6.

THE INFLUENCE OF PARTICLE AND LIQUID PARAMETERS

6.1. Introduction

The results presented in both this and the following chapter were obtained wherever possible by holding all variables except the one under consideration constant. However, where this was not possible, the experimental results (Appendix 4) have been adjusted to a standard condition according to the relationships reported elsewhere within Chapters 6 and 7. Once again, the bulk of the work reported in this chapter was carried out in T_{56} with disc turbine impellers.

6.2. Particle Density

Fig. 4.2 showed the dependence of N_{JS} on $\Delta\rho$ for unaerated systems. These data are presented again, along with that obtained at several gas rates, in Fig. 6.1. Table 6.1 gives the exponents deduced from these results.

Gas Rate Q vvm	Exponent on $\Delta\rho$ - slope in Fig. 6.1	Standard Deviation of data from slope
0	0.40	0.05
0.25	0.21	0.13
0.5	0.22	0.03
1.0	0.24	0.035

Table 6.1 Dependence of N_{JS} on $\Delta\rho$

It appears that, under aerated conditions, the dependence of N_{JS} on $\Delta\rho$ is reduced to

$$N_{JS} \propto \Delta\rho^{\simeq 0.22} \qquad 6.1$$

With the exception of the polystyrene particles, the gas phase was well dispersed before the particles were suspended, i.e. $N_{JS} >> N_{CD}$. The polystyrene particles, however, were suspended just as gas bubbles were first being circulated down the vessel walls towards the

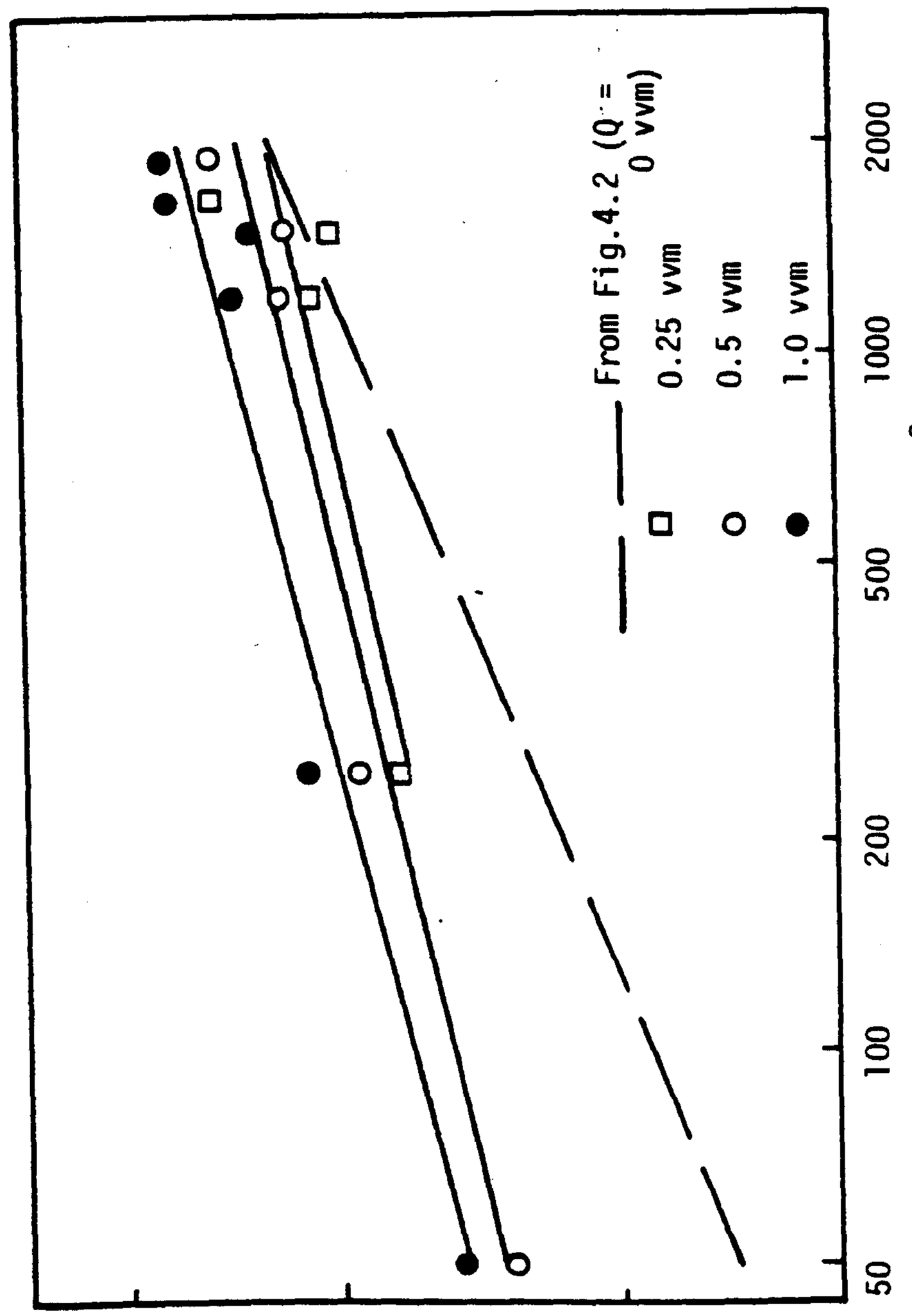

Fig. 6.1 Influence of $\Delta\rho$ on N_{JS} for Various Gas Rates

(T_{56}, D = T/3 DT, c = T/4, X = 1%, d_p = 300 μm)

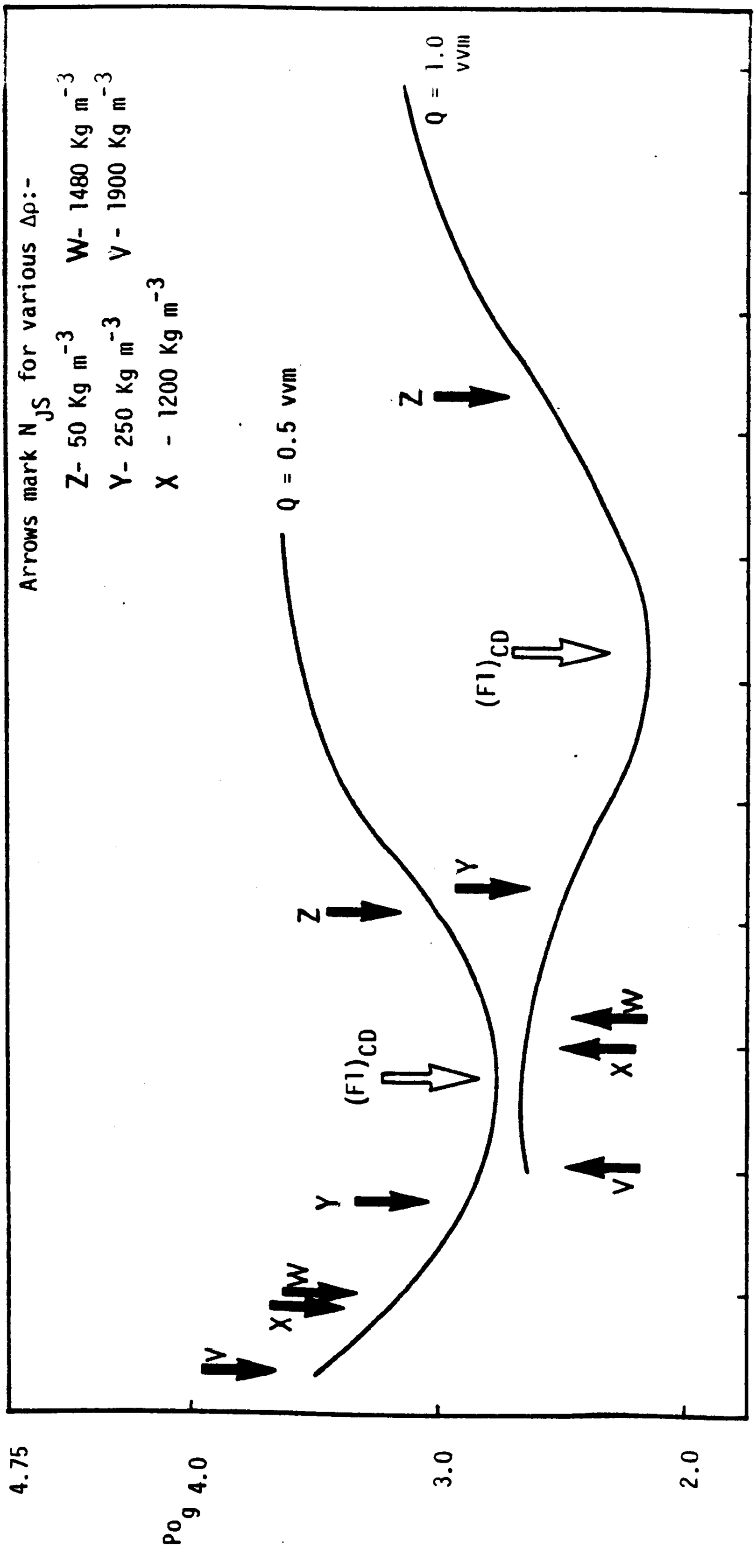

Fig. 6.2 Power number - Flow number plot showing Just-Suspended Condition for Various Particle Densities
(T_{56}, D = T/3 DT, c = T/4, d_p = 300 μm, X = 1%)

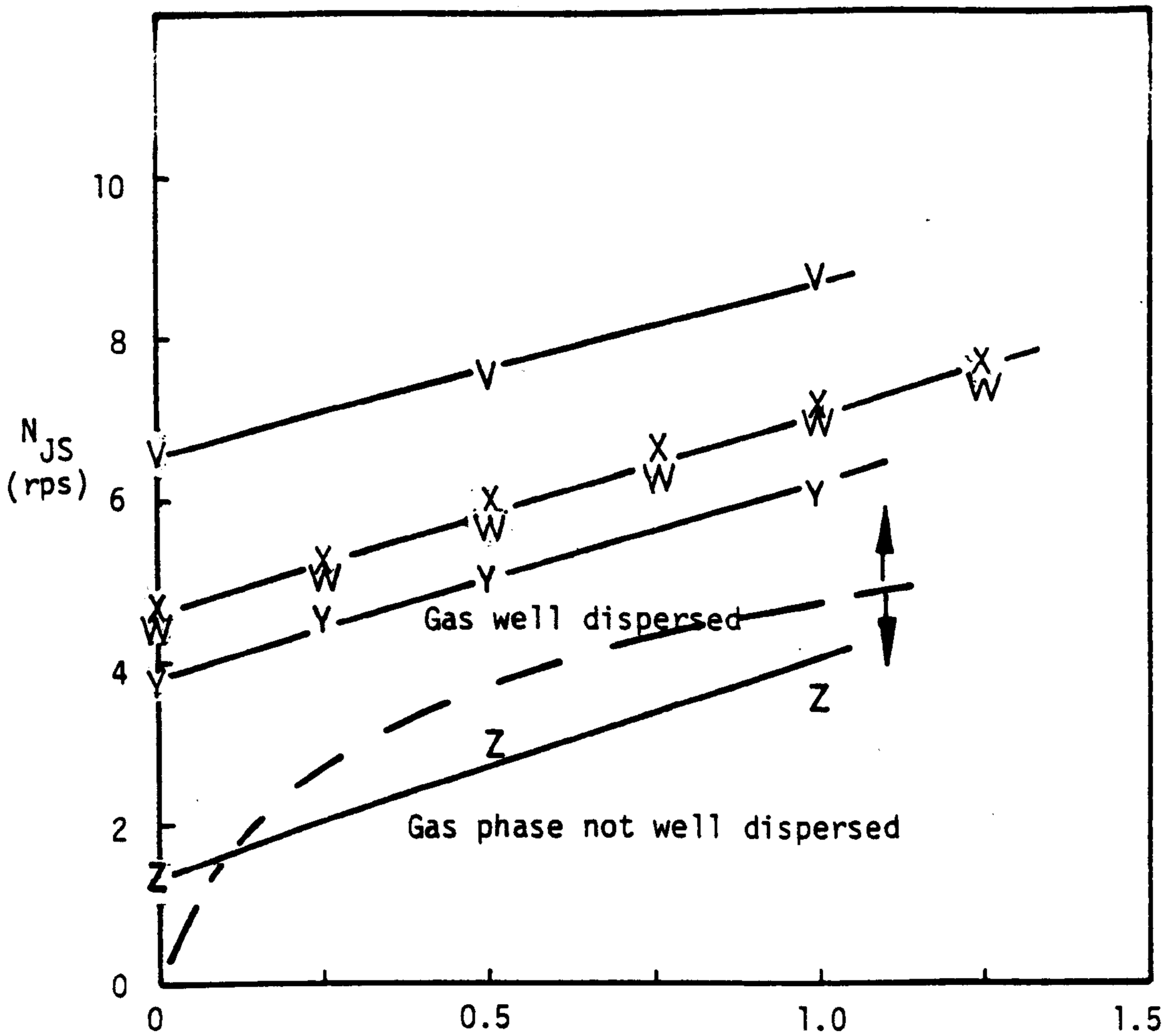

Fig. 6.3 N_{JS} versus Q for Various $\Delta\rho$

(Details and Symbols as in Fig.6.2)

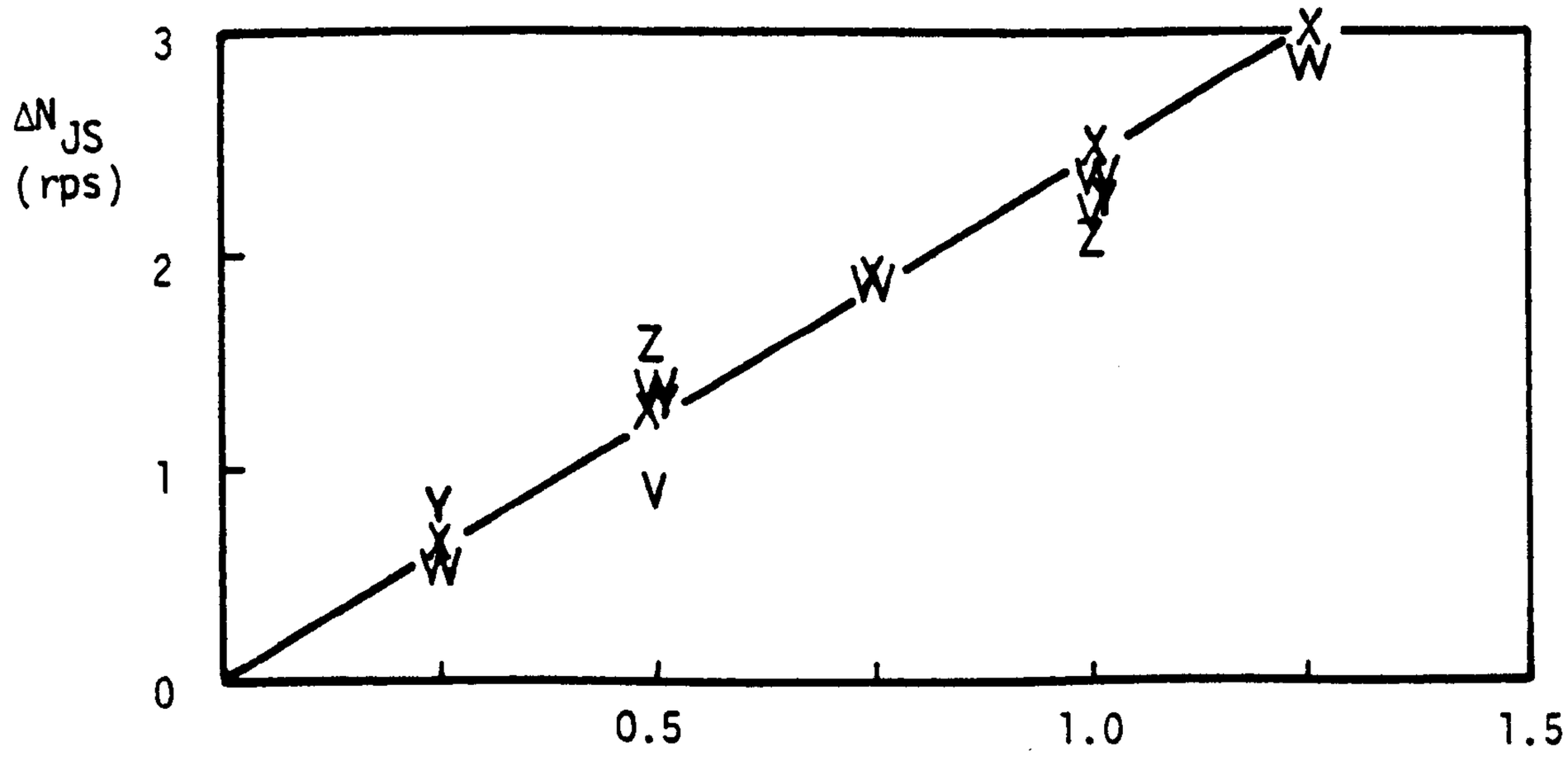

Fig. 6.4 ΔN_{JS} (= $(N_{JS})_g$ - $(N_{JS})_{Q=0}$) Against Gas Rate for Various $\Delta\rho$

(Details and Symbols as in Fig. 6.2)

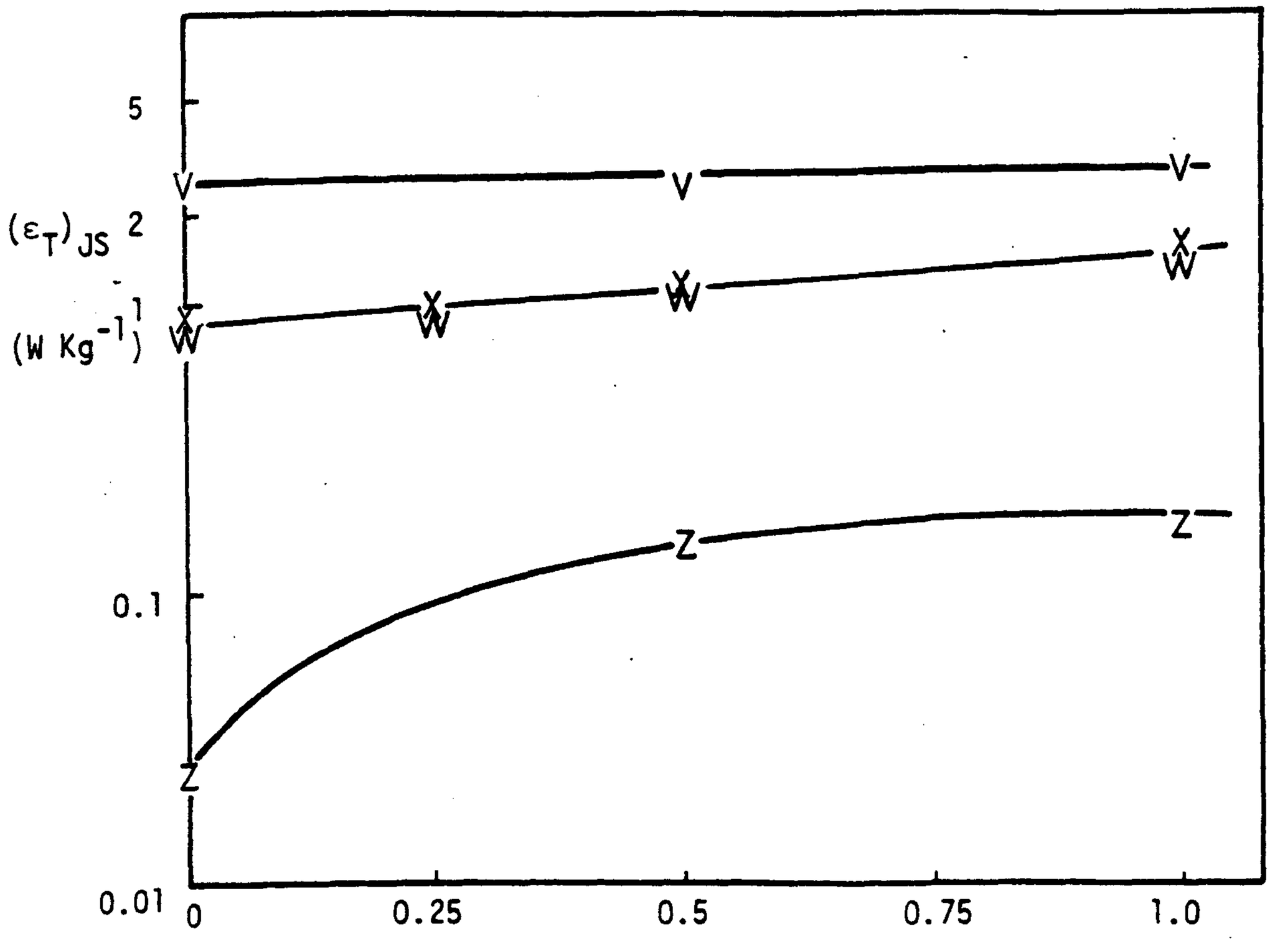

Fig. 6.5 Specific Power Input versus Q for Various $\Delta\rho$

(Details and Symbols as Fig. 6.2)

base. Thus for a fixed gas rate, the lightest suspension duty involved the particles with the lowest density difference, and as $\Delta\rho$ increased so N_{JS} also increased. Fig. 6.2 demonstrates this effect by marking the minimum suspension and gas dispersion criteria for 0.5 and 1 vvm. One point arising from inspection of this figure was that N_{JS} was achieved at a point that remained in approximately the same position on the Po_g - Fl graph in relation to N_{CD} (the minimum) for both gas rates.

Additional gas loading to a system in the just-suspended state resulted in sedimentation since P_g/P decreased. It was found that the same increase in impeller speed was necessary to restore N_{JS}, independent of the density difference. Therefore, if the data presented as N_{JS} against Q in Fig. 6.3 were replotted as ΔN_{JS} $(= (N_{JS})_g - (N_{JS})_{Q=0})$ against Q (Fig. 6.4), then all the data fell on a straight line through the origin. Since the absolute value of N_{JS} for the lead glass Ballotini was approximately five times that for the polystyrene in an unaerated system, then a similar absolute increase in N with Q would result in a very much higher percentage increase in N_{JS} with Q for the least dense particles. Hence a much greater relative increase in power input was required to re-suspend the polystyrene on aeration: this effect is shown in Fig. 6.5. The absolute variation in the specific power input necessary to cause suspension $(\varepsilon_T)_{JS}$, with gas rate was not markedly different between the particle types, but the relative increase in $(\varepsilon_T)_{JS}$ was significantly higher for the least dense particles.

Thus for a very wide range of density differences, and independent of the gas-liquid mixing condition, the increase in impeller speed necessary to restore N_{JS} on increased gassing rate was dependent only on Q for that particular geometry. Therefore on aeration of a system with a very light suspension duty, many times the ungassed

specific power input requirement may be necessary to restore N_{JS}, whereas only a small relative increase in ε_T would be necessary for a difficult suspension duty (e.g. high density difference).

6.3. Particle Concentration

The relationship between N_{JS} and particle concentration given in Eqn. 4.9 for unaerated systems was found to hold equally well in aerated systems, as shown in Fig. 6.6 for both disc turbine and mixed flow impeller systems; i.e.:

$$N_{JS} \alpha X^{0.12} \qquad 4.9$$

Once again slightly higher exponents (0.13 - 0.15) were found when using a $D = T/3$ disc turbine than when using the $D = T/2$ version (0.08 - 0.12).

It was observed that, at low concentrations, particles were dispersed throughout the whole liquid volume at $N << N_{JS}$. However, at very high concentrations, there was a very definite clear layer of liquid near the upper surface for $N << N_{JS}$. Nevertheless, for all the concentrations examined, this clear layer was eliminated and particles dispersed throughout the whole vessel contents independent of gas rate, at $N \leq N_{JS}$, though this should not be interpreted as having any special significance since other workers[2] have observed a clear liquid layer for $N \geq N_{JS}$.

Fig. 6.7 shows ΔN_{JS} against Q for six particle concentrations, covering a ten-fold increase in X. As with $\Delta\rho$, this variation in X appeared to have a negligible effect on the rate of increase of speed (with gas rate) necessary to keep the particles just-suspended, which was once again linear. The increases in specific power input necessary to maintain the systems at N_{JS} are presented in Fig. 6.8 for three different concentrations and show no apparent dependence on X, though as described in the previous section, the relative increase in $(\varepsilon_T)_{JS}$ was higher for the lighter suspension duty, i.e. the lowest concentrations.

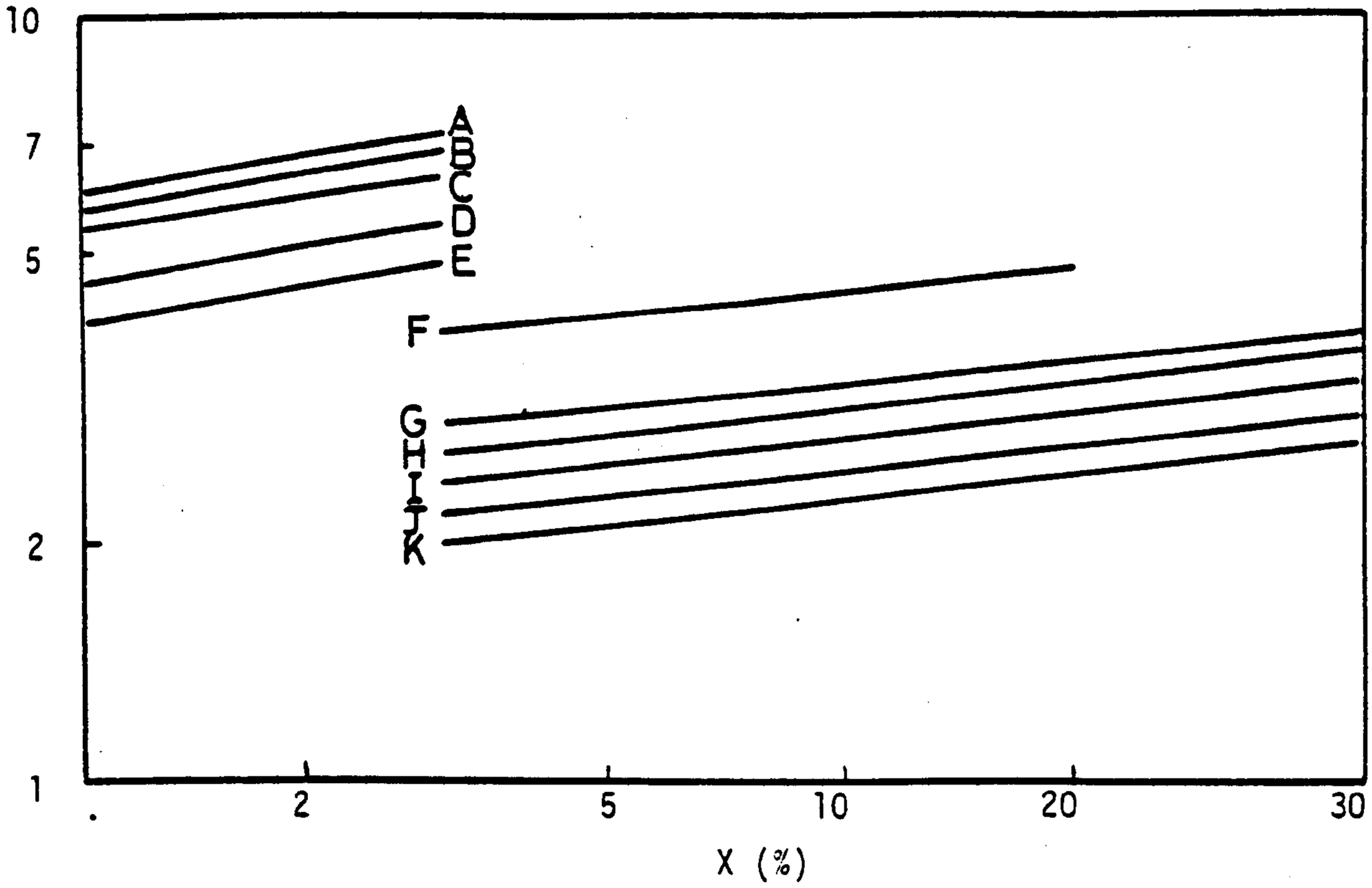

Fig. 6.6 Effect of Varying Particle Concentration on N_{JS} for Various Gas Rates and Impeller Types

(T_{56}, c = T/4, Soda Glass Ballotini)

Symbol	Q (vvm)	Impeller
A	1.0	D = T/3 DT
B	0.75	"
C	0.5	"
D	0.25	"
E	0	"
F	1.0	D = T/2 4 MFU
G	1.0	D = T/2 DT
H	0.75	"
	0	D = T/2 4 MFD
I	0.5	D = T/2 DT
J	0.25	"
K	0	"

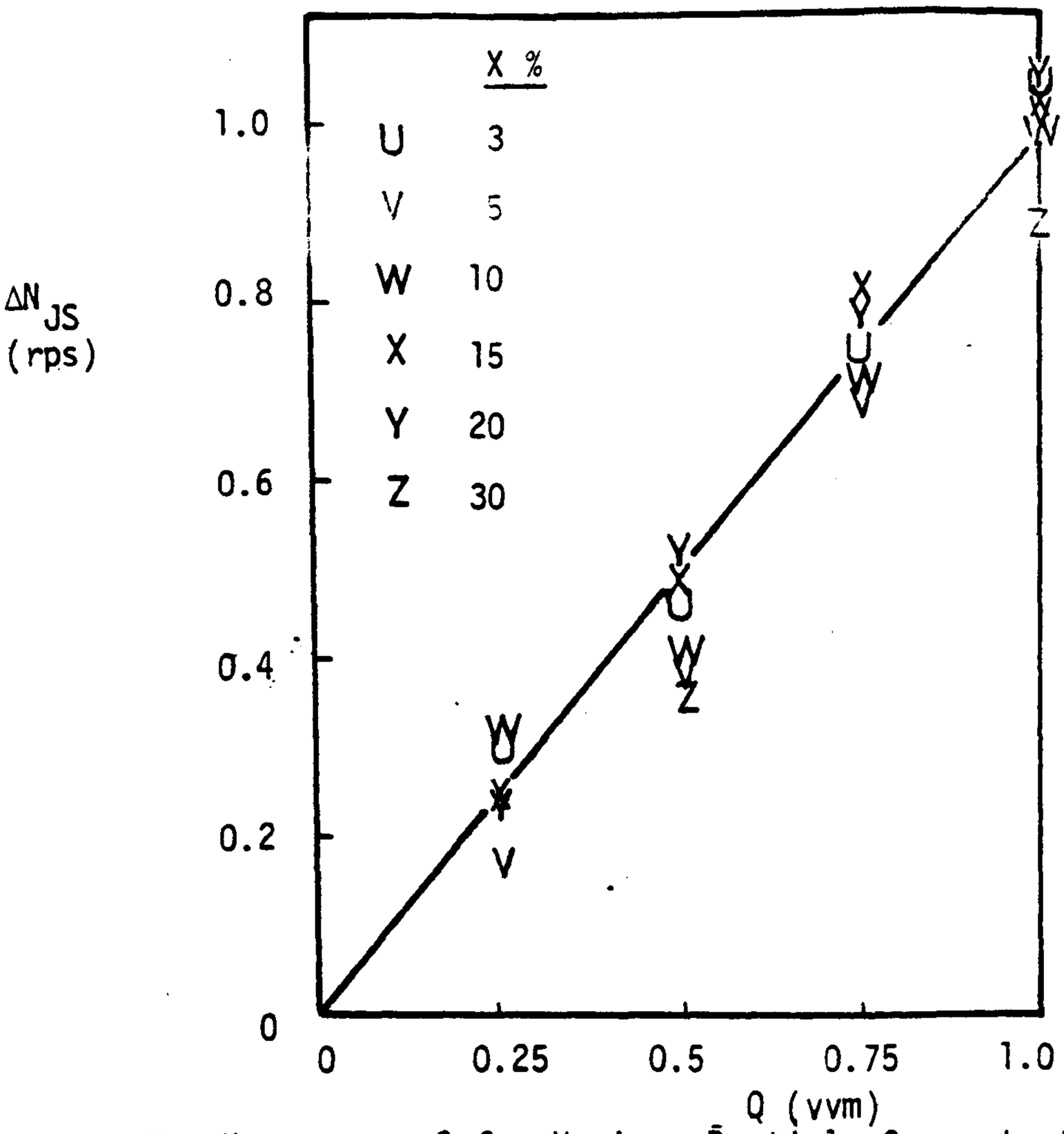

Fig. 6.7 ΔN_{JS} versus Q for Various Particle Concentrations
(T_{56}, D = T/2 DT, e = T/4, Soda Glass Ballotini)

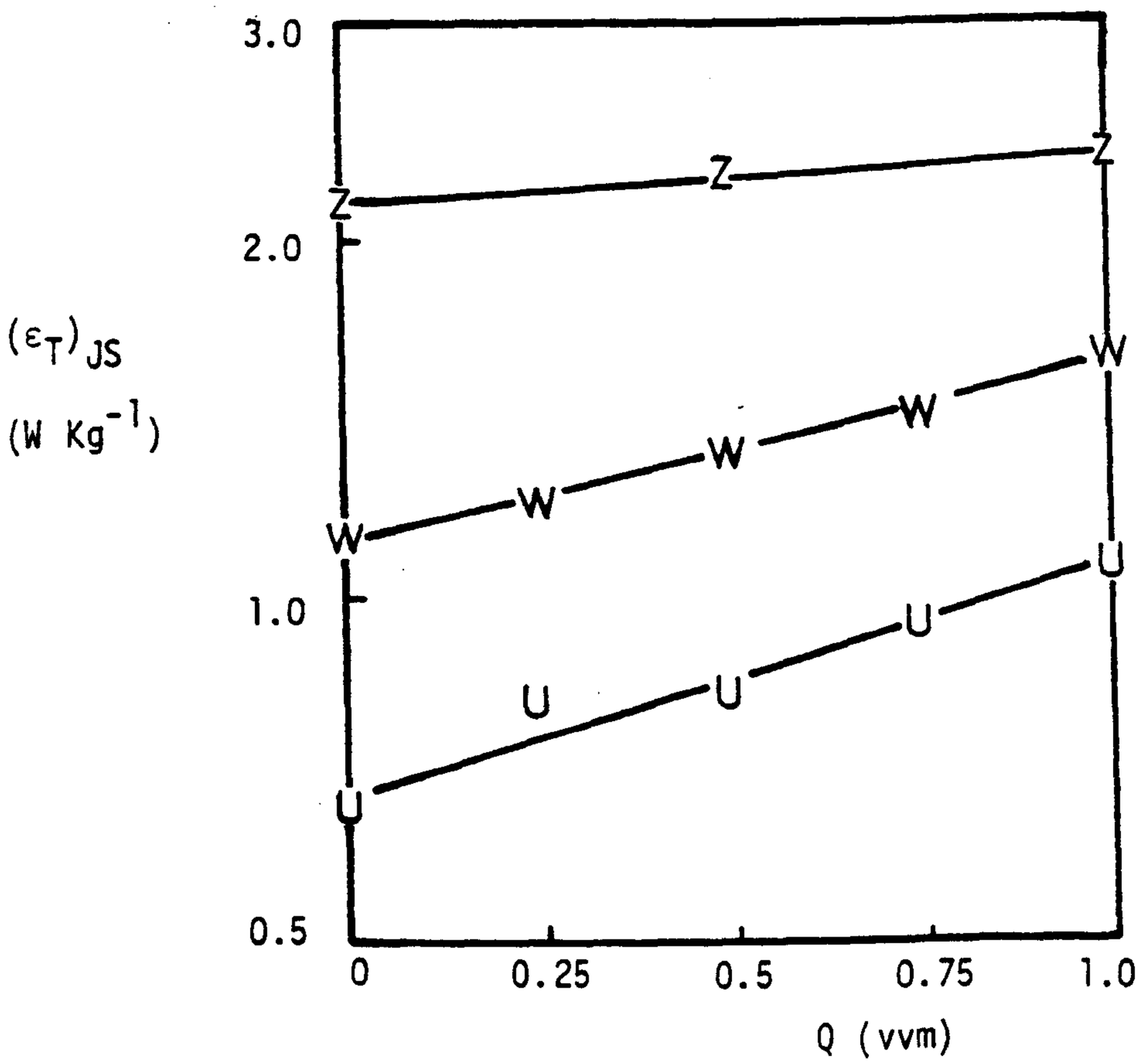

Fig. 6.8 Specific Power Input to Just-Suspend Soda Glass Ballotini versus Gas Rate.

(Details and Symbols as Fig. 6.7)

The gas phase dynamics were affected by variations in X under some circumstances. These effects have already been described in Chapter 5.

6.4. Particle Diameter and Size Distributions

Once again, the gas sparge rate had a negligible effect on the manner in which N_{JS} increased, this time with particle diameter. Fig. 6.9 presents the data for 0, 0.5 and 1 vvm. Conti and Baldi[30] suggested that the mechanism responsible for suspension changed for $d_p < 200$ μm, which is not disproved by this data since the data points relating to the smallest particles ($d_p = 92.5$ μm) appear to be at slightly lower N_{JS} values than expected from inspection of the other results. However, much more information would be required to establish this point and a regression treatment of this data gives:

$$N_{JS} \alpha \begin{cases} d_p^{0.15} & - \quad 0 \text{ vvm} \\ d_p^{0.12} & - \quad 0.5 \text{ vvm} \\ d_p^{0.12} & - \quad 1 \text{ vvm} \end{cases} \qquad 6.2$$

with correlation coefficients of 0.95 or 0.96.

The homogeneity of the dispersions containing the smaller particles was superior to that of the largest size fraction at all impeller speeds. At extremely low impeller speeds ($N << N_{JS}$) the smallest particles were dispersed throughout the whole liquid volume and no interface existed near the surface, whilst the bulk of the particles remained at rest on the base. This suggests that suspension criteria associated with the height of the slurry-clear liquid interface[41] have severe limitations.

The size distributions detailed in Section 4.4.1 fitted the unisized data reasonably well for both 0.5 and 1.0 vvm, when characterized in terms of a mass mean diameter (Fig.6.9), as was the case for the unaerated runs.

The effect of particle size on N_{JS} was very small in aerated

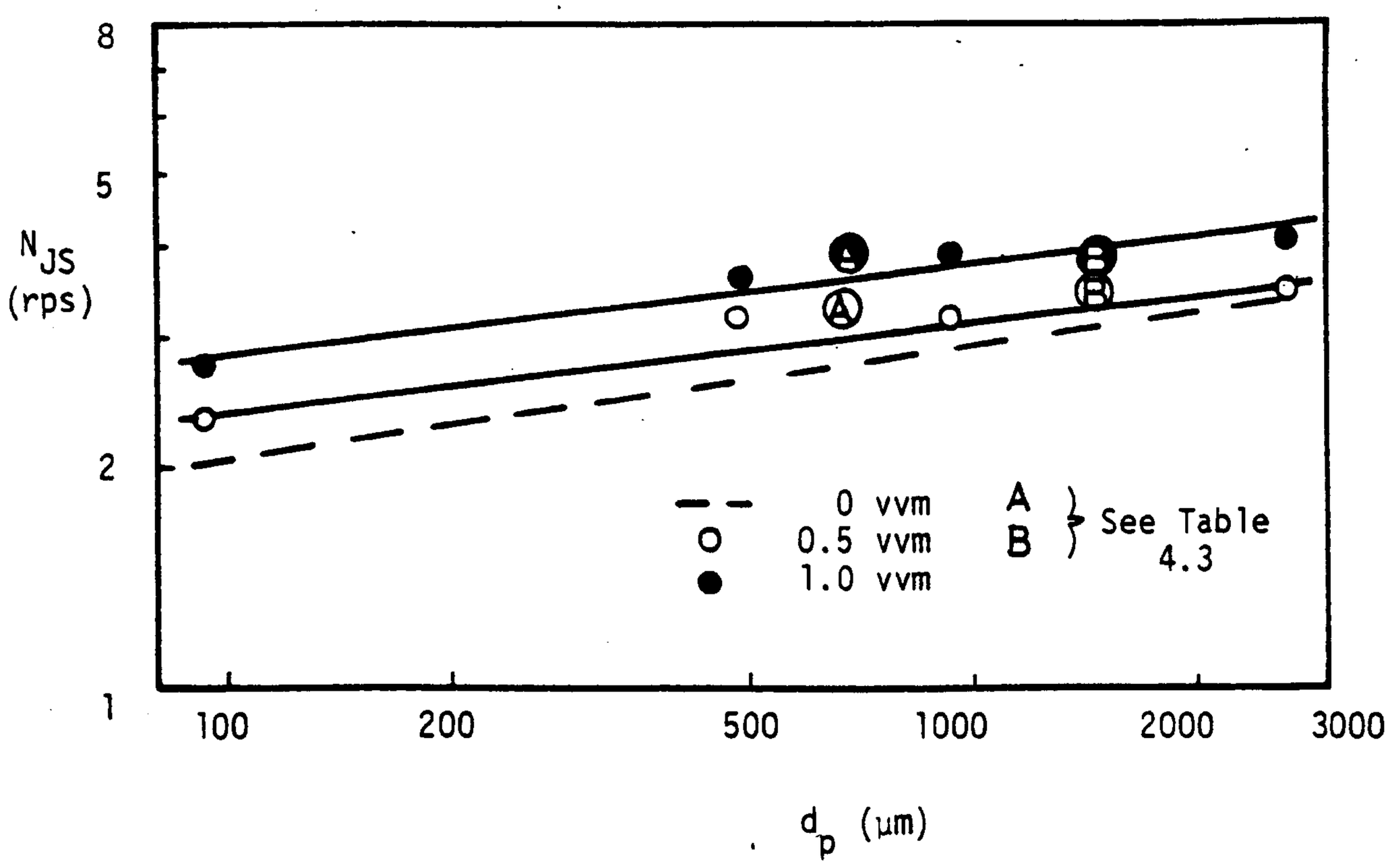

Fig. 6.9 Effect of d_p on N_{JS} for Various Gas Rates

(T_{56}, D = T/2 DT, c = T/4, 1% Lead Glass Ballotini)

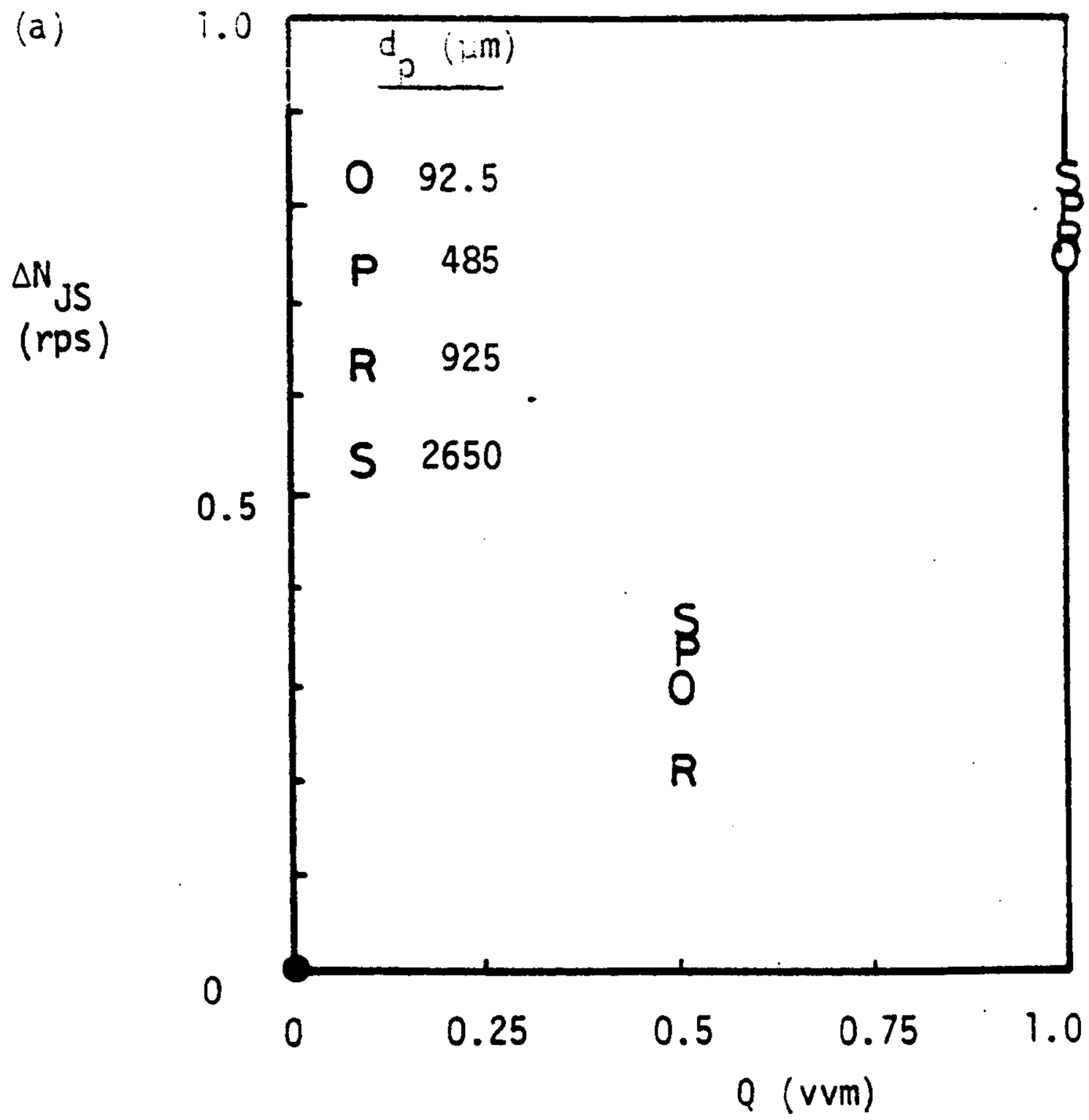

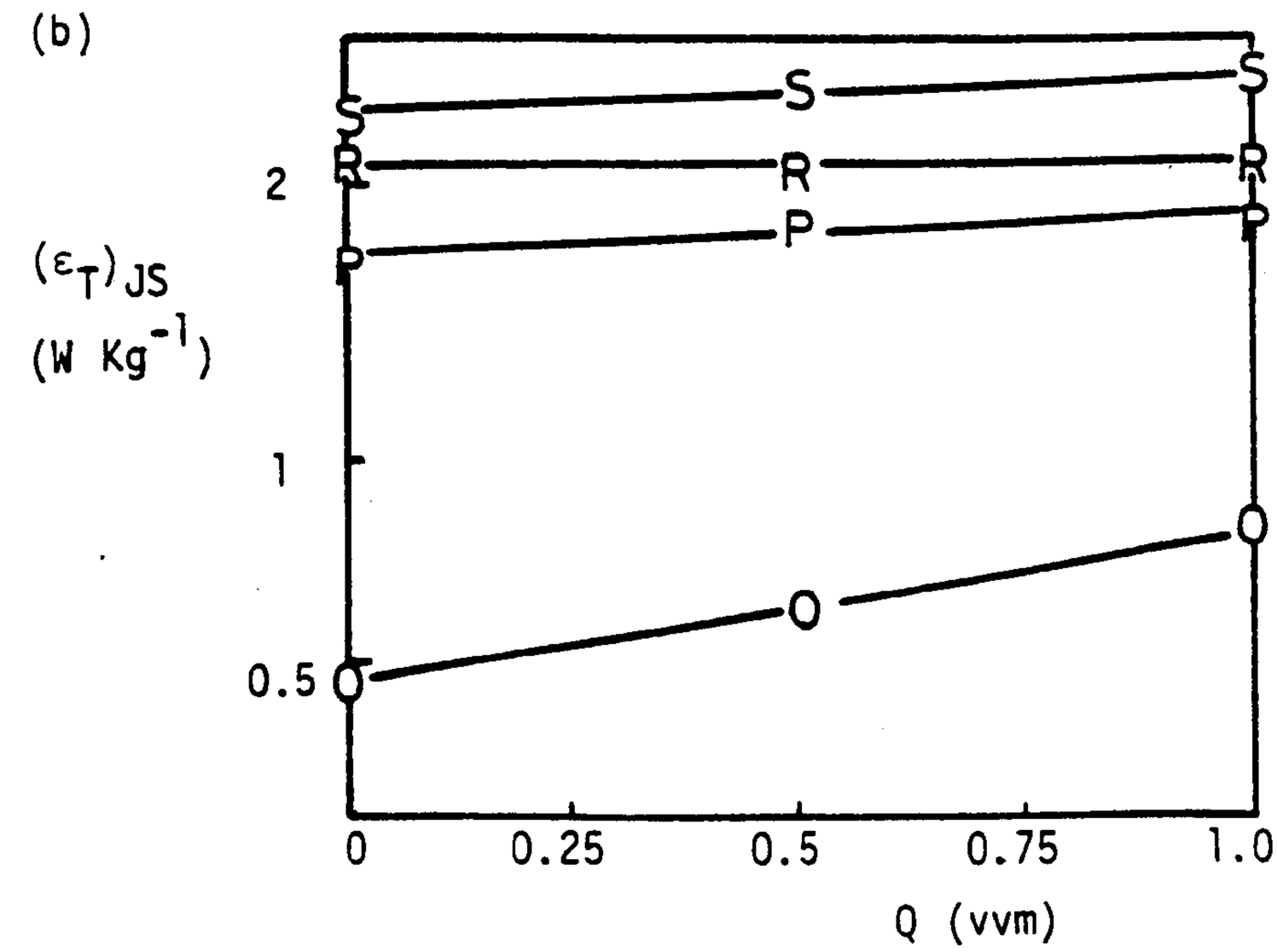

Fig. 6.10 Effect of Q on (a) ΔN_{JS} and (b) $(\varepsilon_T)_{JS}$ for Various d_p
(T_{56}, D = T/2 DT, c = T/4, 1% Lead Glass Ballotini)

and unaerated systems. However, nearly a thirty-fold size range was examined and thus resulted in a considerable increase in $(\varepsilon_T)_{JS}$ with size for any given gas rate. Fig. 6.10b shows that $(\varepsilon_T)_{JS}$ increased very little with gas rate over the range examined. A graph of ΔN_{JS} against Q (Fig. 6.10a) demonstrated the same characteristics as observed with variations in both X and $\Delta\rho$.

6.5. Particle Shape

Despite the extreme shape of the anthracite particles, which necessitated similarly higher than expected speeds and powers to cause suspension for aerated and unaerated systems, the manner in which N_{JS} increased with gas rate was similar to that observed with more spherical particles (Fig. 6.11). Fig. 6.12 shows the specific power inputs necessary to suspend the anthracite (X = 1%, $\Delta\rho$ = 400 Kg m^{-3}, d_p = 550 μm) and a 1% soda glass Ballotini suspension ($\Delta\rho$ = 1480 Kg m^{-3}, d_p = 206 μm) which should theoretically have been a more severe suspension duty, but in fact required only approximately one half of the power consumed to suspend the anthracite.

The effect of particle shape on N_{JS} has previously not been well documented. However, where extreme shapes are being dealt with it appears to have a significant influence on N_{JS}.

6.6. Liquid Viscosity

As well as the unaerated results, little effect of increasing kinematic viscosity between 10^{-6} and 5×10^{-6} $m^2 s^{-1}$ in T_{29} was observed in N_{JS}. Certainly no increase occurred as predicted in Eqn. 4.1 by Zwietering for two phase systems.

6.7. Liquid Level

Liquid levels were increased up to 1.6 T for some additional experiments with the ADT impeller. Although N_{JS} was the same as with a liquid level equal to the tank diameter, the soda glass Ballotini particles were only suspended up to a height of about one tank diameter.

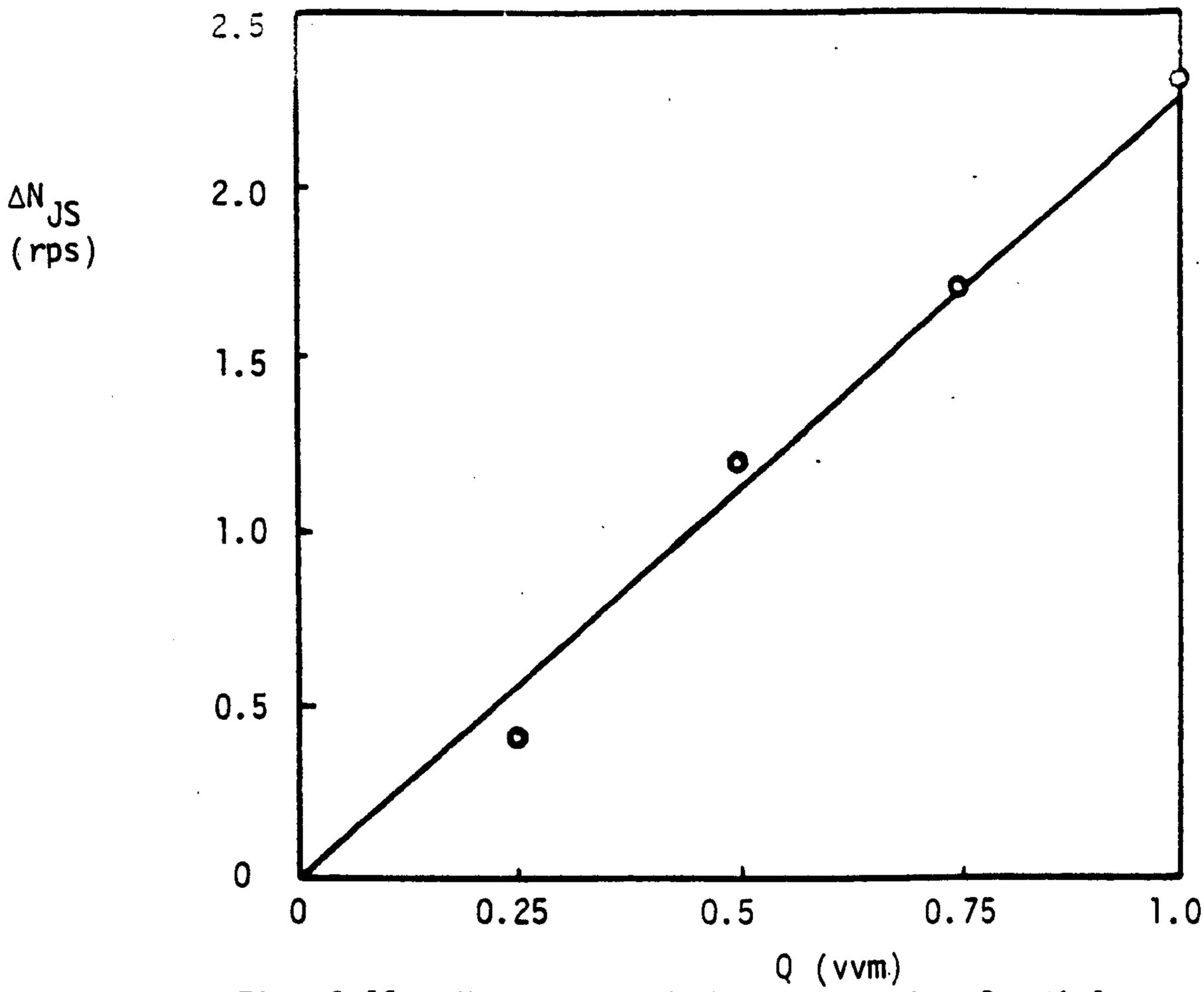

Fig. 6.11 ΔN_{JS} versus Q for Anthracite Particles.
(T_{56}, D = T/3 DT, c = T/4, X = 1%)

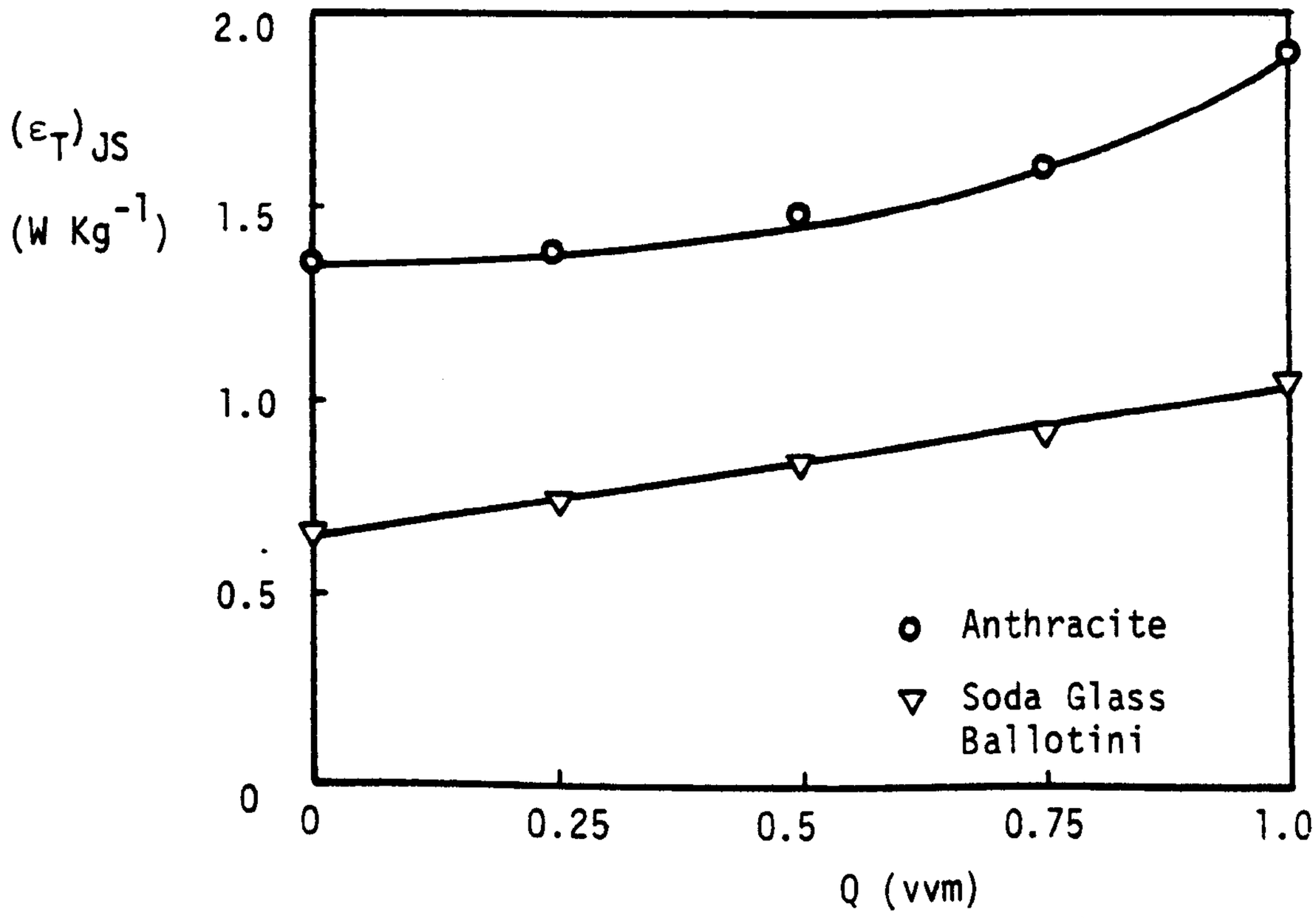

Fig. 6.12 Comparison of $(\varepsilon_T)_{JS}$ versus Q for Anthracite and Soda Glass Ballotini Particles
(T_{56}, D = T/3 DT, c = T/4, X = 1%)

6.8. Conclusions

The relationships presented in Chapter 4, showing the dependence of N_{JS} on various particle properties in unaerated systems, were examined under gassed conditions. The governing exponents were generally slightly lower in aerated systems, though only significantly so for $\Delta\rho$ which was still the most influential particle variable.

For a given disc turbine impeller geometry, the increase in impeller speed necessary to restore N_{JS} on aeration, over the unaerated value of N_{JS}, was almost directly proportional to the gas rate for a very wide range of hydrodynamic conditions, particle densities, sizes, concentrations and shapes. This led to an increase in the specific power inputs necessary to maintain the just-suspended state on aeration. Assuming that a given suspension duty requires a particular turbulence and velocity field on the vessel base, independent of aeration rate, then the increased specific power inputs required on aeration confirm that the gas presence has a damping effect on the flow and turbulence generated by the impeller.

CHAPTER 7.

THE INFLUENCE OF SYSTEM PARAMETERS

7.1. Introduction

The work presented in this chapter will involve presentation of data collected over all the vessels and impellers employed in this study, though the comments made in Section 6.1 still apply.

7.2. Impeller Type

The trends described in Chapter 6 have, in the main, referred to experiments performed using disc turbine impellers for reasons explained earlier. However, the well established advantages of other impeller types with regard to suspension in unaerated systems was confirmed in Section 4.4.2. Also, these alternative impellers have been demonstrated to be capable of satisfactorily dispersing the gas phase with varying degrees of efficiency (Chapter 3). In this section, the influence of aeration on N_{JS} is examined for the various impeller types under consideration.

Fig. 7.1 shows the increase in speed necessary to restore N_{JS} on aeration, ΔN_{JS}, against gas rate for all the impeller types in T_{56} (D = T/2, c = T/4, X = 3% soda glass Ballotini). In accordance with the results reported in Chapter 6, the disc turbine produces a linear increase in ΔN_{JS} with Q. Much further work is required in order to specify exactly the parameters responsible for suspension and then to establish the effect of gas sparging on these parameters. However, it is worth noting that Bryant and Sadeghzadek[56] have reported that average circulation times in a disc turbine agitated vessel also increase linearly with gas rate, but the neutral density radio pill technique they used has some drawbacks and the relevance of average circulation times to suspension is not established. Nevertheless, a great deal of data covering a wide range of operating conditions support this linear relationship between ΔN_{JS} and Q for disc turbines

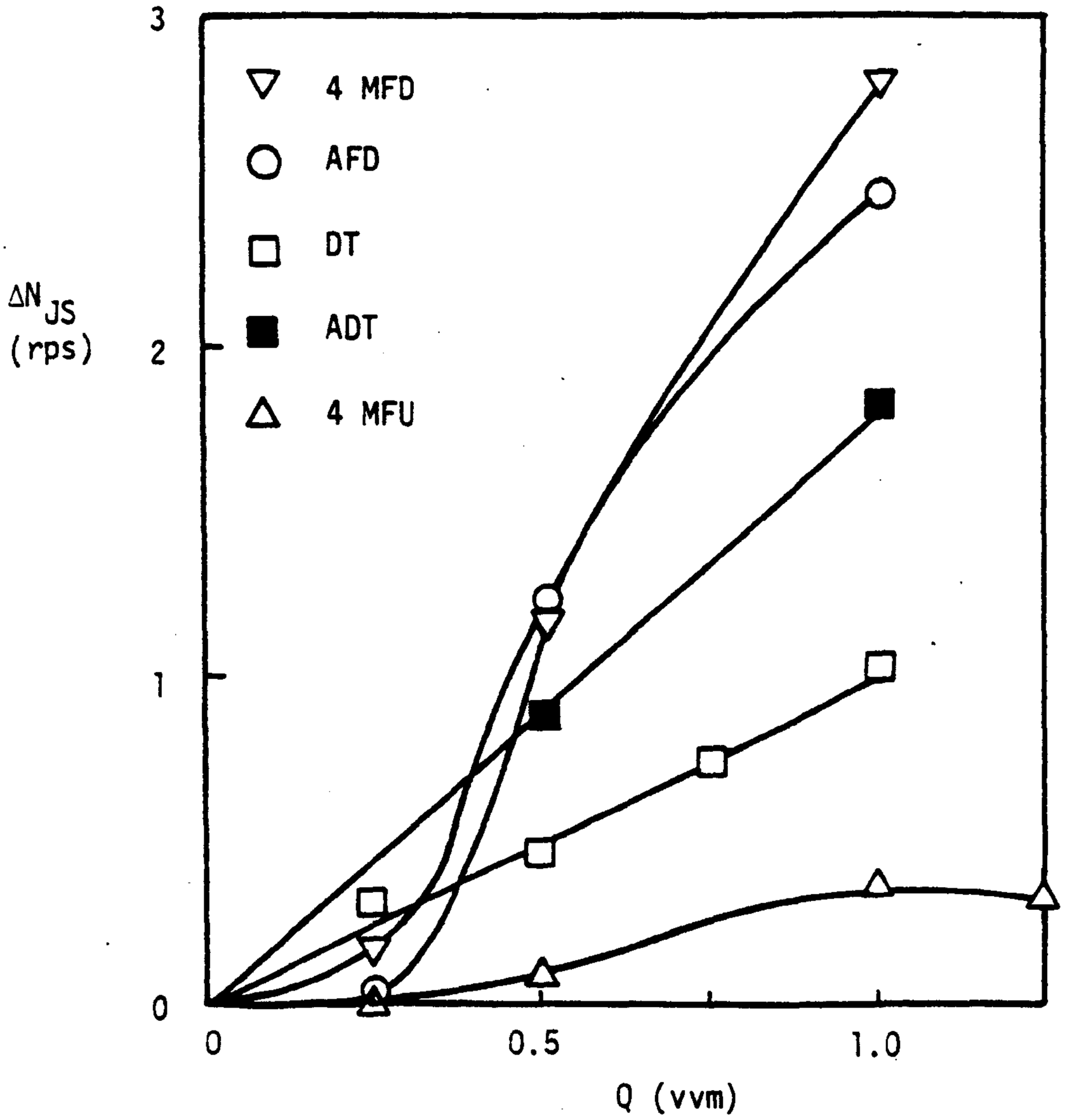

Fig. 7.1 ΔN_{JS} versus Q for Various Impeller Types

(T_{56}, D = T/2, c = T/4, X = 3% Soda Glass Ballotini)

(see Section 7.3).

In Section 3.5.8, a relationship was suggested between the manner in which the ratio P_g/P decreased (with increasing gas rate) for a given impeller system and the capacity of that system to circulate fluid and hence suspend particles. In the case of the disc turbine, the gentle decrease of the ratio P_g/P (or alternatively Po_g) with gas rate for constant speed (Fig. 3.23a) is in accordance with the gradual sedimentation observed when a disc turbine agitated system operates below the just-suspended condition. This confirms that a relationship exists between the cavity formation process which produces this fall in P_g/P and the reduced pumping capacity of the system and thence the ability of the system to suspend particles.

In contrast to the disc turbines, Fig. 7.1 shows that, at low gas rates, the impellers producing axial components of flow (4 MFD, AFD) require only very small increases in speed to maintain the system in the just-suspended condition. However, as Q increases so the rate of increase in speed necessary to restore N_{JS} becomes significantly higher. Fig. 7.2 demonstrates that this characteristic response applies reasonably well to a range of particle conditions for both the 4 MFD and AFD impellers. The results presented by Subbarao et al.[33] were purported to support a linear relationship between ΔN_{JS} and Q for propeller agitated systems but were only presented for low gas rates ($Q < 0.4$ vvm) and thus could have been interpreted as linear.

Generally the disc turbine established a well dispersed gas phase at lower speeds than those for which particle suspension was achieved, except for the lightest of suspension duties. Also, stable operation was possible in terms of power demand for all combinations of suspension and gas dispersion requirements. However, the impellers with a downward axial component of flow displayed fluctuations in power demand and corresponding fluctuations in the degree of gas

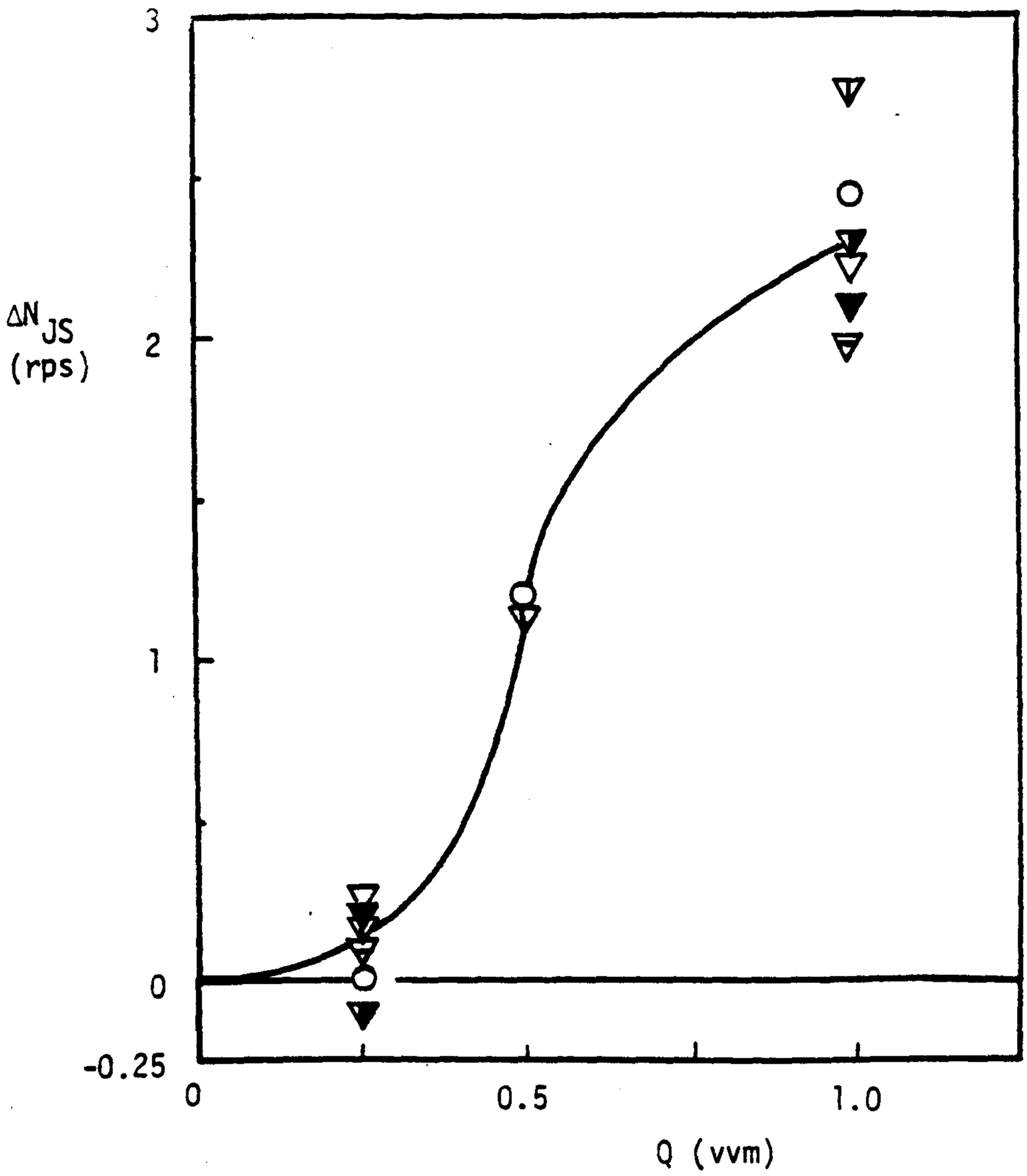

Fig. 7.2 ΔN_{JS} versus Q for Axial and Mixed Flow Impellers Pumping Down. (D = T/2, c = T/4)

▽ 20% Soda Glass Ballotini, 4 MFD, T_{56}

▼ 1% Sand, 4 MFD, T_{56}

▽ 3% Soda Glass Ballotini, 4 MFD, T_{56}

○ 3% Soda Glass Ballotini, AFD, T_{56}

▽ 1% Sand, 4 MFD, T_{91}

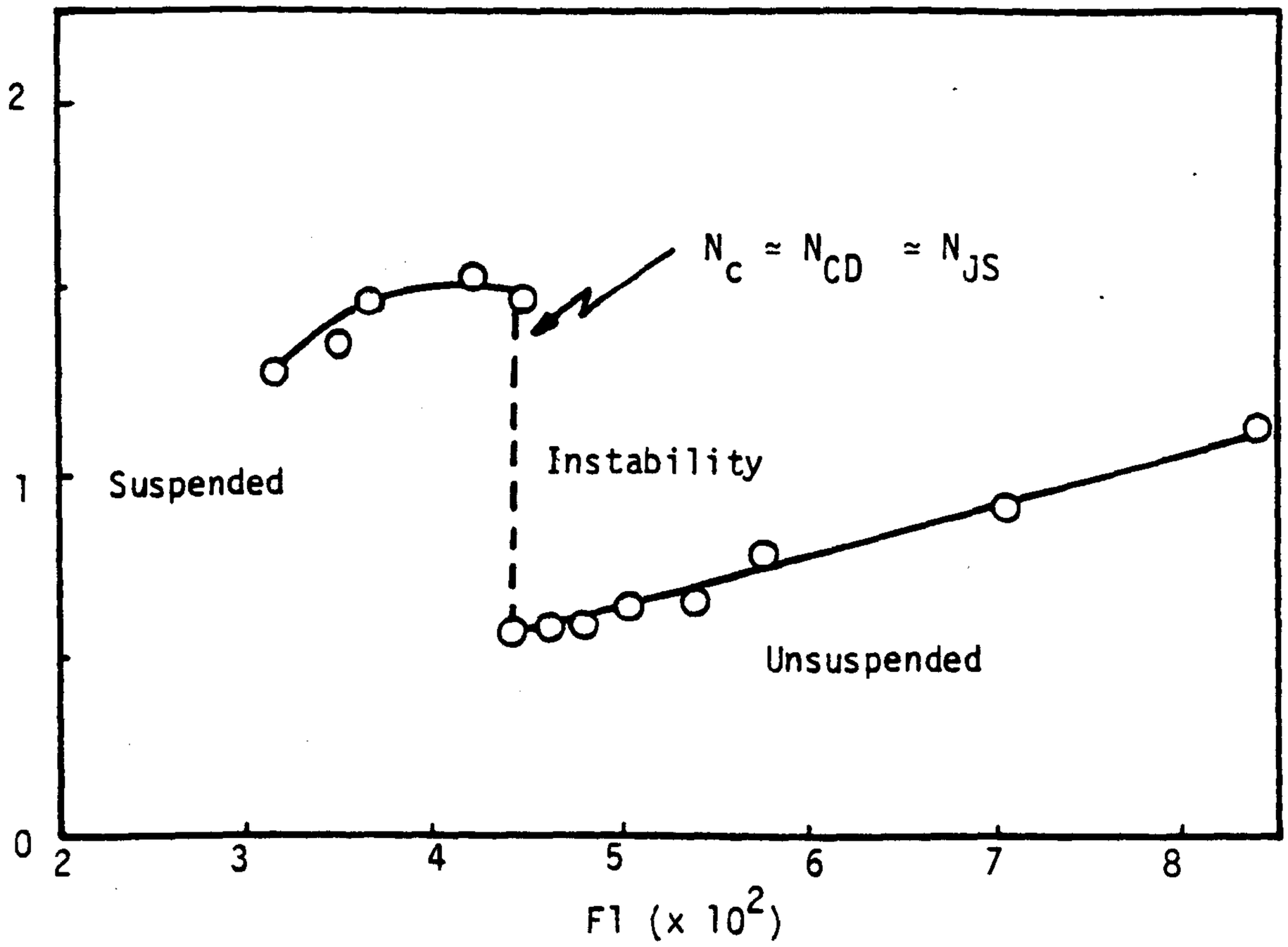

Fig. 7.3 Power number versus Flow number for the D = T/4 4 MFD Impeller (T_{56}, c = T/4, 1% Soda Glass Ballotini, Q = 0.5 vvm)

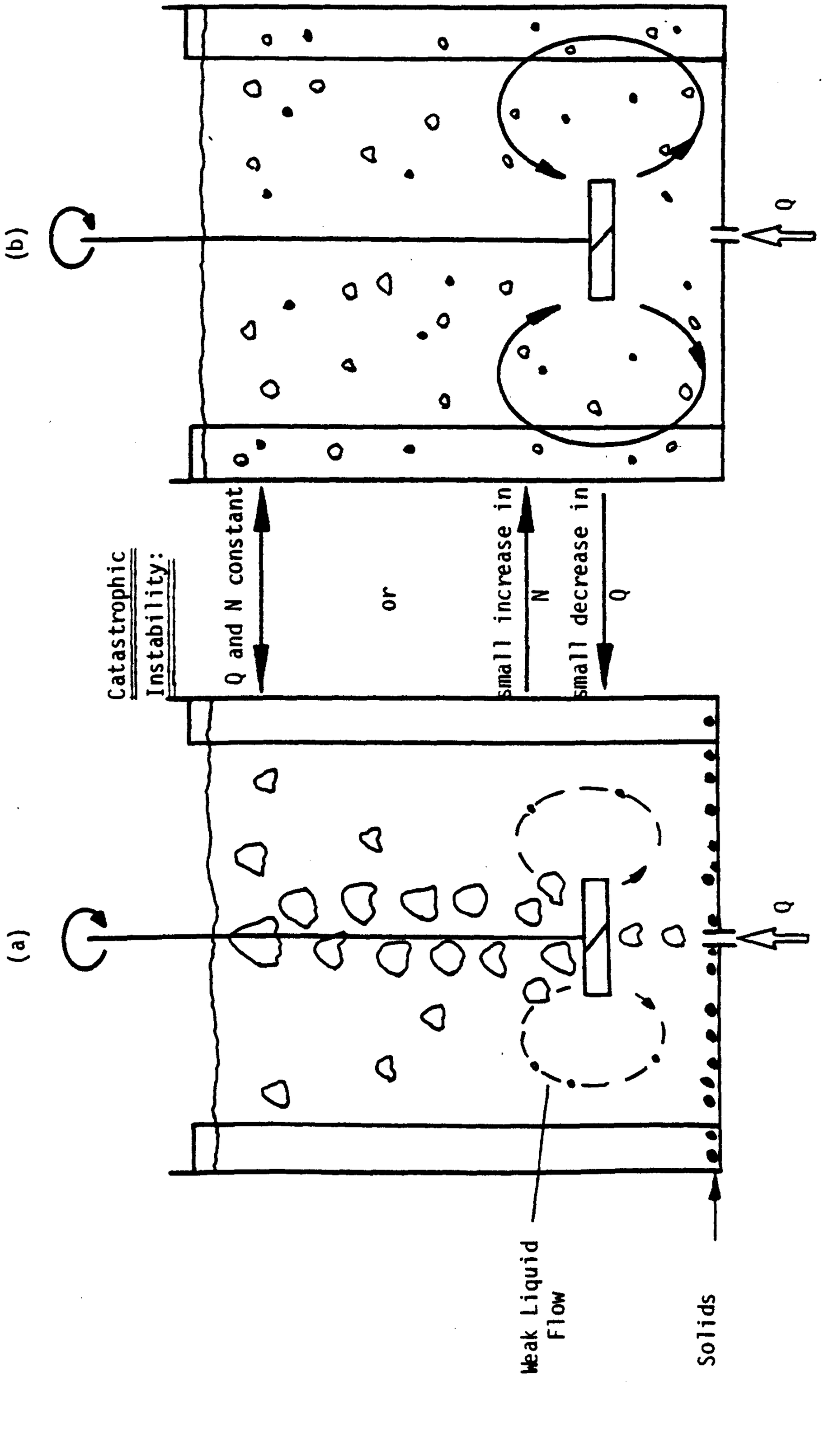

Fig. 7.4 Flow Patterns for an Aerated D = T/4 4 MFD

dispersion (Chapter 3). Fig. 7.3 shows the power number - flow number graph for the smaller (D = T/4) 4 MFD impeller operating at a constant gas rate. As with its gas dispersion behaviour, the smaller impeller displayed more exaggerated but similar trends to the larger version. Consequently when operating the smaller (D = T/4) 4 MFD impeller at its critical condition, the system oscillated between a completely dispersed gas and particulate phase (Fig. 7.4b) and a situation where the particles were completely sedimented and the gas phase badly dispersed (Fig. 7.4a). This regime of instability was relatively narrow and corresponded with the jump in power number (Fig. 7.3). At higher speeds ($N > N_{CD}$) the system remained well mixed. However, at low gas rates (e.g. Q = 0.25 vvm) additional increases in speed over and above N_{CD} were required to achieve N_{JS}. The obvious result of this critical behaviour was that small increases in gas rate could cause sudden and catastrophic sedimentation, as reported by Arbiter et al.[1] for flotation cells. Also, as in Arbiter's work, the severity of this sedimentation corresponded with a sharp drop in the ratio P_g/P with gas input rate (Fig. 3.23b), compared to the more gradual decrease in P_g/P and correspondingly gentle sedimentation observed for disc turbines. The larger impellers (D = T/2) showed basically the same characteristics but in a less severe manner. Instead of oscillating between complete suspension and all the particles being stationary on the vessel base, the flow would tend to stutter so that the particle velocity across the base varied between a high and low value. However, even for $N < N_{CD}$, particles would to some extent be suspended off the base, in contrast to the smaller impeller. N_{JS} would normally correspond with the point when the period of these fluctuations was one to two seconds and thus sometimes occur at $N \leq N_{CD}$, since N_{CD} is defined as the speed at which the torque fluctuations are negligible.

Therefore operation at $N < N_{JS}$ involves a less severe loss of efficiency with larger 4 MFD impellers since sedimentation is less severe than for the smaller version (a slightly more gradual fall in P_g/P with Q - Fig. 3.23a). Fig. 7.5 shows how N_{JS} increases with gas rate for both 0.14 m and 0.28 m diameter 4 MFD impellers, along with the regions of instability (from Fig. 3.12b), the upper limit of which corresponds with N_{CD}. At low gas rates for both impeller sizes, N_{JS} was slightly greater than N_{CD}, implying that the gas phase had been dispersed before complete suspension was achieved. However, as gas rate was increased, these impellers were not so capable of handling the high gas loading, as indicated in Fig. 3.23 by the sharp fall and then a levelling out of the P_g/P curves at comparatively low gas rates, these phenomena corresponding with a fall in pumping capacity of the impeller as the gas flow dominated the impeller action and the bulk of the gas thereafter "chimneyed" up the shaft. Consequently gas dispersion became the more severe duty for $Q \gtrsim 0.25$ vvm. However, even then, $N_{JS} \not\lesssim N_{CD}$ since the reduction in pumping capacity was so great at $N \lesssim N_{CD}$, that only for $N \approx N_{CD}$ was suspension achieved. Therefore, at high gas rates, $N_{CD} \approx N_{JS}$. The possibility of even a very light suspension duty being achieved before the gas phase is dispersed thus seems less likely with MFD impellers because of the more severe difference in P_g/P at the critical condition compared to a disc turbine.

These characteristics, then, are responsible for the responses shown in Fig. 7.1 and 7.2, i.e. for low gas loadings a relatively small increase in speed is necessary to restore N_{JS}, and for higher gas loadings, a much higher rate of increase in speed is needed. The propeller was very similar in behaviour to the MFD impellers, as shown in Figs. 7.1 and 7.2. This corresponds with the similarity in gas dispersion behaviour (Chapter 3). However, the rate of decrease

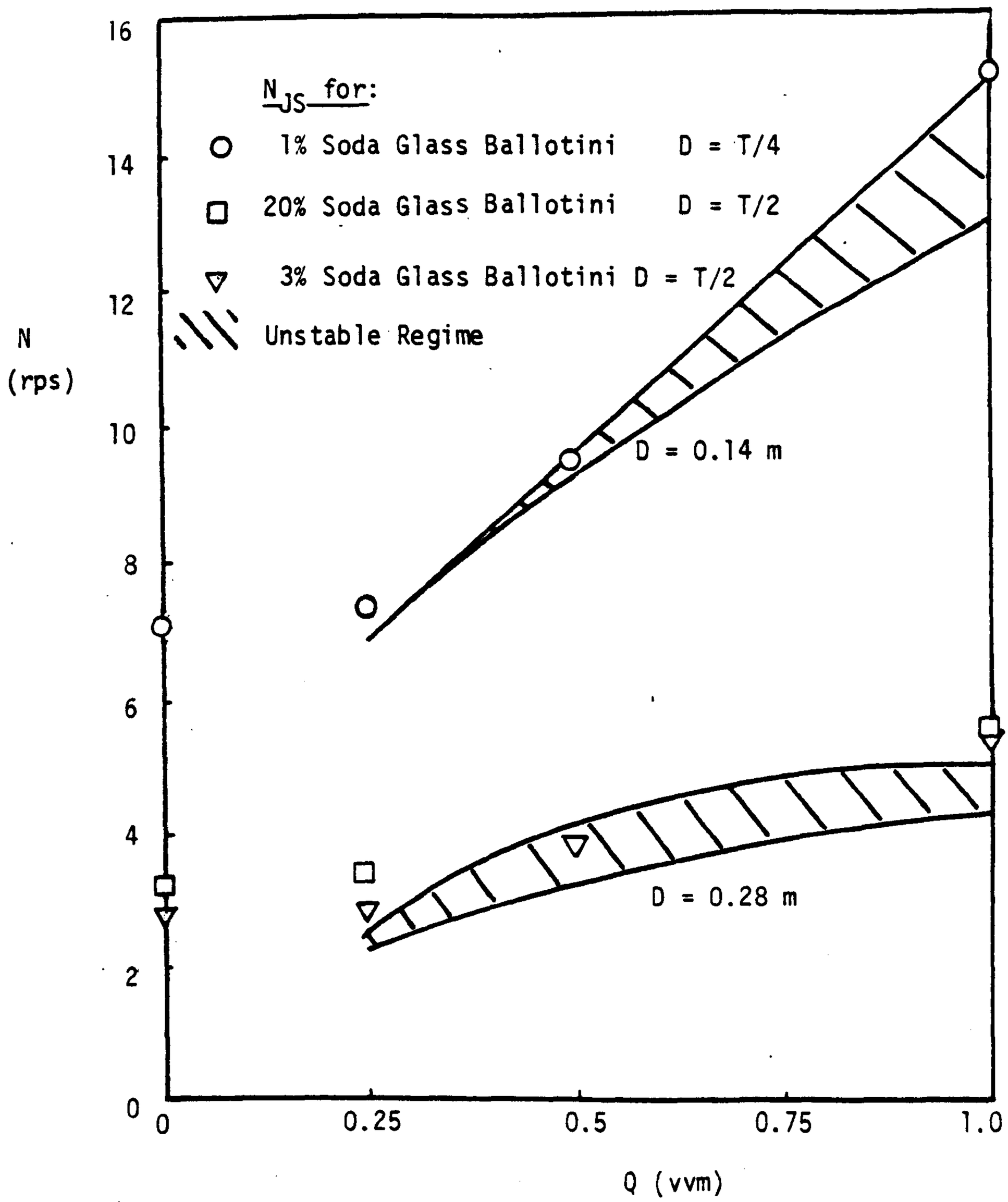

Fig. 7.5 Comparison of Gas Dispersion and Particle Suspension Conditions for 4 MFD Impellers in T_{56}.

of P_g/P with Q (Fig. 3.23a) was less marked than the 4 MFD impellers and suggests that less severe sedimentation occurs as Q increases, although the fluctuations in particle motion on the base were just as noticeable as with the 4 MFD impeller. The increase in power consumption that occurred for low gas rates with the propeller possibly enhanced the flow activity on the vessel base and therefore further reduced the effect of gas on N_{JS} at very low loadings (Fig. 7.2: $\Delta N_{JS} = 0$ for Q = 0.25 vvm).

Only one set of data (for Q = 0.5 and 1.0 vvm) was obtained with the ADT impeller. Nevertheless, inspection of Fig. 7.1 appears to show that, in terms of ΔN_{JS} against Q, it lies somewhere between the disc turbine and the AFD or MFD impellers as might be expected.

The 4 MFU impeller was shown in Section 4.4.2 to be the least energy-efficient impeller with regard to particle suspension in unaerated systems. However, in Chapter 3 it was shown that N_{CD} and P_g/P were relatively insensitive to increases in gas rate (see Figs. 3.19 and 3.23). The result of this insensitivity was that N_{JS} was comparatively insensitive to gas rate since the adverse effects of aeration on the flow produced by the impeller were relatively limited. This is reflected in Fig. 7.1 which shows that comparatively low values of ΔN_{JS} were obtained.

The result of the phenomena described in this section is that the order of merit, in terms of the energy requirement to cause suspension, given in Section 4.4.2, changes with gas rate. Fig. 7.6 shows that, at zero and low gas rates, large energy savings can be made by using AFD or MFD impellers, especially for the smaller versions (D = T/4, Fig. 7.6b). However, as gas rate increases so these impellers lose their advantage and eventually the disc impellers and, more noticeably, the mixed flow impeller pumping upwards become the most energy-efficient. These two types also have the advantage of:

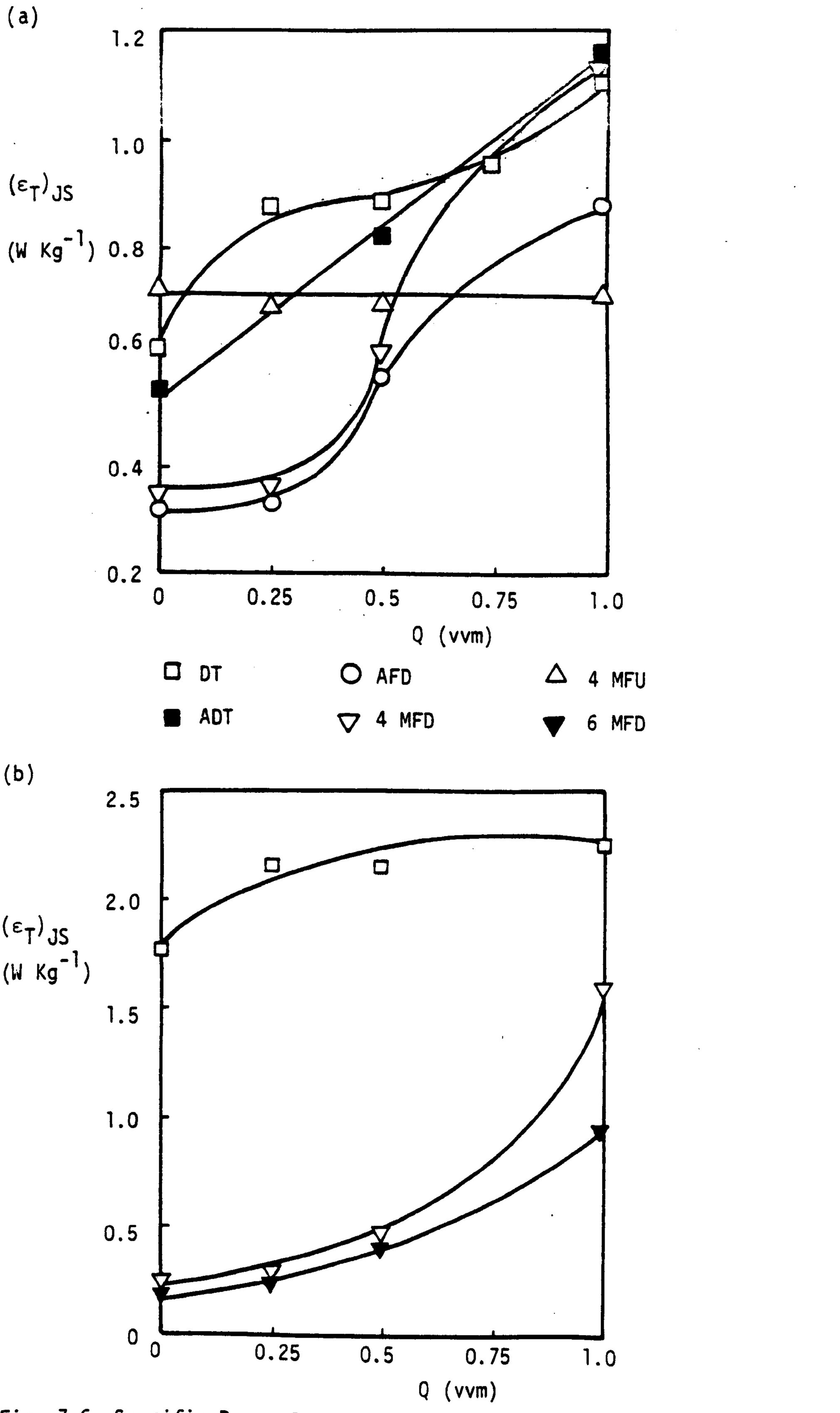

Fig. 7.6 Specific Power Input versus Gas Rate for Various Impeller Types: (a) D = T/2, 3% Soda Glass Ballotini (b) D = T/4, 1% Soda Glass Ballotini (T_{56}, c = T/4)

(a) Not displaying drastic sedimentation if the gas rate fluctuates, thus they can be operated closer to the minimum conditions.

(b) Producing a more homogeneous system for severe suspension duties (e.g. high concentrations) than the AFD or MFD impellers, especially at high gas rates.

Thus the choice of an optimum impeller system depends on the process gassing rate. At low gas rates, the MFD and AFD impellers should be the most suitable, provided that there are no fluctuations in Q since this could result in drastic collapse of suspension. However, with a large safety factor built in, for example operating at $\varepsilon_T = 2(\varepsilon_T)_{JS}$, which will enable larger fluctuations in Q without danger of sedimentation, very large reductions in the specific power input necessary to completely suspend a given particle system can still be achieved. These savings are particularly high for the smaller impellers. If a very high process gas rate is required, a disc turbine or a mixed flow impeller pumping upwards is the optimum choice, though the disc turbine is singularly the most versatile. Perhaps the optimum specification for versatility would be a mixed flow impeller with a reversible mode so that it could be operated pumping upwards or downwards as the situation demanded.

7.3. Impeller Diameter

The relationships found in Chapter 4 relating N_{JS} to impeller diameter in ungassed systems:

$$\text{DT: } N_{JS} \propto D^{-2.45} \qquad 4.14$$

$$\text{4 MFD: } N_{JS} \propto D^{-1.5} \qquad 4.13$$

were found to hold very well in three phase systems as shown in Fig. 7.7 and summarised in Table 7.1 below.

Impeller Type	Gas Rate Q vvm	Exponent of D = slope in Fig. 7.7
DT	0	-2.45
DT	0.5	-2.45
DT	1.0	-2.30
4 MFD	0	-1.5
4 MFD	0.5	-1.45
4 MFD	1.0	-1.45

Table 7.1 Exponents Relating N_{JS} to Impeller Diameter from T_{56}

As with unaerated suspensions, the prediction of power consumption from these relationships should be undertaken with great care since power numbers may vary due to minor dimension inconsistencies between the impellers. Fig. 7.8 seems to indicate that using a disc turbine impeller of diameter less than 0.14 m in T_{56} would require extremely high power inputs. It would be difficult to infer from Fig. 7.8 whether larger or smaller 4 MFD impellers were the most energy-efficient. This seems logical since assuming that:

$$P \propto N^3 D^5 \quad \text{and} \quad N_{JS} \propto D^{-1.5} \qquad 7.1$$

then for constant volume $P_{JS} \propto (\varepsilon_T)_{JS} \propto D^{0.5}$ 7.2

Also, if Zwietering's exponent is used ($N_{JS} \propto D^{-1.67}$), then by similar reasoning to the above:

$$(\varepsilon_T)_{JS} \propto D^0 \qquad 7.3$$

Thus very small or no changes at all would be expected on varying the diameter of a 4 MFD impeller.

The variation of Po_g with impeller size for disc turbine impellers in aerated systems was similar to the variation of Po in unaerated systems (see Appendix 1). However, with the 4 MFD impellers the power number at N_{JS} was not only consistently higher for the smaller version but was also less sensitive to Q than the larger

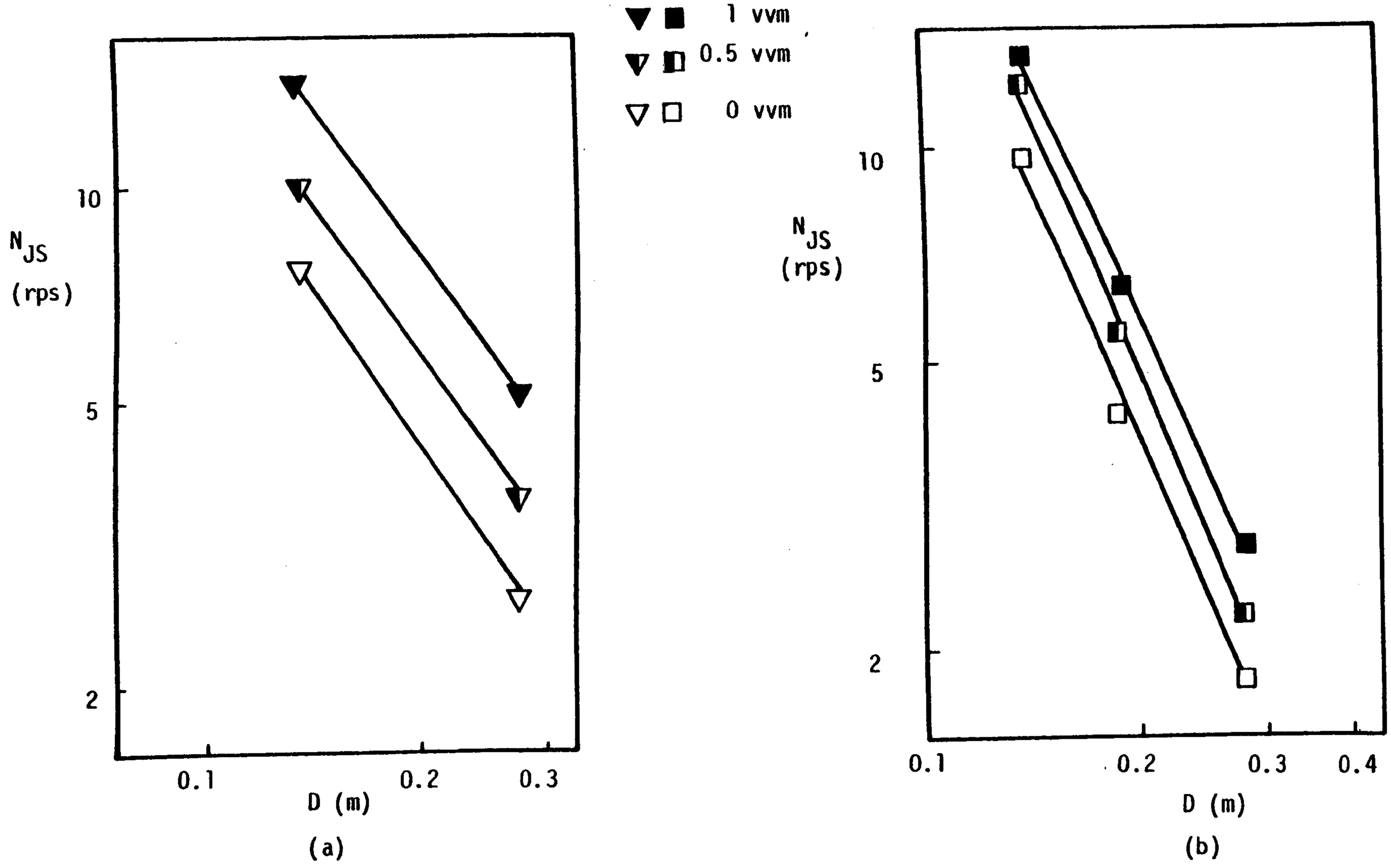

Fig. 7.7 N_{JS} versus Impeller Diameter for (a) 4 MFD and (b) DT Impellers in T_{56} (c = T/4)

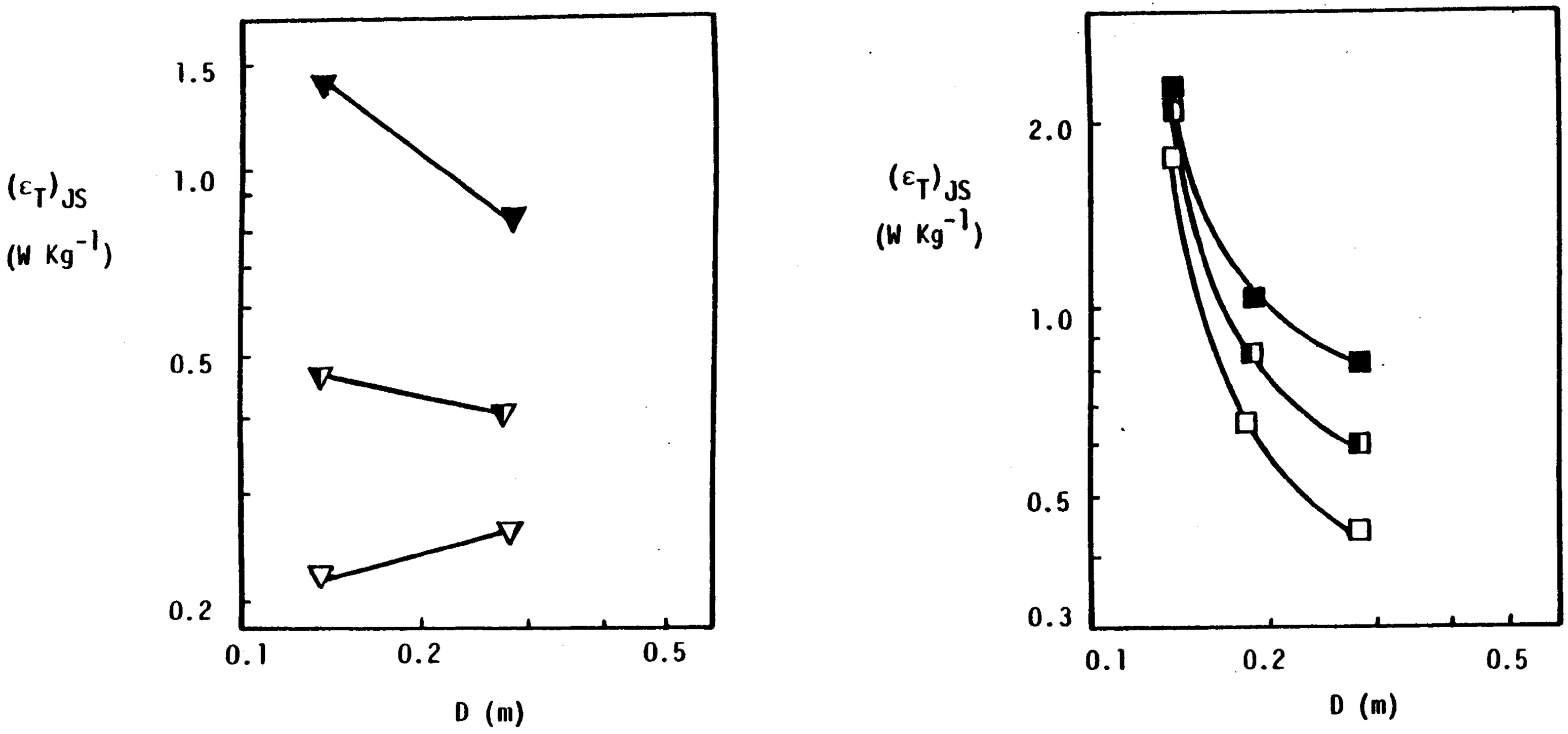

Fig. 7.8 $(\varepsilon_T)_{JS}$ versus D for (a) 4 MFD and (b) DT Impellers in T_{56} (c = T/4)

▽ □ 0 vvm ▼ ◧ 0.5 vvm ▼ ■ 1.0 vvm

version, as shown in Table 7.2 (see Chapter 3).

T (m)	D (m)	Q (vvm)	Po or Po_g at N_{JS}
0.56	0.28	0	1.4
		0.5	0.79
		1.0	0.56
0.56	0.14	0	1.5
		0.5	1.4
		1.0	1.5

Table 7.2 Variation of Power Number with Impeller Size for 4 MFD Impellers for T_{56}

The effect of gas rate on N_{JS} is presented as ΔN_{JS} against Q for the three sizes of disc turbine examined in Fig. 7.9. This figure contains data collected over the complete range of particle variables examined, i.e.:

$$50 \leq \Delta\rho \leq 1900 \quad Kg\ m^{-3}$$

$$92 \leq d_p \leq 2650 \quad \mu m$$

$$0.3 \leq X \leq 30 \quad \%$$

Considering the extremely wide range of variables covered, over the range of gas rates investigated a linear relationship is a reasonable basis for correlating the data, especially for the larger impellers which are the most energy-efficient and for which there is considerable data. Therefore a relationship of the form given in Eqn. 7.4 below can be specified:

$$\Delta N_{JS} = a\ Q \qquad 7.4$$

i.e.
$$(N_{JS})_g - (N_{JS})_{Q=0} = a\ Q \qquad 7.5$$

From Fig. 7.9:

$$a \simeq 0.9\ vvm^{-1}\ s^{-1} \text{ for } D = T/2\ DT \qquad 7.5$$

$$a \simeq 2.4\ vvm^{-1}\ s^{-1} \text{ for } D = T/3\ DT \qquad 7.7$$

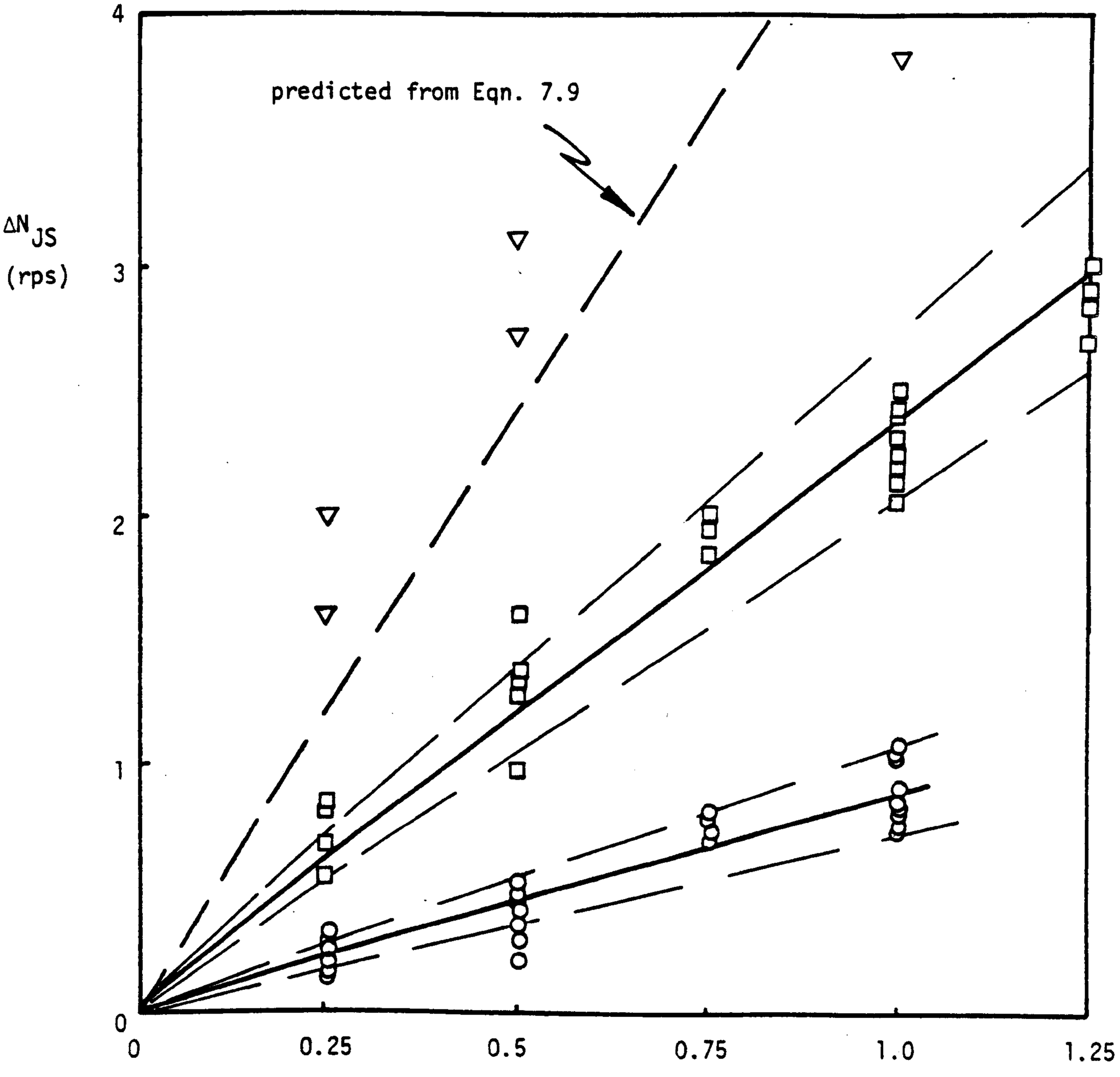

Fig. 7.9 ΔN_{JS} versus Q for 3 sizes of DT Impeller in T_{56} (c = T/4)

○ D = T/2

□ D = T/3

▽ D = T/4

The relationship between 'a' and 'D' can be deduced from:

$$\frac{a_{D=T/2}}{a_{D=T/3}} = \frac{0.9}{2.4} = \left[\frac{3}{2}\right]^{x} \qquad 7.8$$

hence x = -2.42. This is the logical value, since, using the relationships given in Table 7.1, all the data presented in Fig. 7.9 could be adjusted to a particular impeller diameter. Using the value estimated above:

$$a_{D=T/4} = \frac{0.9}{2^{-2.42}} = 4.82 \text{ vvm}^{-1}\text{ s}^{-1} \qquad 7.9$$

which allows prediction of the line in Fig. 7.9 for the D = T/4 impeller. The logical step is therefore to normalise ΔN_{JS} by forming the group $\Delta N_{JS}/(N_{JS})_{Q=0}$ since $(N_{JS})_{Q=0} \propto D^{-2.45}$ which will bring all the data for disc turbines onto one line. Theoretically, the same divergence should have occurred when forming the same ΔN_{JS} v. Q graph for various values of X, $\Delta\rho$, d_p etc. However, the exponents on these variables were so small in comparison to that on impeller diameter that the effect was probably negligible and overcome by experimental errors. Nevertheless this trend is just visible in Figs. 6.7 and 6.10a, and plotting $\Delta N_{JS}/(N_{JS})$ has the effect of correcting all the data to one line since if both $(N_{JS})_{Q=0}$ and $(N_{JS})_g$ are proportional to the various parameters raised to their various powers, then ΔN_{JS} will also be. However, the small variations in the exponents with gas rate, combined with experimental errors, result in the correlation of data by this means displaying more data scatter than the original method (as shown in Fig. 7.10) and thus it is preferable to retain the method used in Fig. 7.9.

The same reasoning will apply to the results for the MFD impellers and this is shown in Fig. 7.11.

7.4. Other Parameters Briefly Studied

This section briefly covers the effect of varying the number of

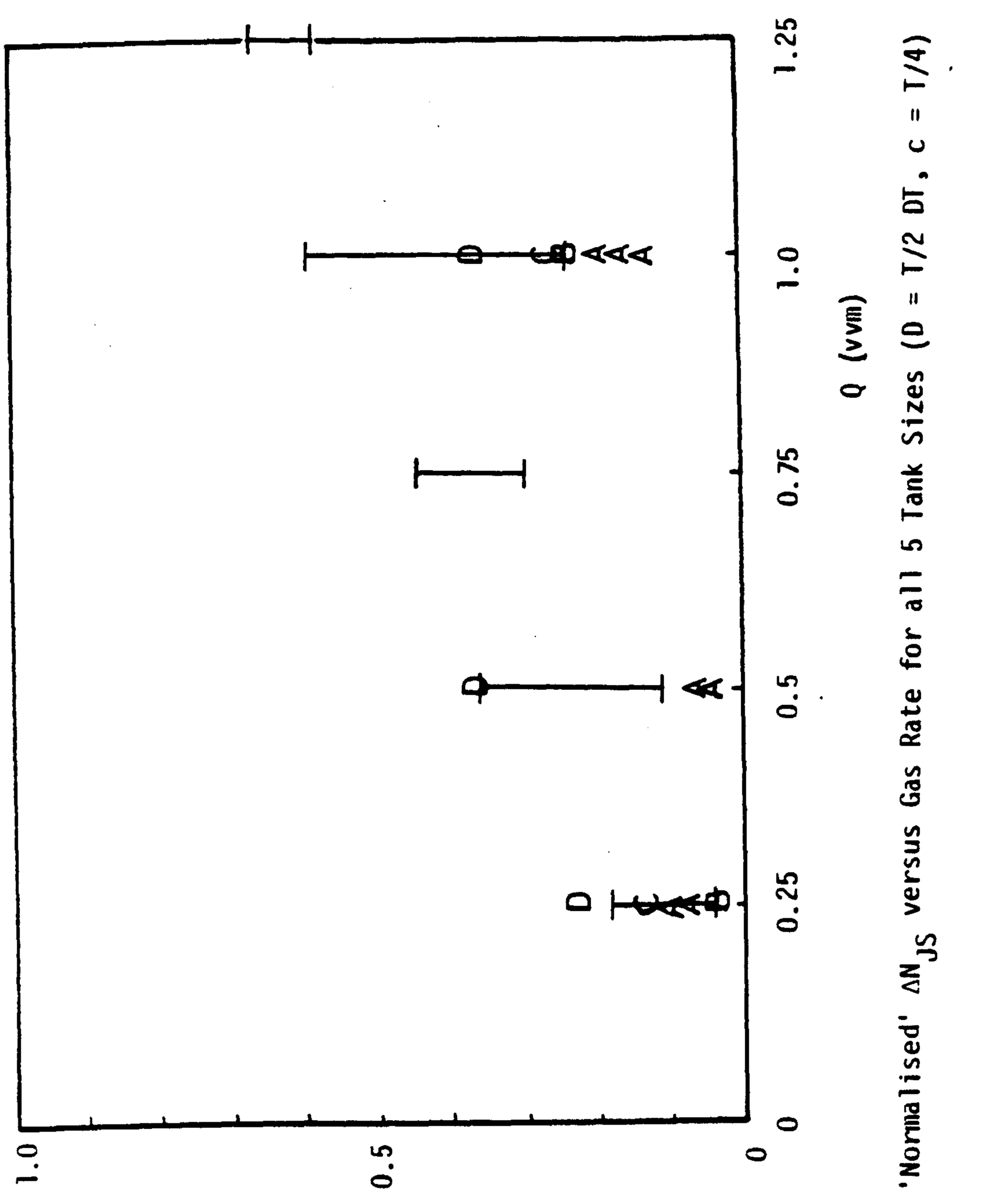
'Normalised' ΔN_{JS} versus Gas Rate for all 5 Tank Sizes (D = T/2 DT, c = T/4)
$\frac{\Delta N_{JS}}{(N_{JS})_{Q=0}}$
Q (vvm)
1.0
0.5
0
0.25
0.5
0.75
1.0
1.25
A
B
C
D
T_{56}
T_{29}
T_{30}
T_{91}
T_{183}

Fig. 7.10

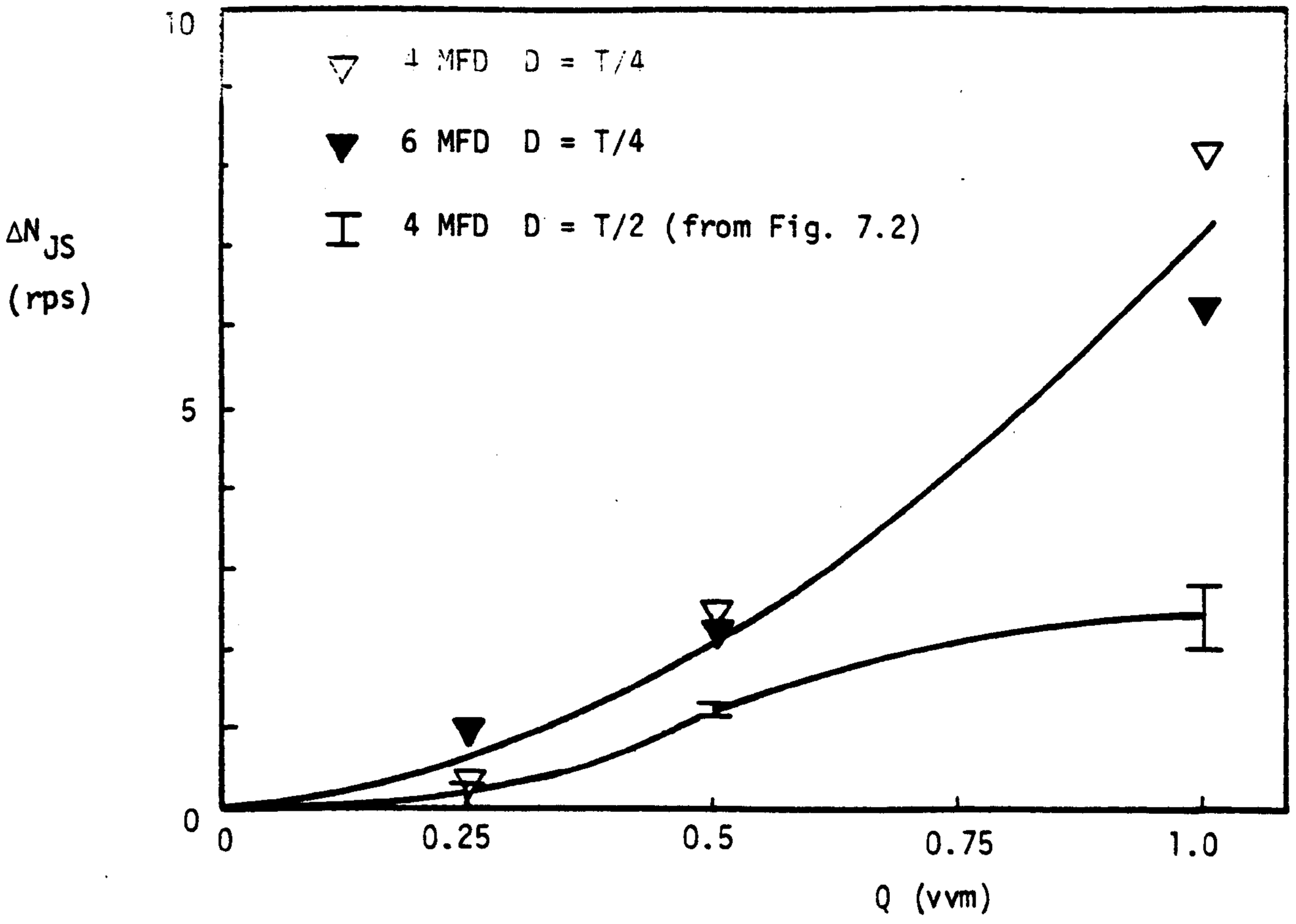

Fig. 7.11 Effect of Varying Impeller Diameter on ΔN_{JS} for 4 MFD and 6 MFD Impellers in T_{56} (c = T/4)

blades on a MFD impeller, using two impellers simultaneously and varying the sparger design.

The 6 MFD impeller has previously been shown to have advantages over the four-bladed version in terms of both its ability to disperse gas (Section 3.5.3) and to suspend particles (Section 4.4.2) in the appropriate two phase system. These advantages are confirmed by the lower increases necessary to restore N_{JS} on aeration (Fig. 7.11) and the resulting reduced power requirements over the 4 MFD, especially at high gas rates (Fig. 7.6b).

Brief tests were carried out to examine the effect of using a double impeller system in T_{56}. The ADT (D = T/2) impeller was placed at a clearance of 0.14 m (c = T/4) and a DT impeller (D = T/2) at a clearance of 0.56 m (c = T) with an increased liquid level of 1.5 T. Increasing liquid level had no effect on N_{JS} (Section 6.7). With a 20% concentration of soda glass Ballotini and a gas rate of 2.5 x 10^{-3} m^3/s (≡ 1.09 vvm on a H = T basis) it was found that this combination of impellers required a specific power input of 1.8 W Kg^{-1} to just-suspend the particles. With the disc turbine removed, the power requirement was only 0.85 W Kg^{-1} but the particles were only suspended to a height of approximately one tank diameter. Thus the extra disc turbine improved homogeneity but also doubled the power requirement to effect suspension. It was noted, however, that a reasonable gas rate applied via a simple sparge ring, in the same position as and replacing the disc turbine, had the same homogeneising effect but without the drawback of extra power demands. Fig. 7.12 shows the power number - flow number plot for the double impeller system at $Q = 2.5 \times 10^{-3}$ $m^3 s^{-1}$.

A test was carried out in T_{56} to estimate the consequences of using a different sparger of industrial utility. This was in the form of two open ended one inch inside-diameter pipes which were positioned

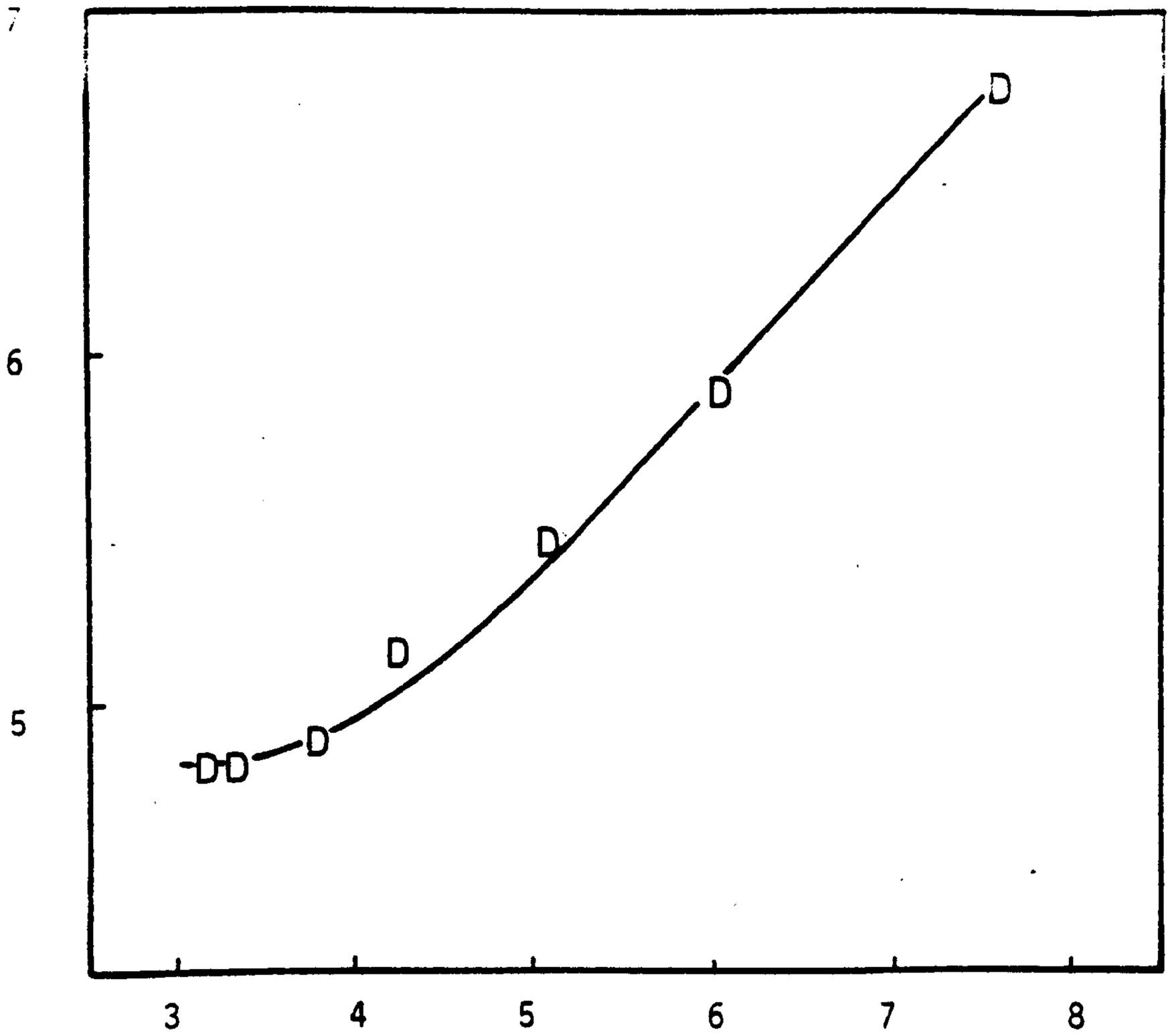

Fig. 7.12 Po_g versus F1 for a Double Impeller System.
(DT at c = T, ADT at c = T/4, H = 1.5 T, Q = 2.5×10^{-3} m^3s^{-1}, T_{56})

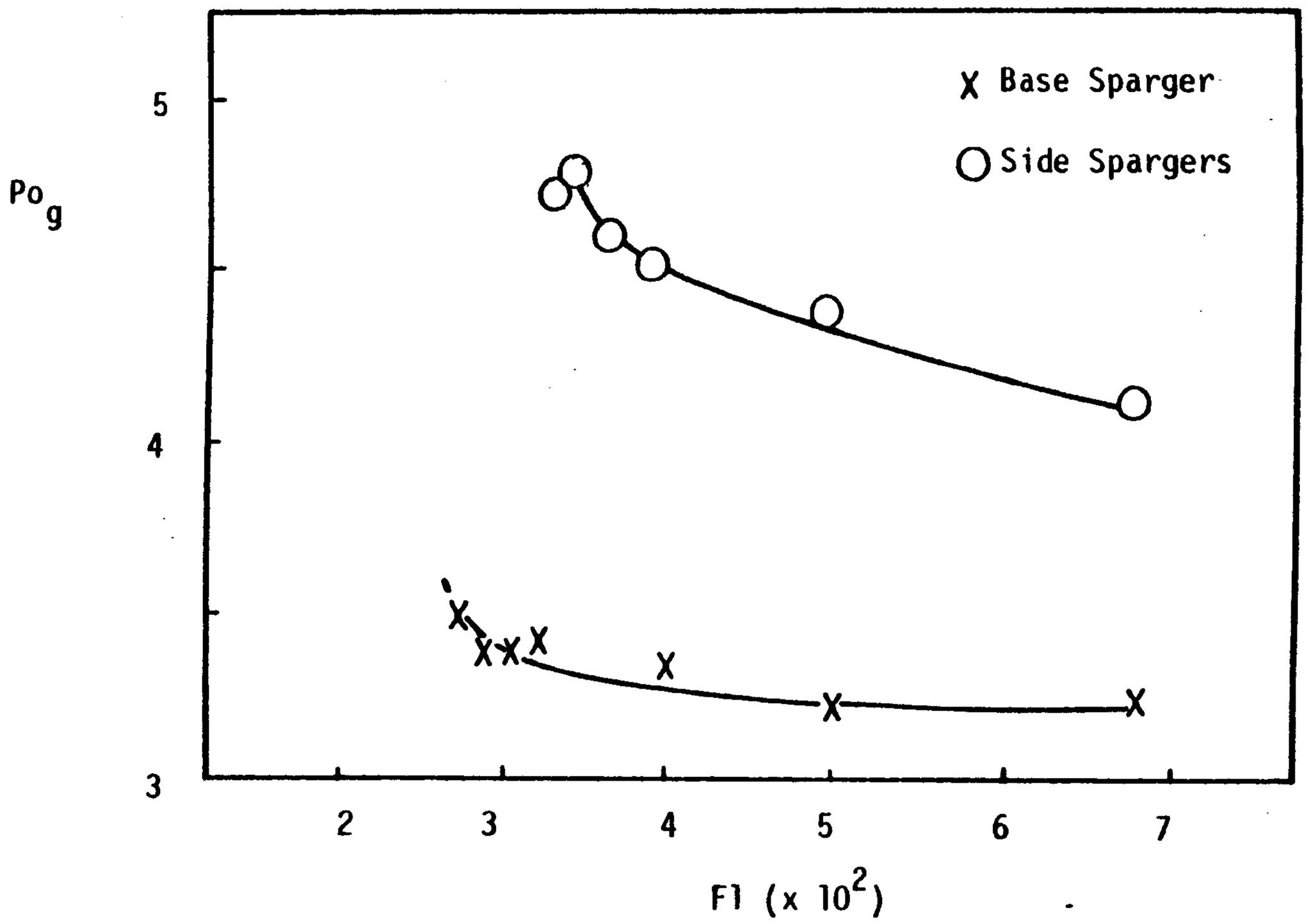

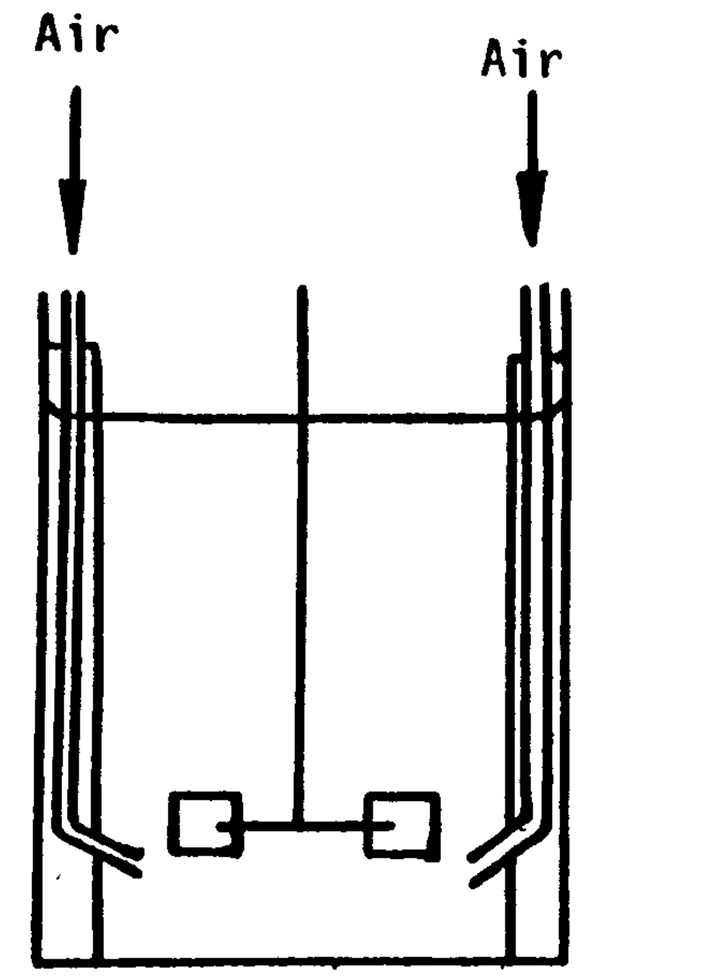

Side Sparging Arrangement

Fig. 7.13 Comparison of Side and Base Spargers (Po_g - Fl)

(T_{56}, D = T/2 DT, c = T/4, 27% Soda Glass Ballotini, Q = 1.1 vvm)

at the same level as the lower blade edge of the D = T/2 disc turbine (Fig. 7.13). A high concentration of soda glass Ballotini (X ≃ 27%) was suspended by this impeller-sparger combination (c = T/4) with a gas rate of 2.5 x 10^{-3} m^3s^{-1} (≃ 1.1 vvm) for approximately the same power input (about 2.2 W Kg^{-1}) as with the standard gas sparging arrangement (Fig. 2.1), though the speed required was slightly lower than with the standard arrangement (3.3 compared with 3.8 rps) and the power numbers higher (Fig. 7.13).

7.5. Impeller Clearance

The combination of lower suspension speeds with a reduced power number was shown to produce considerable decreases in P_{JS} for unaerated systems when the impeller clearance of a D = T/3 disc turbine was reduced (Section 4.4.2). These trends were also found to be true in three phase dispersions, though at high gas rates and low clearance (c = T/6) the effect became gradually less significant, probably due to stagnant areas forming near the periphery of the tank base where fillets of particles were observed to settle and therefore required additional power to suspend them. Table 7.3 reflects this trend, showing a 46% reduction in the power necessary to suspend a 3% soda glass Ballotini suspension with no aeration on reducing the clearance from c = T/4 to c = T/6. However, as Q was increased from 0.25 to 1.25 vvm, so the power saving decreased from 42 to 16%. Though significant reductions in Po_g were obtained throughout, associated with the change in flow pattern from a predominantly radial to a predominantly axial type flow (Section 3.5.5), the reduction in power saving for the clearance change was due to the decreasing reduction obtained in the speed necessary to just-suspend the particles, for the reasons stated above. Eventually, at a gas rate of 1.25 vvm, Table 7.3 shows that N_{JS} was higher for a clearance of c = T/6 than for c = T/4. This trend was reflected in the graph of ΔN_{JS} against Q (Fig. 7.14). Never-

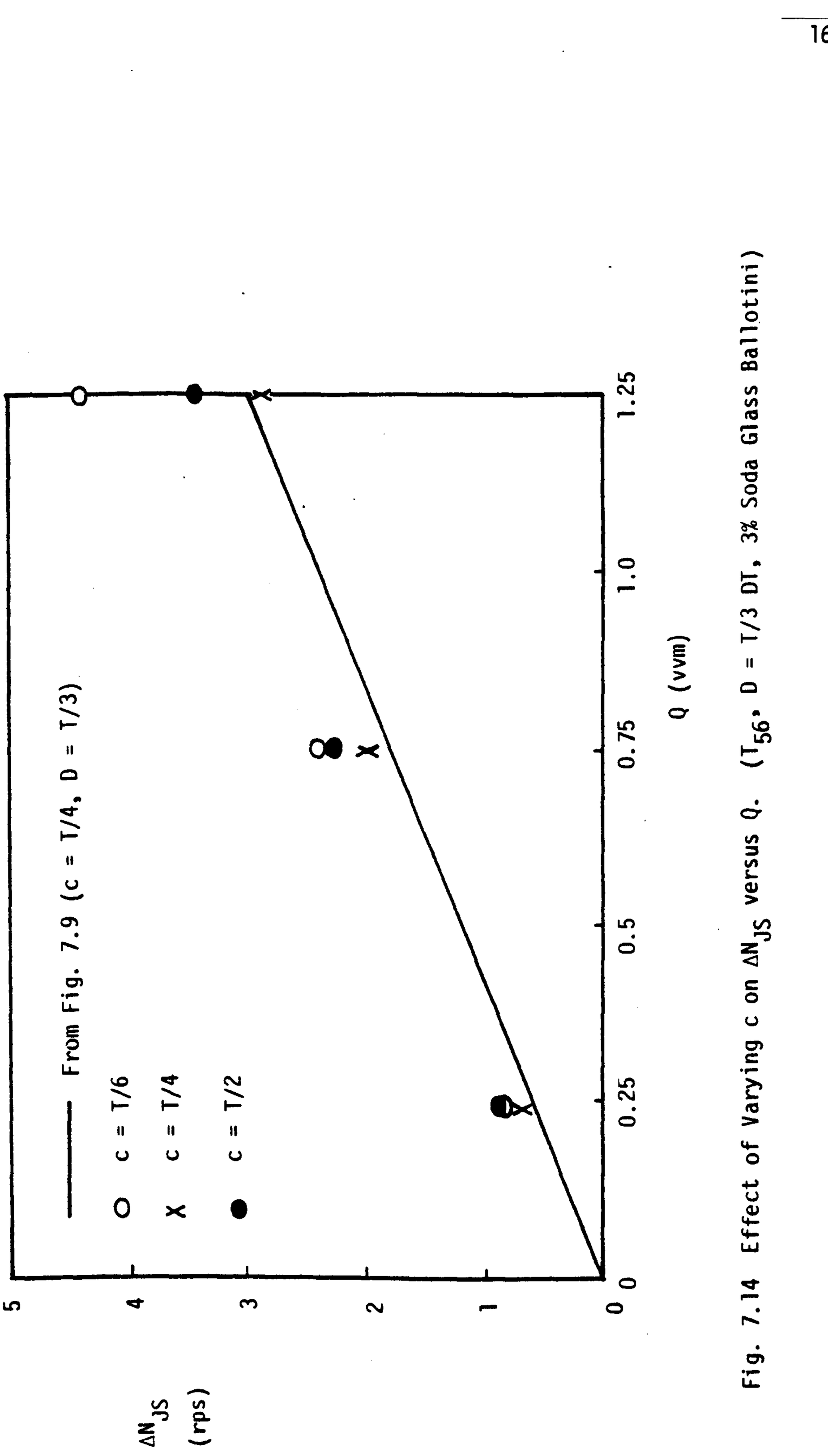

Fig. 7.14 Effect of Varying c on ΔN_{JS} versus Q. (T_{56}, D = T/3 DT, 3% Soda Glass Ballotini)

theless, the overall power saving was retained because of the much reduced value of Po_g at the lower clearance.

Gas Rate Q (vvm)	Impeller Clearance c/T (-)	N_{JS} (rps)	P_{JS} (rps)	$(Po)_{JS}$ or $(Po_g)_{JS}$ (-)
0	0.167	4.28	82	4.6
	0.25	4.95	151	5.5
	0.5	5.90	240	5.4
0.25	0.167	5.07	100	3.4
	0.25	5.62	170	4.35
	0.5	6.73	290	4.1
0.75	0.167	6.67	150	2.2
	0.25	6.90	210	2.8
	0.5	8.18	340	2.7
1.25	0.167	8.65	220	1.5
	0.25	7.78	260	2.5
	0.5	9.33	400	2.2

Table 7.3 Effect of Varying Impeller Clearance (D = T/3)

T_{56} 3% Soda Glass Ballotini

As explained in Chapter 4, a smaller power number was obtained at the highest clearance (c = T/2) than at the standard position (c = T/4) due to surface aeration.

Thus the power savings reported here for the D = T/3 disc turbine were largely due to the change in flow pattern and the resulting drop in power number (see Fig. 3.16). As a result of this, it seems unlikely that such large savings would be achieved for a very light suspension duty since suspension would probably occur at a lower speed than the flow transition. Similarly, the savings obtained by reducing the clearance of a D = T/2 disc turbine (Table 7.4) were relatively low

under aerated conditions in comparison to those obtained for the D = T/3 version since no such flow transition and drop in Po_g occurred for the larger impellers (Section 3.5.5).

Vessel	Q (vvm)	c/T (-)	N_{JS} (rps)	P_{JS} (w)	Po_{JS} or $(Po_g)_{JS}$ (-)
T_{29}	0	0.167	4.77	32.5	4.7
	0	0.25	5.03	39	4.8
	1.0	0.167	5.65	41	3.5
	1.0	0.25	5.93	48	3.6
T_{91}	0	0.167	2.33	1360	5.4
	0	0.25	2.32	1528	6.15
	1.0	0.167	2.88	1473	3.1
	1.0	0.25	3.10	1808	3.0

Table 7.4 Effect of Varying Impeller Clearance (D = T/2)

T_{56} 1% Sand - see Appendix 4 for further examples

There was no apparent difference between the homogeneity of the dispersions for the various impeller clearances. However, gas holdups for the 0.187 m diameter DT in T_{56} were up to 20% lower at the just-suspended condition for the lowest clearance (c = T/6) than for the standard value (c = T/4), the maximum difference being at the lowest gas rates. This is logical since the maximum power savings were achieved for these conditions. Table 7.5 shows that holdups obtained at the highest clearance (c = T/2) were significantly larger, once again due to the higher power inputs necessary to achieve suspension but probably also enhanced by some surface aeration.

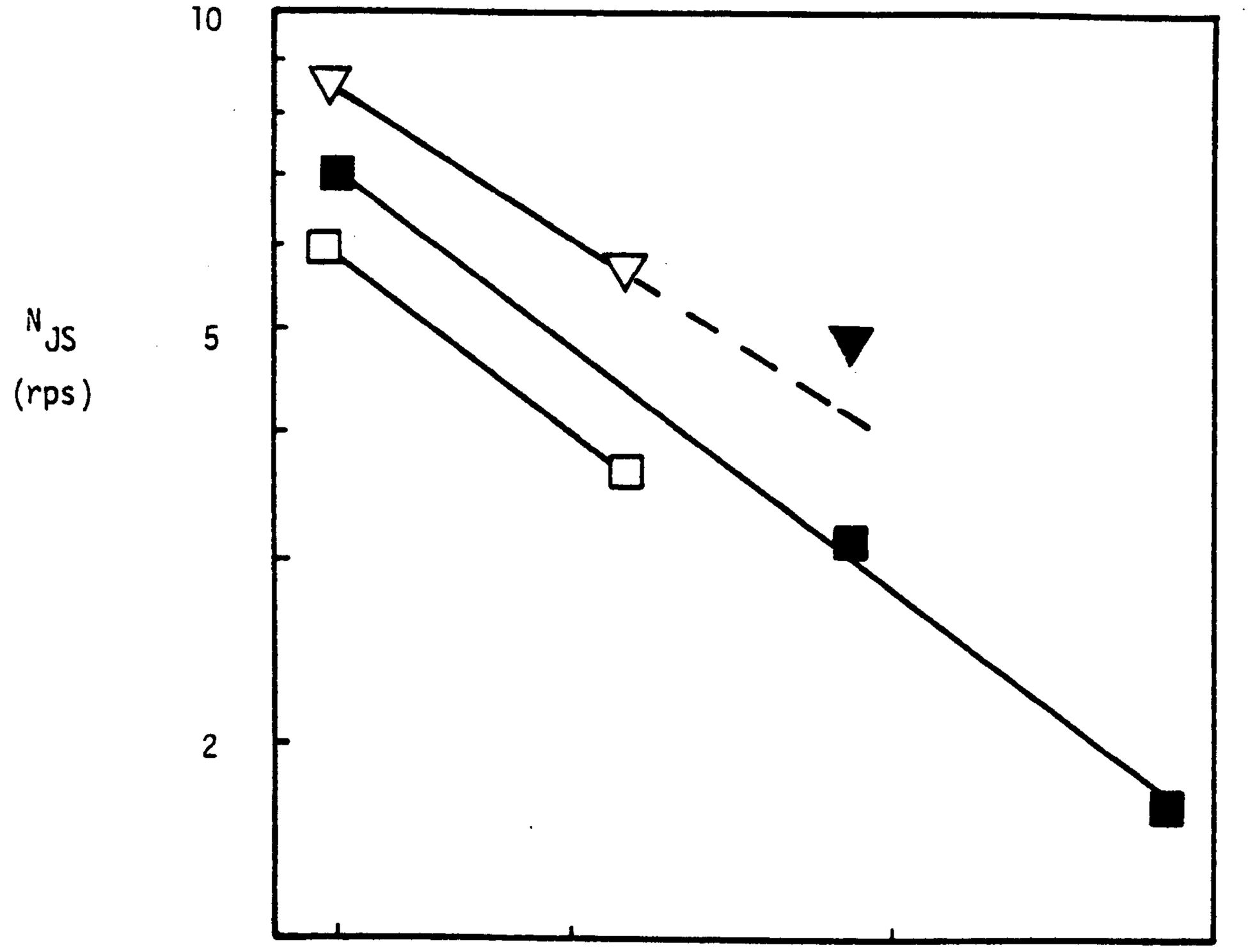

Fig. 7.15 Effect of Scale on N_{JS} for Q = 1 vvm
(D = T/2, c = T/4, X = 1% Sand)

UCL	ICI	
▽	▼	4 MFD
□	■	DT

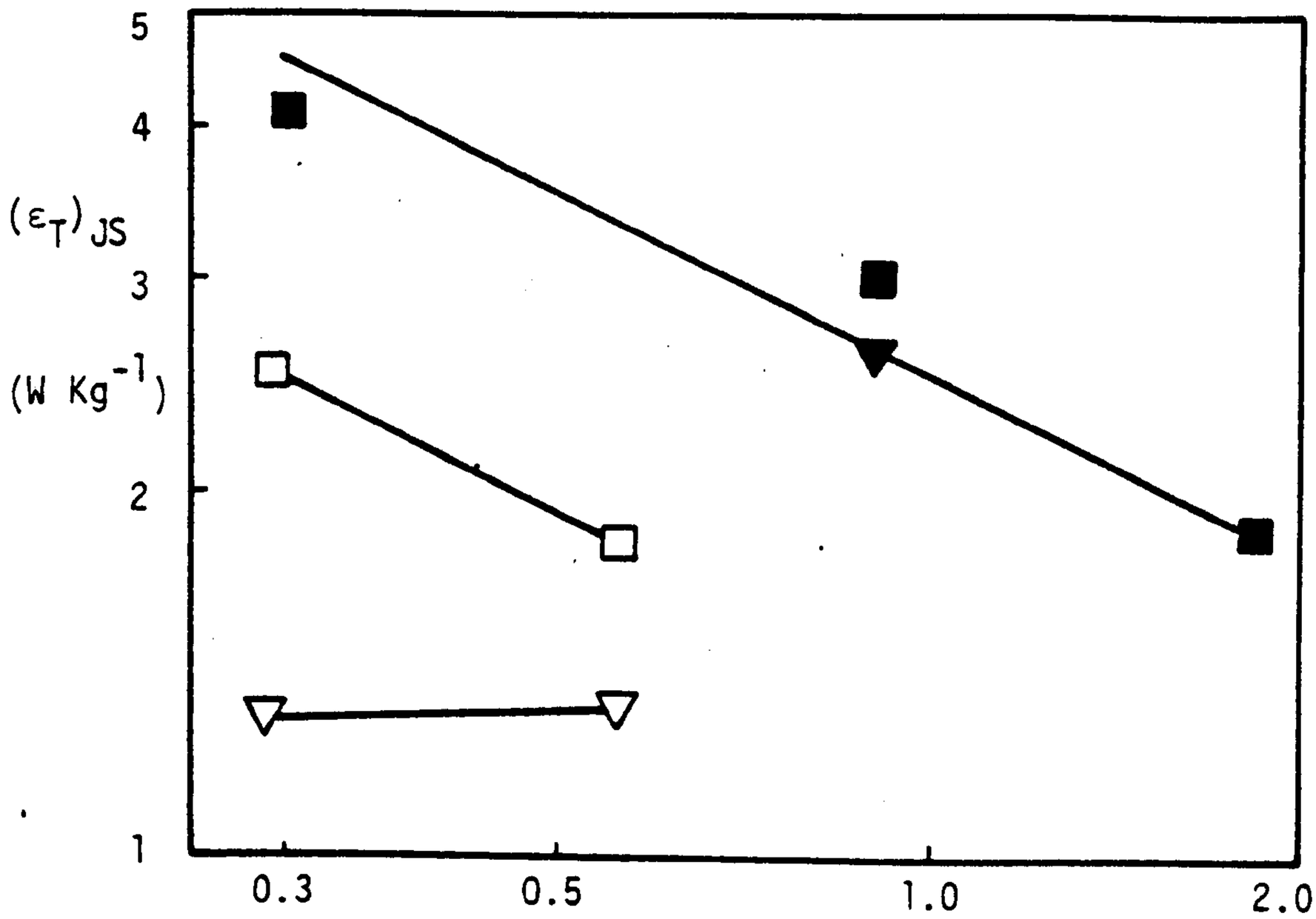

Fig. 7.16 Effect of Scale on $(\varepsilon_T)_{JS}$ for Q = 1 vvm
(D = T/2, c = T/4)

UCL ICI
▽ ▼ 4 MFD
□ ■ DT

Q, vvm →	Exponent on Scale i.e. $N_{JS} \propto T^{?}$			
	0	0.25	0.5	1.0
DT	-0.74	-0.88	-0.82	-0.74
4 MFD	-0.90	-0.76	-	-0.65
4 MFU	-0.78	-	-	-0.65

(a) Data from T_{29} and T_{56} only

c = T/4 D = T/2

Q, vvm →	Exponent on Scale		
	0	0.25	1.0
DT	-0.85	-0.75	-0.80

(b) Data from T_{30}, T_{91} and T_{183} only

c = T/4 D = T/2

	Exponent on Scale		
Q, vvm →	0	0.25	1.0
DT	-0.80	-0.71	-0.72
4 MFD	-0.74	-0.64	-0.54

(c) Combined Data from all 5 Tanks.

c = T/4 D = T/2

Table 7.6 Scale Up Relationships for a 1% Sand Suspension

Once again there is a noticeable decrease in the exponent on tank diameter as gas rate increases. Thus N_{JS} is less sensitive to changes of tank diameter at high gas rates than it is at low gas rates, if the rate of aeration is scaled on tank volumes. Table 7.7 below shows the effect of scaling gas rates by superficial velocities instead of vvm.

Data Source	Impeller Type	Exponent of T for Various Superficial Gas Velocities			
		0	0.4 cms^{-1}	0.6 cms^{-1}	1.4 cms^{-1}
T_{30}, T_{91}, T_{183}	DT	-0.85	-	-0.88	-0.95
T_{29}, T_{56}	DT	-0.74	-	-1.0	-1.12
T_{29}, T_{56}, T_{91}	4 MFD	-0.74	-0.91	-	-

Table 7.7 Effect on Exponents of Scaling Q by Superficial Velocities

The general trend on this basis is for N_{JS} to become a stronger function of vessel size as Q increases. However, if gas rate is scaled on vvm, N_{JS} tends to become a weaker function of scale with increasing gas rate. This also applies for many of the other variables examined (e.g. $\Delta\rho$, d_p, etc.) where tank size did not vary and hence the method of scaling Q is irrelevant. This seems to support the basis set out in Chapter 3 for scaling gas rates in terms of tank volumes.

Fig. 7.17 shows all the data obtained for disc turbine impellers, of diameter T/2 and with a clearance of T/4, over the complete scale and particle property range investigated. A linear regression analysis gives a value for 'a' of 0.94 s^{-1} $(vvm)^{-1}$ with a correlation coefficient of 0.94. Therefore the relationship:

$$(N_{JS})_g - (N_{JS})_{Q=0} = 0.94\ Q \qquad 7.10$$

where Q is in vvm, can be used over a wide scale range provided the deviations shown in Fig. 7.17 are noted and allowed for. More data on the larger and smaller scales and for a variety of particles would be useful in supporting this relationship. Fig. 7.2, showing ΔN_{JS} against Q for the 4 MFD impellers, also confirms that scale has little effect on this more complex relationship between the two variables.

Thus for a given increase of gas rate on any scale of operation, a similar increase in the impeller speed necessary to maintain the "just-suspended" state will be needed, provided geometric similarity

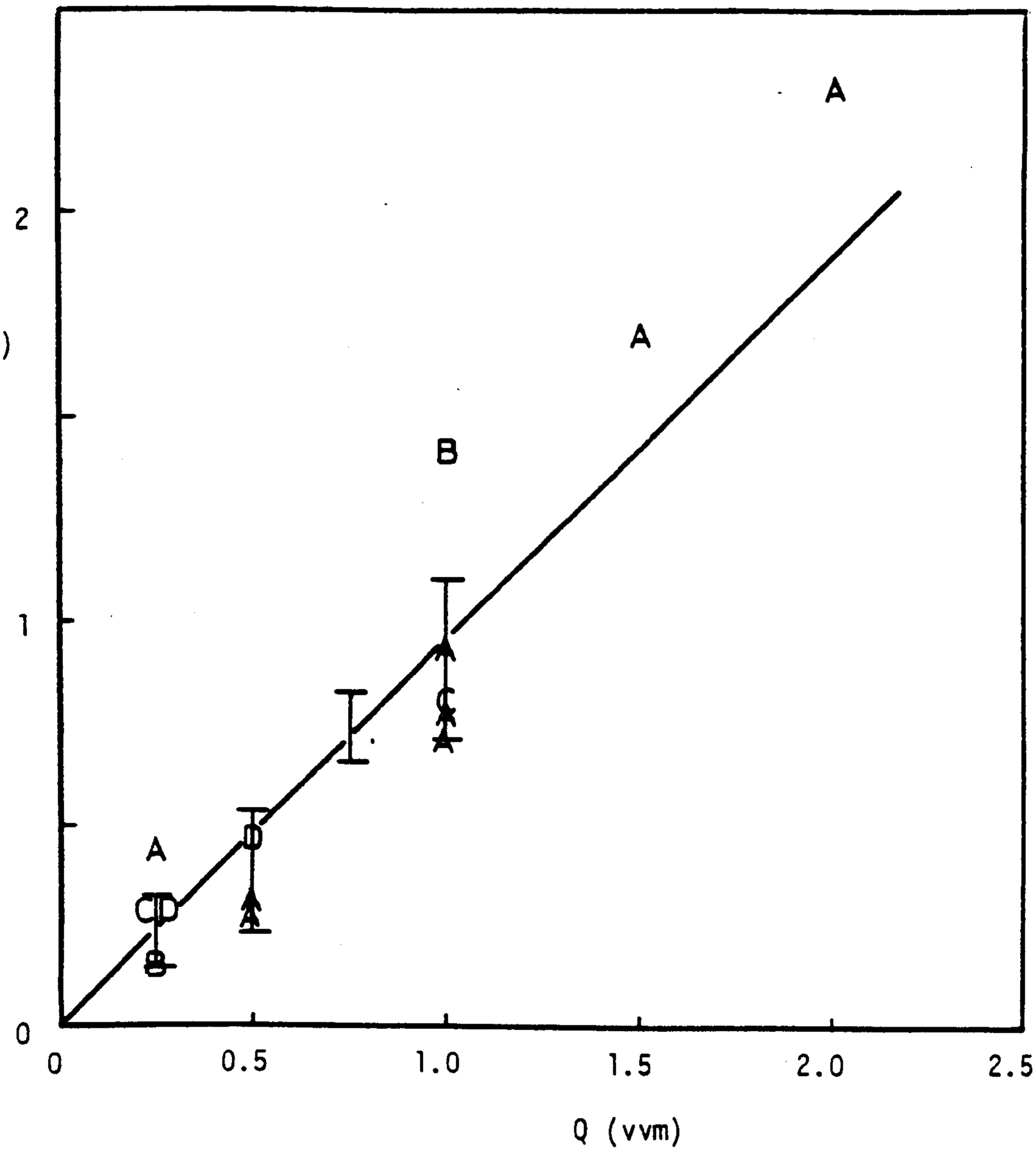

Fig. 7.17 ΔN_{JS} versus Q for 5 vessel sizes
(D = T/2 DT, c = T/4)

I T_{56} - from Fig. 7.9

A T_{29}

B T_{30}

C T_{91}

D T_{183}

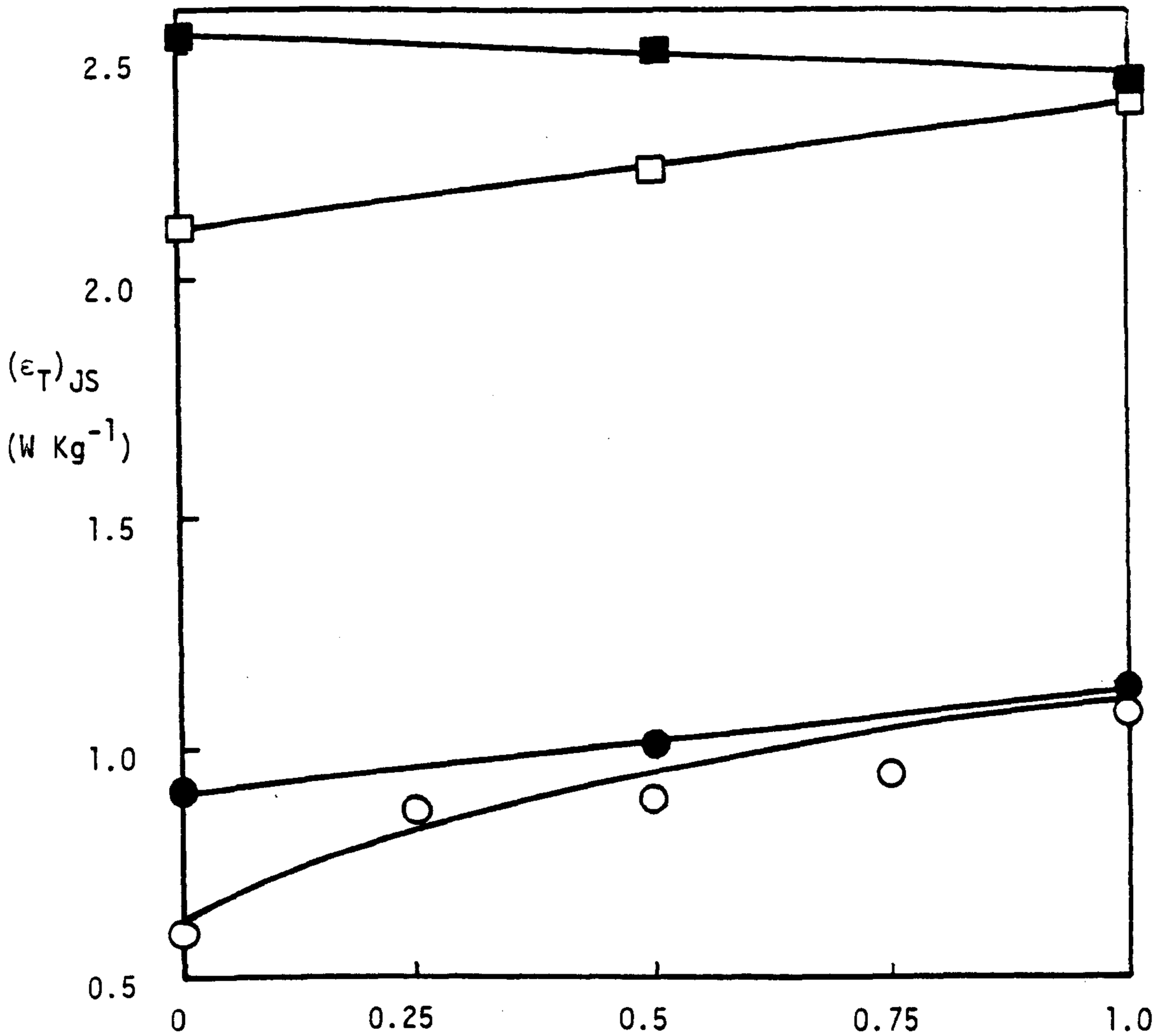

Fig. 7.18 Effect of Scale on $(\varepsilon_T)_{JS}$ versus Q (D = T/2 DT, c = T/4)

T_{56}	T_{29}	
□	■	30% Soda Glass Ballotini
○	●	3% Soda Glass Ballotini

is maintained. This will of course result in a decrease in the magnitude of the exponent relating N_{JS} to tank diameter, as shown in Table 7.6. Also, the exponent will decrease more rapidly for the 4 MFD which shows a higher rate of increase in ΔN_{JS} at high Q than the disc turbine. The most important consequence of this effect is that as the magnitude of the exponent decreases, so the relationship between $(\varepsilon_T)_{JS}$ and T will vary. Thus at high gas rates, an increase in the specific power input, $(\varepsilon_T)_{JS}$, may be necessary on scale up. For example, if $N_{JS} \propto T^{-0.76}$, then this implies a small decrease in $(\varepsilon_T)_{JS}$ on scale up ($(\varepsilon_T)_{JS} \propto T^{-0.28}$). However, if at high Q, $N_{JS} \propto T^{-0.6}$, this implies an increase in specific power input on scale up ($(\varepsilon_T)_{JS} \propto T^{0.2}$). These trends are reflected in Fig. 7.18 which demonstrates how $(\varepsilon_T)_{JS}$ varies with gas rate for two vessel sizes.

7.7. Conclusions

The trends established in Chapter 6, with regard to the effect of increasing gas rate on the exponents governing the relationship between N_{JS} and the particle properties, were also applicable to the system dimensions. These trends were logical in the light of the manner in which impeller speeds and specific power inputs increased in order to maintain the just-suspended condition under aeration.

Those impellers which most efficiently suspended particles in unaerated systems (AFD, MFD) were also the most energy-efficient at low gas rates. However, care was necessary to avoid operation in a regime of flow instability where sudden sedimentation was a possibility if large fluctuations in gas rate occurred. No such instabilities with the associated drastic particle fallout were obtained with disc turbine impellers and mixed flow impellers pumping upwards. Though these impellers were more suited to high gas rate operations, they required higher specific power inputs at low gas rates but had the advantage of more stable operation. The rate of increase of N_{JS}

with gas rate was approximately the same for a very wide range of particle properties and vessel sizes, provided geometrical similarity was maintained. This rate was well characterized for disc turbines.

Scaling up vessel size at high gas rates (Q scaled as vvm) required the specific power input to maintain the just-suspended condition to be kept constant or even increased, depending on the gas rate. There is an interesting compromise when it is considered that Nienow's[5] correlation for N_{CD} (see Fig. 3.19) predicts an increase in $(\varepsilon_T)_{CD}$ on scale up (at constant vvm) and it is generally accepted that there is a decrease in $(\varepsilon_T)_{JS}$ on scale up in unaerated systems.

CHAPTER 8.

GAS-LIQUID MASS TRANSFER

8.1. Introduction

Mass transfer between the gas phase and the liquid phase is often the overriding objective in gas-liquid and gas-liquid-particle dispersions in stirred tanks. The transfer rates can be shown to be controlled by the liquid phase resistance.[57] The gas-liquid mass transfer coefficient generally used to describe the rate is expressed as $k_L A$, the product of a liquid film absorption rate constant and a specific interfacial area. Values of $k_L A$ derived by many different means have been widely published. However, data obtained via chemical methods can often be misleading[58] and recent work[59,60] has shown that neglecting changes in gas holdup composition when using physical absorption techniques can also cause large errors in determining $k_L A$ values. Further, Chandrasekharan and Calderbank[61] demonstrate the dependence of $k_L A$ on the assumed gas phase dynamics (e.g. well mixed or plug flow).

The objective of the work described in this chapter was to devise a method of obtaining reliable $k_L A$ data, which would then allow comparisons to be drawn between the various radial and axial flow impellers as regards their gas-liquid mass transfer potential, and also to assess the effect of particles on gas-liquid mass transfer.

8.2. Literature Survey

8.2.1. Techniques and Calculation Methods

The problems involved in utilizing a chemical technique (commonly the absorption of oxygen in sodium sulphite solution in the presence of a catalyst) were recently reviewed by Van't Riet[62] and Finn.[58] The realization of these problems has led to difficulties in interpreting the data produced and a decline in popularity of the method.

Physical methods can generally be classified into two types:

steady state or transient methods. There is relatively little work available describing steady state methods[63,64,65] but the transient or "dynamic gassing-out" type experiment is well documented. Several other methods are available for estimating mass transfer coefficients and these have recently been reviewed by Figueiredo.[66] Nevertheless, dynamic gassing-out methods still represent the simplest experimental procedure and, provided that the problems set out below are dealt with, it is a useful technique which is not complicated by the presence of a third particulate phase.

The most popular gassing-out method involves deoxygenation of the liquid by, for instance, the passing of nitrogen through it. Generally, a polarographic electrode is then used to follow the dissolved oxygen concentration profile with time after the input gas stream has been changed to air. A mass balance for oxygen in time dt gives:

$$\frac{dc_L}{dt} = k_L A \left[\frac{C_G}{K} - C_L \right] \qquad 8.1$$

Hence, for times t_1 and t_2:

$$k_L A = \frac{\ln \left[\dfrac{\left[\dfrac{C_G}{K}\right] - (C_L)_{t_1}}{\left[\dfrac{C_G}{K}\right] - (C_L)_{t_2}} \right]}{t_2 - t_1} \qquad 8.2$$

The important assumptions relevant in this simple treatment are:

1. Liquid volume remains unchanged.
2. Gas holdup is 100% nitrogen originally.
3. From time t = 0 onwards, the gas holdup is 100% air.
4. The gas and liquid phases are both perfectly mixed.
5. The pressure of the gas is constant throughout the vessel.

Wise[67] outlined this approach in 1951. Latterly it has been

realized that the response time of the polarographic electrode can have a significant effect on $k_L A$ values if it is too long. This applies especially when the electrode time constant, τ (the time needed to achieve 63% of a step change), is not much smaller than the time constant of the mass transfer step, which equals $1/k_L A$. Heineken[68] and Linek[69] have proposed complex models to eliminate the effect of the probe lag, which is mainly due to diffusion through the membrane (except in high viscosity systems[65]) and results in the output not being directly related to the instantaneous oxygen concentration. Van de Sande[70] and Wisdom[3] both demonstrated that electrode response was very close to first order, resulting in a relatively simple treatment to account for it. However, if a fast response probe is used ($\tau \simeq 1 - 3$ seconds) it can easily be demonstrated that the maximum error in $k_L A$ incurred by neglecting the lag due to the probe is only of the order of $\simeq 3\%$ for $k_L A$'s up to $\simeq 0.1\ s^{-1}$[62]. If higher mass transfer rates are to be measured then faster response times are required if a de-convolution procedure, which accounts for probe lag, is to be avoided.

The next problem incurred by the straightforward application of Eqn. 8.2 is caused by the assumption that, the instant that the nitrogen supply is changed to an air supply, the whole gas content of the vessel will immediately change from nitrogen to air. Dunn and Einsele[59] first demonstrated quantitatively the errors involved in this assumption. By assuming that both the gas and liquid phases were well mixed, they simulated concentration versus time curves for both phases. This simulation is reproduced in Fig. 8.1. An oxygen balance on the gas phase with the above assumptions leads to:

$$\begin{bmatrix}\text{Accumulation of}\\ O_2 \text{ in gas phase}\end{bmatrix} = \begin{bmatrix}\text{Rate of } O_2\\ \text{into gas phase}\end{bmatrix} - \begin{bmatrix}\text{Rate of } O_2\\ \text{out of gas}\\ \text{phase}\end{bmatrix} - \begin{bmatrix}\text{Rate of}\\ \text{transfer}\\ \text{of } O_2 \text{ out}\\ \text{of gas phase}\end{bmatrix}$$

or

$$\frac{d(V_G C_G)}{dt} = Q_i C_i - Q_0 C_G - k_L A \left[\frac{C_G}{K} - C_L\right] V_L \qquad 8.3$$

Assuming V_G remains constant and $Q_i \simeq Q_0$:

$$\frac{dC_G}{dt} = \frac{Q}{V_G}(C_i - C_G) - k_L A \left[\frac{C_G}{K} - C_L\right] \frac{V_L}{V_G} \qquad 8.4$$

A similar treatment of the well mixed liquid phase gives

$$\left[\begin{array}{l}\text{Accumulation Rate} \\ \text{of oxygen in liquid}\end{array}\right] = \left[\begin{array}{l}\text{Rate of transfer of} \\ \text{oxygen into liquid}\end{array}\right]$$

or $$\frac{d(V_L C_L)}{dt} = k_L A \left[\frac{C_G}{K} - C_L\right] V_L \qquad 8.5$$

For constant liquid volume this is equivalent to Eqn. 8.1:

$$\frac{dC_L}{dt} = k_L A \left[\frac{C_G}{K} - C_L\right] \qquad 8.6$$

Fig. 8.1 combines Eqns. 8.4 and 8.6, with curves A, B, C and D representing the following conditions applied to Eqn. 8.4:

A) None; i.e. a full solution of the gas phase dynamics assuming a well mixed gas phase.

B) Transfer term negligible; thus $\frac{dC_G}{dt} = \frac{Q}{V_G}(C_i - C_G)$ 8.7

C) Accumulation term negligible; thus a steady state oxygen balance results, i.e. $\frac{Q}{V_G}(C_i - C_G) = k_L A \left[\frac{C_G}{K} - C_L\right] \frac{V_L}{V_G}$ 8.8

D) Both accumulation and transfer terms negligible; the simple model results, i.e. $C_i = C_G$ 8.9

For the conditions chosen by Dunn and Einsele,[59] the divergence of the concentration profiles from the full solution profiles (A), especially in the case of the simple model (D), is particularly marked. Correction factors developed from these curves suggested that $k_L A$ values measured assuming a well mixed gas phase would be considerably higher

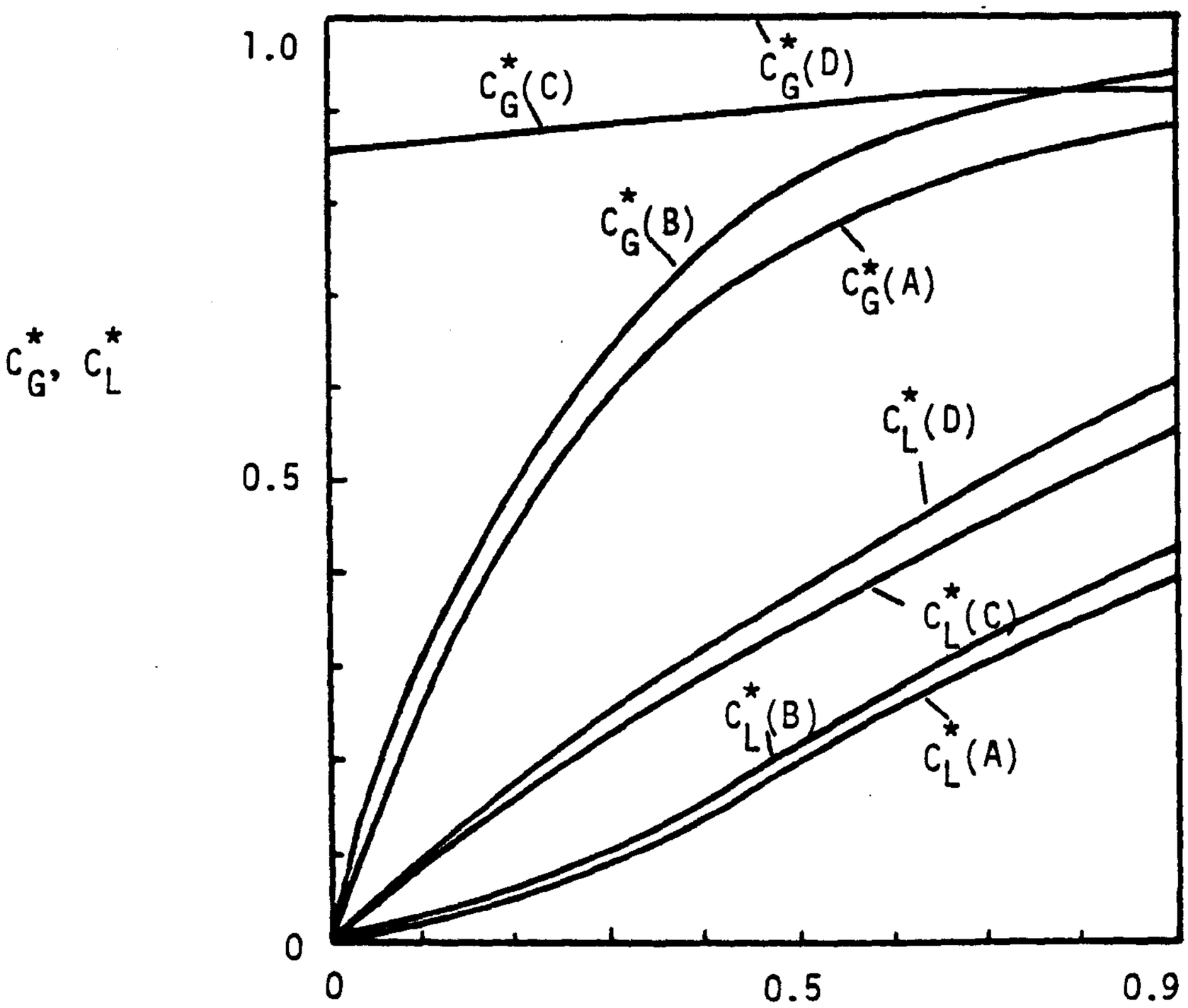

Fig. 8.1 Simulation of Concentration-Time Histories from Dunn and Einsele[59] for models A, B, C and D.

than previous figures. Figueiredo and Calderbank[60] demonstrated the magnitude of this effect, recording, for instance, values of 0.0495 s^{-1} using the simple model (D) compared with 0.1050 s^{-1} using the full solution (A) from identical conditions and concentration versus time data. At very high specific power inputs (approx. 4000 Wm^{-3},Q ≃ 0.5 vvm), and thus enhanced gas holdups, the effect of gas dynamics became more critical and therefore the solutions diverged further, i.e. $k_L A \simeq 0.4\ s^{-1}$ for model A compared to $k_L A \simeq 0.06\ s^{-1}$ for model D. Dang et al.[71] used oxygen to perform step response experiments in a propeller agitated closed system. They present data which show experimental gas phase oxygen concentration - time histories along with theoretical predictions assuming perfect backmixing. However, the theoretical curve is based on the assumption that the transfer term in Eqn. 8.4 can be neglected (model B) which introduces a small error.[59] Nevertheless the agreement between the curves is quite good and supports the proposition that the gas phase can be adequately described as well-mixed. The work of Hanhart et al.,[72] who performed similar tests, confirms Dang's results for impeller speeds above the critical speed defined by Westerterp et al.[73] But it is doubtful whether the well-mixed gas assumption can be made either on larger scale vessels (V_L = 45 l in Dang's work) or at lower impeller speeds or when the liquid height is greater than the tank diameter. Under these conditions, the gas will undoubtedly tend towards plug flow.

The treatment of waste water in vessels with very high liquid levels has resulted in the plug flow assumptions being used.[74,75] Also, Cooke et al.[76] and Chandrasekharan and Calderbank[61] evaluated data assuming the gas throughput was in plug flow. Their results indicate that $k_L A$ values are lower than those obtained assuming the gas phase is well mixed, but higher than those evaluated via the

simple model. This follows since the concentration driving force assuming plug flow will be higher than that assuming a well mixed tank, yet not as high as in the simple model, which always assumes that the maximum possible driving force applies, i.e. $\left[\frac{(C_G)^{\equiv m}}{K} - C_L\right]$. This point is also illustrated by Fig. 8.1.

Chandrasekharan and Calderbank[61] conclude that less than 10% error results from using an arithmetic average value of $k_L A$, derived from the well-mixed and plug flow solutions, and hence make no attempt to analyse the gas phase mixing. However, although their results seem to imply that there is no large difference between the models, their work was carried out only at low specific power inputs, where "well mixed $k_L A$'s" deviate least from the simple model solutions. Also, they used a computed gas holdup, chosen so that the experimental and predicted values would show minimum divergence. This seems reasonable in view of the difficulties in accurately measuring low holdup values. Nevertheless, $k_L A$ is a strong function of holdup and their data show consistent underestimation of the holdup for the well mixed model in comparison to the plug flow model, thus tending to reduce the well mixed $k_L A$ values and bring them closer to the plug flow figures.

Intuitively, under vigorous agitation conditions on a small scale, the gas phase should be adequately described by the well mixed model. However, at high gas rates or in large systems there does appear to be some doubt that this model is still as applicable and the high values of $k_L A$ yielded tend to reinforce this doubt. For these reasons some method is required of either identifying and modelling the gas phase dynamics, or alternatively finding a solution that is independent of them.

8.2.2. Impeller Systems

A recent review by Van't Riet[62] suggests that $k_L A$ is governed by the amount of power dissipated in the fluid, independent of the type

of impeller used in gas-liquid systems. A range of impellers consisting of turbines, paddles, propellers, rods and self sucking agitators was included in this summary of many authors' work. Figueiredo[66] examines several unusual types of agitator (e.g. comb-bladed turbines) and establishes an order of superiority of performance based on equal power dissipation. The extent of this superiority is a strong function of the gas flow model and this suggests that a comparison of several types of impeller which provoke a wide range of gas flow patterns would be a useful exercise if the effect of the differing flow patterns could be prevented from affecting the results. Queneau et al.[49] measured the rate of oxygen mass transfer to lixiviant in a leaching situation and concluded that radial flow turbine impellers generating high shear produced higher $k_L A$ values than axial flow turbines for the same power input.

8.2.3. The Effect of Particle Concentration

Joosten et al.[53] carried out dynamic tests by stripping helium from a small closed helium saturated system using nitrogen sparge gas in a 12.5 cm diameter, disc turbine agitated system. Using various density particles ($900 \leq \rho_S \leq 2500$ Kg m^{-3}) with particle sizes in the range 50 - 250 μm, they determined the effect of volumetric solids concentration on $k_L A$ up to approximately 45% by volume, which for the heaviest particles was about 66% by weight. Their results suggest that, at constant gas rate and power dissipation, increasing solids concentration has a negligible effect on $k_L A$ until a concentration of around 15 - 20% by volume is reached. At this point they found $k_L A$ dropped off at a rate that was dependent on particle size and density. An attempt to correlate this fall in $k_L A$ in terms of the apparent viscosity of the system showed that the fall-off point was reached at an apparent slurry viscosity of around four times the liquid viscosity but this method did not successfully correlate for the various particle

properties. They suggested that the reason for the reduction in $k_L A$ at high solid concentrations was the increased bubble coalescence and therefore reduced interfacial area. This suggests why they could not explain the variation in rate of fall of $k_L A$ with particle concentration in terms of particle size and density. The power dissipation was $1.5\,W\,Kg^{-1}$ but the gas rate was exceedingly high at a superficial velocity of $2.5\ cm\ s^{-1}$, or 12 vvm. This suggests that the state of suspension of the particles varied greatly according to their density. The heavier particles would be more concentrated in the lower regions of the tank and would therefore have no effect on the interfacial area in the upper regions. The lighter particles would be dispersed homogeneously and thus cause a sharp fall-off in $k_L A$ at lower concentrations.

Van den Berg[52] examined a much smaller range of particle concentrations (up to 4% by weight) and found no effect of particle concentration or size (75 - 600 μm) on the gas-liquid interfacial area, which confirms Joosten's results at low particle concentrations. Mehta and Sharma,[77] on the other hand, found that 'A' increased with solids concentration (up to 5% by weight) and that $k_L A$ initially decreased but then increased as solids concentration increased. This is the opposite of the observations of the two previous authors, though the maximum solids concentration examined by Mehta and Sharma was 9% by weight. Also, they used the chemical method to measure 'A' which has since been shown to have disadvantages (see Section 8.2.1).

8.3. The Model

8.3.1. The Determination of Mass Transfer Coefficients from the Liquid and Gas Response Curves

This section describes a theoretical treatment of both gas and liquid response curves to a standard dynamic gassing out test. The $k_L A$ data yielded by this treatment are completely independent of any

assumption with respect to the residence times of the gas bubbles in the system. Thus it is irrelevant to the result whether plug flow or well mixed flow or any other model describes the gas phase dynamics.

A constant volumetric gas flowrate of Q $m^3 s^{-1}$ is sparged in through the base of the vessel with a key component (oxygen) inlet concentration of C_i. It is dispersed into n gas bubbles forming a total volumetric gas holdup of V_G m^3 under steady gas inflow conditions. The key component concentration in the j th bubble (j = 1, 2, 3 ..., n) is C_j, and the average concentration on emerging through the liquid surface is C_o. The volumetric liquid holdup is V_L m^3 and the key component liquid concentration is C_L.

Under steady conditions, in the absence of inlet gas concentration disturbances, C_i, C_j and C_o will all have the same value, C_G, and equilibrium will exist between the gas and liquid phases:

$$C_L = \frac{C_G}{K} \qquad 8.10$$

where K is the Henry's Law constant.

It is assumed that resistance to mass transfer at the gas film is negligible and thus all the resistance is in the liquid film.

If the inlet gas key component concentration is now allowed to vary, equilibrium in the vessel is upset and there will be transfer of the key component across the gas-liquid interface. The liquid phase is assumed to be well mixed (in accordance with all previous models) so that C_L, although now changing with time, is constant throughout the vessel. The bubble concentrations, C_j, will vary according to their individual residence times and C_o will represent the average bubble concentration leaving the liquid surface.

An unsteady state mass balance for the key component in the liquid phase will now be:

$$\sum_{j=1}^{n} \frac{k_L A V_L}{n} \left[\frac{C_j}{K} - C_L\right] = V_L \frac{dC_L}{dt} \qquad 8.11$$

or

$$\left[\begin{array}{l}\text{The sum over all bubbles of the}\\ \text{rate of transfer of key component}\\ \text{from a bubble to the liquid phase}\end{array}\right] = \left[\begin{array}{l}\text{Rate of accumulation of}\\ \text{key component in liquid}\\ \text{phase}\end{array}\right]$$

Implicit in Eqn. 8.11 is the assumption that Henry's Law, Eqn. 8.10, applies at the interface. The symbol 'A' in Eqn. 8.11 represents the total interfacial area of bubbles per total volume of liquid (m^2/m^3) and k_L the liquid film absorption rate constant correlating the mass flux across this area to the driving force. Eqn. 8.11 can be expanded if it is assumed that (AV_L/n) and k_L are constants. The former can be considered to represent the spacially averaged interfacial area per bubble and the latter the spacially averaged liquid film absorption constant. The expansion then gives:

$$\frac{k_L A V_L}{K\,n} \sum_{j=1}^{n} C_j - \frac{k_L A V_L}{n} \sum_{j=1}^{n} C_L = V_L \frac{dC_L}{dt}$$

i.e. $$\frac{1}{Kn} \sum_{j=1}^{n} C_j - C_L = \frac{1}{k_L A} \frac{dC_L}{dt}$$

and therefore $$\frac{1}{n} \sum_{j=1}^{n} C_j = K \left[C_L + \frac{1}{k_L A} \frac{dC_L}{dt}\right] \qquad 8.12$$

If the key component is absent from the system up to time $t = 0$, at which point it is introduced at concentration C_i, via the inlet gas stream, then an overall mass balance for the key component up to any time t will be:

$$\left[\begin{array}{l}\text{Mass of key component}\\ \text{entering the system}\\ \text{up to time t}\end{array}\right] - \left[\begin{array}{l}\text{Mass of key component}\\ \text{leaving the system up}\\ \text{to time t}\end{array}\right] = \left[\begin{array}{l}\text{Mass of key}\\ \text{component in}\\ \text{the liquid}\\ \text{phase}\end{array}\right] + \left[\begin{array}{l}\text{Mass of key component}\\ \text{in the gas phase}\end{array}\right]$$

or
$$Q\int_0^t C_i\,dt - Q\int_0^t C_o\,dt = V_L C_L + V_G \cdot \frac{1}{n}\sum_{j=1}^{n} C_j \qquad 8.13$$

By combining Eqns. 8.12 and 8.13 and rearranging, an expression is obtained which will allow the direct calculation of $k_L A$ at any time t from the concentration-time histories of C_i, C_o and C_L:

$$k_L A = \frac{K\,\dfrac{dC_L}{dt}}{\dfrac{Q}{V_G}\int_0^t (C_i - C_o)dt - C_L\left[\dfrac{V_L}{V_G} + K\right]} \qquad 8.14$$

In practice it is preferable to use a simple step change in C_i such as changing from a nitrogen gas input to an air input.

To avoid the necessity of calibrating the measuring equipment it helps to express Eqn. 8.14 in terms of normalised response concentrations, since these can be obtained directly from the recorder outputs. Thus:

$$C_i^* = C_o^*\,(t = \infty) = C_L^*\,(t = \infty) = 1 \qquad 8.15$$

C_L^* and C_o^* are obtained by dividing the recorded concentrations (C_L and C_o, in arbitrary units) by their final steady state values ($C_L\,(t = \infty)$ and $C_o\,(t = \infty)$ in arbitrary units). Thus:

$$C_L = W_L C_L^* \quad \text{and} \quad C_o = W_G C_o^* \quad \text{and} \quad C_i = W_G C_i^*$$

where $W_{L,G}$ is a constant relating absolute to normalized concentrations and is equal to the final steady state concentration ($C_L\,(t = \infty)$, $C_o\,(t = \infty)$).

Hence Eqn. 8.14 becomes:

$$k_L A = \frac{W_L K\,\dfrac{dC_L^*}{dt}}{\dfrac{QW_G}{V_G}\int_0^t (1 - C_o^*)dt - W_L C_L^*\left[\dfrac{V_L}{V_G} + K\right]} \qquad 8.16$$

But since $$\frac{1}{K} = \frac{C_L}{C_G} = \frac{W_L C_L^*}{W_G C_G^*} = \frac{1}{K^*}\frac{W_L}{W_G} = \frac{W_L}{W_G} \qquad 8.17$$

Then by substituting for K in Eqn. 8.16 and dividing by W_G, Eqn. 8.14 in a normalized form becomes:

$$k_L A = \frac{\dfrac{dC_L^*}{dt}}{\dfrac{Q}{V_G}\displaystyle\int_0^t (1 - C_o^*)dt - C_L^*\left[\frac{V_L}{KV_G} + 1\right]} \qquad 8.18$$

The integral and derivative terms in Eqn. 8.18 are evaluated numerically from the normalized response curves at selected times, t_j (j = 1, 2, 3, ...) as indicated in Fig. 8.2, to arrive at a value for $k_L A$. An optimum value of $k_L A$ can be obtained by plotting the numerator of Eqn. 8.18 against the denominator for a number of values of t_j, to produce a straight line that passes through the origin of slope $k_L A$.

8.3.2. Determination of $k_L A$ from the Initial Liquid Response

A disadvantage of the technique described in the previous section is that both the liquid and gas concentrations must be monitored continuously. This inconvenience is well compensated for by the elimination of the gas residence time distribution model from the analysis. However, it is possible to demonstrate, in principle at least, that $k_L A$ can be evaluated from the liquid response alone.

The expression for $k_L A$, Eqn. 8.18, is indeterminate at t = 0 and t = ∞. The significance of the second indeterminancy is discussed in Section 8.5.1 but the first one leads to an alternative expression for $k_L A$.

Using L' Hospital's rule at t = 0:

$$k_L A = \frac{\left.\dfrac{d^2 C_L^*}{dt^2}\right|_{t=0}}{\dfrac{Q}{V_G}(1 - C_o^*) - \left.\dfrac{dC_L^*}{dt}\right|_{t=0}\left[\dfrac{V_L}{KV_G} + 1\right]} \qquad 8.19$$

Since at $t = 0$; $C_o^* = 0$ and $\left.\dfrac{dC_L}{dt}\right|_{t=0} = 0$

Then

$$k_L A = \frac{V_G}{Q}\left.\frac{d^2 C_L^*}{dt^2}\right|_{t=0} \qquad 8.20$$

8.4. Experimental

8.4.1. The System

All mass transfer measurements were carried out in the T_{56} vessel. Four impellers were examined (DT, AFD, 4 MFD, 4 MFU), all of diameter approximately 0.28 m (T/2) and all positioned 14 cm (T/4) from the base of the vessel. The liquid medium was de-ionised water at 25^o C $\pm$ 1^o C with the liquid level kept at H = T. Some workers (Van't Riet[22]) have used higher liquid levels than standard to avoid any complications due to surface aeration, but Chapman et al.[78] show that under gas sparged conditions the volume of gas entrained through the liquid surface is negligible for this geometry. All experiments were performed at solid concentrations of 0, 3 or 20% by weight particles. A range of impeller speeds were used such that in all cases when particles were present, $N \geq N_{JS}$, so as to ensure:

(a) A reasonable similarity of hydrodynamic conditions between the different impeller systems with regard to particle suspension, i.e. to ensure the entire vessel contents were a three phase mixture in all cases.

(b) That a valid comparison of the mass transfer potential of the impellers was made in a realistic operating range for

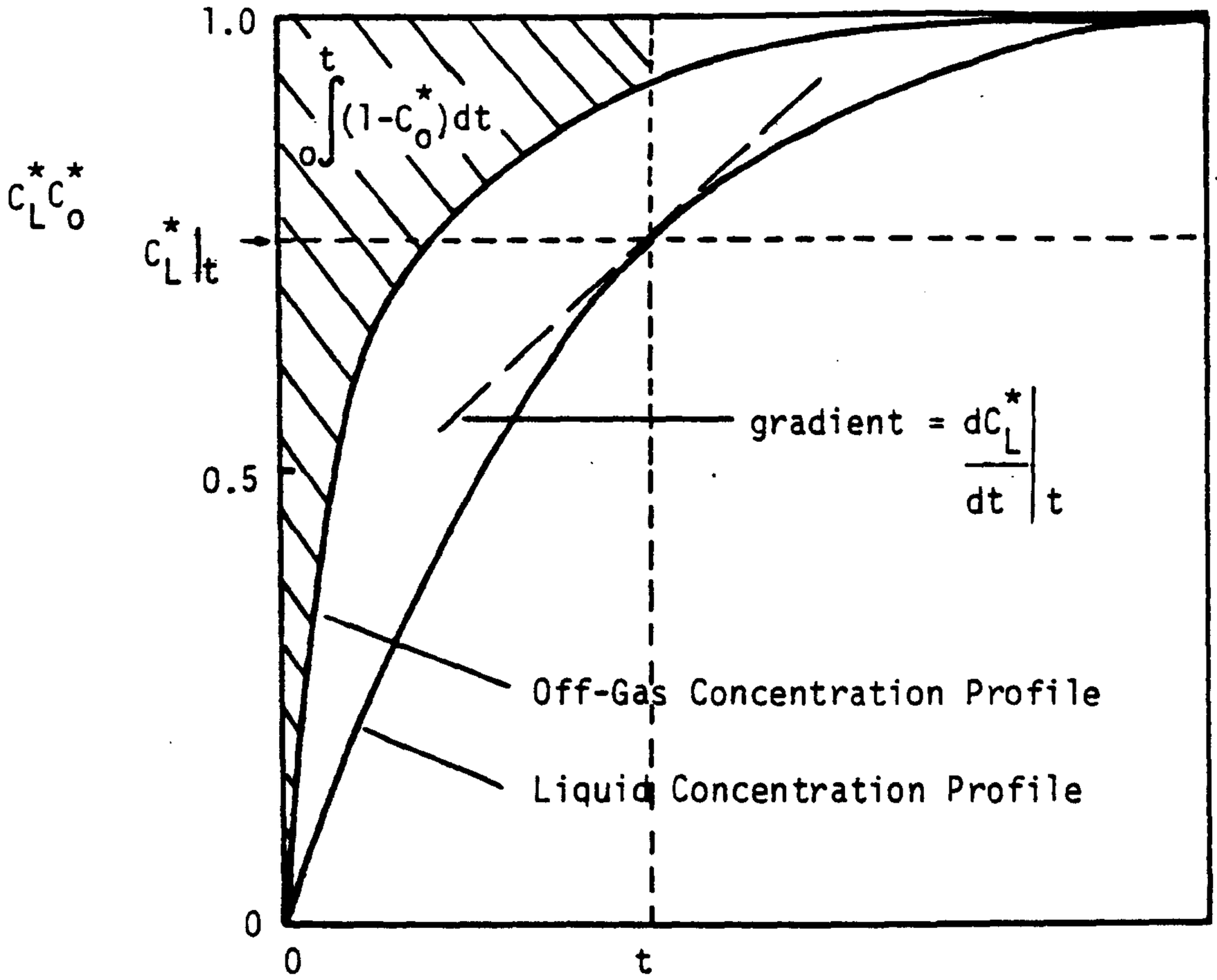

Fig. 8.2 Terms used in the Evaluation of $k_L A$ from Eqn. 8.18

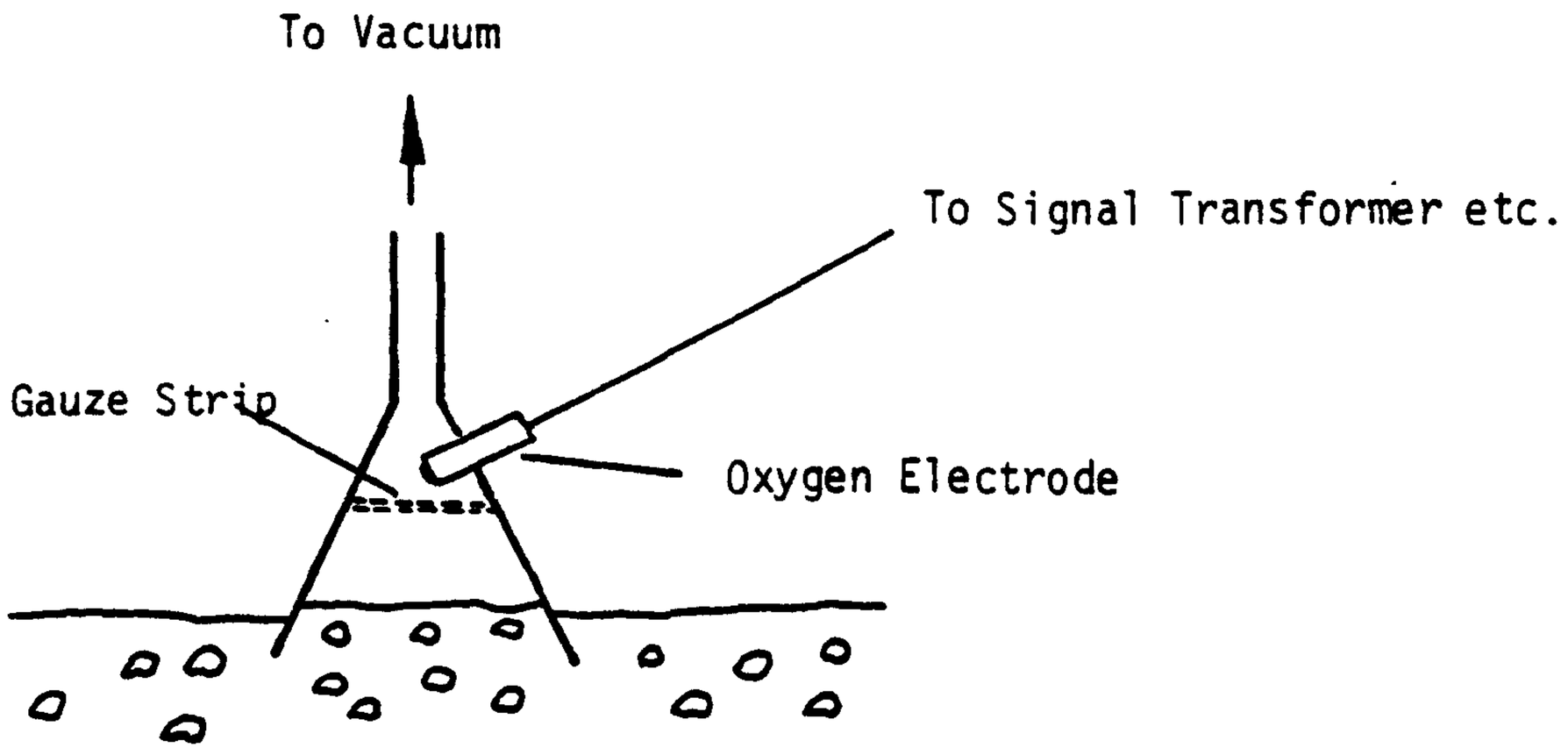

Fig. 8.3 Off-Gas Measuring Apparatus

that impeller.

Two gas rates (0.25 and 1 vvm) were used.

8.4.2. The Technique

The vessel contents were de-aerated by gassing with nitrogen until a steady and very low (effectively zero) oxygen level was attained. The nitrogen sparge rate was the same as the air rate was to be during the run, thus ensuring that no variation in gas holdup occurred on changing to air. For similar reasons the impeller speed during de-aeration was also set at the value to be used during the run. When steady conditions existed, the nitrogen supply was changed stepwise to air in such a manner that there was no burst of gas into the tank which might have influenced the initial response of the system. Two rapid response oxygen electrodes (see Section 8.4.3) were used to follow the oxygen concentration with time in the off-gas at the top of the tank and in the liquid. Because the electrodes had such fast response times ($0.4s < \tau < 2$ s), the positioning of the liquid measuring probe was critical since in the wrong position it would detect the presence of individual bubbles. However, it was possible to find an orientation for each impeller system where a smooth response was obtained by placing the probe, mounted in a copper tube, close to the impeller so that a vigorous flow existed at about 45^{o} to the sensing membrane. Fig. 8.3 shows the method used to follow the off-gas concentration profile. Here the probe was held in an inverted funnel, which was positioned with its lip just under the top surface of the dispersion, thus preventing entrainment of atmospheric air into the funnel. A strip of gauze was placed just below the oxygen electrode to reduce the possibility of liquid splashing onto the sensing membrane. A slight vacuum was applied to the funnel to increase the quantity and velocity of gas passing over the sensing membrane.

Impeller speed, gas rate, gas holdup and power were recorded

for each run.

8.4.3. The Measuring Apparatus

The two oxygen electrodes employed were designed and supplied by ICI Corporate Laboratory. They incorporated platinum and silver electrodes with 10% potassium chloride as the electrolyte sealed by a 1.27×10^{-2} mm P.T.F.E. membrane. The response time of the probes could be varied by altering the tension on the membrane, through which oxygen diffused to be electro-chemically reduced and cause a current proportional to the local partial pressure of oxygen. The probes were each connected to signal transformers which provided them with an applied voltage of about 0.6 volts from the mains supply and provided a zero to fifty millivolt output to a two-pen JJ Instruments CR600 recorder.

The response time of the combined oxygen electrode, signal transformer and recorder was measured by either plunging the probes from a completely de-aerated liquid to a completely air saturated liquid (water) or by directing a nitrogen stream at the sensing membrane and then abruptly replacing it by an air stream. Both methods yielded the same results. The sum of the response lags could be treated as a single first order lag and the data de-convoluted accordingly, i.e.:

$$C_{actual} = \tau \frac{dC_{measured}}{dt} + C_{measured} \qquad 8.21$$

where $\tau = \tau_L$ or τ_G as appropriate. Typical test responses for both the gas and liquid probes are given in Appendix 5. Obtaining the actual concentration profile from the measured one was slightly more complicated for the off-gas. In this case the output would contain a pure time delay plus a response time that depended on the volume of gas in the funnel and the degree of mixing that occurred within this gas volume. These data were obtained with the probe and funnel in situ. The tank would be completely de-aerated by sparging with nit-

rogen at the appropriate rate (i.e. 0.25 or 1 vvm). A source of air was then instantly inserted just under the lip of the funnel, simultaneously recording the time of application of air on the recorder. After a short pure time delay, a response would be observed on the recorder (Appendix 5) which could again be treated as a first order response lag. A time constant (τ_G) was then evaluated, which accounted for the combined probe, funnel, analyzer and recorder responses. Off-gas data were therefore deconvoluted by first allowing for the pure time delay and then treating in the same manner as the liquid response data (i.e. according to Eqn. 8.21). Details of the deconvolution procedure are given in Appendix 6.

The liquid probe was found to have a first order time lag, τ_L, of 0.4 s. The gas probe lag, τ_G, was much larger (4 - 10 s) and a function of gas rate since it was dominated by the mixing process in the funnel, the volume of which was about one litre compared to system gas holdups in the range 3 - 12 litres. Since the funnel volume varied in practice, depending on the vacuum applied, there was a degree of uncertainty in the measured value of τ_G. Fortunately, τ_G could also be deduced from individual run data by invoking the mean residence time theorum as discussed later. As can be seen in Appendix 6, the liquid response was little affected by the deconvolution process but the gas concentration profile was significantly altered.

Due to the variation of time constants with membrane tension, the probe responses were checked before and after every set of experiments, but found to vary very little unless the probe was dismantled.

8.5. Results and Discussion

8.5.1. The Model

The experimental conditions, with corresponding $k_L A$ values determined using Eqn. 8.18, are presented in Appendix 7. Fig. 8.4 shows the numerator of Eqn.8.18 plotted against the denominator for a

number of arbitrary times in the transient response interval for three typical runs (26, 28 and 29). These data show the predicted linear form with very little scatter and enable $k_L A$ to be determined with a fair degree of confidence. Using the data from four runs, Table 8.1 compares the $k_L A$ values obtained from Eqn. 8.18 with evaluations that assume specific models for gas mixing. As is to be expected, the simple 'no depletion' model consistently underestimates $k_L A$, implying as it does an excessive concentration driving force (see Fig. 8.1). At the higher gas rate (Q = 1 vvm) there is good agreement between the

Run	$k_L A$ (s^{-1})			
	Gas mixing model			
	No depletion ($C_i = C_o = C_G$) (D - Fig. 8.1)	Perfect mixing (A - Fig.8.1)	Plug flow	Unspecified
26	0.035	0.070	0.045	0.055
27	0.037	0.097	0.052	0.062
28	0.066	0.119	0.081	0.077
29	0.089	0.199	0.115	0.107

Table 8.1 The Effect of Gas-Liquid Mixing Assumption on $k_L A$ Evaluation

present work and the assumption of gas plug flow, whereas at the low gas rate (Q = 0.25 vvm) the results lie between those obtained assuming perfect gas mixing and those obtained assuming plug flow. Though these results relate only to a disc turbine impeller, they emphasize the dangers involved in assuming a particular mode of gas flow and applying it over a wide range of hydrodynamic conditions. It is interesting to note that the impeller speeds used in Runs 26, 27 and 29 were well in excess of N_R [5], the speed at which gas recirculation to the cavities in the impeller region becomes significant (Chapter 3), and approximately

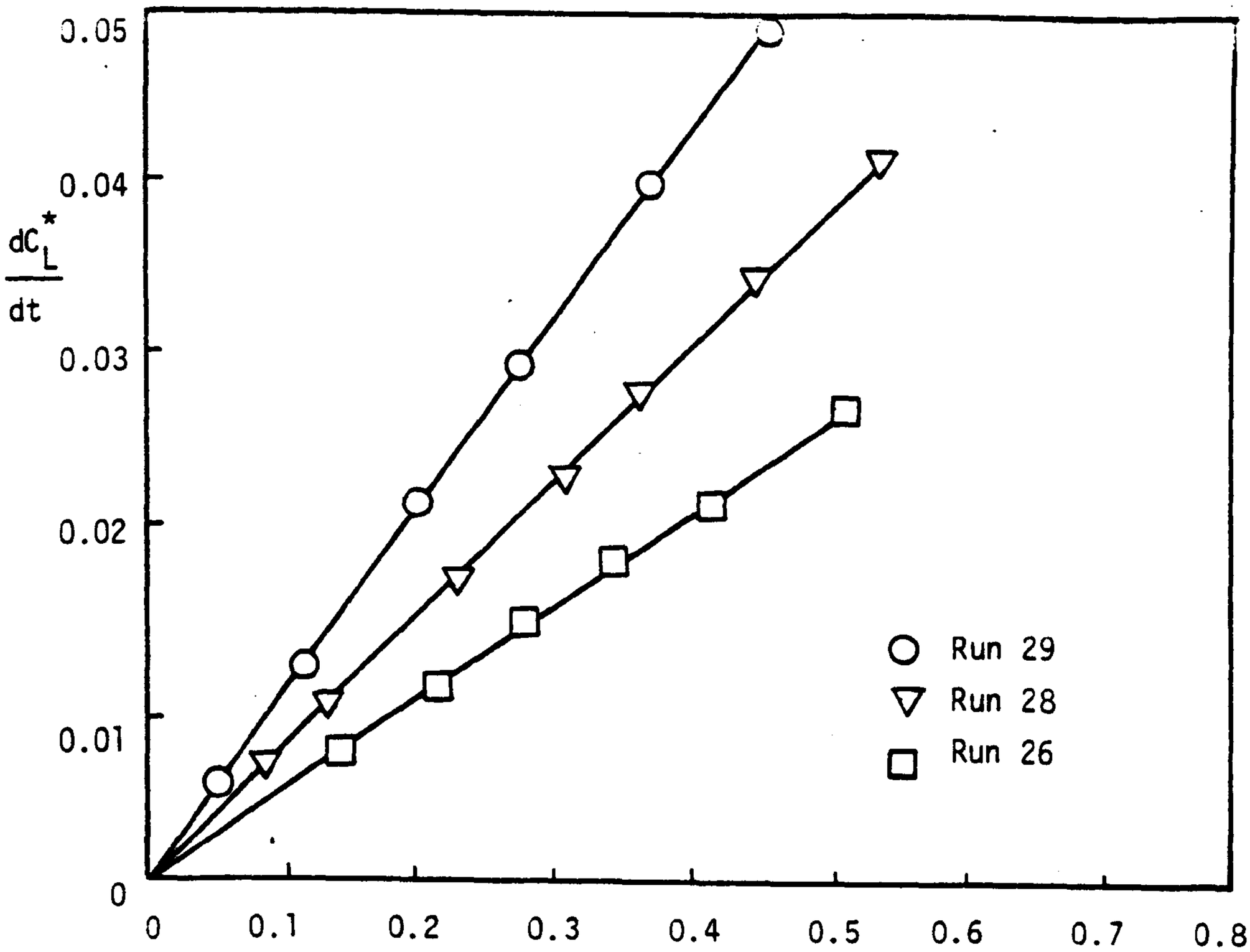

$$\left[\frac{Q}{V_G}\int_o^t (1-C_o^*)dt \;-\; C_L^*\left[\frac{V_L}{KV_G}+1\right]\right]$$

Fig. 8.4 Estimation of $k_L A$ from Eqn. 8.18

equal to N_R for Run 28.

An empirical correlation summarizing the $k_L A$ data in the literature was recently published in a review article by Van't Riet[62]. As such, this correlation was principally based on data evaluated via the 'no-depletion' model since the drawbacks and alternatives to this treatment are relatively recent developments (Section 8.2.1). Nevertheless, the $k_L A$ values evaluated via the 'no'depletion' model for this work were some 50% higher than the values predicted using Van't Riet's equation. This is just outside his quoted error band of $\pm$ 20 - 40%.

The major uncertainties in the experimental data used to extract $k_L A$ by means of Eqn. 8.18 are the first order time constant of the gas concentration detection system, τ_G, and the gas holdup, V_G; τ_G affects the gas concentration response, C_o^*, quite markedly, as is demonstrated in Appendix 6; its value is determined for each run as follows. The mean residence time theorem[79] states that for steady state multicomponent systems, the mean residencetime of any conserved component is equal to the total holdup of that component in the system divided by its flow rate through the system. Applying this to the oxygen component in the system under consideration when the steady state is reached ($t = \infty$), we have:

$$\text{Mean Residence Time of oxygen} = \frac{V_G C_i + \left[\frac{V_L C_i}{K}\right]}{Q C_i} = \frac{V_G + (V_L/K)}{Q} \qquad 8.22$$

For linear systems this mean residence time may also be obtained from the normalized step response of the system[80]:

$$\text{Mean Residence Time of oxygen} = \int_0^\infty (1 - C_o^*)dt \qquad 8.23$$

Eqns. 8.22 and 8.23 indicate that the denominator of Eqn. 8.18 must

approach zero as t approaches infinity; we make use of this by finding by iteration the value of τ_G that satisfies this condition. An example of this process is given in Appendix 6. The problems involved in accurately estimating the gas holdup, ε, and hence V_G, have been described earlier (Chapters 2 and 3). Since variations in V_G led to variations of similar magnitude in $k_L A$, then for further work on the method it would be desirable to improve on the technique used here to measure gas holdup.

As the expression for $k_L A$ is indeterminate at $t = 0$ and $t = \infty$, then large errors occur for evaluations at small and large times. These show up as a cloud of points near the origin (Fig. 8.5a) for Run 27 but for clarity are not recorded for Runs 26, 28 and 29 in Eqn. 8.4.

Problems were encountered in attempts to evaluate $k_L A$ from the initial second derivative of the liquid responses (Eqn. 8.20). This method was certainly unsuitable for high gas flows where sharp changes in slope occurred very soon after the step change. For Run 27 a well defined initial liquid response was obtained (Fig. 8.5b) that yielded a $k_L A$ value of 0.071 s^{-1} from the second derivative. This is some 15% higher than the value obtained from the slope of Fig. 8.5a. The obvious advantages of this method of evaluating $k_L A$ - only the liquid response curve is required, which is considerably easier to measure than that of the gas, and the method is independent of both gas mixing effects and the equilibrium parameter, K - are hindered by the difficulty in obtaining a very precise indication of the starting point of the experiment and a clean initial portion of the response curve, uninfluenced by flow disturbances due to the step change initiation.

In the extreme, where a very high sparge rate ($Q \to \infty$) affects the system so much as to make the assumption $C_i^* = C_o^*$ valid (equivalent to the 'no depletion' model), then Eqn. 8.18 reduces to:

(a)

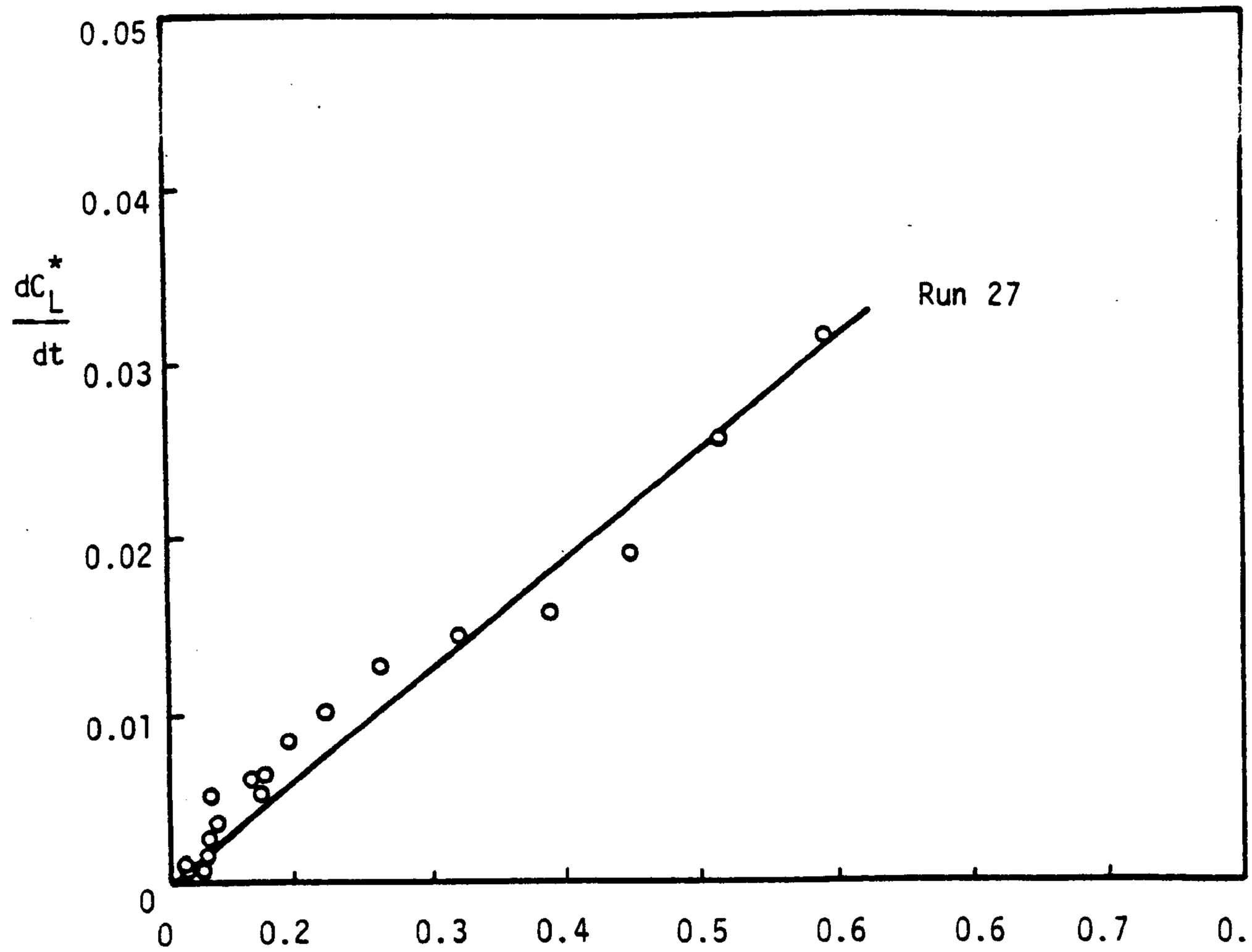

$$\left[\frac{Q}{V_G}\int_0^t (1-C_o^*)dt \;-\; C_L^*\left[\frac{V_L}{KV_G}+1\right]\right]$$

(b)

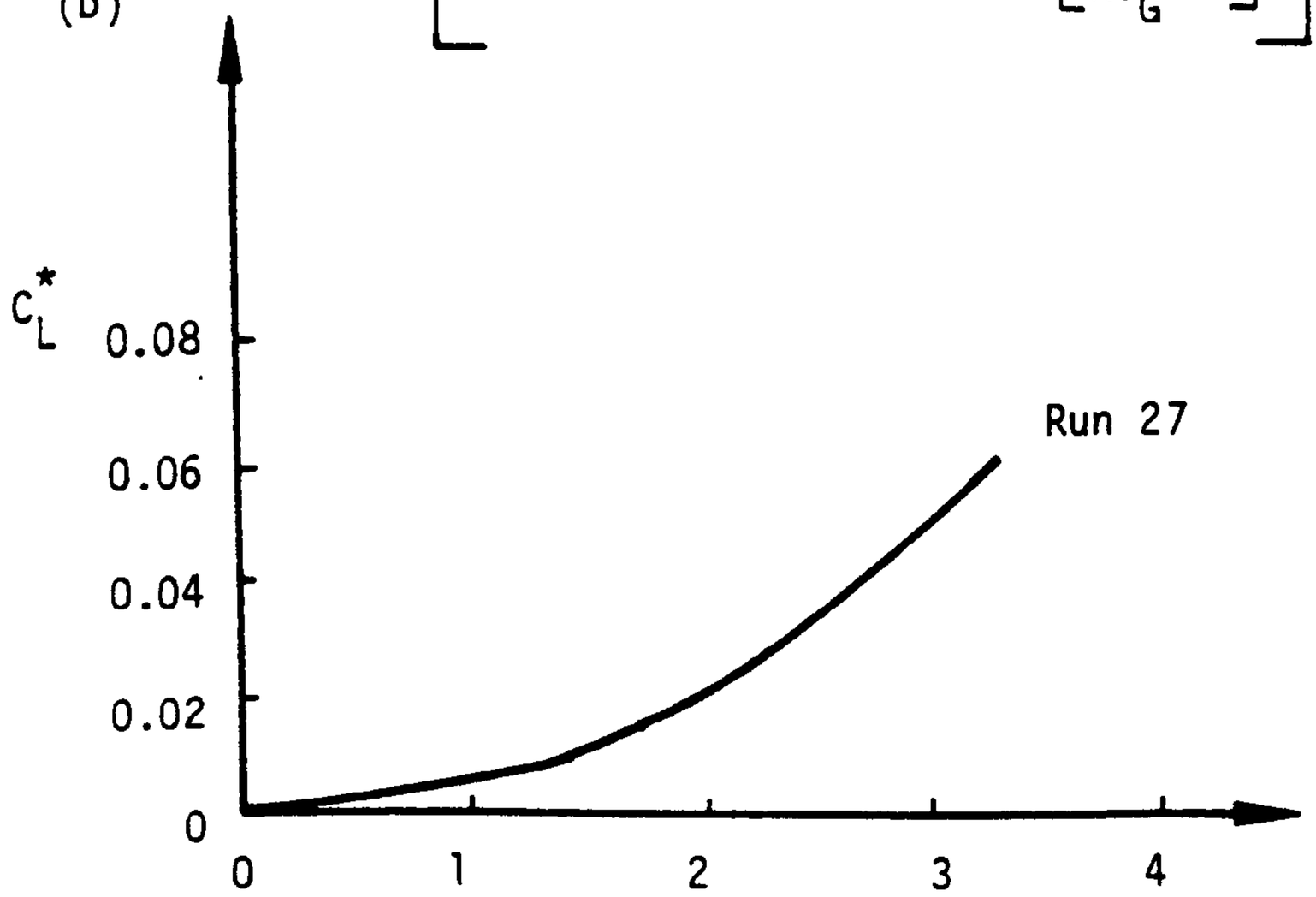

Fig. 8.5 Estimatation of $k_L A$ for Run 27 using (a) the Gas and Liquid Response Curves and (b) the Initial Liquid Response

$$k_L A = \left.\frac{dC_L^*}{dt}\right|_{t=0} \qquad (t = 0 \Rightarrow C_L^* = 0) \qquad 8,24$$

This hypothesis was tested with the 4 MFU impeller at the highest gas rate (Runs 19 and 20) but predictably it was very difficult to specify an accurate initial slope. However, the range of possible solutions appeared reasonable (see Section 8.5.2).

8.5.2. Comparison of Impellers

The restrictions imposed on these experiments (i.e. $N > N_{JS}$ and N_{CD}) meant that a larger range of specific power inputs could be examined for the lower gas rate (0.25 vvm) than could be for the higher rate (1 vvm). Van't Riet's conclusion[62] that $k_L A$ was dependent only on power input and gas rate and independent of impeller type, seems reasonable when considering Fig. 8.6 which shows $k_L A$ against specific power input for the four impeller types studied at a sparge rate of 0.25 vvm. Although there is some scatter and little overlap of power inputs, the $k_L A$ values seem to vary little with impeller type, but show a gradual drop in the rate of increase in $k_L A$ with power input. The disc turbine produces the highest mass transfer coefficients, but also requires the highest power inputs to simultaneously disperse the gas and suspend the particles. The 4 MFU impeller appears to be marginally less efficient than the other impellers at the lower power inputs, but for $\varepsilon_T > 1$ W Kg^{-1} each impeller produces approximately similar $k_L A$ values. However, at the higher gas rate (1 vvm), there appears to be a definite advantage in using a disc turbine or 4 MFU impeller at specific power inputs of around 1 W Kg^{-1} (Fig. 8.7). At higher power inputs the data suggest that the advantage of any one impeller type will diminish as for the lower gas rate, though there are not enough data to confirm this trend. The broken lines on Fig. 8.7 represent the range of uncertainty in evaluating $k_L A$ for the 4 MFU

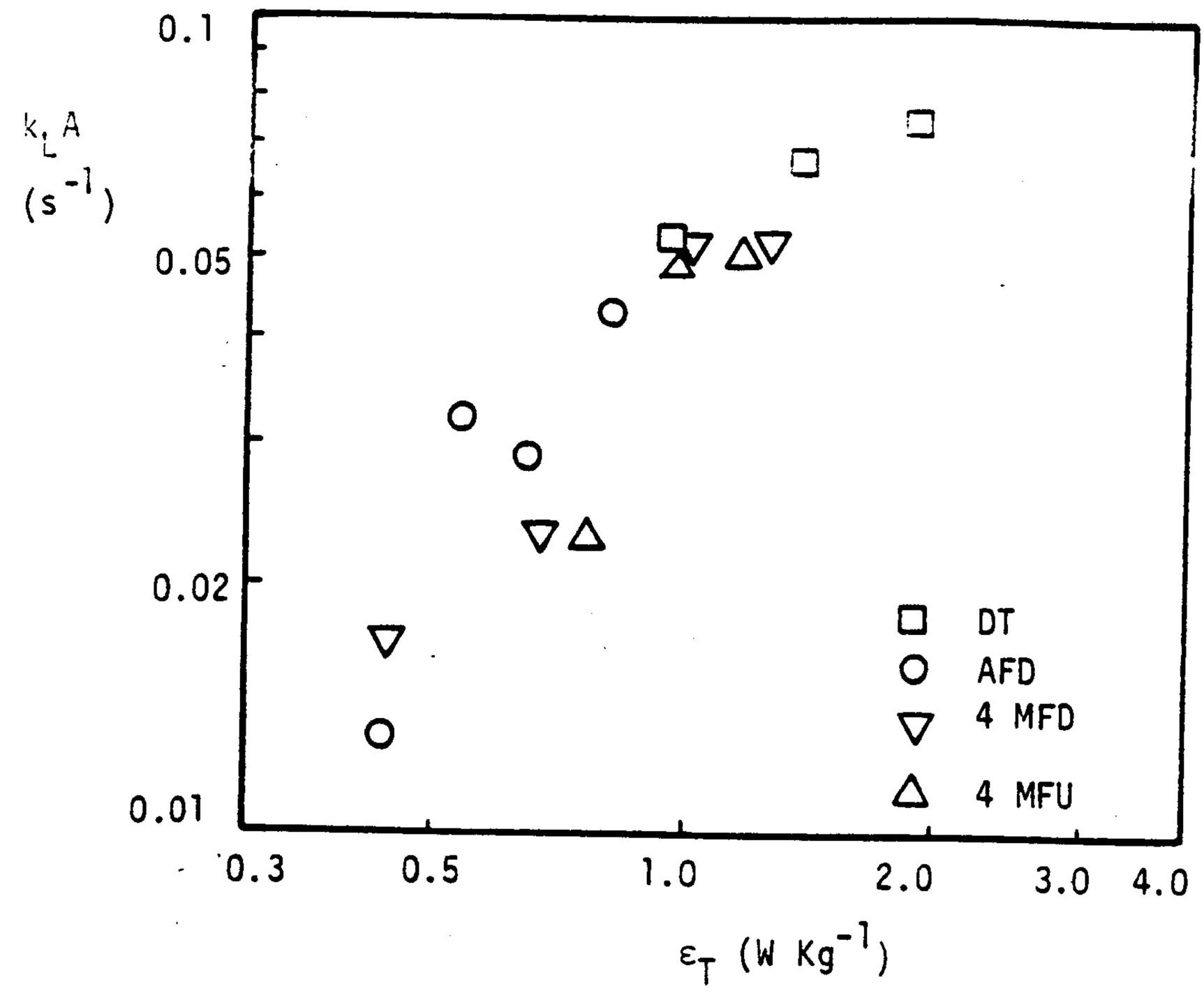

Fig. 8.6 $k_L A$ versus ε_T for Various Impeller Types, Q = 0.25 vvm.
(D = T/2, c = T/4, T_{56})

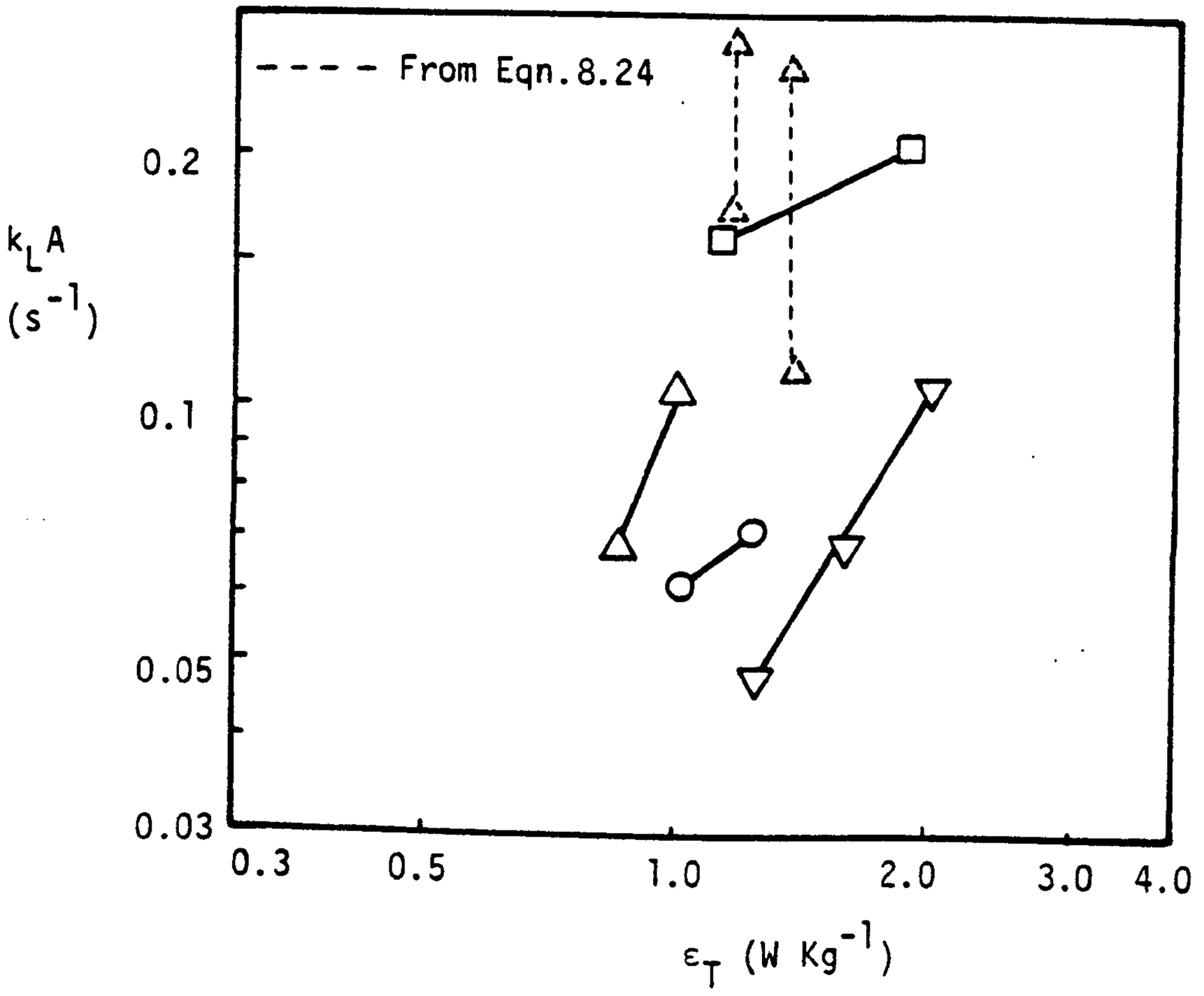

Fig. 8.7 $k_L A$ versus ε_T for Various Impeller Types, Q = 1 vvm.
(Details and Symbols as Fig. 8.6)

impeller (Runs 20 and 21) via Eqn. 8.24.

The conclusions drawn from Chapter 3 with regard to the changing dispersion efficiency of the various impellers with gas rate - i.e. the impellers with discs and the 4 MFU impeller showed increasing advantages at higher gas rates - seem to be supported by the results presented in Fig. 8.7.

Thus the disc turbine impeller consistently produced the highest $k_L A$ values, especially at the highest gas rate. At very high specific power inputs there appears to be little advantage in using any one impeller type and also there appears to be a smaller return on any extra power input.

The runs represented in Fig. 8.7 were also treated according to the 'no depletion', well mixed and plug flow gas phase assumptions, and the results are presented in Fig. 8.8. This figure confirms the superiority of the disc turbine, independent of the gas flow model, whereas the 4 MFU impeller is shown to produce relatively low $k_L A$ values (in relation to the 4 MFD and AFD impellers) when compared to those derived using Eqn. 8.18.

8.5.3. The Effect of Particle Concentration

Examination of the data in Appendix 7 shows that the trends reported by Joosten et al.[53] were generally confirmed by this work. For instance, with an aeration rate of 1 vvm the AFD impeller gave a $k_L A$ value of 0.05 s^{-1} for a specific power input of 1.33 W Kg^{-1} and a particle concentration of 20% by weight compared to a $k_L A$ value of 0.07 s^{-1} for a specific power input of only 1.24 W Kg^{-1} and a 3% particle concentration. Similarly, the 4 MFU impeller produced a higher value of $k_L A$ (0.104 s^{-1} compared to 0.075 s^{-1}) for a lower value of ε_T [1.01 W Kg^{-1} compared to 1.54 W Kg^{-1}) when a lower particle concentration was used [3% compared to 20%) with a gas rate of 1 vvm.

The only results obtained with a two phase gas-liquid only

(a)

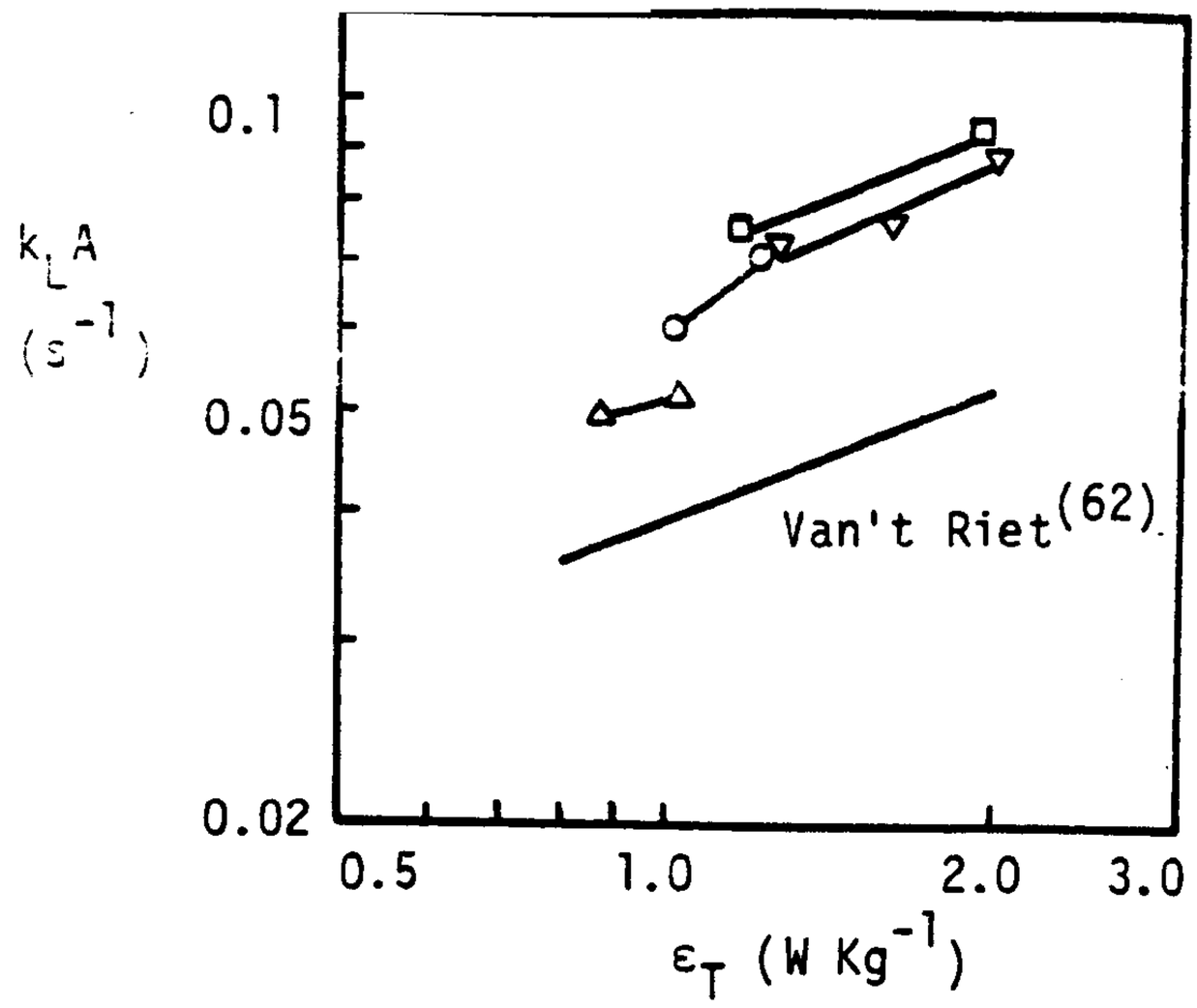

(b)

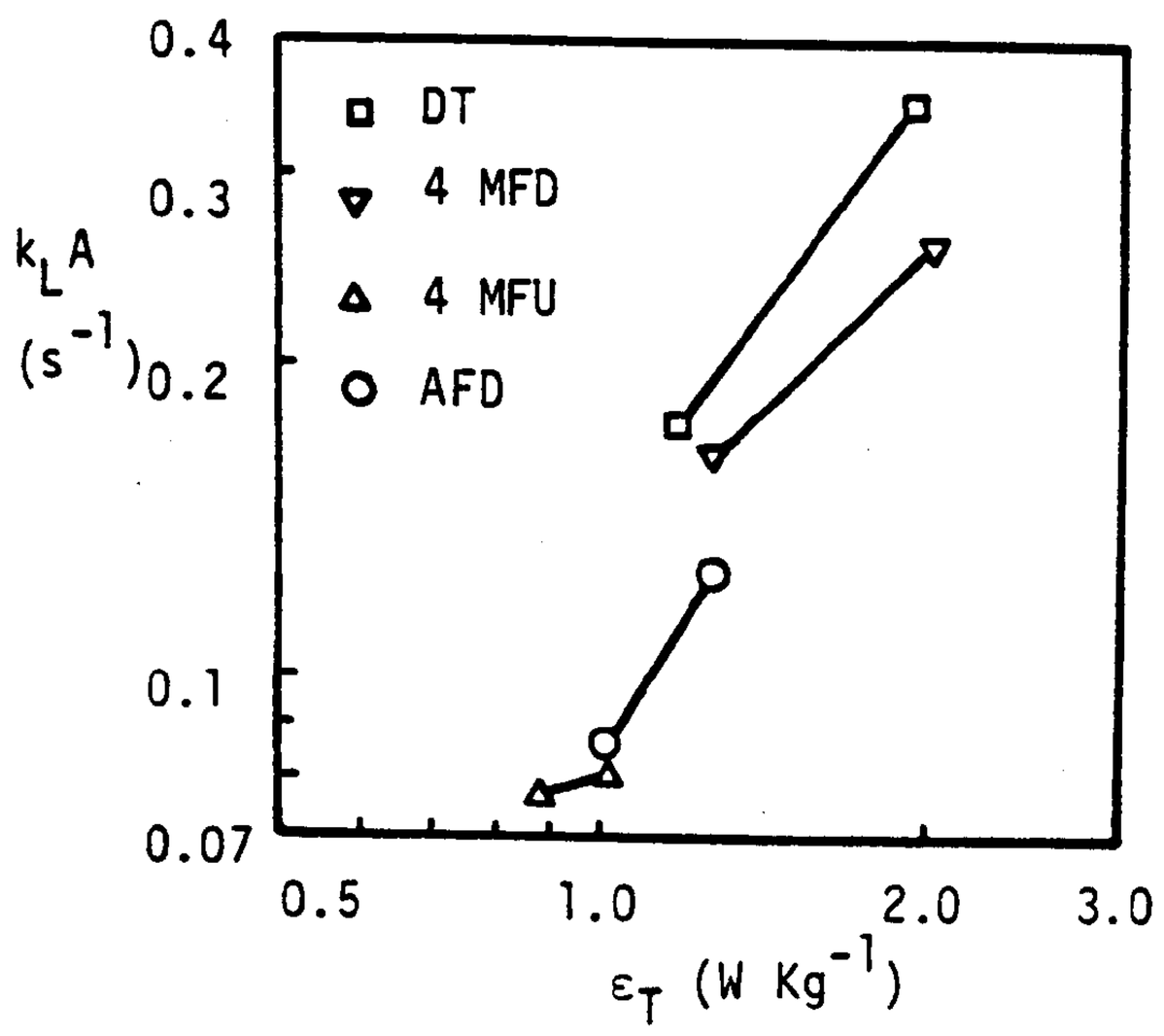

(c)

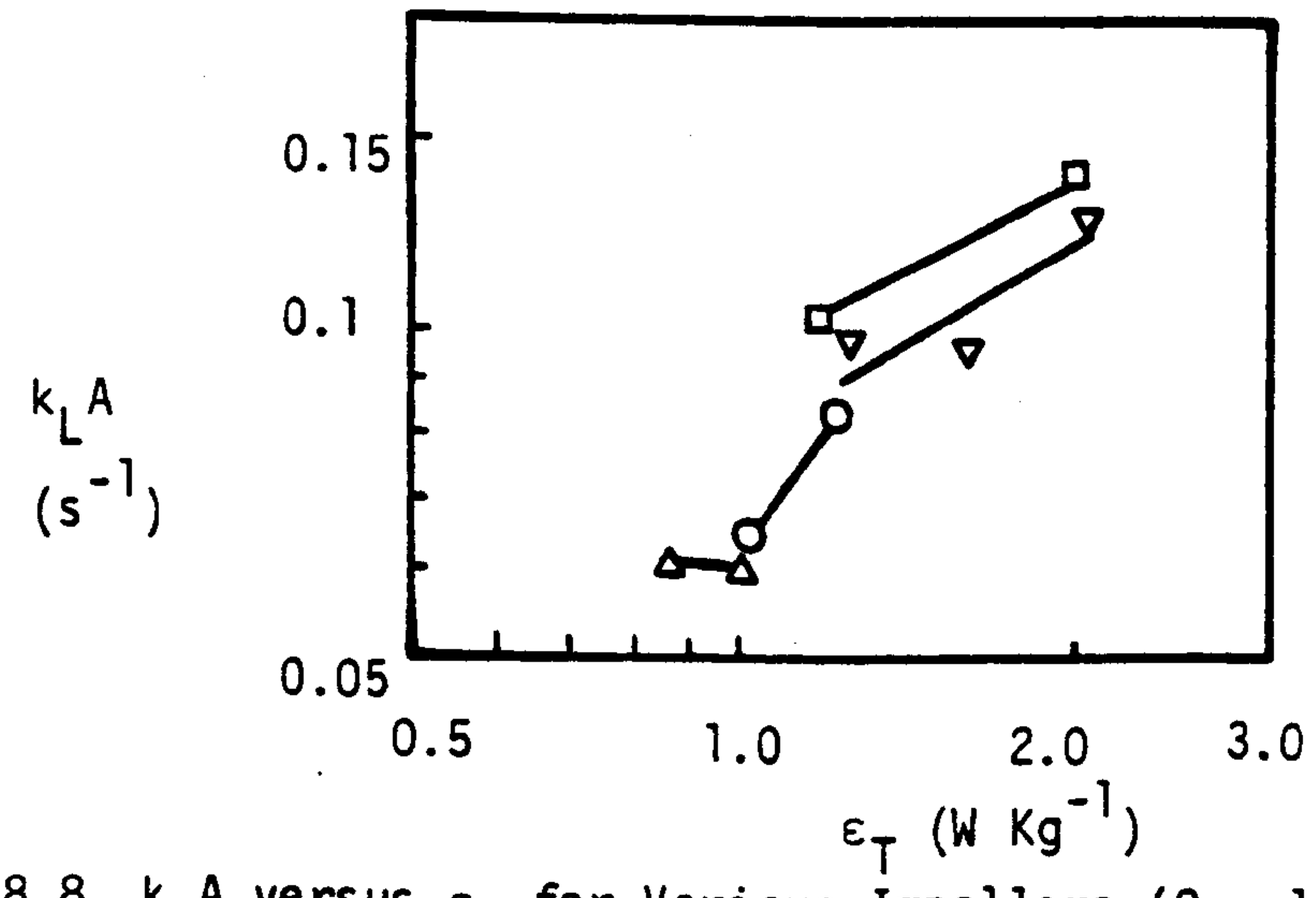

Fig. 8.8 $k_L A$ versus ε_T for Various Impellers (Q = 1 vvm) where $k_L A$ is evaluated according to: (a) the Simple Model, (b) the well-mixed gas phase model, (c) the Plug-Flow Model.

dispersion were for the disc turbine impeller. With Q = 0.25 vvm, the value of $k_L A$ fell from 0.074 s^{-1} to 0.052 s^{-1} as X increased from 3 to 20% with an identical specific power input in each case of 1.88 W Kg^{-1}. However, with no particles present, $k_L A$ was 0.062 s^{-1} but with ε_T only 1.71 W Kg^{-1}. This suggests that the presence of the particles had very little effect when X was low, but a reasonable damping effect on $k_L A$ at high particle concentrations.

As stated above, these characteristics fall into line with those described by Joosten et al. However, the small rise they sometimes observed in $k_L A$ (10 - 20%) when very low solid concentrations were added was noted only for the disc turbine at a gas rate of 1 vvm, but on this occasion $k_L A$ was nearly doubled (0.107 → 0.206 s^{-1}) when X was increased from 0 to 3% ($\varepsilon_T \simeq$ 2.0 W Kg^{-1} in each case). This result seems unlikely in the light of those reported above, yet obvious explanations such as an erroneous gas holdup etc. do not account for such a large difference. Nevertheless, for the same conditions and power input, $k_L A$ fell to below the non-particulate system level when the concentration of solids was increased to 20%, in accordance with all the previously reported data.

8.6. Conclusions

The method of treating transient absorption data proposed in this chapter yields $k_L A$ values which are independent of the gas residence time distribution and hence do not rely on any assumptions with regard to the gas phase dynamics. The results demonstrate the hazards involved in assuming a particular description of the gas flow and applying it to a wide range of conditions. Consequently, further work on two fronts is necessary, the first being to improve the experimental technique, with particular reference to:

(a) Estimating an accurate start time for the runs.

(b) Improving the off gas sampling apparatus.

(c) Measuring V_G more accurately.

The second entails a very detailed comparison of $k_L A$ evaluations by this model with those obtained via the other models which assume plug flow or well-mixed gas flow. As a result of that work, insight may be gained into any possible advantage of re-appraising all previously published mass transfer coefficients obtained by the transient response technique.

As a result of the independence of $k_L A$ from the gas phase dynamics, it was possible to confidently compare the gas-liquid mass transfer potential of four impeller types even though they caused very different gas flow patterns. Disc turbine impellers were shown to produce high $k_L A$ values but required the highest specific power inputs, though at high gas rates they had a distinct advantage over other impeller types on an equal power input basis. The 4 MFU impeller appeared to be more efficient (i.e. produce higher $k_L A$ values) relative to the other impeller types at high gas rates, though the more traditional methods of estimating $k_L A$ did not confirm this result.

The general trends of Joosten et al.[53] with regard to the effect of solids concentration on gas-liquid mass transfer coefficients were confirmed.

CHAPTER 9.

FINAL CONCLUSIONS AND SUGGESTIONS FOR FURTHER WORK

9.1. Conclusions

The decrease in impeller power consumption on aeration has been shown to have serious effects on the particle suspension capability of an impeller, resulting in a given suspension duty requiring higher impeller speeds and power inputs to achieve the just-suspended state as gas rate is increased. The manner in which P_g decreases with increasing Q gives an indication of the severity of these problems, which vary with impeller geometry. Impellers which produce a component of flow in the opposite direction to the overall direction of gas flow through the vessel can experience severely unstable behaviour which in turn can result in dramatic sedimentation of the suspended solids.

The consequence of these interactions is that the optimum impeller choice for a given duty in a two phase system is not necessarily the best choice in a three phase system. The way in which $(\varepsilon_T)_{JS}$ increases over the ungassed value as sparge rate increases varies with impeller type and thus, although the AFD and MFD impellers are in some ways superior at zero and low gas rates, they require the largest energy inputs at high gas rates.

It should be noted that the necessary increases in agitation to maintain the just-suspended state are dependent only on the interaction between the gas sparge and the impeller pumping capacity. Hence on aeration, for a given impeller system, a very light suspension duty will require a similar increase in N_{JS} and $(\varepsilon_T)_{JS}$ to a very severe suspension duty, resulting in a much more significant fractional increase in agitation conditions for the lighter duty.

9.2. Design Recommendations for Gas-Liquid-Particle Mixing

The following recommendations are made as a basis for the design of a three phase system:

1) An economic and/or hazard analysis of the system should be carried out to identify the most important constraints on the design. For example:
   (a) Stability: operation at speeds below N_{JS} and/or N_{CD} might result in dangerous heat build-up or unacceptable conversion losses etc.
   (b) Mass transfer: a high $k_L A$ value might be essential to the reaction or absorption system.
   (c) Power consumption: high power costs may necessitate operation at minimum possible power input.
2) Impeller choice: this depends on the most important constraints (see above) and the required process aeration rate. At very low gas rates, the AFD and MFD impellers sometimes require considerably lower power inputs to achieve N_{JS}, but, unless a considerable safety margin is used, flow instabilities may occur if there are any fluctuations in gas rate. Also, if a high $k_L A$ is required, their advantage is diminished since correspondingly high power inputs will then be necessary and the disc turbine becomes a better choice since it produces no flow instabilities.

   At high rates of aeration, the disc turbine and MFU impellers appear superior in terms of energy requirements, system stability and mass transfer coefficients. The ADT impeller showed no significant advantage over the standard disc turbine.
3) Of all the impellers studied, the disc turbine appears to be singularly the most versatile for three phase operations. It has been shown for this impeller type, over a wide range of vessel sizes ($0.019 \leq V_L \leq 4.41\ m^3$), that the impeller speed required to achieve the just-suspended state can be

estimated by a relationship of the form given in Eqn.7.10 from a knowledge of N_{JS} in the corresponding unaerated system. Zwietering's expression (Eqn. 4.1) remains the best basis for estimating $(N_{JS})_{Q=0}$. However, the data presented in Chapters 4 and 7 show that some care should be taken in scaling up using this relationship.

The expressions governing scale up in aerated systems differ slightly from those applicable in unaerated systems. In terms of specific power inputs these differences are magnified and under various conditions it is necessary to increase $(\varepsilon_T)_{JS}$ on scale up.

9.3. Further Work

Throughout this thesis there have been references to aspects of the subject that would benefit from further investigation.

The techniques used here to characterize the agitation of gas-liquid dispersions using various impeller types have proved fruitful. However, observation of the gas and liquid flows around the impeller blades in order to detect any role played by gas filled cavities might be very useful in further explaining the gassed power characteristics of the 4 MFD, AFD and 4 MFU impellers particularly. Linking the power characteristics and cavity behaviour to experimental measurements of the volumetric liquid pumping capacity of the impeller is complicated by the difficulties involved in measuring the latter. Nevertheless, if this could be achieved it would allow a less speculative interpretation of the suspension results to be made.

With regard to particle suspension, it was clearly shown in Chapter 4 that the mechanisms responsible for lifting the particles are still not fully understood. An attempt to observe particle behaviour in the presence of various scales of turbulent eddies (promoted using grids upstream) might give some indication of the applicability of the model proposed by Baldi et al.[26] The anomaly

referred to in Chapters 4 and 7 suggests that care must be taken in relating results obtained in different tanks and the effect of surface fungal growth on suspension requires illumination.

The extreme difficulty encountered in suspending the very flat and angular anthracite particles suggests that the effect of particle shape on N_{JS} should be further investigated. Also, though electrolytes have significant effects on bubble properties, it has not been established here whether or not there would be any effect on suspension. However, it should be possible to predict this on the basis of power measurements in non-coalescing systems.

In industry very fine particles are commonly used (e.g. in slurry reactors). These present further difficulties in that there may be interface effects (particle to bubble) which influence mass transfer as well as suspension. Now that a basis has been established in terms of relatively simple experimental systems, it should be possible to continue the work into areas where additional complicating factors are involved.

NOTATION

(Unless otherwise stated in the text.)

a	-	constant in Eqns. 7.4 to 7.10	$vvm^{-1}\ s^{-1}$
A	-	specific interfacial area	m^{-1}
c	-	impeller clearance above base of tank	m
C	-	concentration of key component (oxygen)	Moles m^{-3} or arbitrary units
d_b	-	bubble diameter	m
d_p	-	particle diameter	μm
D	-	impeller diameter	m
F	-	net force	N
g	-	acceleration due to gravity	ms^{-2}
G	-	mass flowrate	$Kg\ s^{-1}$
h	-	increase in height of dispersion on aeration	m
H	-	unaerated height of liquid	m
J	-	an area (see Fig. A6.1)	s
k_L	-	liquid film absorption rate constant	ms^{-1}
$k_L A$	-	mass transfer coefficient	s^{-1}
K	-	Henry's Law constant	vol/vol
M	-	an area (see Fig. A6.1)	s
n	-	number of bubbles in vessel	-
N	-	impeller speed (see subscripts)	rps or s^{-1}
P	-	power input to impeller (see subscripts)	W
Q	-	volumetric gas flowrate	vvm or $m^3 s^{-1}$
S	-	parameter in Eqn. 4.1	-
t	-	time	s
T	-	tank diameter	m
U	-	linear velocity	ms^{-1}
V	-	volume (see subscripts)	m^3

v_s	-	superficial gas velocity (= $4Q/\pi T^2$)	ms^{-1}
vvm	-	volumetric gas flowrate per unit volume of liquid	$minutes^{-1}$
W	-	final steady state concentration values (t=∞)	arbitrary units
x	-	exponent in Eqn. 7.8	-
X	-	mass concentration (= mass particles/mass of suspension)	%
Y, Y', Y''	-	constants in Eqns. 3.8 - 3.10	various
Z	-	dimensionless parameter defined in Eqn. 4.2	-

Dimensionless Numbers

Fl	-	flow number (= Q/ND^3)	-
Po	-	power number (= $P/\rho_L N^3 D^5$)	-
Re	-	Reynolds number (= $\rho_L ND^2/\mu$)	-

Greek Symbols

α	-	normalised particle concentration (= sample concentration/bulk concentration)	-
β	-	critical liquid pumping rate (Eqns.3.15 to 3.16)	m^3s^{-1}
δ	-	constant in Eqns. 3.12 - 3.18	-
$\Delta\rho$	-	density difference between solid and liquid phases (= $\rho_S-\rho_L$)	$Kg\ m^{-3}$
ε	-	volumetric gas holdup (= h/H+h)	-
ε_T	-	specific power dissipation (see subscripts) based on mass of liquid in tank containing liquid only	$W\ Kg^{-1}$
μ	-	liquid viscosity	$Ns\ m^{-2}$
ν	-	kinematic viscosity (= μ/ρ)	m^2s^{-1}
ρ	-	density (see subscripts)	$Kg\ m^{-3}$
σ_Z	-	standard deviation of Z from a mean value	-
τ	-	first order time lag (see subscripts)	s

Subscripts

b	-	of bubble
B	-	on the vessel base
c	-	at the condition where flow fluctuations occur

$\frac{C}{T}$	Gas holdup, ε (%) at various Q		
	0.25 vvm	0.75 vvm	1.25 vvm
0.167	2.3	5.1	8.5
0.25	2.9	5.7	8.2
0.50	3.9	7.4	9.2

Table 7.5 Effect of Impeller Clearance on Gas Holdup at N_{JS}

(D = T/3 DT T_{56} 3% Soda Glass Ballotini)

7.6. Scale Up

In Chapter 4 (Section 4.4.2), the N_{JS} data obtained in the ICI tanks (T_{30}, T_{91}, T_{183}) were shown to be self consistent but significantly higher than that obtained in the U.C.L. tanks (T_{29}, T_{56}), which were also self consistent. Fig. 7.15 shows an equivalent graph to Fig. 4.7 but for a gas rate of 1 vvm and with the two sets of tanks treated as producing separate data. Once again the difference between the two data sets is very marked, especially if viewed in terms of the power requirements to achieve N_{JS} at this gas rate (Fig. 7.16).

Table 7.6(a-c) gives the exponents on T to be used on scale up for each impeller type at gas rates between 0 and 1 vvm.

CD - at the completely dispersed condition

g - with sparged aeration

G - of the gas phase

i - at the inlet

j - an integer referring to the gas phase concentration in a particular bubble or at a time

JS - at the just-suspended condition

L - of the liquid phase

O - at the outlet

PJS - at the discontinuity in the sampled concentration v. N plot

R - at the condition where recirculation of gas to the impeller cavities occurs

S - of the solid phase

$\equiv^{m}$ - at equilibrium

Superscripts

* normalised value

\- mean value

REFERENCES

1. N. Arbiter, C.C. Harris and R.F. Yap, Trans. A.I.M.E., 1969, 244, 134.

2. A.W. Nienow, Chem. Eng. Sci., 1968, 23, 1453.

3. D.J. Wisdom, Ph.D. Thesis, University of London, 1974.

4. A.W. Nienow and D. Miles, J. Sci. Inst., 1969, 2, 994.

5. A.W. Nienow, D.J. Wisdom and J.C. Middleton, Second European Conference on Mixing (BHRA), Cambridge 1977, F1-1 to F1-16.

6. T.N. Zwietering, Chem. Eng. Sci., 1958, 8, 224.

7. J. Rennie and F.H.H. Valentin, Chem. Eng. Sci., 1968, 23, 663.

8. A.W. Nienow and D.J. Wisdom, Chem. Eng. Sci., 1974, 29, 1994.

9. K. Van't Riet and J.M. Smith, Chem. Eng. Sci., 1973, 28, 1031.

10. W. Bruijn, K. Van't Riet and J.M. Smith, Trans. Instn. Chem. Engrs., 1974, 52, 88.

11. M.M.C.G. Warmoeskerken, J. Feijen and J.M. Smith, The Instn. Chem. Engrs. Symp. Ser., 1981, 64, J1.

12. Y. Oyama and K. Endoh, Chem. Eng. (Tokyo), 1955, 19, 2.

13. A.W. Nienow, C.M. Chapman and J.C. Middleton, Chem. Eng. J., 1979, 17, 111.

14. H. Brauer and H. Schmidt-Traub, Chem. Ing. Tech., 1972, 44, 1329.

15. A.W. Nienow and D.J. Wisdom, Inst. of Chem. Engrs. Third Annual Research Meeting, Salford 1976.

16. J.H. Rushton and J.J. Bimbinet, Can. J. Chem. Eng., 1968, 46, 16.

17. K.R. Westerterp,L.L. van Dierendonck and J.A. De Kraa, Chem. Eng. Sci., 1963, 18, 157.

18. The Institution of Chemical Engineers Fluid Mixing Group, The Chemical Engineer, August/September 1980.

19. A.W. Nienow and D. Miles, Chem. Eng. J., 1978, 15, 13.

20. G.B. Tatterson, S.Y. Hsien Hwa and R.S. Brodkey, Chem. Eng. Sci., 1980, 35, 1369.

21. J.F. Davidson and D. Harrison, Fluidised Particles, Cambridge University Press, 1963.

22. K. Van't Riet, Ph.D. Thesis, Tech. Univ. of Delft, 1973.

23. F. Kneule, Chem. Ing. Tech., 1956, 28, 221.

24. P. Harriott, A.I. Ch. E. J., 1962, 8, 93.

25. S. Narayanan, V.K. Bhatia, D.K. Guha and M.N. Rao, Chem. Eng. Sci., 1969, 24, 223.

26. G. Baldi, R. Conti and E. Alaria, Chem. Eng. Sci., 1978, 33, 21.

27. J. Weisman and L.E. Efferding, A.I. Ch. E. J., 1960, 6, 419.

28. J.R. Bourne and R.N. Sharma, First European Conference on Mixing (BHRA), Cambridge 1974, B3-25 to B3-38.

29. L. Musil, Coll. Czech. Chem. Commun., 1976, 41, 839.

30. R. Conti and G. Baldi, International Symposium on Mixing, Mons 1978, B2-1 to B2-17.

31. A.W. Nienow, Inst. of Chem. Engrs. Sponsored Course,"Mixing in the Process Industries". Bradford, 1980.

32. A.W. Nienow and D. Miles, Chem. Eng. J., 1978, 15, 13.

33. D. Subbarao and V.K. Taneja, Third European Conference on Mixing (BHRA), York 1979, 229-240.

34. L. Musil and J. Vlk, Chem. Eng. Sci., 1978, 33, 1123.

35. I.S. Pavlushenko et al. Zh. Prikl. Khim., 1957, 30, 1160.

36. Y. Oyama and K. Endoh, Chem. Eng. (Tokyo), 1956, 20, 66.

37. V. Kolar, Coll. Czech. Chem. Commun., 1967, 32, 526.

38. A.W. Nienow and D. Miles, Ind. Eng. Chem. Proc. Des. Devel ., 1971, 10, 41.

39. D.B. Holmes, R.M. Voncken and J.A. Dekker, Chem. Eng. Sci., 1964, 19, 201.

40. S. Nagata, Mixing Principles and Applications, Kodansha Ltd., Tokyo, 1975.

41. W.D. Einenkel and A. Mersmann, VerFahrenstechnik, 1977, 11, 90.

42. J.R. Bourne and M. Zabelka, Chem. Eng. Sci., 1980, 35, 533.

43. R.L. Bates, P.L. Fondy and R.R. Corpstein, Ind. Eng. Chem. Process. Des. Devel ., 1963, 2, 310.

44. M.J. Cliff, M.F. Edwards and I.N. Ohiaeri, Inst. of Chem. Engrs. Symp. Ser. No. 64, M1-M11.

45. L.E. Gates, J.R. Morton, P.L. Fondy, Chemical Engineering, May 24th 1976, 144.

46. R.V. Chaudhari and P.A. Ramachandran, A.I. Ch. E. J., 1980, 26, 177.

47. M. Zlokarnik and H. Judat, Chem. Ing. Tech ., 1969, 41, 1270.

48. J.Y. Oldshue, Ind. Eng. Chem., 1969, 61, 79.

49. P.B. Queneau, R.J. Jan, R.S. Rickard and D.F. Lowe, Metallurgical Trans., 1975, 6B, 149.

50. J.A. Wiedmann, A. Steiff, P.M. Weinspach, Chem. Eng. Commun., 1980, 6, 245.

51. A.M. Jahnse and E.J. de Jong, Industria Chemica and Petrolifera, 1974, 11, 26.

52. H.J. Van den Berg, Chemical Reaction Engineering, Advances In Chemistry Series 109, Washington, Americal Chemical Society, 1972, p.240.

53. G.E.H. Joosten, J.G.M. Schilder, J.J. Janssen, Chem. Eng. Sci., 1977, 32, 563.

54. L. Massimilla, A. Solimando and E. Squillace, Brit. Chem. Engng., 1961, 6, 232.

55. D. Adlington and E. Thompson, Proc. Third European Symposium on Chemical Reaction Engineering, 1965, 203.

56. J. Bryant and S. Sadeghzadek, Third European Conference on Mixing (BHRA), York 1979, F3.

57. A.W. Nienow, Symposium on the Profitable Aeration of Waste Water (BHRA), London 1981, Paper 1.

58. R.K. Finn, Biochemical and Biological Engineering Science, N. Blakenbrough, Ed., Academic Press, London 1967.

59. I.J. Dunn and A. Einsele, J. Appl. Chem. Biotechnol., 1975, 25, 707.

60. M.M. Lopes de Figueiredo and P.H. Calderbank, Chem. Eng. Sci., 1979, 34, 1333.

61. K. Chandrasekharan and P.H. Calderbank, Chem. Eng. Sci., 1981, 36, 819.

62. K. Van't Riet, Ind. Eng. Chem. Process. Des. Devel., 1979, 18, 357.

63. C.W. Robinson and C.R. Wilke, Biotechnol. Bioeng., 1973, 15, 755.

64. P.H. Calderbank, Trans. Inst. Chem. Engrs., 1959, 37, 173.

65. J. Solomon, Ph.D. Thesis, University of London, 1980.

66. M.M. Lopes de Figueiredo, Ph.D. Thesis, University of Edinburgh, 1978.

67. W.S. Wise, J. Gen. Microbiol., 1951, 5, 167.

68. F.G. Heineken, Biotechnol. Bioeng., 1971, 13, 599.

69. V. Linek, Biotechnol. Bioeng., 1972, 14, 285.

70. E. Van de Sande, Ph.D. Thesis, Tech. Univ. of Delft., 1974.

71. N.D.P. Dang, D.A. Karrer and I.J. Dunn, Biotechnol. Bioeng., 1977, 19, 853.

72. J. Hanhart, H. Kramers and K.R. Westerterp, Chem. Eng. Sci., 1963, 18, 503.

73. K.R. Westerterp, L.L. Van Dierendonck and J.A. de Kraa, Chem. Eng. Sci., 1963, 18, 157.

74. M. Lakin, R. Salzman, J. Oldshue and H. Gray, Int. Symp. on Mixing, Mons 1978, C2-1 to C2-39.

75. M. Roustan, J.M. Charles and J.P. Martinet, Int. Symp. on Mixing, Mons 1978, C1-1 to C1-19.

76. M. Cooke, J.C. Middleton and P. Lynch. To be published.

77. V.D. Mehta and M.M. Sharma, Chem. Eng. Sci., 1971, 26, 461.

78. C.M. Chapman, A.W. Nienow and J.C. Middleton, Biotechnol. Bioeng., 1980, 22, 981.

79. B.A. Buffham, Proc. Roy. Soc. London, 1973, A.333, 89.

80. L.G. Gibilaro and S.P. Waldram, Chem. Eng. J., 1972, 4, 197.

APPENDIX 1.

TWO PHASE SUSPENSION DATA

For Disc Turbines

D = T/4

Run No.	T (m)	D (m)	c/T (-)	$\Delta\rho$ Kgm^{-3}	X %	d_p (μm)	N_{JS} (rps)	P_{JS} (W)	$(Po)_{JS}$ (-)	Z (-)	$Re^* \times 10^{-4}$ (-)	N_{JS}' (rps)	N_{JS}'' (rps)	S_{exp} (-)
1	0.56	0.14	0.25	1480	1	206	9.58	243	5.16	0.84	4.69	9.79	9.79	11.7
2	0.56	0.14	0.25	50	1	300	2.62	-	-	0.60	1.28	2.30	2.30	13.7
3	0.56	0.14	0.25	200	1	600	5.2	39	5.04	0.68	2.55	4.9	4.9	12.7

Notation:

Z - see Eqn. 4.2 (corrected to X = 1%)

Re^* - see Eqn. 4.3.

N_{JS}' - From Zwietering[6]

N_{JS}'' - From Nienow[2]

S_{exp} - Experimental evaluation of Zwietering's S Group

Run No.	T (m)	D (m)	c/T (-)	$\Delta\rho$ Kgm^{-3}	X %	d_p (μm)	N_{JS} (rps)	P_{JS} (W)	$(Po)_{JS}$ (-)	Z (-)	$Re^* \times 10^{-4}$ (-)	N_{JS}' (rps)	N_{JS}'' (rps)	S_{exp} (-)
4	0.56	0.187	0.25	50	1	300	1.34	-	-	0.71	1.56	1.13	1.20	8.9
5	0.56	0.187	0.25	400	1	550	5.3	184	5.55	0.56	6.19	3.22	3.43	12.3
6	0.56	0.187	0.25	1200	0.3	309	3.83	73	5.6	1.05	5.17	4.02	4.29	7.1
7	0.56	0.187	0.25	1480	1	206	4.2	90	5.4	1.16	4.90	4.8	5.12	6.6
8	0.56	0.187	0.25	1480	2	206	4.5	110	5.51	1.17	4.83	5.23	5.58	6.5
9	0.56	0.187	0.25	1480	3	206	4.95	151	5.47	1.12	5.07	5.51	5.88	6.7
10	0.56	0.187	0.5	1480	3	206	5.9	240	5.36	0.94	6.04	5.51	-	8
11	0.56	0.187	0.167	1480	3	206	4.28	82.4	4.61	1.37	4.38	5.51	5.0	5.8
12	0.29	0.097	0.25	1480	3	206	10.9	34.5	3.15	0.96	3.0	9.64	10.3	8.5
13	0.56	0.187	0.25	250	1	500	3.63	61	5.58	0.63	4.24	2.55	2.72	12

D = T/3

DT

D = T/2

DT

Run No.	T	D	c/T	Δρ	X	d_p	N_{JS}	P_{JS}	$(Po)_{JS}$	Z	$Re^* \times 10^{-4}$	N_{JS}'	N_{JS}''	S_{exp}
14	0.56	0.28	0.25	1480	3	206	2.01	84	6.02	1.37	6.82	2.09	2.35	3.8
15	"	"	"	"	5	"	2.21	114	6.15	1.30	7.14	2.23	2.51	4.0
16	"	"	"	"	10	"	2.42	146	5.97	1.31	6.85	2.44	2.75	4.0
17	"	"	"	"	15	"	2.48	162	6.2	1.31	7.02	2.57	2.90	3.9
18	"	"	"	"	20	"	2.6	188	6.31	1.30	7.1	2.67	3.0	3.9
19	"	"	"	"	30	"	2.95	295	6.74	1.17	7.7	2.82	3.17	4.2
20	0.29	0.145	"	"	3	"	3.85	17.4	4.76	1.19	4.05	3.65	4.11	4.2
21	0.29	0.145	"	"	32.4	"	5.25	49.5	5.34	1.12	5.52	4.98	5.60	4.2
22	0.56	0.28	"	1900	1	2650	3.14	314	5.9	1.33	12.3	3.38	3.80	3.7
23	"	"	"	"	1	925	3.06	290	5.9	1.14	12.0	2.73	3.08	4.5
24	"	"	"	"	1	485	2.82	222	5.7	1.13	11.05	2.4	2.7	4.7
25	"	"	"	"	1	92.5	1.99	78	5.8	1.21	7.8	1.72	1.94	4.6
26	"	"	"	1650	1	470	2.92	245	5.7	1.01	11.4	2.24	2.52	5.2
27	"	"	0.167	1650	1	470	2.55	152	5.33	1.53	10.0	2.24	2.24	4.6

D = T/2
continued

DT

Run No.	T	D	c/T	Δρ	X	d_p	N_{JS}	P_{JS}	$(Po)_{JS}$	Z	$Re^* \times 10^{-4}$	N_{JS}'	N_{JS}''	S_{exp}
28	0.29	0.145	0.25	1650	1	470	5.03	39	4.8	0.97	5.29	3.92	4.41	5.1
29	0.29	0.145	0.167	"	"	"	4.77	32	4.7	1.02	5.01	3.92	3.92	4.9
30	0.30	0.15	0.25	"	"	"	5.58	85	5.95	0.79	6.28	3.81	4.29	5.9
31	0.91	0.455	0.25	"	"	"	2.32	1528	6.15	1.16	24.0	1.48	1.67	6.3
32	0.91	0.455	0.167	"	"	"	2.30	1360	5.4	1.22	23.8	1.48	1.48	6.2
33	1.83	0.915	0.25	"	"	"	1.28	7200	5.25	1.07	53.6	0.82	0.92	6.2
34	1.83	0.915	0.167	"	"	"	1.41	8353	4.58	1.02	59.0	0.82	0.82	6.9

For 4 MFD Impellers - All D/T Ratios

Run No.	T	D	c/T	Δρ	X	d_p	N_{JS}	P_{JS}	$(Po)_{JS}$	Z	$Re^* \times 10^{-4}$	N_{JS}'	N_{JS}''	S_{exp}
35	0.56	0.14	0.25	1480	1	206	7.18	30.5	1.53	1.67	3.52	-	-	7.1
36	0.29	0.072	"	1650	1	470	12.7	5	1.23	1.94	1.63	-	-	7.1
37	0.56	0.28	"	1480	3	206	2.74	48	1.37	1.64	9.3	-	-	5.25
38	0.56	0.28	"	1480	20	206	3.32	90	1.40	1.75	8.71	-	-	5.0
39	0.56	0.28	"	1650	1	470	3.63	108	1.31	1.33	14.2	-	-	6.5
40	0.29	0.145	"	1650	1	470	6.45	21	1.22	1.19	6.78	-	-	6.6
41	0.91	0.455	"	1650	1	470	2.87	838	1.78	1.09	29.7	-	-	7.7

For Other Impeller Types

Run No.	Impeller Type	T	D	c/T	Δρ	X	d_p	N_{JS}	P_{JS}	$(Po)_{JS}$	Z	$Re^{*}x10^{-4}$	N_{JS}'	N_{JS}''	S_{exp}
42	6 MFD	0.56	0.14	0.25	1480	1	206	6.55	26.5	1.76	-	-	-	-	6.5
43	ADT	"	0.28	"	"	3	"	2.67	75	2.3	-	-	-	-	5.1
44	AFD	"	0.29	"	"	3	"	3.55	45	0.48	-	-	3.13	-	6.8
45	4 MFU	"	0.28	"	"	3	"	3.6	100	1.25	1.12	14.1	-	-	6.9
46	4 MFU	"	0.28	"	"	20	"	4.28	184	1.36	0.92	16.8	-	-	6.4
47	4 MFU	"	0.28	"	1650	1	470	4.67	216	1.23	1.05	18.3	-	-	8.3
48	4 MFU	0.29	0.145	"	1650	1	470	7.83	42.4	1.38	0.94	8.23	-	-	8.0

Additional Runs

49	DT	0.56	0.28	0.25	1900	1	A	3.07	-	-	-	-	-	-	- Size Distribution A & B: see Section 4.4.1
50	DT	0.56	0.28	"	1900	1	B	3.0	-	-	-	-	-	-	-
51	DT	0.29	0.145	"	1650	1	470	5.37	-	-	-	-	-	-	- $\nu=1.1x10^{-6}m^2s^{-1}$
52	DT	0.29	0.145	"	1650	1	470	4.67	35.0	-	-	-	-	-	- $\nu=1.55x10^{-6}\ m^2s^{-1}$
53	DT	0.29	0.145	"	1650	1	470	4.67	34.6	-	-	-	-	-	- $\nu=4.9x10^{-6}m^2s^{-1}$
54	ADT + DT	0.56	0.28	0:25+ 1.0	1480	20	206	NOT SUSPENDED							Double impeller H= 1.5T

APPENDIX 2.

Notation within this appendix is independent of the rest of the thesis.

UNSUCCESSFUL TECHNIQUES

Attempts were made to measure local holdups of either the particulate, or all three phases, in situ. A photographic technique, involving a camera with a specially built 90 cm long extension piece fitted with lenses, was tested. The basis of this technique was that the photograph taken of the dispersion at the end of the extension piece (which focussed on a plane approximately 1 cm from the end) could be analysed to give a measure of local particle concentration. However, difficulties were experienced in preventing bubbles from sticking to the lens extension and blurring the picture. Also, it was very difficult to distinguish the particles at fairly low concentrations but impossible at high concentrations or high gassing rates.

The other technique considered was based on γ ray absorption. The principle was that two γ ray sources should be used which had absorption coefficients in the liquid and solid phases such that:

$$\left[\frac{\lambda_L}{\lambda'_L}\right] \neq \left[\frac{\lambda_S}{\lambda'_S}\right] \qquad \text{A.1}$$

where λ_L and λ_S were the linear absorption coefficients for source 1 in the liquid and solid phases respectively, and λ'_L, λ'_S the equivalent coefficients for source 2. The absorption in the gas phase was negligible, hence an absorption equation could be written for each source:

$$\ln\left[\frac{I_1}{I_0}\right] = -\lambda_L \varepsilon_L x - \lambda_S \varepsilon_S x \qquad \text{A.2}$$

$$\ln\left[\frac{I'_1}{I'_0}\right] = -\lambda'_L \varepsilon_L x - \lambda'_S \varepsilon_S x \qquad \text{A.3}$$

where I_1 (I'_1) = count per unit time in three phase dispersion

I_0 (I'_0) = count per unit time in air

x = distance between source and counter

$\epsilon_{S,\ L,G,}$ = volumetric holdup of solid, liquid or gas phase

Thus, in theory, provided the constraint expressed in Eqn. A.1 was observed, the simultaneous solution of Eqns. A.2 and A.3 with Eqn. A.4 should yield the local holdups of all three phases in the vessel.

$$\epsilon_S + \epsilon_L + \epsilon_G = 1 \qquad A.4$$

The fork shaped probe consisted of a reversible rod with a well shielded source in each side as one leg and a sensitive sodium iodide crystal and photomultiplier tube as the other leg. Thus a count could be made with one source, the rod rotated and a count taken with the other source.

However, although the method should have worked in theory - by careful choice of different energy sources, Eqn. A.1 could be satisfied - the calibration of the sources (i.e. evaluation of λ_L, λ_S, λ_L' and λ_S') was made prohibitively difficult by the sensitivity of the equipment to the presence of the vessel walls, impeller, temperature changes, etc., etc. This extreme sensitivity to all manner of things made the technique totally impractical in a stirred vessel.

APPENDIX 3.

CIRCUIT DIAGRAMS FOR THE LIGHT CELL

Light Cell and Associated Circuits

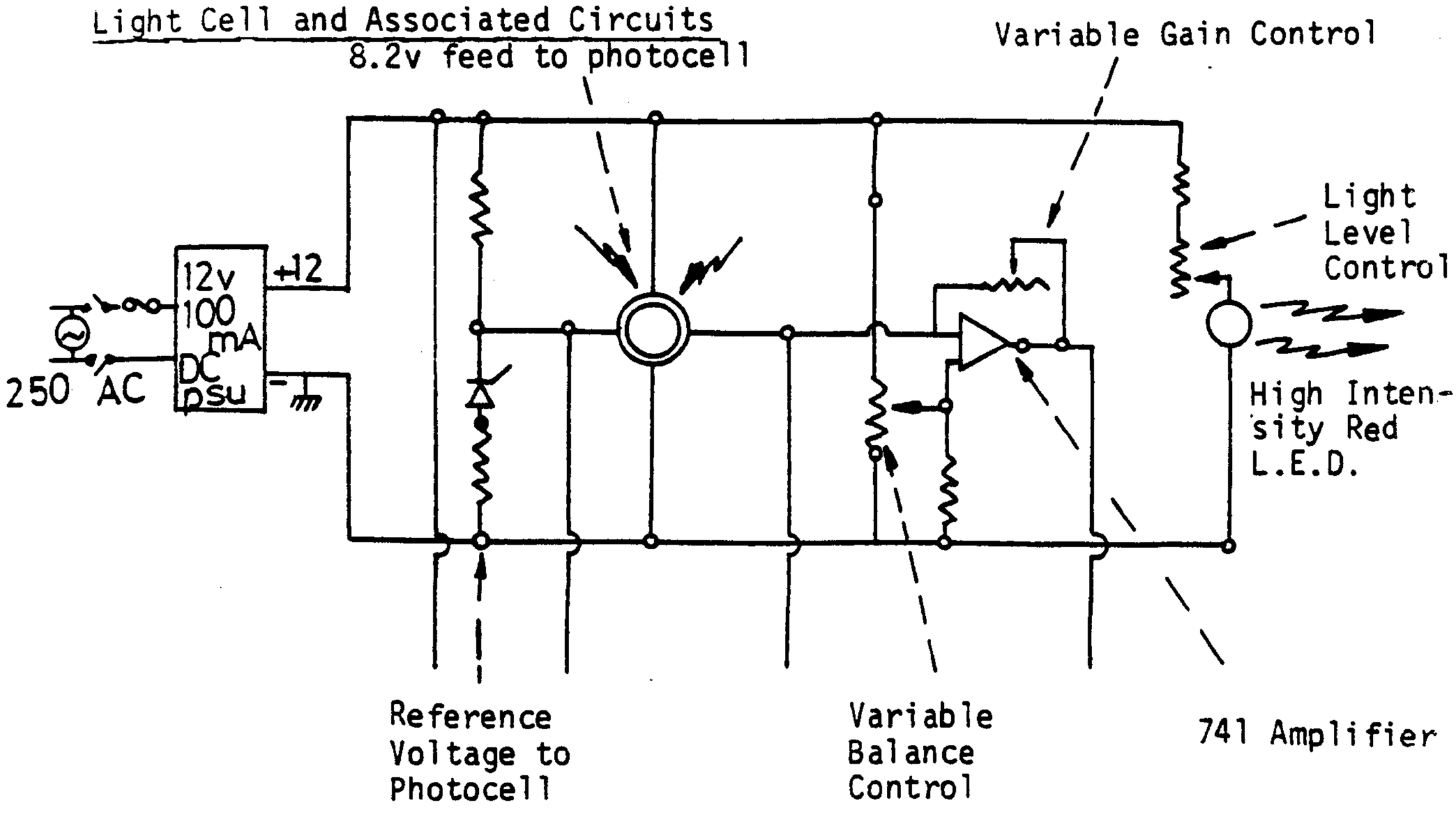

Overall Circuit

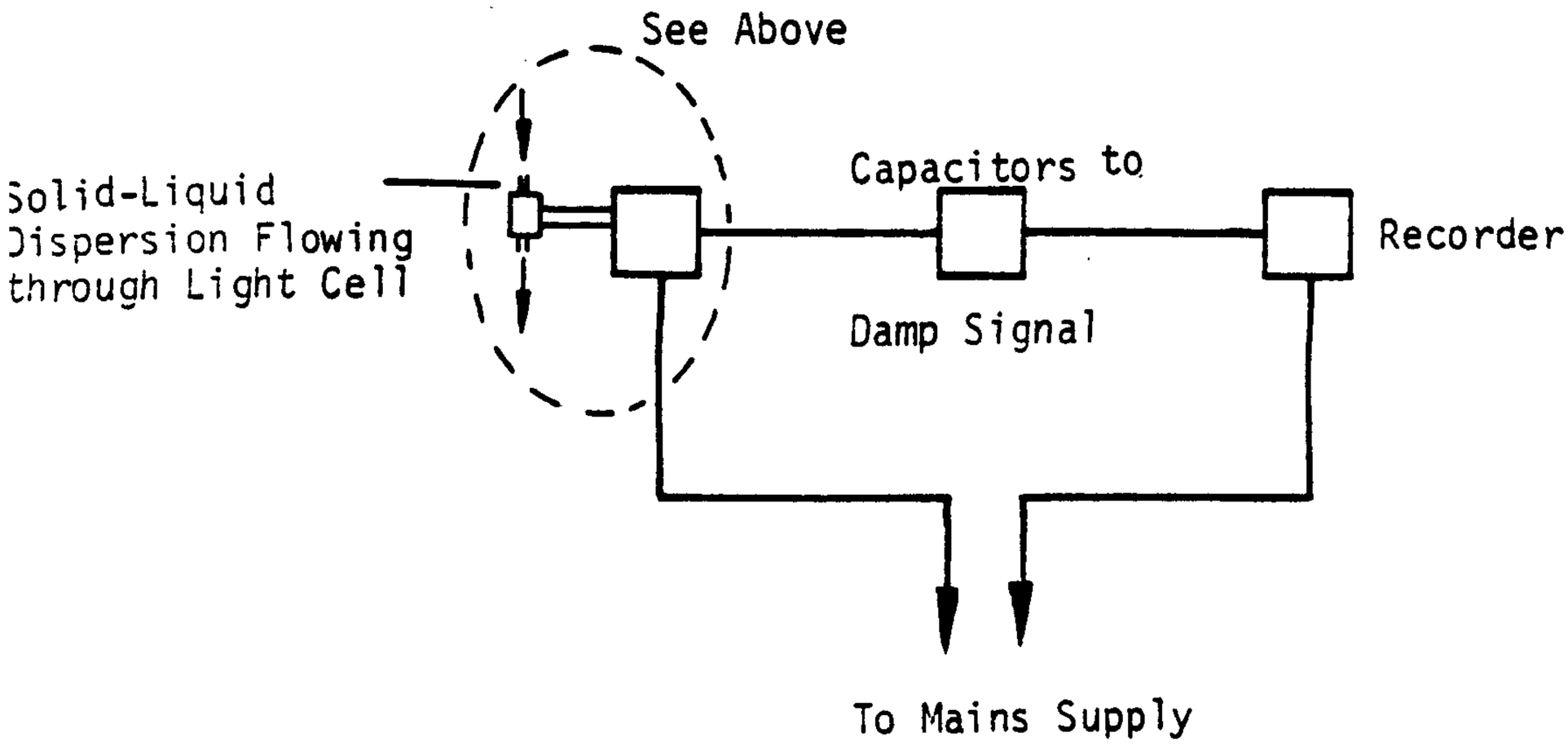

APPENDIX 4.

THREE PHASE SUSPENSION DATA

All details of the individual runs can be obtained from Appendix 1.

Run No.	Q vvm	N_{JS} rps	P_{JS} W	$(\epsilon_T)_{JS}$ W Kg^{-1}	$(Po_g)_{JS}$ -
1	0.25	11.2	296	2.15	3.96
	0.5	12.3	299	2.17	3.03
	1.0	13.4	311	2.26	2.42
2	0.25	4.62	-	-	-
	0.5	5.71	-	-	-
3	No data - wetting problems				
4	0.5	2.94	17.5	0.13	3.05
	1.0	3.41	23.1	0.17	2.60
5	0.25	5.7	191	1.39	4.53
	0.5	6.5	204	1.48	3.29
	0.75	7.0	220	1.60	2.78
	1.0	7.6	262	1.90	2.64
6	0.25	4.3	78.6	0.57	4.35
	0.5	4.85	80	0.58	3.10
	0.75	5.5	105	0.76	2.78
	1.0	6.08	132	0.96	2.60
	1.25	6.37	139	1.01	2.40
7	0.25	4.7	100	0.73	4.4
	0.5	5.5	115	0.83	3.1
	0.75	5.9	126	0.91	2.7
	1.0	6.35	142	1.03	2.4
	1.25	6.9	171	1.24	2.3
8	0.25	5.3	145	1.05	4.4
	0.5	6.1	170	1.23	3.2
	0.75	6.5	176	1.28	2.8
	1.0	7.0	200	1.45	2.6
	1.25	7.2	216	1.57	2.5
9	0.25	5.62	172	1.25	4.35
	0.5	6.32	186	1.35	3.25
	0.75	6.9	212	1.54	2.84
	1.0	7.37	240	1.74	2.65
	1.25	7.78	263	1.91	2.47
10	0.25	6.73	288	2.03	4.13
	0.75	8.18	338	2.45	2.70
	1.25	9.33	403	2.92	2.18
11	0.25	5.07	997	0.72	3.38
	0.75	6.67	147.3	1.07	2.18
	1.25	8.65	220	1.60	1.54
12	0.5	11.5	32.0	1.67	2.55
	1.0	12.83	37.2	1.94	2.1

Run No.	Q vvm	N_{JS} rps	P_{JS} W	$(\varepsilon_T)_{JS}$ W Kg^{-1}	$(Po_g)_{JS}$ -
13	0.25	4.48	84	0.61	4.1
	0.5	5.03	91	0.66	3.1
	1.0	6.02	126	0.91	2.5
14	0.25	2.32	120	0.87	5.70
	0.5	2.48	121	0.88	4.64
	0.75	2.76	130	0.94	3.58
	1.0	3.06	153	1.11	3.12
15	0.25	2.38	129	0.94	5.53
	0.5	2.60	138	1.0	4.55
	0.75	2.90	151	1.09	3.57
	1.0	3.23	180	1.31	3.09
16	0.25	2.60	165	1.20	5.43
	0.5	2.82	178	1.29	4.62
	0.75	3.13	190	1.38	3.62
	1.0	3.43	220	1.60	3.16
17	0.25	2.73	197	1.43	5.6
	0.5	2.97	208	1.51	4.7
	0.75	3.30	223	1.62	3.62
	1.0	3.52	240	1.74	3.2
18	0.25	2.82	216	1.57	5.6
	0.5	3.11	241	1.75	4.7
	0.75	3.38	246	1.78	3.7
	1.0	3.63	271	2.0	3.3
19	0.5	3.30	307	2.23	4.98
	1.0	3.83	333	2.41	3.46
20	0.5	4.12	19.3	1.01	4.31
	1.0	4.57	20.4	1.06	3.34
21	0.5	5.5	48.7	2.54	4.58
	1.0	6.0	46.0	2.40	3.30
22	0.5	3.49	338	2.45	4.63
	1.0	4.01	348	2.52	3.02
23	0.5	3.27	280	2.03	4.68
	1.0	3.83	296	2.15	3.08
24	0.5	3.16	249	1.81	4.61
	1.0	3.62	247	1.79	3.04
25	0.5	2.30	95.4	0.69	4.59
	1.0	2.75	113	0.82	3.16
26	0.25	3.05	255	1.85	5.22
	1.0	3.62	250	1.81	3.08
27	0.25	3.32	199	1.45	4.74
	1.0	3.47	226	1.64	3.15

Run No.	Q vvm	N_{JS} rps	P_{JS} W	$(\epsilon_T)_{JS}$ W Kg^{-1}	$(Po_g)_{JS}$ -
28	0.25	5.47	48	2.52	4.58
	1.0	5.93	48	2.50	3.59
29	0.25	5.25	41.1	2.16	4.43
	1.0	5.65	40.9	2.15	3.54
30	0.25	5.75	82.5	3.71	5.28
	1.0	7.0	91.0	4.09	3.22
31	0.25	2.62	1895	3.16	5.3
	1.0	3.1	1808	3.01	3.04
32	0.25	2.6	1657	2.76	4.72
	1.0	2.88	1473	2.45	3.08
33	0.25	1.58	10136	2.3	4.0
	0.5	1.75	10184	2.31	2.96
	1.0	1.75*	8201	1.86	2.4
34	0.25	1.5	8385	1.9	3.87
	1.0	1.75	8201	1.86	2.39
35	0.25	7.44	32	0.23	1.43
	0.5	9.57	65	0.47	1.47
	1.0	15.3	176	1.28	1.48
36	0.25	13.3	6.1	0.32	1.28
	1.0	20.8	11 - 21	0.6 - 1.1	0.6 - 1.2
37	0.25	2.9	49	0.36	1.16
	0.5	3.9	83	0.60	0.79
	1.0	5.5	158	1.13	0.56
38	0.25	3.55	85	0.62	1.1
	1.0	5.53	176	1.28	0.60
39	0.25	3.8	117	0.85	1.24
	1.0	5.7	184	1.33	0.58
40	0.25	6.3	19	1.0	1.19
	1.0	8.7	24	1.3	0.58
41	0.25	2.95	772	1.29	1.51
	1.0	4.83	1573	2.62	0.69
42	0.25	7.5	38	0.28	1.68
	0.5	8.83	54	0.39	1.46
	1.0	12.7	130	0.94	1.20
43	0.5	3.55	113	0.82	1.46
	1.0	4.49	163	1.18	1.05

* This result was attained at the maximum impeller speed and is a little suspect.

Run No.	Q vvm	N_{JS} rps	P_{JS} W	$(\epsilon_T)_{JS}$ W Kg^{-1}	$(Po_g)_{JS}$ -
44	0.25	3.55	45	0.33	0.48
	0.5	4.78	83	0.60	0.36
	1.0	6.0	123	0.89	0.27
45	0.25	3.55	92	0.67	1.21
	0.5	3.7	100	0.73	1.15
	1.0	3.98	102	0.74	0.95
46	0.25	4.25	177	1.28	1.3
	1.0	5.07	210	1.52	0.94
47	1.0	6.4	302	2.19	0.67
48	0.25	8	41.2	2.2	1.26
	1.0	9.67	52.8	2.8	0.91
49	0.5	3.4	-	-	-
	1.0	3.9	-	-	-
50	0.5	3.3	-	-	-
	1.0	3.8	-	-	-
51	0.25	5.67	-	-	-
	1.0	6.37	-	-	-
52	0.25	5.1	42.0	2.19	-
	1.0	5.75	37.9	1.98	-
53	0.25	4.83	35.5	1.85	-
	1.0	5.83	41.7	2.18	-
54	2.5×10^{-3} m^3s^{-1}	3.52	357	1.8	-

Text cut off in original

APPENDIX 5: τ_L and τ_G MEASUREMENTS

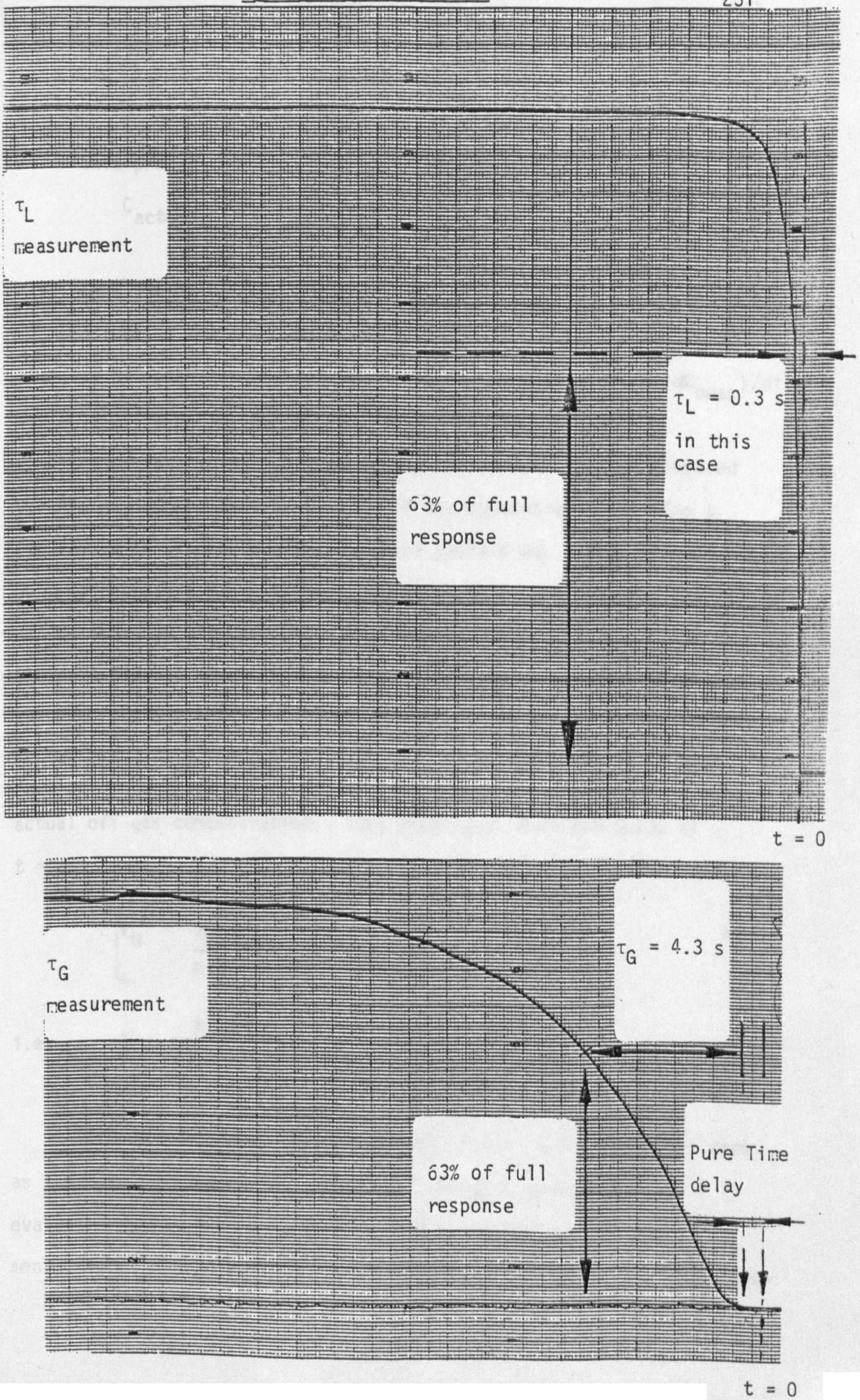

APPENDIX 6.

DE-CONVOLUTION PROCEDURE & ESTIMATION OF τ_G

This process was carried out according to Eqn. 8.21.

$$C_{actual} = \tau \frac{dC_{measured}}{dt} + C_{measured} \qquad 8.21$$

Thus the actual concentration data were obtained by evaluating the gradient of the measured concentration-time history curve at a time, t, after the experiment started. The resulting value $(dC_{meas})/dt$ was multiplied by the appropriate experimentally obtained first order lag (τ_L or τ_G), and adding this product to the measured concentration gave an actual value of the concentration at time t. Fig. A6.1a shows that the liquid phase profile was virtually unaffected by this procedure since τ_L was so small ($\simeq$ 0.4 s). However, the effect on the measured off-gas concentration profile was noticeable, as shown in Fig. A6.1b. The resulting <u>difference</u> in the area above the curve before and after this treatment (i.e. the region marked 'J') is equivalent to τ_G, and the area 'M' = $\int_0^\infty (1-C_o^*)\, dt$ where C_o^* is the actual off-gas concentration. Thus from Eqns. 8.22 and 8.23, at $t = \infty$:

$$\left[V_G + \frac{V_L}{K}\right]/Q = \int_0^\infty (1-C_o^*)\, dt \qquad A6.1$$

i.e.
$$\frac{Q}{V_G} \int_0^\infty (1-C_o^*)\, dt = 1 + \left[\frac{V_L}{KV_G}\right] \qquad A6.2$$

This confirms that the denominator in Eqn. 8.18 approaches zero as $t \to \infty$ ($C_L^* = 1$ at $t = \infty$). Since the integral term in Eqn. A6.2 is evaluated during the computation of $k_L A$, then by using the experimental value of τ_G, a value can be assigned to the area (J + M) because:

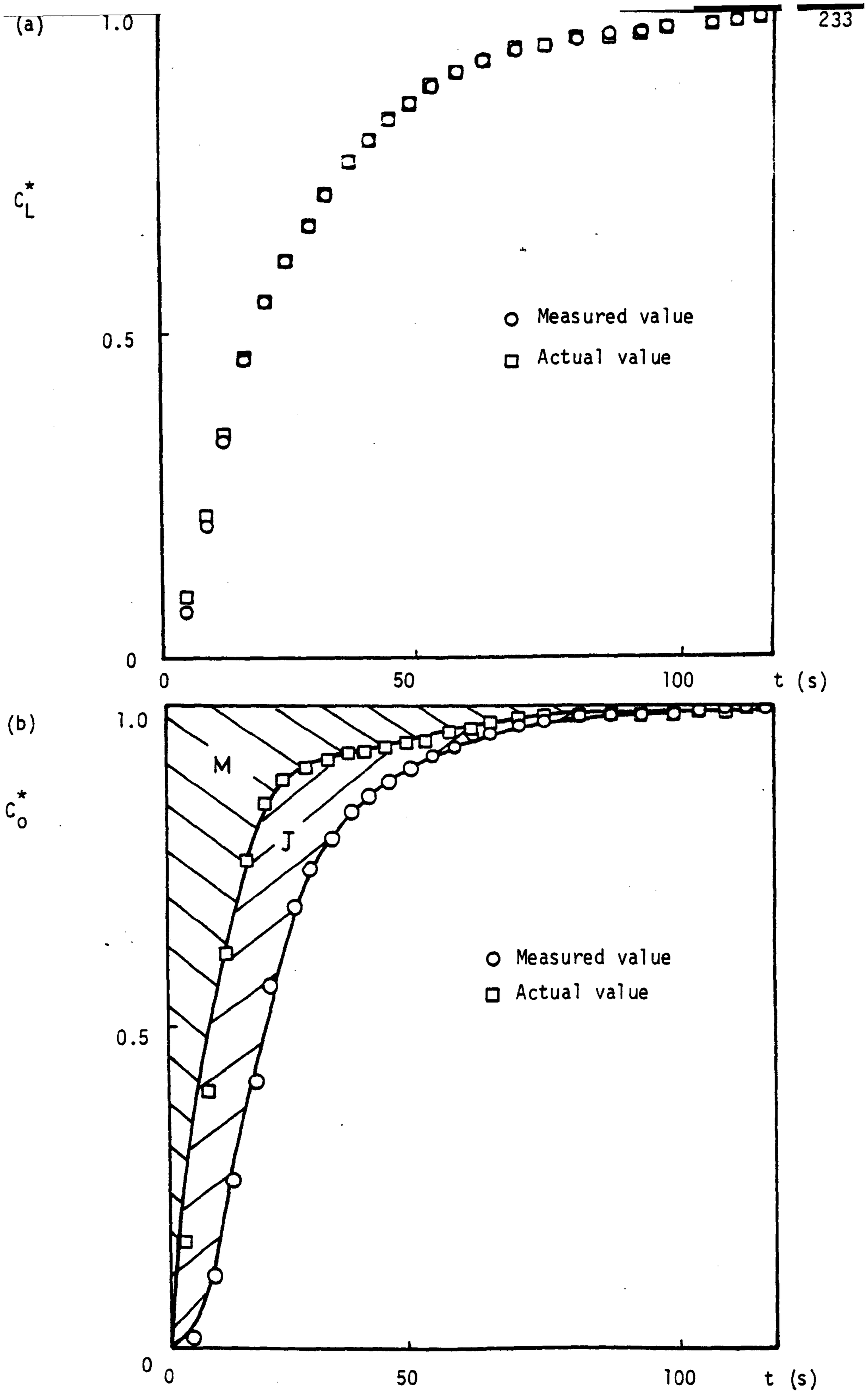

Fig. A6.1 Effect of Deconvolution for Run 27: (a) Liquid phase (b) off-gas

$$\frac{Q}{V_G}\int_0^\infty (1-C_o^*)\,dt = \frac{Q}{V_G}(M) = \frac{Q}{V_G}\left[(J+M) - \tau_G\right] \qquad A6.3$$

where $J = \tau_G$ A6.4

and from Eqn. A6.2, the value of (J+M) can be computed assuming the necessary knowledge of V_L, V_G and K. In this work the value of the Henry's Law constant (K) was taken as 0.0274 (litres of air/litres of water) for an air-water system at 25^o C.

Thus the following procedure was undertaken to satisfy the above relationships and evaluate $k_L A$:

1. τ_L and τ_G evaluated from experimental tests - see Appendix 5.
2. Both gas and liquid measured concentration profiles deconvoluted to give actual concentration profiles.
3. $k_L A$ estimated from Eqn. 8.18 at various times in the transient response period, right up to equilibrium conditions, i.e. $t \to \infty$.
4. From Eqn. A6.2, K can be evaluated at $t = \infty$ since

$$K = \frac{\frac{V_L}{V_G}}{\left[\frac{Q}{V_G}\int_0^\infty (1-C_o^*)\,dt - 1\right]} \qquad A6.5$$

5. From Eqns. A6.2 and A6.3:

$$\frac{Q}{V_G}\left[(J+M) - \tau_G\right] = 1 + \frac{V_L}{KV_G} \qquad A6.6$$

hence from the experimental value of τ_G and the value of K evaluated from Eqn. A6.5, the area (J+M) can be deduced.

6. If the literature value of K is now substituted back into Eqn. A6.6, along with the value of (J+M) deduced in step 5, then a new value of τ_G results and the process is repeated from step 1 until the value of K from Eqn. A6.5 is equal to

0.0274 l air/l water.

This process resulted in τ_G values that differed by up to 50% from the experimental measured values. However, the self consistency of Eqn. 8.18 meant that these errors normally had a remarkably small effect on the eventual $k_L A$ value produced.

APPENDIX 7.

GAS-LIQUID MASS TRANSFER RESULTS

Section 1 : Q = 0.25 vvm; X = 3% Soda Glass Ballotini

Section 2 : Q = 1.0 vvm; X = 3% Soda Glass Ballotini

Section 3 : Gas-Liquid only; Q = 0.25 and 1.0 vvm

Section 4 : Q = 0.25 or 1.0 vvm; X = 20% Soda Glass Ballotini

Key to gas mixing model:

(i) Simple 'no depletion' model (D - Fig. 8.1)

(ii) Gas phase Perfectly Mixed (A - Fig. 8.1)

(iii) Gas phase in Plug Flow

(iv) Unspecified - this work

The $k_L A$ values for specific gas mixing models (i, ii and iii) were provided by ICI Corporate Laboratory.

MASS TRANSFER RESULTS

All impellers are D = T/2, c = T/4

Section 1

1a) Disc Turbine N_{CD} = 1.15 rps N_{JS} = 2.3

Run	ε_T WK_g^{-1}	N rps	V_G $m^3 \times 10^3$	k_LA (s^{-1}) for various gas mixing models			
				(i) No depletion	(ii) Perfect mixing	(iii) Plug flow	(iv) Unspecified (this work)
1	0.96	2.4	3.4	-	-	-	0.053
2	1.34	2.7	4.5	-	-	-	0.0655
3	1.88	3.0	5.15	0.042	0.23	0.064	0.074

1b) 4 MFU N_{CD} = 2.5 rps N_{JS} = 3.55 rps

Run	ε_T	N	V_G	k_LA (i)	k_LA (ii)	k_LA (iii)	k_LA (iv)
4	0.76	3.55	3.4	-	-	-	0.023
5	0.96	3.85	3.7	-	-	-	0.050
6	1.15	4.2	3.9	-	-	-	0.052

1c) 4 MFD N_{CD} = 2.6 rps N_{JS} = 2.9 rps

Run	ε_T	N	V_G	k_LA (i)	k_LA (ii)	k_LA (iii)	k_LA (iv)
7	0.44	3.0	3.4	-	-	-	0.017
8	0.67	3.4	3.9	-	-	-	0.023
9	1.0	3.85	3.9	0.032	0.061	0.040	0.052
10	1.27	4.2	4.7	-	-	-	0.051

1d) AFD N_{CD} = 2.5 rps N_{JS} = 3.55 rps

Run	ε_T	N	V_G	k_LA (i)	k_LA (ii)	k_LA (iii)	k_LA (iv)
11	0.44	3.6	3.7	-	-	-	0.013
12	0.54	3.9	3.7	-	-	-	0.032
13	0.65	4.2	3.9	0.026	0.041	0.030	0.029
14	0.82	4.7	3.9	-	-	-	0.043

Section 2

2a) Disc Turbine N_{CD} = 2.35 rps N_{JS} = 3.05 rps

Run	ε_T	N	V_G	k_LA (i)	k_LA (ii)	k_LA (iii)	k_LA (iv)
15	1.17	3.1	11.05	0.076	0.17	0.10	0.160
16	1.97	3.7	12.3	0.093	0.35	0.14	0.21

2b) 4 MFU N_{CD} = 2.8 rps N_{JS} = 4.0 rps

Run	ε_T	N	V_G	k_LA (i)	k_LA (ii)	k_LA (iii)	k_LA (iv)
17	0.87	4.05	9.3	0.052	0.078	0.062	0.068
18	1.01	4.3	10.1	0.053	0.08	0.061	0.104
19	1.2	4.7	10.3	-	-	-	- *
20	1.4	5.0	11.1	-	-	-	- *

* Simple model Soln. - see Fig. 8.7

2c) 4 MFD N_{CD} = 5.25 rps N_{JS} = 5.5 rps

Run	ε_T	N	V_G	k_LA (i)	k_LA (ii)	k_LA (iii)	k_LA (iv)
21	1.27	5.5	11.3	0.072	-	0.097	0.047
22	1.63	5.85	11.3	0.076	0.146	0.094	0.066
23	2.01	6.3	11.3	0.088	0.26	0.13	0.104

2d) AFD N_{CD} = 3.65 rps N_{JS} = 6.0 rps

Run	ε_T	N	V_G	k_LA (i)	k_LA (ii)	k_LA (iii)	k_LA (iv)
24	1.02	6.05	10.6	0.060	0.085	0.064	0.062
25	1.24	6.55	10.8	0.071	0.126	0.085	0.070

Section 3.

Disc Turbine

Run	Q vvm	ε_T	N	V_G	k_LA (i)	k_LA (ii)	k_LA (iii)	k_LA (iv)
26	0.25	1.45	2.8	3.5	0.035	0.070	0.045	0.055
27	0.25	1.71	3.0	3.9	0.037	0.097	0.052	0.062
28	1.0	1.17	3.1	10.8	0.066	0.119	0.081	0.077
29	1.0	1.96	3.8	11.3	0.089	0.199	0.115	0.107

Section 4.

Run	Impeller	Q	ε_T	N	V_G	k_LA (i)	k_LA (ii)	k_LA (iii)	k_LA (iv)
30	AFD	1.0	1.33	6.6	9.9	-	-	-	0.05
31	4 MFU	1.0	1.54	5.0	9.6	-	-	-	0.075
32	DT	0.25	1.88	3.0	3.9	-	-	-	0.052
33	DT	1.0	2.08	3.7	10.95	-	-	-	0.079